PTEP

Prog. Theor. Exp. Phys. **2023** 043I02(11 pages)
DOI: 10.1093/ptep/ptad050

Movable but unavoidable nodal lines through high-symmetry points in 2D materials

Vladimir Damljanović*

Institute of Physics Belgrade, University of Belgrade, Pregrevica 118, 11080 Belgrade, Serbia
*E-mail: damlja@ipb.ac.rs

Received February 24, 2023; Accepted April 13, 2023; Published April 14, 2023

In 2D materials, electronic band contacts often make a non-trivial contribution to a material's topological properties. Besides band contacts at high-symmetry points (HSPs) in the Brillouin zone (BZ), like those in graphene, there are nodal lines that form various patterns in the reciprocal space. In this paper we have found all movable nodal lines, whose shape depends on the model, that pass through HSPs in the presence of time-reversal symmetry. Cases with and without spin–orbit coupling are included by studying all 80 layer groups and their double extensions. Eight single and six double groups, including three symmorphic, necessarily host Dirac and Weyl nodal lines that extend through the whole BZ, respectively. Our research might be of interest in designing new materials with interesting physical properties.

Subject Index I90, I95

1. Introduction

The physics of 2D materials has become one of the focal points of solid-state science since the electric field effect was reported in atomically thin graphene in 2004. The Brillouin zone (BZ) of 2D materials is an even-dimensional manifold, and topological invariants are used in explaining the properties of 2D materials, such as the integer quantum Hall effect. A non-zero topological charge originates from singularities of electron wave functions in the reciprocal space, and these singularities appear at BZ points where two or more electron bands touch [1].

In two dimensions, bands can touch at isolated points or lines. Band touchings can be essential [2,3] or accidental [4]. The former are induced by the crystal and time-reversal symmetry (TRS), they are pinned to a high-symmetry point (HSP) or line (HSL), and they remain intact by symmetry-preserving perturbations. Accidental band contacts change their position in the BZ by perturbations that keep the symmetry, they cannot be removed if protected by topology, and can be removed in the opposite case (truly accidental band contacts). So far, the existence of such movable but unavoidable nodal points (MNPs) and lines (MNLs) has been almost exclusively linked to non-symmorphic symmetries of a crystal [5–9]. We show below that MNLs exist in some symmorphic groups too.

Nodal lines are further classified according to dispersion in the directions perpendicular to the line. For higher-order nodal lines, the splitting is of order higher than one. In 3D non-magnetic materials with spin–orbit coupling (SOC) such nodal lines are of order two and three [10]. Weyl (WNLs) and Dirac nodal lines (DNLs) have linear splitting, with twofold and fourfold degeneracy on the line, respectively. The existence of WNLs or DNLs in bulk band structure leads to interesting physical properties, such as *drumhead* edge states, which are nearly dispersionless

and hence exhibit strong electron correlations [11,12]. The existence of nodal lines in three dimensions is connected with a particular symmetry element [13–18], and can also be analyzed by the use of point groups [19], all 230 space groups [20], and 3D magnetic groups [21]. These publications are augmented with exhaustive tables of all possible quasiparticles in 3D magnetic and non-magnetic crystals [22–26].

In two dimensions, WNLs are predicted in the GaTeI family [27] and in ferromagnetic layers [28–30]. For determination of the properties of 2D materials using symmetry, characters or irreducible (co)representations of layer groups are necessary. Those are tabulated for double layer little groups [31], for generators of single layer groups [32], and for maximal symmetry of hexagonal materials [33]. Recently, a full tabulation of layer groups, single and double, gray and ordinary, has been published [34]. We used Ref. [34] together with tables for (3D) space groups from the Bilbao Crystallographic Server [35,36] as a starting point for our research.

Here we present all MNLs that pass through HSPs in layer groups with TRS, with and without SOC. We show that these MNLs are unavoidable for crystals belonging to eight layer groups (describing systems without SOC) and six double layer groups (for crystals with SOC). We give dispersions and effective Hamiltonians near the mentioned HSPs and illustrate our theory with a few examples. An interesting curiosity are three symmorphic layer groups that support MNLs when SOC is included. Finally, we compare our results with those published in the literature on related topics.

2. Method

With $\mathbf{k}_0$ being a BZ point (an HSP), $\mathbf{q}$ a small wave vector, R the allowed irreducible (co)representation of the little group $G_{\mathbf{k}_0}$ of $\mathbf{k}_0$, and $g = \left\{\widehat{h}\middle|\ \tau_{\widehat{h}}\right\}$ an element (in Seitz notation) of $G_{\mathbf{k}_0}$, the following formula holds [37]:

$$\widehat{H}\left(\mathbf{k}_0+\mathbf{q}\right) = \widehat{R}^{\dagger}\left(g\right)\widehat{H}\left(\mathbf{k}_0+\widehat{h}'\mathbf{q}\right)\widehat{R}\left(g\right), \tag{1a}$$

where $\widehat{h}'$ is the operator reduction of $\widehat{h}$ to 2D BZ. If, in addition, $-\mathbf{k}_0$ belongs to the star of $\mathbf{k}_0$, then TRS (denoted by θ) gives:

$$\widehat{H}'^{*}\left(\mathbf{q}\right) = \widehat{R}^{\dagger}\left(\theta g_s\right)\widehat{H}'\left(-\widehat{h}'_s\mathbf{q}\right)\widehat{R}\left(\theta g_s\right), \tag{1b}$$

where $\widehat{H}'(\mathbf{q}) = \widehat{H}(\mathbf{k}_0+\mathbf{q}) - \widehat{H}(\mathbf{k}_0)$, $g_s = \left\{\widehat{h}_s\middle|\ \tau_{\widehat{h}_s}\right\}$ and $\widehat{h}_s\mathbf{k}_0$ differs from $-\mathbf{k}_0$ by a reciprocal lattice vector. By differentiating these relations with respect to $\mathbf{q}$ at $\mathbf{q}=0$ once, twice, etc., we obtain relations between Hamiltonian derivatives and derive dispersions in the vicinity of the HSP. We have considered Hamiltonians including the second (third) order for the case without (with) SOC. We obtained groups and HSPs that are not located at HSLs and that have line-like solutions for vanishing splitting terms. In all such cases, two-component Hamiltonians contain only one Pauli matrix (in addition to the unit matrix), which we choose to be $\widehat{\sigma}_1$. Since the nth-order Hamiltonian derivatives transform as $[\Gamma_{\mathrm{2DPV}}^{\otimes n}] \otimes R^* \otimes R$, and since, in all cases of interest (except for the double group 74^D at the BZ center), $\Gamma_{\mathrm{2DPV}}^{\otimes 3} = 4\Gamma_{\mathrm{2DPV}}$ (or $\Gamma_{\mathrm{2DPV}}^{\otimes 3} = 2\Gamma_1 + 3\Gamma_{\mathrm{2DPV}}$, for 74^D at the BZ center), we can exclude the possibility that some higher-order derivatives couple with any other Pauli matrix, except the ones already contained in the linear or quadratic (linear, quadratic, or cubic for 74^D at the BZ center) terms in the Taylor expansion of the Hamiltonian, which would cause energy splitting. Γ_{2DPV} denotes the 2D polar-vector representation that acts in 2D reciprocal space and Γ_1 is the unit representation, while $[\Gamma_{\mathrm{2DPV}}^{\otimes n}]$ is the symmetrized nth power of Γ_{2DPV}. It turns out that the four-component Hamiltonians

that do not correspond to the fortune-teller (FT) dispersion [38,39] do not support MNLs. Since gray single and double layer groups have little group corepresentations of dimensions two and four (besides 1D), our method exhausts all possibilities.

We now prove that, if an MNL exists in the vicinity of an HSP, it must continue further. With $\mathbf{k}_0$ now being the touching point of two bands located near an HSP, its little group contains only the horizontal reflection plane as a non-trivial element. Both bands can be approximated by $E_1 = p_1q_1 + p_2q_2$ and $E_2 = c_1q_1 + c_2q_2$ respectively, so that $p_1 \neq c_1$ and $p_2 \neq c_2$ (at $\mathbf{q} = 0$ two bands touch by the initial assumption; $\mathbf{k}_0$ is now not an HSP but lies close to it). Now $E_1 = E_2$ has the solution $q_2 = q_1(p_1 - c_1)/(c_2 - p_2)$, which means that the line continues. We can repeat the same reasoning for another point close to $\mathbf{k}_0$ and so on. In other words, MNLs cannot be interrupted.

Finally, guided by the result described in the previous paragraph, we have included groups that host FT states described in Refs. [38] and [39] for non-SOC and SOC cases, respectively, and that are also experimentally observed [40]. Among the conclusions of the previous paragraph is that FT states cannot be the only features at the Fermi level. This holds no matter if the Chern number of FT states is integer or not.

3. Results

In what follows, c denotes a real parameter, while q_1 and q_2 are projections of $\mathbf{q}$ to orthonormal basis vectors $\mathbf{e}_1$ and $\mathbf{e}_2$, respectively. The orientation of the basis vectors is arbitrary since no little group of HSPs in question contains a horizontal rotation axis or vertical reflection plane, except for groups hosting FT dispersion. However, depending on the parameters of the model, sometimes it is more convenient to switch to another orthonormal basis $\mathbf{e}'_1$, $\mathbf{e}'_2$, which will be defined below. In these cases, projections of $\mathbf{q}$ to this new basis are denoted by q'_1 and q'_2. Finally, $V^{(2)}_{l,m}$ ($V^{(3)}_{l,m,n}$) are the second- (third-)order derivatives of certain components of the Hamiltonian. These are real parameters, symmetric under any permutation of indices, but with no additional symmetry. The superscript D denotes a double group, which is the symmetry of the system with SOC.

Groups and HSPs hosting MNLs when SOC is neglected are shown in Table 1, those with SOC in Table 2. For groups 5, 7, 36, 48, 52 (points $(0, \pm 1/2)$, $(\pm 1/2, 0)$), 4^D, 5^D, 35^D, and 74^D (points $(0, \pm 1/2)$, $(\pm 1/2, 0)$, $\pm(1/2, 1/2)$), the Hamiltonian and dispersion are:

$$\widehat{H} = \left(E_0 + \sum_{l,m=1}^{2} V^{(2)}_{l,m} q_l q_m\right)\widehat{\sigma}_0 + \left(c_1q_1 + c_2q_2 + \sum_{l,m,n=1}^{2} V^{(3)}_{l,m,n} q_l q_m q_n\right)\widehat{\sigma}_1, \tag{2a}$$

$$E_{1,2} = E_0 + \sum_{l,m=1}^{2} V^{(2)}_{l,m} q_l q_m \pm \left|c_1q_1 + c_2q_2 + \sum_{l,m,n=1}^{2} V^{(3)}_{l,m,n} q_l q_m q_n\right|. \tag{2b}$$

For the new basis given by:

$$\mathbf{e}'_1 = \frac{c_1\mathbf{e}_1 + c_2\mathbf{e}_2}{\sqrt{c_1^2 + c_2^2}},$$

$$\mathbf{e}'_2 = \frac{-c_2\mathbf{e}_1 + c_1\mathbf{e}_2}{\sqrt{c_1^2 + c_2^2}}, \tag{2c}$$

the Hamiltonian and dispersion are:

Table 1. Single layer groups hosting unavoidable accidental nodal lines through HSPs. The notation for the layer and space groups as well as the primitive basis vectors is according to Refs. [42] and [43], respectively. The coordinates of the HSPs in the last column are in the primitive basis $\{\mathbf{b}_1, \mathbf{b}_2\}$ of the reciprocal 2D lattice.

Single layer group		Corresponding space group			Diperiodic plane	HSP
5	$p\,1\,1\,b$	7	$P\,1\,c\,1$	C_s^2	$y=0$	$(0,\pm\frac{1}{2})$
						$(\pm\frac{1}{2},\pm\frac{1}{2})$
7	$p\,1\,1\,2/b$	13	$P\,1\,2/c\,1$	C_{2h}^4	$y=0$	$(0,\pm\frac{1}{2})$
						$(\pm\frac{1}{2},\pm\frac{1}{2})$
33	$p\,b\,2_1\,a$	29	$P\,c\,a\,2_1$	C_{2v}^5	$y=0$	$(\pm\frac{1}{2},\pm\frac{1}{2})$
36	$c\,m\,2\,e$	39	$A\,e\,m\,2$	C_{2v}^{15}	$x=0$	$(0,\pm\frac{1}{2})$
						$(\pm\frac{1}{2},0)$
43	$p\,2/b\,2_1/a\,2/a$	54	$P\,2_1/c\,2/c\,2/a$	D_{2h}^8	$y=0$	$(\pm\frac{1}{2},\pm\frac{1}{2})$
45	$p\,2_1/b\,2_1/m\,2/a$	57	$P\,2/b\,2_1/c\,2_1/m$	D_{2h}^{11}	$x=0$	$(\pm\frac{1}{2},\pm\frac{1}{2})$
48	$c\,2/m\,2/m\,2/e$	67	$C\,2/m\,2/m\,2/e$	D_{2h}^{21}	$z=0$	$(0,\pm\frac{1}{2})$
						$(\pm\frac{1}{2},0)$
52	$p\,4/n$	85	$P\,4/n$	C_{4h}^3	$z=0$	$(0,\pm\frac{1}{2})$
						$(\pm\frac{1}{2},0)$
						$(\pm\frac{1}{2},\pm\frac{1}{2})$

Table 2. Double layer groups hosting unavoidable accidental nodal lines through HSPs. The notation for the layer and space groups as well as the primitive basis vectors is according to Refs. [42] and [43], respectively. The coordinates of the HSPs in the last column are in the primitive basis $\{\mathbf{b}_1, \mathbf{b}_2\}$ of the reciprocal 2D lattice.

Double layer group		Corresponding double space group			Diperiodic plane	HSP
4^D	$p\,1\,1\,m$	6^D	$P\,1\,m\,1$	C_s^1	$y=0$	$(0,0)$
						$(\pm\frac{1}{2},0)$
						$(0,\pm\frac{1}{2})$
						$(\pm\frac{1}{2},\pm\frac{1}{2})$
5^D	$p\,1\,1\,b$	7^D	$P\,1\,c\,1$	C_s^2	$y=0$	$(0,0)$
						$(\pm\frac{1}{2},0)$
29^D	$p\,b\,2_1\,m$	26^D	$P\,m\,c\,2_1$	C_{2v}^2	$x=0$	$(0,\pm\frac{1}{2})$
						$(\pm\frac{1}{2},\pm\frac{1}{2})$
33^D	$p\,b\,2_1\,a$	29^D	$P\,c\,a\,2_1$	C_{2v}^5	$y=0$	$(0,\pm\frac{1}{2})$
35^D	$c\,m\,2\,m$	38^D	$A\,m\,m\,2$	C_{2v}^{14}	$x=0$	$(0,\pm\frac{1}{2})$
						$(\pm\frac{1}{2},0)$
74^D	$p\,\bar{6}$	174^D	$P\,\bar{6}$	C_{3h}^1	$z=0$	$(0,0)$
						$(\pm\frac{1}{2},0)$
						$(0,\pm\frac{1}{2})$
						$\pm(\frac{1}{2},\frac{1}{2})$

$$\widehat{H} = \left(E_0 + \sum_{l,m=1}^{2} V'^{(2)}_{l,m} q'_l q'_m\right)\widehat{\sigma}_0 + \sqrt{c_1^2 + c_2^2}\left(q'_1 + c_0 q'^3_2\right)\widehat{\sigma}_1, \tag{2d}$$

$$E_{1,2} = E_0 + \sum_{l,m=1}^{2} V'^{(2)}_{l,m} q'_l q'_m \pm \sqrt{c_1^2 + c_2^2}\left|q'_1 + c_0 q'^3_2\right|, \tag{2e}$$

with $c_0 = (c_1^3 V^{(3)}_{222} - 3c_1^2 c_2 V^{(3)}_{122} + 3c_1 c_2^2 V^{(3)}_{112} - c_2^3 V^{(3)}_{111})/(c_1^2 + c_2^2)^2$. Since $q'_1 + c_0 q'^3_2 = 0$ has one solution, one MNL passes through $\mathbf{q} = 0$. In Eqs. (2d) and (2e), we neglect energy splitting terms that contain products of q'_1 with q'_2, in comparison to q'_1. Such HSPs were mentioned in Ref. [41] as having linearity rank equal to one.

For group 52 near BZ corners, the following relations hold:

$$\widehat{H} = \left(E_0 + c\mathbf{q}^2\right)\widehat{\sigma}_0 + \left(c_1 q_1^2 + c_2 q_1 q_2 - c_1 q_2^2\right)\widehat{\sigma}_1, \tag{3a}$$

$$E_{1,2} = E_0 + c\mathbf{q}^2 \pm \left|c_1 q_1^2 + c_2 q_1 q_2 - c_1 q_2^2\right|. \tag{3b}$$

In the new basis,

$$\begin{aligned} \mathbf{e}'_1 &= \frac{\mathbf{e}_1 + \lambda \mathbf{e}_2}{\sqrt{1+\lambda^2}}, \\ \mathbf{e}'_2 &= \frac{-\lambda \mathbf{e}_1 + \mathbf{e}_2}{\sqrt{1+\lambda^2}}, \end{aligned} \tag{3c}$$

where $\lambda = (c_2 + \sqrt{c_2^2 + 4c_1^2})/(2c_1)$, the following holds:

$$\widehat{H} = \left(E_0 + c\mathbf{q}'^2\right)\widehat{\sigma}_0 - \sqrt{c_2^2 + 4c_1^2}\, q'_1 q'_2 \widehat{\sigma}_1, \tag{3d}$$

$$E_{1,2} = E_0 + c\mathbf{q}'^2 \pm \sqrt{c_2^2 + 4c_1^2}\left|q'_1 q'_2\right|. \tag{3e}$$

Since $q'_1 q'_2 = 0$ has two solutions, two MNLs intersect at a right angle for $\mathbf{q} = 0$.

For group 74^D near the BZ center ($\mathbf{k}_0 = 0$) the Hamiltonian and energies are:

$$\widehat{H} = \left(E_0 + c\mathbf{q}^2\right)\widehat{\sigma}_0 + \left(c_1 q_1\left(q_1^2 - 3q_2^2\right) + c_2 q_2\left(q_2^2 - 3q_1^2\right)\right)\widehat{\sigma}_1, \tag{4a}$$

$$E_{1,2} = E_0 + c\mathbf{q}^2 \pm \left|c_1 q_1\left(q_1^2 - 3q_2^2\right) + c_2 q_2\left(q_2^2 - 3q_1^2\right)\right|. \tag{4b}$$

The new basis is given by:

$$\begin{aligned} \mathbf{e}'_1 &= \frac{c_2 \mathbf{e}_1 + c_1 B \mathbf{e}_2}{\sqrt{c_2^2 + c_1^2 B^2}}, \\ \mathbf{e}'_2 &= \frac{-c_1 B \mathbf{e}_1 + c_2 \mathbf{e}_2}{\sqrt{c_2^2 + c_1^2 B^2}}, \end{aligned} \tag{4c}$$

where $B = 1 + 2\sqrt{1 + c_2^2/c_1^2}\cos[(1/3)\arccos(1/\sqrt{1 + c_2^2/c_1^2})]$ is a real solution of the cubic equation $(c_1/c_2)^2 B^3 - 3(c_1/c_2)^2 B^2 - 3B + 1 = 0$. In the new basis the Hamiltonian and dispersion are:

$$\widehat{H} = \left(E_0 + c\mathbf{q}'^2\right)\widehat{\sigma}_0 - \frac{c_1^2(B^2 - 2B) - c_2^2}{\sqrt{c_2^2 + c_1^2 B^2}} q'_2\left(q'^2_2 - 3q'^2_1\right)\widehat{\sigma}_1, \tag{4d}$$

$$E_{1,2} = E_0 + c\mathbf{q}'^2 \pm \frac{c_1^2(B^2 - 2B) - c_2^2}{\sqrt{c_2^2 + c_1^2 B^2}}\left|q'_2\left(q'^2_2 - 3q'^2_1\right)\right|. \tag{4e}$$

Here we note that $c_1^2(B^2 - 2B) - c_2^2 > 0$. Since $q'_2(q'^2_2 - 3q'^2_1) = 0$ has three solutions, three MNLs intersect at $\mathbf{q} = 0$ at angles of $\pi/3$.

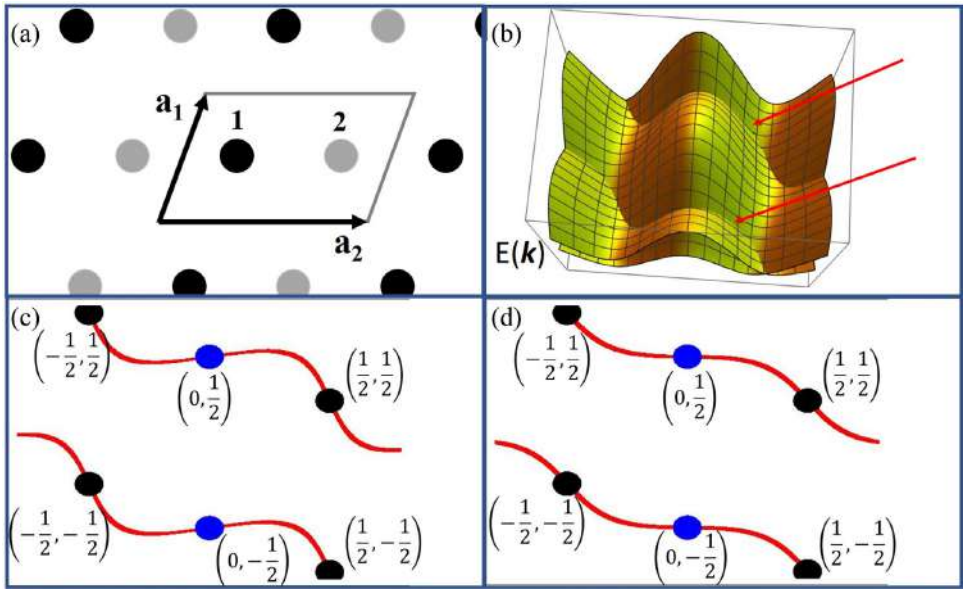

Fig. 1. Tight-binding model for $p112/b$: (a) crystal structure (all nuclei are of the same type; black and gray circles denote nuclei above and below the drawing plane, respectively; visualization by VESTA [44]); (b) electronic band structure for f_0, f_1, f_2, and f_3 equal to 4.2, 1.3, 0.9, and 0.5 in arbitrary units (a.u.), respectively (red arrows denote MNLs); (c) position of MNLs in the reciprocal space, (d) same as (c) for f_0, f_1, f_2, and f_3 equal to 3.6, 3.1, 2.7, and 0.9 a.u., respectively. In (c) and (d) numbers in brackets denote coordinates of special points in the reciprocal basis (blue and black circles). Mutually equivalent points are denoted by circles of the same color.

Groups 33, 43, 45, 29^D, and 33^D host fortune-teller (FT) dispersion, which is described in more detail in Refs. [38,39]. Here we only give the dispersion:

$$E_{j,l} = j|c_1|q_1| + lc_2|q_2||, (j, l \in \{+, -\}), \tag{5}$$

where c_1 and c_2 are (only in this equation) positive quantities. The bands are ordered in the following way: $E_{-,+} \leq E_{-,-} \leq E_{+,-} \leq E_{+,+}$. It follows that MNLs $E_{-,-} = E_{+,-}$ are given by $c_1q_1 = c_2q_2$ and $c_1q_1 = -c_2q_2$. Two MNLs intersect at $\mathbf{q} = 0$ at an angle that depends on c_1 and c_2. Those MNLs arising from FT dispersion are at constant energy only in the linear approximation. When quadratic corrections to the Hamiltonian are accounted for, the MNLs remain unsplit, but the overall energy shift is quadratic in $q_{||}$ (the wave vector along the MNL).

4. Illustrative examples

We first consider the tight-binding model composed of the s-orbitals, without SOC, on the structure shown in Fig. 1(a), which belongs to layer group $p112/b$(No. 7). The occupied Wyckoff position is $2d$ with $z = 1.3$ Å. The Hamiltonian and its eigenvalues are:

$$\widehat{H}(\mathbf{k}) = \begin{pmatrix} f_0 + 2f_1\cos(\mathbf{k}\cdot\mathbf{a}_1) & 2e^{-\frac{i}{2}\mathbf{k}\cdot\mathbf{a}_2}\left(f_2\cos\left(\frac{1}{2}\mathbf{k}\cdot\mathbf{a}_2\right)\right. \\ & \left. +f_3\cos\left(\mathbf{k}\cdot\mathbf{a}_1 - \frac{1}{2}\mathbf{k}\cdot\mathbf{a}_2\right)\right) \\ 2e^{\frac{i}{2}\mathbf{k}\cdot\mathbf{a}_2}\left(f_2\cos\left(\frac{1}{2}\mathbf{k}\cdot\mathbf{a}_2\right)\right. & \\ \left. +f_3\cos\left(\mathbf{k}\cdot\mathbf{a}_1 - \frac{1}{2}\mathbf{k}\cdot\mathbf{a}_2\right)\right) & f_0 + 2f_1\cos(\mathbf{k}\cdot\mathbf{a}_1) \end{pmatrix}, \tag{6a}$$

$$E_{1,2}(\mathbf{k}) = f_0 + 2f_1\cos(\mathbf{k}\cdot\mathbf{a}_1) \pm 2\left|f_2\cos\left(\frac{1}{2}\mathbf{k}\cdot\mathbf{a}_2\right) + f_3\cos\left(\mathbf{k}\cdot\mathbf{a}_1 - \frac{1}{2}\mathbf{k}\cdot\mathbf{a}_2\right)\right|. \tag{6b}$$

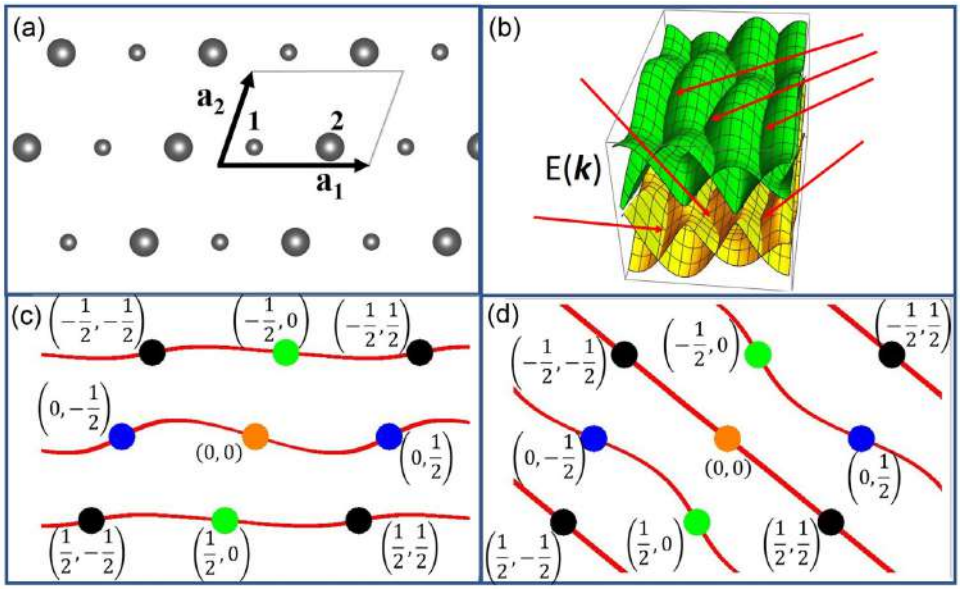

Fig. 2. Tight-binding model for symmorphic $p11m$: (a) crystal structure (nuclei of both types are located on one plane; visualization by VESTA [44]); (b) electronic band structure for f_0, f_1, z_1, z_2, and z_3 equal to 2, 3, $4+2i$, $3-6i$, and $1+2i$ a.u., respectively (red arrows denote MNLs); (c) position of MNLs in the reciprocal space; (d) same as (c) for f_0, f_1, z_1, z_2, and z_3 equal to 4.2, 1.3, $-2.4+1.2i$, $3.4-5.6i$, and $6.1+1.2i$ a.u., respectively. In (c) and (d) numbers in brackets denote coordinates of special points in the reciprocal basis (blue, orange, green, and black circles). Mutually equivalent points are denoted by circles of the same color.

Here f_0, f_1, f_2, and f_3 are real hopping parameters for the zeroth, first, second, and third neighbors, respectively. The two energies coincide for:

$$\mathbf{k}\cdot\mathbf{a}_2 \in \left\{-2\arctan\left(\frac{f_2+f_3\cos(\mathbf{k}\cdot\mathbf{a}_1)}{f_3\sin(\mathbf{k}\cdot\mathbf{a}_1)}\right)+2m\pi\right\}, \tag{6c}$$

where m is any integer. Equation (6c) is well defined for all possible values of hopping parameters. The full band structure for particular values of parameters is shown in Fig. 1(b), where band touching lines are clearly visible. The positions of the lines in the reciprocal space are shown in Fig. 1(c). By varying the parameters, the shape of the lines changes, but the lines always pass through points (0, 1/2) and (1/2, 1/2), and through ones equivalent to them, as shown in Table 1 and Figs. 1(c), (d).

We next consider the tight-binding model on the structure shown in Fig. 2(a), which belongs to the symmorphic (double) layer group $p11m$ (4^D). We choose basis functions $|s_1\uparrow\rangle$, $|s_1\downarrow\rangle$, $|s_2\uparrow\rangle$, $|s_2\downarrow\rangle$, where s_1, s_2 are s-orbitals for atoms 1 and 2, respectively, while $\uparrow$ and $\downarrow$ denote spinors for up and down spins, respectively. Since the horizontal reflection plane is the symmetry of the system, the *up* and *down* states are decoupled from each other, so that the Hamiltonian is block-diagonal:

$$\widehat{H} = \begin{pmatrix} \widehat{H}_\uparrow & \widehat{0} \\ \widehat{0} & \widehat{H}_\downarrow \end{pmatrix}, \tag{7a}$$

with

$$\widehat{H}_\uparrow(\mathbf{k}) = \widehat{H}^*_\downarrow(-\mathbf{k}) = \begin{pmatrix} f_0 & z_1 e^{-i\mathbf{k}\cdot\mathbf{a}_1} + z_2 + z_3 e^{i\mathbf{k}\cdot(\mathbf{a}_2-\mathbf{a}_1)} \\ z_1^* e^{i\mathbf{k}\cdot\mathbf{a}_1} + z_2^* + z_3^* e^{-i\mathbf{k}\cdot(\mathbf{a}_2-\mathbf{a}_1)} & g_0 \end{pmatrix}. \tag{7b}$$

Here f_0 and g_0 are real, on-site hopping parameters for sites 1 and 2, respectively, while z_1, z_2, and z_3 are complex hopping parameters for the first, second, and third neighbors, respectively. The full band structure is:

$$E_2^{\uparrow,\downarrow}(\mathbf{k}) = \frac{f_0+g_0}{2} + \frac{1}{2}\sqrt{(f_0-g_0)^2 + 4|z_1 e^{\mp i\mathbf{k}\cdot\mathbf{a}_1} + z_2 + z_3 e^{\pm i\mathbf{k}\cdot(\mathbf{a}_2-\mathbf{a}_1)}|^2}, \tag{7c}$$

$$E_1^{\uparrow,\downarrow}(\mathbf{k}) = \frac{f_0+g_0}{2} - \frac{1}{2}\sqrt{(f_0-g_0)^2 + 4|z_1 e^{\mp i\mathbf{k}\cdot\mathbf{a}_1} + z_2 + z_3 e^{\pm i\mathbf{k}\cdot(\mathbf{a}_2-\mathbf{a}_1)}|^2}. \tag{7d}$$

Both nodal lines $E_1^{\uparrow} = E_1^{\downarrow}$ and $E_2^{\uparrow} = E_2^{\downarrow}$ are given by:

$$h_3 \sin(\mathbf{k}\cdot\mathbf{a}_1) + h_2 \sin(\mathbf{k}\cdot\mathbf{a}_2) + h_1 \sin[\mathbf{k}\cdot(\mathbf{a}_2-\mathbf{a}_1)] = 0, \tag{7e}$$

where $h_1 = -i(z_2^* z_3 - z_2 z_3^*)$, $h_2 = -i(z_1^* z_3 - z_1 z_3^*)$ and $h_3 = -i(z_1^* z_2 - z_1 z_2^*)$ are real parameters. Equation (7e) has the following solution:

$$\mathbf{k}\cdot\mathbf{a}_2 \in \left\{\Phi - \arcsin\left(\frac{h_3}{h_1}\sin\Phi\right) + 2m\pi\,,\ \Phi + \arcsin\left(\frac{h_3}{h_1} sin\Phi\right) + (2m+1)\pi\right\}, \tag{7f}$$

with m being any integer and

$$\sin(\Phi) = \frac{h_1 \sin(\mathbf{k}\cdot\mathbf{a}_1)/h_3}{\sqrt{\left(h_1^2+h_2^2\right)/h_3^2 + 2h_1h_2\cos(\mathbf{k}\cdot\mathbf{a}_1)/h_3^2}}, \tag{7g}$$

$$\cos(\Phi) = \frac{h_1 \cos(\mathbf{k}\cdot\mathbf{a}_1)/h_3 + h_2/h_3}{\sqrt{\left(h_1^2+h_2^2\right)/h_3^2 + 2h_1h_2\cos(\mathbf{k}\cdot\mathbf{a}_1)/h_3^2}}. \tag{7h}$$

The argument of arcsin in Eq. (7f) has modulus less or equal to one except if $(h_1/h_3)^2$ and $(h_2/h_3)^2$ are both less than one. In that case, $-1 \le \cos(\mathbf{k}\cdot\mathbf{a}_1) \le t_2$ or $t_1 \le \cos(\mathbf{k}\cdot\mathbf{a}_1) \le 1$ must hold ($t_{1,2} = -h_1h_2/h_3^2 \pm \sqrt{(1-h_1^2/h_3^2)(1-h_2^2/h_3^2)}$). The band structure shown in Fig. 2(b) for particular values of parameters confirms the existence of MNLs. In this case h_1^2 and h_2^2 are both less than h_3^2, while in the case shown in Fig. 2(d) this does not hold, with a clear difference in the accidental degeneracy pattern. In any case, MNLs pass through HSPs as shown in Table 2 and in Figs. 2(c), (d).

5. Discussion and conclusions

We compare our results with those on related topics published in the literature. Analysis of all 3D crystallographic double point groups, for systems with SOC, that shows in which cases movable or unmovable nodal lines exist has been reported [45]. These results can be used for symmorphic little groups, since allowed representations are then just a product of point group irreducible representations with the phase factors that represent translations. Point groups $\underline{C}_s^D$ and $\underline{C}_{3h}^D$ hosts one and three MNLs, respectively [45]. This is in accordance with our results in Table 2 (the little group for 74^D in the BZ center is $\underline{C}_{3h}^D$; for the remaining symmorphic groups it is $\underline{C}_s^D$). On the other hand, the HSPs for non-symmorphic 29^D and 33^D from Table 2 host two intersecting MNLs, while Ref. [45] predicts one nodal line along the axis of order two for $\underline{C}_{2v}^D$. This difference is because 29^D and 33^D are non-symmorphic and because band degeneracy at HSPs hosting FT states is four, while Ref. [45] considers two-band models.

The origin of doubly degenerate nodal lines that connect time-reversal invariant momenta in 3D crystals with SOC is reported in Ref. [46]. The list of symmorphic 3D space groups that host such lines [46] contains all corresponding symmorphic space groups in Table 2, which supports our findings. Compound $PbTaSe_2$ is a symmorphic 3D metal with SOC that exhibits nodal lines in experiments [47], as predicted in Ref. [46]. To avoid Kramer's degeneracy in the whole BZ,

the authors of Ref. [46] considered non-centrosymmetric 3D crystals. They show that a nodal line through an HSP exists if its little groups have at least one improper rotation (symmetry element with determinant -1). In our cases this is always fulfilled, since at least the horizontal plane must be present in order to avoid band repulsion due to the non-crossing rule.

To illustrate their own results, the authors of Ref. [48] used a tight-binding model with SOC on a structure that belongs to group 74^D ($p\bar{6}$). Three nodal lines intersect symmetrically at the BZ center and also pass through the middle of the BZ edges, thus confirming our prediction. Numerical calculations [49] suggest that a boron bilayer adopts a structure with the symmetry $p\bar{6}$. Since boron is a light element, the reported band structure lacks SOC [49]. Future research could show whether it is possible to enhance SOC using bilayered boron as a starting material.

Group theoretical conditions for semi-Dirac dispersion in non-magnetic 2D materials with negligible SOC are reported [50]. All groups and HSPs from Ref. [50] are here included in Table 1. The tight-binding model for group $c\,2/m\,2/m\,2/e$ gives a line of degeneracy that depends on the numerical values of the tight-binding parameters [50]; hence it is an MNL as predicted here. Moreover, the dispersion near the (0, 1/2) point in Ref. [50] matches that for group $c\,2/m\,2/m\,2/e$ given here in Eq. (2e). Similarly, the tight-binding model for group $p\,1\,1\,b$, published in Ref. [51], exhibits MNLs across the whole BZ with the same dispersion near the HSPs indicated in Table 1. Lines of accidental degeneracy, noticed in Ref. [51], have gained a full explanation in the present work. Group $c\,m\,2\,e$ is omitted in Ref. [50], due to a bug in the REPRES program on the Bilbao Crystallographic Server, which was fixed recently. According to Ref. [50], the authors used REPRES [35] for finding allowed representations of layer groups via their corresponding space groups. Finally, one can point out that groups from Ref. [50] give semi-Dirac dispersion (quadratic in one direction of the BZ that splits linearly in the perpendicular direction) while the bands do not form cones. The formation of semi-Dirac cones requires a Hamiltonian of the form $c_1 q_1 \widehat{\sigma}_j + c_2 q_2^2 \widehat{\sigma}_l$ (or, in the more general case, $c_1 q_1 \widehat{\sigma}_j + c_2 q_2^n \widehat{\sigma}_l$), with two different Pauli matrices ($j \neq l$) and with n-natural number greater than one. We have omitted the term with the unit matrix $\widehat{\sigma}_0$, since it does not lead to band splitting. In this case the band splitting is $\pm\sqrt{c_1^2 q_1^2 + c_2^2 q_2^4}$ (in the more general case it is $\pm\sqrt{c_1^2 q_1^2 + c_2^2 q_2^{2n}}$), with $\mathbf{q} = 0$ as the only touching point. Detailed analysis of all HSPs of all gray single or double layer groups does not give any HSPs with semi-Dirac cones [41].

In summary, we have determined all layer groups that host nodal lines through high-symmetry BZ points, and whose shapes depend on the model parameters (MNLs). In our analysis we have included both cases without and with SOC in the presence of TRS. Although we did not restrict our search to Weyl or Dirac nodal lines only, it turns out that all the MNLs that we found are either DNLs (in cases without SOC) or WNLs (in cases with SOC). Since little group representations responsible for MNLs are the only allowed ones in listed HSPs, the existence of MNLs is guaranteed by the layer groups from Tables 1 and 2. On the other hand, it is not guaranteed that MNLs are at constant energy, nor that they lie close to the Fermi level, although such cases are not necessarily excluded. Our finding extends the knowledge of band degeneracies in 2D materials and might be useful for designing 2D materials whose sensitivity to external conditions like temperature, pressure, strain, etc. is yet to be studied.

Acknowledgements

The author acknowledges funding from the Ministry of Science, Technological Development and Innovation of the Republic of Serbia provided by the Institute of Physics Belgrade, University of Belgrade.

References

[1] X. Feng, J. Zhu, W. Wu, and S. A. Yang, Chin. Phys. B **30**, 107304 (2021).
[2] L. P. Bouckaert, R. Smoluchowski, and E. Wigner, Phys. Rev. **50**, 58 (1936).
[3] C. Herring, Phys. Rev. **52**, 361 (1937).
[4] C. Herring, Phys. Rev. **52**, 365 (1937).
[5] S. M. Young and C. L. Kane, Phys. Rev. Lett. **115**, 126803 (2015).
[6] B. J. Wieder and C. L. Kane, Phys. Rev. B **94**, 155108 (2016).
[7] J. Zhang, Y.-H. Chan, C.-K. Chiu, M. G. Vergniory, L. M. Schoop, and A. P. Schnyder, Phys. Rev. Mater. **2**, 074201 (2018).
[8] M. M. Hirschmann, A. Leonhardt, B. Kilic, D. H. Fabini, and A. P. Schnyder, Phys. Rev. Mater. **5**, 054202 (2021).
[9] A. Leonhardt, M. M. Hirschmann, N. Heinsdorf, X. Wu, D. H. Fabini, and A. P. Schnyder, Phys. Rev. Mater. **5**, 124202 (2021).
[10] Z.-M. Yu, W. Wu, X.-L. Sheng, Y. X. Zhao, and S. A. Yang, Phys. Rev. B **99**, 121106 (2019).
[11] C. Fang, H. Weng, X. Dai, and Z. Fang, Chin. Phys. B **25**, 117106 (2016).
[12] S.-Y. Yang, H. Yang, E. Derunova, S. S. P. Parkin, B. Yan, and M. N. Ali, Adv. Phys. X **3**, 1414631 (2018).
[13] C. Fang, Y. Chen, H.-Y. Kee, and L. Fu, Phys. Rev. B **92**, 081201 (2015).
[14] Y. Kim, B. J. Wieder, C. L. Kane, and A. M. Rappe, Phys. Rev. Lett. **115**, 036806 (2015).
[15] Z. Gao, M. Hua, H. Zhang, and X. Zhang, Phys. Rev. B **93**, 205109 (2016).
[16] B.-J. Yang, T. A. Bojesen, T. Morimoto, and A. Furusaki, Phys. Rev. B **95**, 075135 (2017).
[17] Z. Song, T. Zhang, and C. Fang, Phys. Rev. X **8**, 031069 (2018).
[18] H. Li, C. Fang, and K. Sun, Phys. Rev. B **100**, 195308 (2019).
[19] S. Kobayashi, Y. Yamakawa, A. Yamakage, T. Inohara, Y. Okamoto, and Y. Tanaka, Phys. Rev. B **95**, 245208 (2017).
[20] L. Wu, F. Tang, and X. Wan, Phys. Rev. B **104**, 045107 (2021).
[21] J. Yang, C. Fang, and Z.-X. Liu, Phys. Rev. B **103**, 245141 (2021).
[22] F. Tang and X. Wan, Phys. Rev. B **104**, 085137 (2021).
[23] Z.-M. Yu, Z. Zhang, G.-B. Liu, W. Wu, X.-P. Li, R.-W. Zhang, S. A. Yang, and Y. Yao, Sci. Bull. **67**, 375 (2022).
[24] G.-B. Liu, Z. Zhang, Z.-M. Yu, S. A. Yang, and Y. Yao, Phys. Rev. B **105**, 085117 (2022).
[25] Z. Zhang, G.-B. Liu, Z.-M. Yu, S. A. Yang, and Y. Yao, Phys. Rev. B **105**, 104426 (2022).
[26] F. Tang and X. Wan, Phys. Rev. B **105**, 155156 (2022).
[27] W. Wu, Y. Jiao, S. Li, X.-L. Sheng, Z.-M. Yu, and S. A. Yang, Phys. Rev. Mater. **3**, 054203 (2019).
[28] B. Feng, R.-W. Zhang, Y. Feng, B. Fu, S. Wu, K. Miyamoto, S. He, L. Chen, K. Wu, K. Shimada, T. Okuda, and Y. Yao, Phys. Rev. Lett. **123**, 116401 (2019).
[29] L. Jin, X. Zhang, T. He, W. Meng, X. Dai, and G. Liu, Appl. Surf. Sci. **520**, 146376 (2020).
[30] F. Zhou, Y. Liu, M. Kuang, P. Wang, J. Wang, T. Yang, X. Wang, Z. Cheng, and G. Zhang, Nanoscale **13**, 8235 (2021).
[31] D. B. Litvin and T. R. Wike, Character Tables and Compatibility Relations of the Eighty Layer Groups and Seventeen Plane Groups (Plenum, New York, 1991).
[32] I. Milosevic, B. Nikolic, M. Damnjanovic, and M. Krcmar, J. Phys. A: Math. Gen. **31**, 3625 (1998).
[33] V. Damljanović, R. Kostić, and R. Gajić, Phys. Scr. **2014**, 014022 (2014).
[34] B. Nikolić, I. Milošević, T. Vuković, N. Lazić, S. Dmitrović, Z. Popović, and M. Damnjanović, Acta Crystallogr. A **78**, 107 (2022). https://onlinelibrary.wiley.com/doi/abs/10.1107/S20532733210 1322X
[35] M. I. Aroyo, A. Kirov, C. Capillas, J. M. Perez-Mato, and H. Wondratschek, Acta Crystallogr. A **62**, 115 (2006).
[36] L. Elcoro, B. Bradlyn, Z. Wang, M. G. Vergniory, J. Cano, C. Felser, B. Andrei Bernevig, D. Orobengoa, G. de la Flor, and M. I. Aroyo, J. Appl. Crystallogr. **50**, 1457 (2017).
[37] J. L. Mañes, Phys. Rev. B **85**, 155118 (2012).
[38] V. Damljanović, I. Popov, and R. Gajić, Nanoscale **9**, 19337 (2017).
[39] V. Damljanović, N. Lazić, A. Šolajić, J. Pešić, B. Nikolić, and M. Damnjanović, J. Phys.: Condens. Matter **32**, 485501 (2020).
[40] M. Kopciuszyński, M. Krawiec, L. Zurawek, and R. Zdyb, Nanoscale Horiz. **5**, 679 (2020).

[41] N. Lazić, V. Damljanović, and M. Damnjanović, J. Phys. A: Math. Theor. **55**, 325202 (2022).
[42] V. Kopsky and D. B. Litvin, International Tables of Crystallography Volume E: Subperiodic Groups (Kluwer, Dordrecht, 2002).
[43] T. Hahn, International Tables of Crystallography Volume A: Space-Group Symmetry (Springer, Berlin, 2005).
[44] K. Momma and F. Izumi, J. Appl. Crystallogr. **44**, 1272 (2011).
[45] A. Knoll and C. Timm, Phys. Rev. B **105**, 115109 (2022).
[46] Y.-M. Xie, X.-J. Gao, X. Y. Xu, C.-P. Zhang, J.-X. Hu, J. Z. Gao, and K. T. Law, Nat. Commun. **12**, 3064 (2021).
[47] G. Bian et al., Nat. Commun. **7**, 10556 (2016).
[48] Z. Zhang, W. Wu, G.-B. Liu, Z.-M. Yu, S. A. Yang, and Y. Yao, Phys. Rev. B **107**, 075405 (2023).
[49] S.-G. Xu, B. Zheng, H. Xu, and X.-B. Yang, J. Phys. Chem. C **123**, 4977 (2019).
[50] V. Damljanović and R. Gajić, J. Phys.: Condens. Matter **29**, 185503 (2017).
[51] V. Damljanović, Opt. Quantum Electron. **50**, 272 (2018).

Nanoscale

PAPER

View Article Online
View Journal | View Issue

Cite this: *Nanoscale*, 2017, **9**, 19337

Fortune teller fermions in two-dimensional materials†

Vladimir Damljanović, *[a] Igor Popov [a,b] and Radoš Gajić[c]

Dirac-like electronic states are the main engines powering tremendous advancements in the research of graphene, topological insulators and other materials with these states. Zero effective mass, high carrier mobility and numerous applications are some consequences of linear dispersion that distinguishes Dirac states. Here we report a new class of linear electronic bands in two-dimensional materials with zero electron effective mass and sharp band edges, and predict stable materials with such electronic structures utilizing symmetry group analysis and an *ab initio* approach. We make a full classification of completely linear bands in two-dimensional materials and find that only two classes exist: Dirac fermions on the one hand and fortune teller-like states on the other hand. The new class supports zero effective mass similar to that of graphene and anisotropic electronic properties like that of phosphorene.

Received 18th October 2017,
Accepted 15th November 2017

DOI: 10.1039/c7nr07763g

rsc.li/nanoscale

1. Introduction

Electrons can move in certain materials as if they have no mass. Massless fermions in solid state materials have played an increasingly important role since the discovery of graphene,[1] a material where zero electron effective mass is caused by linear Dirac-like dispersion. While the first mapping of the electronic structure of graphene to the Dirac equation was an interesting theoretical curiosity,[2] the true significance of the Dirac-like states in solid state systems became apparent upon identification of many physical, measurable consequences of the linear dispersion.[3] For instance, the existence of massless fermions in graphene yields extraordinarily high electron and hole mobilities[4] with revolutionary implications in electronics. Other implications include, and are not limited to, Klein tunneling in single- and bi-layer graphene,[5] and the quantum Hall[6] and fractional quantum Hall[7] effects at room temperature. The two-dimensional (2D) nature of graphene and related materials brings numerous additional advantages including mechanical flexibility, optical transparency,[8] and possibilities for engineering heterostructures with the desired properties by stacking of two or more 2D materials.[9] There is a whole plethora of various 2D materials beyond graphene with a linear dispersion in their band structure,[10] including topological insulators[11] and semimetals.[12]

Although the behavior of electrons in the vicinity of K and K' points of graphene's 2D Brillouin zone (BZ) is actually described by the Weyl equation, such points are, for historical reasons, called 2D Dirac points (occasionally, 2D Weyl points).[13] Their generalizations to 3D bulk single crystals are called (spin-1/2) Weyl points. According to the fermion doubling theorem, Weyl points (fermions) must appear in pairs of opposite chirality in the BZ. Two such Weyl fermions appearing at the same point in the BZ are called a 3D Dirac point,[14] while a pair of 3D Dirac points at the same k-vector forms a double Dirac point.[15] Note that at a band crossing, a Weyl point (3D Dirac point, double Dirac point) is two-fold (four-fold, eight-fold) degenerate. Generalizations for higher pseudo-spins are possible. Recent *ab initio* calculations show spin-1 Weyl and spin-3/2 Rarita–Schwinger–Weyl fermions in transition metal silicides,[16] such as RhSi.[17] An additional type of Dirac point appears in antiferromagnetic (AFM) 2D layers.[18,19] Here the crossing point is four-fold degenerate, the corresponding Chern number of each band is zero and such crossings can appear as a single point in the BZ. Quasiparticles in solids can even go beyond their Weyl and Dirac counterparts as shown by the classification of linear and quadratic three-, six- and eight-band crossings in 3D crystals with a strong spin–orbit coupling (SOC).[20] Other studies also discuss three-,[16] six-,[16,17] and eight-fold[15] degenerate fermions. Different types of electronic dispersions are intricately linked to symmetry, as also exemplified with cone engineering by symmetry manipulation,[21] whereas new 2D Dirac cones have been generated in graphene under an external periodic potential.[22] Mañes has used space group representations to find sufficient

[a]*Institute of Physics Belgrade, University of Belgrade, Pregrevica 118, 11080 Belgrade, Serbia. E-mail: damlja@ipb.ac.rs; Fax: +381 11 3162 190; Tel: +381 11 3713 060*
[b]*Institute for Multidisciplinary Research, University of Belgrade, Kneza Višeslava 1, 11030 Belgrade, Serbia*
[c]*Graphene Laboratory (GLAB) of Center for Solid State Physics and New Materials, Institute of Physics Belgrade, University of Belgrade, Pregrevica 118, 11080 Belgrade, Serbia*

†Electronic supplementary information (ESI) available: Group-theoretical derivations, the effective mass and density of states calculation as well as the outline of the algorithm used in *ab initio* calculations. See DOI: 10.1039/C7NR07763G

conditions for the existence of spin-1/2 Weyl points in the BZ of 3D single crystals, and enumerated the possible *T*-symmetric corepresentations of such points for spinless systems (single groups).[23] Recently, a set of symmetry conditions that guarantees 2D Dirac-like dispersion in the vicinity of high symmetry points in the BZ of any non-magnetic 2D material with negligible SOC has been reported.[24,25] Also, the existence of 2D Dirac fermions in bilayer non-honeycomb crystals using symmetry analysis has been indicated.[26] It has recently been shown that certain non-symmorphic symmetries induce new band hourglass-like dispersion at the surface of some 3D single crystals.[27] Non-symmorphic symmetries also cause a similar dispersion in 2D (layer) systems with SOC.[28,29] Topologically protected band touchings (TPBT) were found on the BZ surface of a SnTe 3D material class[30] and the A_2B_3 family of materials.[31] Note that such band touchings[27,30,31] are located away from the high-symmetry points of the BZ, and that they *can be moved but cannot be removed* by the change of model parameters used to calculate the band structure. Surprisingly, the existence of classes of massless fermions other than 2D Dirac-like, in 2D non-magnetic, time-reversal symmetric (TRS), materials with negligible SOC has not been addressed yet.

Here we report that combined TRS and certain crystal non-symmorphic symmetries of 2D materials lead to the emergence of peculiar massless linearly dispersive bands which we call fortune teller (FT) states. The geometries of these FT states in reciprocal space are pyramidal and paper fortune teller-like, unnoticed in solid state matter before. Our analysis indicates that these states and the Dirac cones are the unique possibilities for essential linear dispersive bands in all diperiodic directions of non-magnetic 2D materials without SOC. Our results are based on the analysis of all eighty layer single groups, which are all possible symmetries of non-magnetic 2D materials with negligible SOC. Inclusion of SOC would require an analysis of eighty layer double groups. These are distinct mathematical entities, and the results for the SOC-case do not apply to the non-SOC-case or *vice versa*. For this reason we treat here the non-SOC-case and leave analogous analysis for the SOC-case for future research. Similar search for Dirac-like and other (unconventional) quasiparticles has already been performed in the SOC-case.[15,20,28,29] Finally, we predict stable 2D materials with our new massless fermions using DFT and our own-developed software. The *ab initio* calculations have confirmed the existence of the predicted electronic dispersion and quantitatively determined structural and electronic properties, which can be utilized in further experimental realizations of the new class of 2D materials.

2. Classification of linear states in 2D materials

We consider all possible symmetry groups of non-magnetic crystals with negligible SOC, which are periodic in two spatial directions and finite in the perpendicular direction. These are the so-called layer single groups (or diperiodic groups). This implies that spinful degeneracy of a band is twice the spinless (orbital) degeneracy. Representation-protected band spinless degeneracy at the wave vector $\mathbf{k}_0$ in the 2D BZ, for bands belonging to the allowed[32] (relevant,[33] small[34]) irreducible representation (irrep) R of the group of the wave vector (little group) $G(\mathbf{k}_0)$, is given by the dimension of R. For all eighty layer single groups irreps R are either one- or two-dimensional.[32,35] TRS either doubles spinless band-degeneracy at given $\mathbf{k}_0$ or leaves it unchanged.[36] Therefore, possible essential spinless band-degeneracies are one, two or four.

Since the orbitally (spinless) non-degenerate band is smooth, its second derivative is finite and the effective mass, being inversely proportional to the second derivative,[37] is nonzero. Therefore, the bands carrying zero effective mass are possible only in the vicinity of points in the BZ where the electron energy is orbitally (spinless) degenerate. We show in the ESI† that in the vicinity of a spinless double degenerate point, 2D Dirac bands are the only possible massless bands.

The behavior of the bands near four-fold orbitally (spinless) degenerate points in non-magnetic 2D materials with no SOC has not been examined thus far and we perform this task as described in the next section. Before that, we comment on why we think that four-fold spinless degeneracies can only be caused by combined TRS and crystal symmetry. It is well-known that some crystal non-symmorphic symmetries combined with certain topological properties can lead to touching of two bands somewhere on high symmetry lines in the BZ. We call this topologically protected band touchings (TPBT). In such TPBT, band degeneracy is larger than required by dimensionality of irreps of the corresponding little group. Such an approach started with Zak's introduction of elementary band representations[38] (EBR) and culminated with the recent classification of all possible 10 403 band structures in double space groups.[39] Essentially, the presence of TPBT can be established by investigation of compatibility relationships of irreps along certain closed loops in the BZ.[40] Alternative formulation is in terms of non-symmorphic symmetry eigenvalues.[28,29] It sometimes happens that a band belongs to different irreps at two end points in the symmetry line and consequently must have touched another band an odd number of times (most probably once). The method cannot determine where exactly in the symmetry line two bands touch. Such a position depends on the model used to calculate the band structure. In layer single groups irreps of little groups for symmetry lines are one-dimensional inside BZ. BZ edges have either several one-dimensional irreps or only one two-dimensional irrep or two one-dimensional irreps related by TRS.[32] Corresponding three-fold (four-fold *etc.*) spinless degeneracy would require TPBT of three (four *etc.*) bands *at the same point in the BZ* which we assume is unlikely. In addition, all these three (four *etc.*) bands would have to belong to different irreps of the little group, which at some point becomes impossible. On the other hand, two double-degenerate bands at the edge of the BZ belong to the same irrep and therefore cannot touch.[41] For these reasons, we assume that TPBT can lead at most to double spinless degeneracy and to Dirac-like dispersion. The

same assumption holds even for band touchings that are not protected by topology but are model-dependent (accidental band touchings). Note that above arguments do not apply to the SOC case. For example, TPBT of two two-fold spinful degenerate bands exist in some layer double groups.[28]

3. Fortune teller states

In the following, the functional form of the new linear dispersion relation that corresponds to the vicinity of four-fold spinless degeneracy will be presented and compared to 2D Dirac-like dispersion. As before, we assume that $\mathbf{q}$ is a wave vector of small modulus, $\mathbf{t}$ a real 2D vector, u_1, u_2 positive quantities and q_1, q_2 projections of $\mathbf{q}$ along certain, mutually orthogonal directions. If $\mathbf{k}_0$ is a point that hosts a pair of 2D Dirac cones, then the Taylor expansion of the electron energy around this point reads:

$$E_{1,2}(\mathbf{k}_0+\mathbf{q}) \approx E_0 + \mathbf{t}\cdot\mathbf{q} \pm \sqrt{u_1 {q_1}^2 + u_2 {q_2}^2}. \quad (1)$$

For $u_1 = u_2$, 2D Dirac cones are isotropic and for $\mathbf{t} \neq 0$, the cones are tilted.[42,43] The new electronic dispersion presented in this paper is:

$$E_{1,2,3,4}(\mathbf{k}_0+\mathbf{q}) \approx E_0 \ \pm\ |u_1|q_1|\ \pm\ u_2|q_2||. \quad (2)$$

While the 2D Dirac band has the geometric form of a simple cone with a circular or elliptical cross section, the geometry of dispersion (2) consists of two different geometric forms. The plus sign under the absolute value yields the geometry of a four-sided pyramid, whereas the minus sign corresponds to a more complex geometry, which looks like the paper origami called paper fortune tellers [Fig. 2(b)]. Since both forms always appear together, we label dispersion (2) using one name – the fortune teller (FT) dispersion.

Next, we state the conditions that lead to four-fold essential spinless degeneracy. According to Herring,[36] there are, in principle, two possibilities for achieving this. The first one is:

O_1: $\mathbf{k}_0$ is equivalent to its inverse $-\mathbf{k}_0$,

O_2: R is two-dimensional,

O_3: R is pseudo-real or complex.

The second one is: $\mathbf{k}_0$ is not equivalent to $-\mathbf{k}_0$, $-\mathbf{k}_0$ is in the star of $\mathbf{k}_0$, R is two-dimensional, $R_{\mathrm{in}} = R{\uparrow}G$ is pseudo-real or complex (R_{in} is the representation of the whole layer single group G, obtained by induction from R). Detailed case-by-case study of representations of layer single groups[32] shows, by exhaustion, that the second possibility never occurs in 2D non-magnetic materials with negligible SOC. A more detailed discussion on the conditions for four-fold spinless degeneracy and the classification of all massless bands in non-magnetic 2D materials with weak SOC is given in the ESI.† Therefore conditions O_1–O_3 are the only essential four-fold spinless degeneracies in such systems.

Now we show how the linear dispersion (2) is connected to TRS and crystal symmetry. A general matrix form of the Taylor expansion of a four-component Hamiltonian around a given $\mathbf{k}_0$ point of BZ is:

$$\hat{H}(\mathbf{k}_0+\mathbf{q}) \approx E_0\hat{I}_4 + \hat{H}', \quad (3)$$

where

$$\hat{H}' = \hat{W}(\hat{I}_4 \otimes |\vec{q}\rangle), \quad (4)$$

and

$$\hat{W} = \left[\left\langle \frac{\partial}{\partial \mathbf{q}}\right| \hat{H}(\mathbf{k}_0+\mathbf{q})\right]_{\mathbf{q}=0}. \quad (5)$$

$\hat{I}_4$ is a four-dimensional unit matrix, $\otimes$ denotes the Kronecker product, $\langle\partial/\partial\mathbf{q}|$ is the transposed gradient at $\mathbf{q} = 0$, hence $\hat{W}$ is a four-by-eight matrix. We can combine the representation R and its complex conjugate R^* to obtain one four-dimensional, physically irreducible, real representation D in the following way: $D = R\oplus R^*$. It follows that we can choose the basis functions $\{\varphi_1, \ldots, \varphi_4\}$ for D to be real at $\mathbf{k}_0$ so that TRS imposes the following (* denotes complex conjugation):[23]

$$\hat{H}^*(\mathbf{k}_0+\mathbf{q}) = \hat{H}(\mathbf{k}_0-\mathbf{q}). \quad (6)$$

Taking the first order derivative of this equation with respect to $\mathbf{q}$, at $\mathbf{q}$= 0 gives the following condition for $\hat{W}$:

$$\hat{W}^* = -\hat{W}. \quad (7)$$

Taking into account in addition the hermicity of the Hamiltonian, we obtain for $\hat{H}'$ the following:

$$\hat{H}' = \mathrm{i}\begin{pmatrix} 0 & \mathbf{v}_1\cdot\mathbf{q} & \mathbf{v}_2\cdot\mathbf{q} & \mathbf{v}_3\cdot\mathbf{q} \\ -\mathbf{v}_1\cdot\mathbf{q} & 0 & \mathbf{v}_4\cdot\mathbf{q} & \mathbf{v}_5\cdot\mathbf{q} \\ -\mathbf{v}_2\cdot\mathbf{q} & -\mathbf{v}_4\cdot\mathbf{q} & 0 & \mathbf{v}_6\cdot\mathbf{q} \\ -\mathbf{v}_3\cdot\mathbf{q} & -\mathbf{v}_5\cdot\mathbf{q} & -\mathbf{v}_6\cdot\mathbf{q} & 0 \end{pmatrix}, \quad (8)$$

where $\mathbf{v}_j$ are real 2D vectors. Since $\hat{H}'$ is purely imaginary, for every eigenstate ψ_n corresponding to energy E_j, there exists an eigenstate ψ_n^* that corresponds to the energy $-E_j$. Therefore, eigenvalues of $\hat{H}'$ come in pairs (E_j, $-E_j$) and the Hamiltonian $\hat{H}'$ obeys the particle-hole symmetry. The eigenvalues of $\hat{H}(\mathbf{k}_0)$ + $\hat{H}'$ given by eqn (9) confirm our statement:

$$E_{1,2,3,4} = E_0 \pm \frac{1}{\sqrt{2}}\sqrt{\sum_{j=1}^{6}(\mathbf{v}_j\cdot\mathbf{q})^2 \pm \sqrt{\left[\sum_{j=1}^{6}(\mathbf{v}_j\cdot\mathbf{q})^2\right]^2 - 4[(\mathbf{v}_1\cdot\mathbf{q})(\mathbf{v}_6\cdot\mathbf{q}) - (\mathbf{v}_2\cdot\mathbf{q})(\mathbf{v}_5\cdot\mathbf{q}) + (\mathbf{v}_3\cdot\mathbf{q})(\mathbf{v}_4\cdot\mathbf{q})]^2}}. \quad (9)$$

Note that particle-hole symmetry is not accidental, but it is a consequence of the fact that complex conjugation is a symmetry operation. More precisely, in our case the combination of TRS, reality of representation D and the fact that $\mathbf{k}_0$ is time-reversal invariant momentum leads to purely imaginary $\hat{H}'$, and to particle-hole symmetry with respect to E_0.

To further simplify eqn (9) we use the following identity[23] valid for every element (in Seitz notation) $(\hat{h}|\tau_{\hat{h}} + \mathbf{R})$ of the little group $G(\mathbf{k}_0)$:

$$\hat{H}(\mathbf{k}_0 + \mathbf{q}) = \hat{D}^{+}((\hat{h}|\tau_{\hat{h}} + \mathbf{R}))\hat{H}(\mathbf{k}_0 + \hat{h}'\mathbf{q})\hat{D}((\hat{h}|\tau_{\hat{h}} + \mathbf{R})), \quad (10)$$

where $\hat{D}((\hat{h}|\tau_{\hat{h}} + \mathbf{R}))$ is the matrix of the representation D that corresponds to the element $(\hat{h}|\tau_{\hat{h}} + \mathbf{R})$ and $\hat{h}'$ is the reduction (as an operator) of $\hat{h}$ to two-dimensional $\mathbf{k}$-space. After differentiating (10) with respect to $\mathbf{q}$, at $\mathbf{q} = 0$ we obtain (T denotes transposition):

$$\hat{W} = \hat{D}((\hat{h}|\tau_{\hat{h}} + \mathbf{R}))\hat{W}[\hat{D}((\hat{h}|\tau_{\hat{h}} + \mathbf{R})) \otimes \hat{h}']^{\mathrm{T}}. \quad (11)$$

Eqn (11) is a consequence of crystal symmetry. If we write the matrix $\hat{W}$ as a column-vector $|\hat{W}\rangle$, eqn (11) becomes:

$$[\hat{D}((\hat{h}|\tau_{\hat{h}} + \mathbf{R})) \otimes \hat{D}((\hat{h}|\tau_{\hat{h}} + \mathbf{R})) \otimes \hat{h}']|\hat{W}\rangle = |\hat{W}\rangle. \quad (12)$$

It follows that the matrix $\hat{W}$ belongs to the totally symmetric part of the representation $D \otimes D \otimes \Gamma_{2\mathrm{DPV}}$, where $\Gamma_{2\mathrm{DPV}}$ is a two-dimensional polar-vector representation. For all groups that satisfy conditions O_1–O_3 we have, using Wigner's method of group projectors, found the form that symmetry imposes on the matrix $\hat{W}$ and consequently on vectors $\mathbf{v}_j$, and inserted the result in eqn (9). In all cases, the equation for eigenvalues (9) reduces to the dispersion (2). More details on the application of group projectors are given in the ESI.†

It turns out that only three out of eighty layer single groups have allowed representations satisfying the conditions O_1–O_3. Groups allowing the dispersion (2) are listed in Table 1. All three groups are non-symmorphic and belong to the rectangular system. The component q_1 can be chosen as projection of $\mathbf{q}$ along a direction that is parallel to any screw axis 2_1, q_2 is a projection along the perpendicular direction. The points $\mathbf{k}_0$ hosting the dispersion (2) are located at the corners $(\pm\pi/a, \pm\pi/b)$ of the rectangle that presents the BZ border. The corresponding space group from Table 1 denotes the space group that is obtained by periodic repetition of layer groups' elements along the axis perpendicular to the diperiodic plane. The diperiodic plane in Table 1 denotes the position of the layer single group plane within the corresponding 3D space group. The effective mass of both dispersions (1) and (2) is zero, as shown in the ESI† using the usual formula for $\hat{m}_{\mathrm{eff}}$.[37]

Analogous four-fold degeneracies are present in bulk 3D systems,[16,17] on the surface of 3D systems[31] or in 2D AFM crystals.[18,19] These are all spinful degeneracies in the presence of SOC. Dispersion of Rarita–Schwinger–Weyl fermions[16] is proportional to $S_z\sqrt{q_x^2 + q_y^2 + q_z^2}$, where S_z is a projection of pseudo-spin $S = 3/2$ along the z-axis, while the unconventional fermion at the BZ center of RhSi is a combination of two $S = 1/2$ and two $S = 3/2$ states with a similar dispersion.[17] In 2D AFM systems the dispersion $\pm\sqrt{q_x^2 + q_y^2}$ is double degenerate,[18,19] and the same holds for surface Dirac fermions.[31] The dispersion (2) differs from these Dirac-like dispersions, it is a property specific to 2D materials and consequently falls into the range of nanophysics.

Orbital wave functions must belong to an allowed irrep at a given point in the BZ. This statement is valid irrespective of strength of electronic correlations, since the Coulomb repulsion between electrons has the same transformation properties as the rest of the Hamiltonian. The allowed irreps of the groups listed in Table 1 are the only ones at these points of the BZ, hence the electronic correlations cannot change the form of the dispersion (2) *as long as TRS and crystal symmetries are preserved*. Even if the band picture fails the energy of all electrons in the crystal has dispersion (2). If one acts simultaneously by a space group element to radius vector of every electron in the crystal the many-body wave function has the same symmetry as the single-particle wave function of the corresponding non-interacting model. On the other hand, a combination of SOC and Hubbard interaction can result in an AFM order, which then breaks TRS.[46,47] The same effect might occur even without SOC.[48] Our analysis does not refer to such cases so a detailed *ab initio* investigation of particular material should show whether transition to the AFM order occurs.

Symmetry of the crystal lattice is responsible for (an)isotropy of single crystals.[49] For example, isotropy of the electric susceptibility tensor in silicon is caused by the cubic symmetry, while the in-plane isotropy of graphene is caused by the hexagonal symmetry. In our cases, crystal axes are maximally of the second order, the irreps of the corresponding point groups are all one-dimensional and the materials belonging to layer groups listed in Table 1 are expected to be *anisotropic*.

From the analysis of irreps of layer double groups[50] we conclude that in the presence of SOC, originally eight-fold, spinful degeneracy splits into four doubly spinful degenerate levels for Dg33 and two four-fold spinful degenerate levels for Dg43 and Dg45. Since Dg43 and Dg45 contain inversion, bands are at least spinful double-degenerate, so the four-fold spinful degenerate level cannot split into four non-degenerate ones along *e.g.* the BZ-diagonal. On the other hand, layer double group

Table 1 Layer single groups hosting the dispersion (2) in the vicinity of the BZ corners: $\mathbf{k}_0 = (\pm\pi/a, \pm\pi/b)$. The notation for layer- and space-groups are according to Kopsky and Litvin[44] and Hahn,[45] respectively. The x-, y- and z-axes are along a-, b- and c-directions of the orthorhombic 3D unit cell, respectively. The notation for allowed representation in the last column is according to the Bilbao Crystallographic Server.[32] Symbol ⇔ denotes equivalence between representations. In all three cases the little group $G(\mathbf{k}_0)$ is the whole layer single group

Layer single group		Corresponding space group			Diperiodic plane	irreps R at $\mathbf{k}_0$
Dg33	$pb2_1a$	29	$Pca2_1$	C_{2v}^{5}	$y = 0$	$U_1 \Leftrightarrow U_1^*$
Dg43	$p2/b2_1/a2/a$	54	$P2_1/c2/c2/a$	D_{2h}^{8}	$y = 0$	$U_1, U_2 \Leftrightarrow U_1^*$
Dg45	$p2_1/b2_1/m2/a$	57	$P2/b2_1/c2_1/m$	D_{2h}^{11}	$x = 0$	$T_1, T_2 \Leftrightarrow T_1^*$

Dg33 does not support four-fold degeneracy at the BZ corners, which is necessary for FT dispersion. We conclude that SOC destroys FT dispersion at BZ corners of layer groups from Table 1. This result is valid irrespective of the strength of SOC. The four-fold orbital, and therefore eight-fold spinful degeneracy in layer single groups from Table 1 leads to electron band filling of $8n$ (n = 1, 2, 3, ...), as a necessary condition for bands to be either completely filled or completely empty.[51,52] This requirement remains even in the SOC case.[28] In fact Dg33, Dg43 and Dg45 are the only layer double groups with band filling $8n$ necessary for insulating systems.[28] In contrast to layer single groups from Table 1, essential eight-fold spinful degeneracy does not exist in their double group counterparts.[50] Instead, four spinful double-degenerate bands are tangled together in an hourglass manner in double-Dg43 and Dg45, while in non-centrosymmetric double-Dg33, eight non-degenerate bands form a "cat's cradle" structure.[28] Analysis of band connectivity[28] for double-Dg33, Dg43 and Dg45 confirms our prediction of SOC splitting for bands at the corners of the BZ for groups from Table 1.

Since there is only one FT dispersion in the first BZ of each group from Table 1, it is interesting to investigate if band topology requires appearance of additional dispersions somewhere else in the first BZ. According to Chern, the following integral must be an integer C_n:

$$C_n = \frac{\mathrm{i}}{2\pi}\int\int_{1^{\mathrm{st}}\,\mathrm{BZ}} \nabla_{\mathbf{q}} \times \langle \psi_n(\mathbf{q})|\nabla_{\mathbf{q}}\psi_n(\mathbf{q})\rangle \cdot \mathrm{d}^2\mathbf{S}, \qquad (13)$$

where ψ_n is the eigenstate of n^{th} level, C_n is the Chern number, while $\mathrm{i}\nabla_{\mathbf{q}} \times \langle \psi_n(\mathbf{q})|\nabla_{\mathbf{q}}\psi_n(\mathbf{q})\rangle$ is the Berry curvature.[11,53] In the case of graphene, each Dirac point gives contribution of 1/2 to the C_n and consequently, the number of Dirac points in the first BZ must be even. This is a 2D version of the Fermion doubling theorem. In contrast to graphene, our dispersion leads to zero Berry curvature for each of four states in each of the three groups. Consequently, the Berry phase is zero along any closed contour in the BZ, which gives $C_n = 0$ for all n = 1, 2, 3, 4. It follows that topology does not forbid FT to be the only dispersion at the Fermi level. Similar conclusion holds for *e.g.* AFM Dirac cone, where the contact point is also four-fold degenerate.[18]

Next we discuss the behavior of FT dispersion under strain. Application of strain that deforms the rectangular primitive cell into an oblique one, lowers the symmetry from a Dg33 to a Dg5 layer group, *i.e.* from Dg43 and Dg45 to Dg7. Since both Dg5 and Dg7 necessarily host the semi-Dirac dispersion,[54] FT dispersion splits into two pairs of semi-Dirac cones. The Chern number of semi-Dirac dispersion is zero, so such bands are topologically trivial. It follows that any linear combination of single band Chern numbers, such as mirror Chern number or spin Chern number, is also zero in this case. For strain that does not deform the rectangular primitive cell, the behavior of FT dispersion is determined by *translationengleiche* subgroups of Dg33, Dg43 and Dg45. As detailed analysis of band degeneracies in all layer single groups shows, breaking of horizontal glide plane symmetry of Dg33, splits an FT point into two spinless double-degenerate points, both belonging to double spinless degenerate lines. Such splitting occurs also in Dg43 and Dg45, when one breaks any symmetry element of their subgroup Dg33. On the other hand, breaking of any element belonging to Dg43 or Dg45 but not to Dg33 gives the final group Dg33 and FT states are robust against such deformations.

Density of states (DOS) per unit area/volume for the n^{th} energy band is given by the following formula: $\rho_n(\varepsilon) = (1/2\pi)^{D_{\mathrm{im}}}\int\int_{1^{\mathrm{st}}\,\mathrm{BZ}} \delta(\varepsilon - \varepsilon_n(\mathbf{q}))\mathrm{d}^{D_{\mathrm{im}}}\mathbf{q}$. Here, the dimensionality D_{im} is equal to three (two) for 3D (2D) systems. For Dirac dispersion $\pm v|\mathbf{q}|$ in 3D (in 2D), it is convenient to change to spherical (polar) coordinates. DOS is proportional to $\int_0^{\mathrm{bzb}} q^{D_{\mathrm{im}}-1}\delta(\varepsilon - vq)\mathrm{d}q$, where the BZ border bzb depends on the azimuthal and polar angles. For a sufficiently small energy ε measured from the bands contact point, we obtain, after including the particle-hole symmetry, $\rho_n(\varepsilon) \sim |\varepsilon|$ for 2D, *i.e.* $\rho_n(\varepsilon) \sim \varepsilon^2$ for 3D Dirac dispersion. In both cases, DOS becomes vanishingly small in the vicinity of contact points of the cones. This result refers, among other cases, also to four-fold spinful degenerate fermions in 3D.[16,17] On the other hand, change to polar coordinates does not help in calculating DOS for dispersion (2). It is more convenient to introduce linear transformations of q_1 and q_2 such that expression under the Dirac delta function contains only one variable of integration. Details of calculations are given in the ESI,† while the final result is:

$$\rho(\varepsilon) \approx \frac{3}{\pi\hbar}\left[\frac{1}{av_b} + \frac{1}{bv_a}\right], \qquad (14)$$

with degeneracy due to the spin included. Here a and b are lattice constants while v_a and v_b are Fermi velocities along a and b. It is worth noting that DOS of FT is constant around E_{F} in contrast to DOS of Dirac states in graphene. This unique coexistence of zero electron effective mass and non-zero DOS at E_0 might have consequences on *e.g.* charge transport properties. For example, a smaller sensitivity of conductance is expected when charged impurities are introduced in materials with FT states.

4. *Ab initio* search for realistic materials

Next we report examples of (meta)stable 2D materials with the desired layer groups predicted using *ab initio* calculations. We have developed and utilized software that automatically searches for materials with a given group, analyzes their stability and band structure. The outline of the algorithm is listed in the ESI.† Since the atomic SOC strength increases as the fourth power of the atomic number,[13] we limited our search only to light elements of the periodic table. For the sake of demonstration of the new electronic dispersion in real materials, we have searched for stable crystals with the above

stated symmetry groups among a few light elements, including B, C, Si and P. These are known to build stable 2D materials of various crystal symmetries and have negligible SOC. Note that the materials presented here are for demonstration purposes only, without intent to be a complete list. More elemental crystals with given symmetries are possible, while the list exponentially grows when compounds of two or more elements per unit cell are considered. Our symmetry arguments do not determine the position of FT states on the energy scale, so it is not guaranteed that the Fermi level will cross the energy near E_0. We have applied band filling theory[28,51,52] to our groups and found that the number of valence electrons per primitive cell must be an odd multiple of four, for FT states to touch exactly at E_F and that no other bands cross the Fermi level. The simplest structures satisfying these necessary (but non-sufficient) conditions have four identical nuclei in the primitive cell and belong to Dg45. The structures are listed in Table 2.

Note that we mean the *structural stability* here when we write about stability. Our DFT calculations have been conducted for the materials in an absolute vacuum. This has been a common approach in related papers.[15–18,20,27,30,31] Here we propose a new class of materials which may include dozens of materials. Their chemical stability, *i.e.* stability in the atmosphere and reactivity with oxygen and other chemicals depend on the particular material's chemical composition, hence the chemical stability varies among materials in the class. For instance, phosphorene (double layer) has a Dg45 symmetry group (hence it belongs to the new class), while its reactivity with hydrogen, oxygen and fluorine has been analyzed in detail.[55] Questions of chemical stability of other found and yet to be found materials in the new class are to be answered in future research.

A stable structure with FT contact points positioned exactly at the Fermi level [P(Dg45), marked with bold letters in Table 2] is shown in Fig. 1(a). It consists of zig-zag chains of P atoms placed alternately at two parallel planes. The potential energy surface (PES) of elemental phosphorus has multiple local minima, *i.e.* many allotropes have been recently predicted,[56] hence there are numerous (meta)stable phases of phosphorus with different symmetries. P(Dg45) is a new one, placed at the distinct local minimum of PES in the configuration subspace with the Dg45 group and 4-fold multiplicity of Wyckoff positions [Fig. 1(b)]. Its stability is further confirmed by molecular dynamics simulations at 100 K.

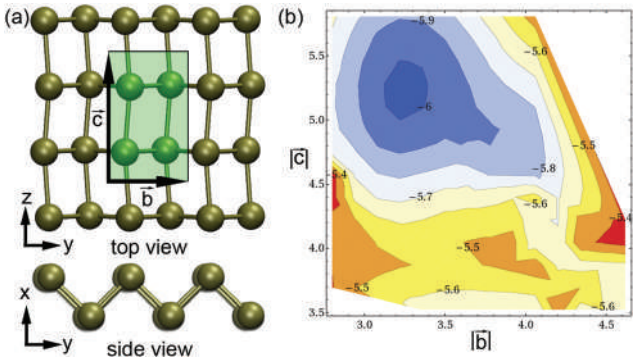

Fig. 1 Example of a stable structure with FT states at E_F. Top and side views of the optimized geometry of P(Dg45) is shown in panel (a). An elementary unit cell is marked with a green rectangle together with lattice vectors. Potential energy surface (atomization energy is given in eV per atom) in the configuration space constrained by the Dg45 group and 4-fold multiplicity of Wyckoff positions is shown in (b). The lattice parameters are given in Angstroms. Calculations are not done in the white region of panel (b) since the search algorithm predetermined instability of the crystal in this region.

The band structure of P(Dg45) along lines between high symmetry points is shown in Fig. 2(a). At Y–R–Z section of the BZ, four states touch at E_F (both upper and lower states are doubly spinless degenerate), yielding 4-fold spinless degeneracy at the point of contact (E_F). Constant and non-zero DOS in the vicinity of E_F confirms our prediction given by eqn (14). The bands around R point obey the electron–hole symmetry, in agreement with our discussion related to eqn (9). The Fermi velocities of these states in the Y–R and R–Z directions are 1.08×10^6 m s^{-1} and 0.46×10^6 m s^{-1}, which are in the range of the Fermi velocity of graphene.

The Fermi velocity of P(Dg45) is highly anisotropic. Therefore anisotropic electronic properties are expected to be similar to those of doped phosphorene.[57] The 2-fold spinless degeneracy of both lower and upper bands at R is lifted along the diagonal direction (Γ–R). Note another set of bands between Z and Γ, with 2-fold spinless degeneracy below E_F. More geometry details of the states around R are visible in Fig. 2(b). These states look exactly the same as the symmetry analysis predicted above: the FT states consisting of two pyramid-like and two paper fortune teller-like bands that touch at their tips and two lines, respectively. Sharp edges of the dispersion are unique among the electronic structure of

Table 2 Examples of stable 2D crystals with the Dg45 group. Mult. is multiplicity of Wyckoff position. E_{at} is atomization energy, b and c are lattice parameters. Coordinates of only one atom are given for each element. Other coordinates can be obtained from Wyckoff positions. $\Delta E_F = E_{FT} - E_F$ – energy difference between the Fermi level and nearest FT states. Group velocities v_b and v_c are calculated using $v_j = \frac{1}{\hbar}\frac{\partial E(k_1,k_2)}{\partial k_j}$ where index j corresponds to b or c lattice directions. A corresponding stable structure for carbon was not found

Element	E_{at} [eV per atom]	b [Å]	c [Å]	Coordinates [Å]	ΔE_F [eV]	v_b [10^6 m s^{-1}]	v_c [10^6 m s^{-1}]
B	−6.51	3.12	2.97	(0.390 0.387 0.743)	−0.65	1.22	1.52
Si	−5.56	3.74	4.64	(0.765 0.583 1.160)	−2.30	0.91	0.79
P	**−6.03**	**3.22**	**5.24**	**(0.780 0.708 1.310)**	**0.00**	**1.08**	**0.40**

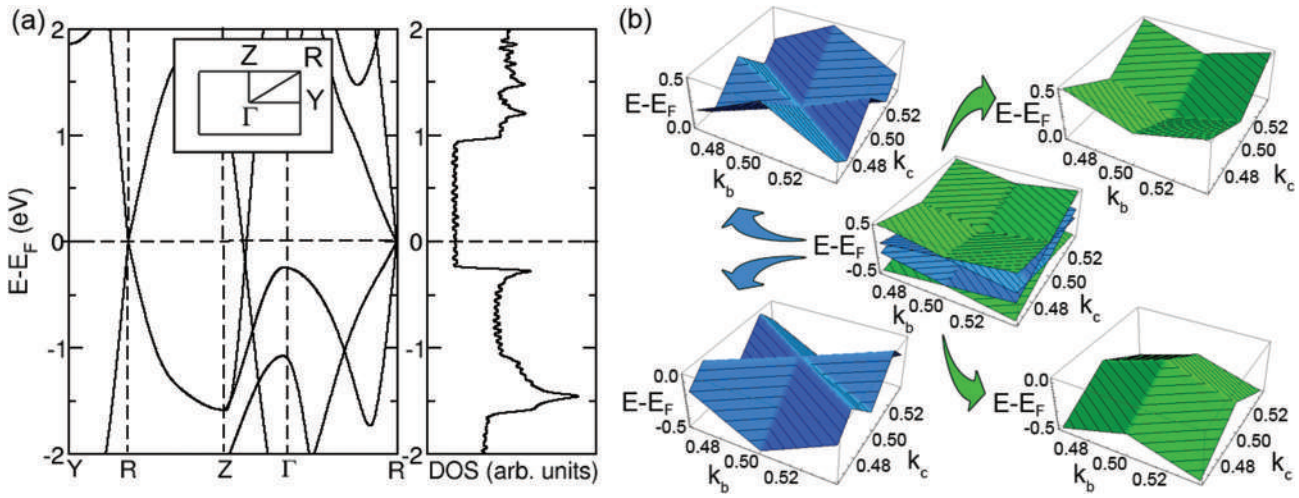

Fig. 2 The band structure of P(Dg45). (a) Electronic band structure along the lines between high-symmetry k-points (left panel) and the corresponding density of states (right panel). (b) FT states consisting of pyramidal (green) and paper fortune teller-like (blue) bands at point R. Energies are in units of eV relative to E_F, k-points are in units of $2\pi/|\mathbf{b}|$ and $2\pi/|\mathbf{c}|$. Coordinates of the R-point are (0.5, 0.5), while the $R-Z$ direction ($R-Y$ direction) is parallel to the $\mathbf{k_b}$ ($\mathbf{k_c}$) axis.

any known crystal, and particularly in contrast to the smooth features of Dirac cones.

In order to image experimentally the sharp edges as the unique signature of the FT state, angle-resolved photoemission spectroscopy (ARPES)[58] can be utilized. ARPES can probe the momentum-dependent electronic band structure of 2D materials providing detailed information on the band dispersion and Fermi surface. Importantly for the fine structural feature of edges, recent progress of this technique allows ARPES measurements with a precision of roughly 1 meV energy resolution and 0.1 degree angular resolution. Prior to application of ARPES the material should be doped to move the Fermi level from the contact point and reach a doped Fermi surface with edges. Doping can be achieved by electron transfer between the target material and a substrate which acts as a donor or an acceptor of electrons. In order to preserve the symmetry, the donor/acceptor should be sputtered to both surfaces of the target material. The contact between the substrate and only one face of the sample would reduce the symmetry of the system and open a gap. The same holds for gating, when an electric field is applied perpendicularly to the sample. These symmetry arguments explain *e.g.* the gap opening in bilayer graphene under gating.[59] On the other hand, adding dopant elements to the target material in a way that preserves the original symmetry does not affect the FT dispersion. Even though preserving symmetry in highly doped systems is a formidable task, a light doping, in percent or even ppm ranges, would be sufficient for shifting of the Fermi level from the contact points, depending on a particular material. Light doping is still negligible for breaking of crystal symmetry. Other than ARPES, inverse photoemission spectroscopy can be used to probe the unoccupied states in the electronic band structure. In addition to the edges as a very unique feature of the novel FT state, transport measurements would address the anisotropic electronic nature of the states.

5. Conclusions

In conclusion, we have established a full classification of states with linear dispersions in non-magnetic, time-reversal symmetric 2D materials with a negligible spin–orbit coupling, based on group theory analysis, and found that only one additional massless state to the Dirac one is possible. These states have not only unique and interesting geometric forms, but they also can open new horizons for both fundamental research and applications. For instance, these fermions in 2D materials do not have a counterpart in elementary particle physics, in analogy to some new fermions predicted for the 3D space groups.[15–17,20] The sharp edges in the electronic bands have been neither predicted nor measured before, so their existence in the FT states may spawn new phenomena in solid state materials. Materials with FT bands can be competitive to the popular phosphorene due to the importance of anisotropy of its electronic structure.[57] Our unified classification of linearly dispersive bands paves the way to engineer new materials with Dirac and FT states. We hope that findings presented here will be of great motivation for experimental groups to bring these materials into existence.

Author contributions

VD performed the symmetry group analysis, discovered FT dispersion, analytically calculated the effective mass, density of states and the Berry curvature, and wrote the corresponding

parts of the manuscript. IP developed and used the software for *ab initio* search, conceptualized and wrote the larger part of the manuscript. RG initiated the research with the idea that Dirac dispersion can be a consequence of symmetry.

Conflicts of interest

There are no conflicts to declare.

Acknowledgements

We are thankful to Jelena Pešić, Marko Spasenović and Andrea Damascelli for discussions and suggestions related to this work. DFT calculations were performed using computational resources at the Center of Surface and Nanoanalytics, Johannes Kepler University, Linz, Austria. We are grateful to Prof. Kurt Hingerl for providing the necessary computational resources at JKU. This work was supported by the Serbian Ministry of Education, Science and Technological Development under project numbers OI 171005 and III 45016.

References

1 K. S. Novoselov, A. K. Geim, S. V. Morozov, D. Jiang, Y. Zhang, S. V. Dubonos, I. V. Grigorieva and A. A. Firsov, *Science*, 2004, **306**, 666–669.
2 G. W. Semenoff, *Phys. Rev. Lett.*, 1984, **53**, 2449–2452.
3 A. H. Castro Neto, F. Guinea, N. M. R. Peres, K. S. Novoselov and A. K. Geim, *Rev. Mod. Phys.*, 2009, **81**, 109–162.
4 K. Bolotin, K. Sikes, Z. Jiang, M. Klima, G. Fudenberg, J. Hone, P. Kim and H. Stormer, *Solid State Commun.*, 2008, **146**, 351–355.
5 M. I. Katsnelson, K. S. Novoselov and A. K. Geim, *Nat. Phys.*, 2006, **2**, 620–625.
6 Y. Zhang, Y.-W. Tan, H. L. Stormer and P. Kim, *Nature*, 2005, **438**, 201–204.
7 X. Du, I. Skachko, F. Duerr, A. Luican and E. Y. Andrei, *Nature*, 2009, **462**, 192–195.
8 D. Akinwande, N. Petrone and J. Hone, *Nat. Commun.*, 2014, **5**, 5678.
9 A. K. Geim and I. V. Grigorieva, *Nature*, 2013, **499**, 419–425.
10 J. Wang, S. Deng, Z. Liu and Z. Liu, *Natl. Sci. Rev.*, 2015, **2**, 22–39.
11 M. Z. Hasan and C. L. Kane, *Rev. Mod. Phys.*, 2010, **82**, 3045–3067.
12 Z. K. Liu, B. Zhou, Y. Zhang, Z. J. Wang, H. M. Weng, D. Prabhakaran, S.-K. Mo, Z. X. Shen, Z. Fang, X. Dai, Z. Hussain and Y. L. Chen, *Science*, 2014, **343**, 864–867.
13 S. A. Yang, *SPIN*, 2016, **06**, 1640003.
14 S. M. Young, S. Zaheer, J. C. Y. Teo, C. L. Kane, E. J. Mele and A. M. Rappe, *Phys. Rev. Lett.*, 2012, **108**, 140405.
15 B. J. Wieder, Y. Kim, A. M. Rappe and C. L. Kane, *Phys. Rev. Lett.*, 2016, **116**, 186402.
16 P. Tang, Q. Zhou and S.-C. Zhang, *Phys. Rev. Lett.*, 2017, **119**, 206402.
17 G. Chang, S.-Y. Xu, B. J. Wieder, D. S. Sanchez, S.-M. Huang, I. Belopolski, T.-R. Chang, S. Zhang, A. Bansil, H. Lin and Z. M. Hasan, *Phys. Rev. Lett.*, 2017, **119**, 206401.
18 S. M. Young and B. J. Wieder, *Phys. Rev. Lett.*, 2017, **118**, 186401.
19 J. Wang, *Phys. Rev. B: Condens. Matter Mater. Phys.*, 2017, **95**, 115138.
20 B. Bradlyn, J. Cano, Z. Wang, M. G. Vergniory, C. Felser, R. J. Cava and B. A. Bernevig, *Science*, 2016, **353**, aaf5037.
21 L. A. Ponomarenko, R. V. Gorbachev, G. L. Yu, D. C. Elias, R. Jalil, A. A. Patel, A. Mishchenko, A. S. Mayorov, C. R. Woods, J. R. Wallbank, M. Mucha-Kruczynski, B. A. Piot, M. Potemski, I. V. Grigorieva, K. S. Novoselov, F. Guinea, V. I. Fal'ko and A. K. Geim, *Nature*, 2013, **497**, 594–597.
22 C.-H. Park, L. Yang, Y.-W. Son, M. L. Cohen and S. G. Louie, *Phys. Rev. Lett.*, 2008, **101**, 126804.
23 J. L. Mañes, *Phys. Rev. B: Condens. Matter Mater. Phys.*, 2012, **85**, 155118.
24 V. Damljanović and R. Gajić, *J. Phys.: Condens. Matter*, 2016, **28**, 085502.
25 V. Damljanović and R. Gajić, *J. Phys.: Condens. Matter*, 2016, **28**, 439401.
26 G. van Miert and C. M. Smith, *Phys. Rev. B: Condens. Matter Mater. Phys.*, 2016, **93**, 035401.
27 Z. Wang, A. Alexandradinata, R. J. Cava and B. A. Bernevig, *Nature*, 2016, **532**, 189–194.
28 B. J. Wieder and C. L. Kane, *Phys. Rev. B: Condens. Matter Mater. Phys.*, 2016, **94**, 155108.
29 S. M. Young and C. L. Kane, *Phys. Rev. Lett.*, 2015, **115**, 126803.
30 T. H. Hsieh, H. Lin, J. Liu, W. Duan, A. Bansil and L. Fu, *Nat. Commun.*, 2012, **3**, 982.
31 B. J. Wieder, B. Bradlyn, Z. Wang, J. Cano, Y. Kim, H.-S. Kim, A. M. Rappe, C. L. Kane and A. B. Bernevig, arXiv:1705.01617, 2017.
32 M. I. Aroyo, A. Kirov, C. Capillas, J. M. Perez-Mato and H. Wondratschek, *Acta Crystallogr., Sect. A: Found. Crystallogr.*, 2006, **62**, 115–128.
33 J. F. Cornwell, *Group Theory in Physics, Volume I*, Academic Press, 1984.
34 C. J. Bradley and A. P. Cracknell, *The Mathematical Theory of Symmetry in Solids*, Clarendon, 2010.
35 I. Milošević, B. Nikolić, M. Damnjanović and M. Krčmar, *J. Phys. A: Math. Gen.*, 1998, **31**, 3625.
36 C. Herring, *Phys. Rev.*, 1937, **52**, 361–365.
37 N. W. Aschroft and N. D. Mermin, *Solid State Physics*, Saunders College Publishing, 1972.
38 J. Zak, *Phys. Rev. B: Condens. Matter Mater. Phys.*, 1982, **26**, 3010–3023.
39 B. Bradlyn, L. Elcoro, J. Cano, M. G. Vergniory, Z. Wangl, C. Felser, M. I. Aroyo and A. B. Bernevig, *Nature*, 2017, **547**, 298–305.

40 L. Michel and J. Zak, *Phys. Rep.*, 2001, **341**, 377–395.
41 L. D. Landau and L. M. Lifshitz, *Quantum Mechanics: Non-Relativistic Theory*, Butterworth-Heinemann, 1981.
42 S. Katayama, A. Kobayashi and Y. Suzumura, *J. Phys. Soc. Jpn.*, 2006, **75**, 054705.
43 M. O. Goerbig, J.-N. Fuchs, G. Montambaux and F. Piéchon, *Phys. Rev. B: Condens. Matter Mater. Phys.*, 2008, **78**, 045415.
44 V. Kopsky and D. B. Litvin, *International Tables of Crystallography Volume E: Subperiodic Groups*, Kluwer Academic Publishers, 2002.
45 T. Hahn, *International Tables of Crystallography Volume A: Space-Group Symmetry*, Springer, 2005.
46 J.-M. Carter, V. V. Shankar, M. A. Zeb and H.-Y. Kee, *Phys. Rev. B: Condens. Matter Mater. Phys.*, 2012, **85**, 115105.
47 G. Sharma, Z. Zhao, P. Sarker, B. A. Nail, J. Wang, M. N. Huda and F. E. Osterloh, *J. Mater. Chem. A*, 2016, **4**, 2936–2942.
48 D. Di Sante, A. Hausoel, P. Barone, J. M. Tomczak, G. Sangiovanni and R. Thomale, *Phys. Rev. B: Condens. Matter Mater. Phys.*, 2017, **96**, 121106.
49 A. S. Nowick, *Crystal Properties Via Group Theory*, Cambridge University Press, 2005.
50 L. Elcoro, B. Bradlyn, Z. Wang, M. G. Vergniory, J. Cano, C. Felser, B. A. Bernevig, D. Orobengoa, G. de la Flor and M. I. Aroyo, *J. Appl. Crystallogr.*, 2017, **50**, 1457–1477.
51 H. Watanabe, H. C. Po, M. P. Zaletel and A. Vishwanath, *Phys. Rev. Lett.*, 2016, **117**, 096404.
52 H. Watanabe, H. C. Po, A. Vishwanath and M. Zaletel, *Proc. Natl. Acad. Sci. U. S. A.*, 2015, **112**, 14551–14556.
53 M. V. Berry, *Proc. R. Soc. London, Ser. A*, 1984, **392**, 45–57.
54 V. Damljanović and R. Gajić, *J. Phys.: Condens. Matter*, 2017, **29**, 185503.
55 D. W. Boukhvalov, A. N. Rudenko, D. A. Prishchenko, V. G. Mazurenko and M. I. Katsnelson, *Phys. Chem. Chem. Phys.*, 2015, **17**, 15209–15217.
56 J. Guan, Z. Zhu and D. Tománek, *Phys. Rev. Lett.*, 2014, **113**, 046804.
57 J. Kim, S. S. Baik, S. H. Ryu, Y. Sohn, S. Park, B.-G. Park, J. Denlinger, Y. Yi, H. J. Choi and K. S. Kim, *Science*, 2015, **349**, 723–726.
58 A. Damascelli, *Phys. Scr.*, 2004, **T109**, 61–74.
59 K. F. Mak, C. H. Lui, J. Shan and T. F. Heinz, *Phys. Rev. Lett.*, 2009, **102**, 256405.

Electronic Supplementary Information for the paper "Fortune teller fermions in two-dimensional materials" by V. Damljanović, I. Popov and R. Gajić

Classification of linear states in 2D

We first show that in the vicinity of spinless double degenerate point, 2D Dirac bands are the only possible massless bands. Eigenvalues of any two-component, $\boldsymbol{k}$-dependent Hamiltonian $\hat{H}(\boldsymbol{k})$ are:

$$E_{1,2}(\boldsymbol{k}) = f_0(\boldsymbol{k}) \pm \sqrt{\sum_{j=1}^{3}\left[f_j(\boldsymbol{k})\right]^2}\,, \tag{S1}$$

where

$$(\forall j = \overline{0,3}) f_j(k) = \tfrac{1}{2} Tr\left[\hat{H}(\boldsymbol{k})\hat{\sigma}_j\right] \tag{S2}$$

are real functions and $\hat{\sigma}_{1,2,3}$ ($\hat{\sigma}_0$) are the Pauli matrices (is the unit matrix). If $\boldsymbol{k}_0$ is crossing point of two bands and $\boldsymbol{q}$ is a wave vector of small modulus then $f_1(\boldsymbol{k}_0) = f_2(\boldsymbol{k}_0) = f_3(\boldsymbol{k}_0) = 0$ and:

$$E_{1,2}(\boldsymbol{k_0} + \boldsymbol{q}) \approx f_0(\boldsymbol{k_0} + \boldsymbol{q}) \pm \sqrt{u q_1^{2n_1} + v q_2^{2n_2}} \tag{S3}$$

In Eq. (S3), u and v are positive quantities, n_1 and n_2 are natural numbers and q_1 and q_2 are projections of $\boldsymbol{q}$ along certain, mutually orthogonal directions. Since the expression under the square root in Eq. (S3) cannot be negative, the powers on q_1, q_2 must be even. Eq. (S3) is obtained by the Taylor expansion of f_j, (j=1, 2, 3) around the point $\boldsymbol{k}_0$. In order to obtain the effective mass we need second order derivatives with respect to q_1, q_2 at

$\boldsymbol{q}$=0. If x denotes q_1 or q_2, the second derivative of $|x|^n$ (n=2,3,4,..) depends on whether n is even (n=2s, s=1,2,3,..):

$$\frac{d^2}{dx^2}|x|^{2s} = 2s(2s-1)x^{2s-2},$$

or odd (n=2s+1):

$$\frac{d^2}{dx^2}|x|^{2s+1} = 2s(2s-1)|x|^{2s-1} + 4sx^{2s-1}\theta(x) + 2x^{2s}\delta(x).$$

Here $\theta(x)$=1 ($\theta(x)$=-1) for x>0 (x<0) and $\delta(x)$ is Dirac delta-function. For n=2 second derivative at x=0 is a positive constant, which gives rise to finite effective mass. For n>2 second derivative is zero at x=0 and the contribution to the effective mass comes from second derivatives of f_0 in Eq. (S3). Again, the effective mass is finite. The only remaining case n_1=n_2=1 gives zero effective mass and corresponds to 2D Dirac-like dispersion (see Eq. (1) of the main text and this text below).

Next, we classify all possibilities for linear dispersions in the band structure of 2D materials. In order to achieve this aim we define a set of parameters, which values determine possible existence of linear dispersions in 2D crystals. If $G(\boldsymbol{k}_0)$ is the group of the wave vector $\boldsymbol{k}_0$ and R is allowed [32] (relevant [33], small [34]) irreducible representation (irrep) of $G(\boldsymbol{k}_0)$, then the set of parameters consists of

-equivalence of $\boldsymbol{k}_0$ and its inverse $-\boldsymbol{k}_0$,

-dimensionality of representation R,

-reality of representation R.

We consider all possible symmetry groups of crystals which are periodic in 2 spatial directions and finite in the perpendicular direction. These are the so called layer groups (or diperiodic groups). Layer groups have only 1D or 2D allowed irreps [32, 35], while they can be real on one hand or pseudo-real or complex on the other hand. When complex conjugation is a symmetry operation, reality of irreps determines if it causes additional degeneracy. For single crystals the corresponding theory was developed in 1937 [36]. Therefore, each of these parameters can obtain one of two options; hence there are 8 possible combinations, as illustrated in figure S1.

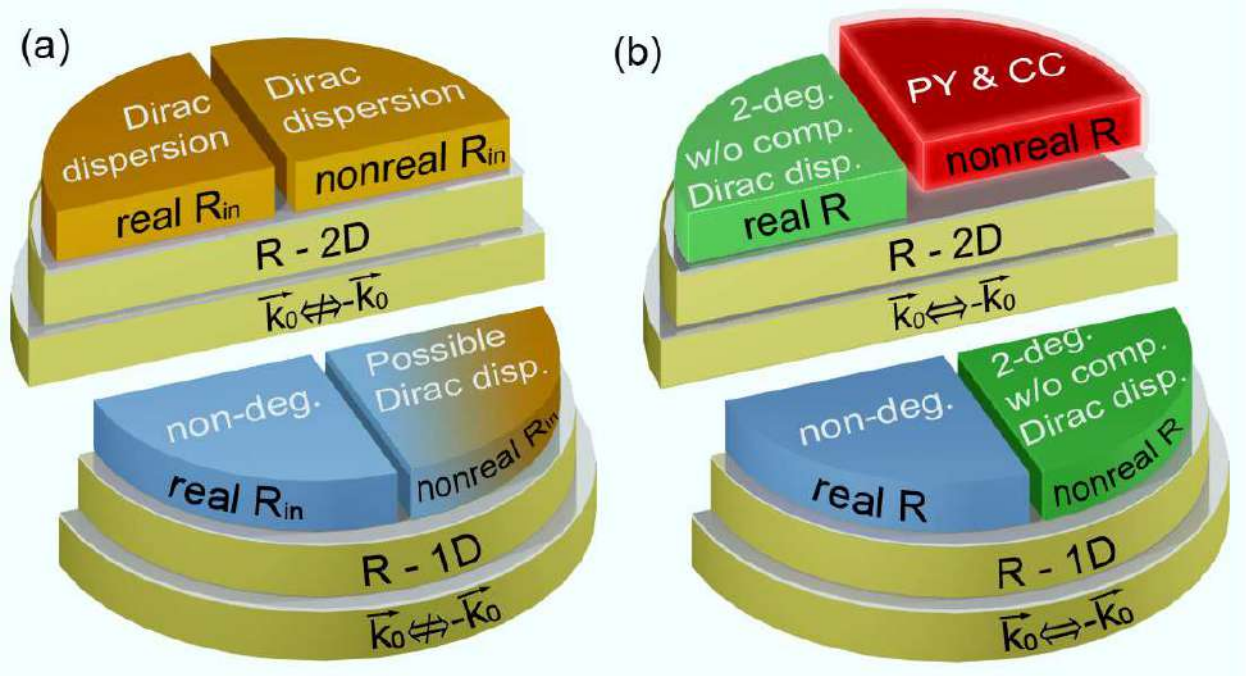

Figure S1. Full classification of linearly dispersive electronic bands in non-magnetic 2D materials based on symmetry conditions. Panel (a) corresponds to the case $\boldsymbol{k}_0 \not\Leftrightarrow -\boldsymbol{k}_0$ and panel (b) to the case $\boldsymbol{k}_0 \Leftrightarrow -\boldsymbol{k}_0$. 2-deg. w/o comp. Dirac. disp. means doubly-degeneracy without complete Dirac dispersion, non-deg. means a non-degenerate state.

Firstly, we consider the case $\boldsymbol{k}_0 \nLeftrightarrow -\boldsymbol{k}_0$ (figure S1a). The wave vector $\boldsymbol{k}_0$ must have a locally maximal symmetry, otherwise linear dispersion cannot appear, due to either too many band contacts [S1] or none at all. If R is two-dimensional, and the irrep R_{in} of the whole layer group G, which is obtained by induction from R ($R_{in} = R{\uparrow}G$) is real, Dirac-like dispersion appears [24] (orange upper left section). If R_{in} is not real, $-\boldsymbol{k}_0$ is not in the star of $\boldsymbol{k}_0$ [32] than the additional degeneracy due to TRS does not appear. This case also leads to Dirac dispersion [24] (orange upper right section). In the last two cases double degeneracy at Dirac point is caused by the crystal symmetry. For R one-dimensional and R_{in} real (left panel blue section), the energy level E_0 at $\boldsymbol{k}_0$ is non-degenerate preventing Dirac dispersion in the vicinity of $\boldsymbol{k}_0$. For R one-dimensional and R_{in} pseudoreal or complex (blue-orange section) there are two possibilities. If $-\boldsymbol{k}_0$ is not in the star of $\boldsymbol{k}_0$, E_0 is non-degenerate while in the opposite case TRS causes E_0 to be double degenerate with a complete Dirac-like dispersion around $\boldsymbol{k}_0$ [25]. Next we consider the case $\boldsymbol{k}_0 \Leftrightarrow -\boldsymbol{k}_0$ (figure S1b). If R is one-dimensional and real, the energy level E_0 at $\boldsymbol{k}_0$ is non-degenerate and linear dispersion cannot appear (right panel blue section). If R is one-dimensional and not real (right panel green section down), TRS causes E_0 to be double degenerate, but complete linear Dirac-like dispersion is not possible since the TRS causes $u_2=0$ (u_2 is a coefficient in the expression for Dirac dispersion [24], see the expression (1) in the main text). The same statement holds for two-dimensional, real R (right panel green section up). The remaining case in which R is two-dimensional and pseudoreal or complex will be treated in more detail in the main text (right panel red section).

Group-theoretical derivations

We show more details in obtaining the dispersion relation (2) of the manuscript. For obtaining irreps *R* of layer single groups we used Bilbao Crystallographic Server [32] for space groups that correspond to the layer single groups of interest. Obtained matrices are given in Tables S1-S3.

Table S1 Matrices of representation U_1 and 2DPV corresponding to *Dg*33. Diperiodic plane is *xz*.

*Dg*33	$(\hat{E}\|\vec{0})$	$\left(\hat{C}_2^z\middle\|\frac{1}{2}\vec{a}_3\right)$	$\left(\hat{\sigma}_{xz}\middle\|\frac{1}{2}\vec{a}_1\right)$	$\left(\hat{\sigma}_{yz}\middle\|\frac{1}{2}\vec{a}_1+\frac{1}{2}\vec{a}_3\right)$
U_1	$\begin{pmatrix}1 & 0\\ 0 & 1\end{pmatrix}$	$\begin{pmatrix}i & 0\\ 0 & -i\end{pmatrix}$	$\begin{pmatrix}0 & -1\\ 1 & 0\end{pmatrix}$	$\begin{pmatrix}0 & i\\ i & 0\end{pmatrix}$
$\hat{h}'$	$\begin{pmatrix}1 & 0\\ 0 & 1\end{pmatrix}$	$\begin{pmatrix}-1 & 0\\ 0 & 1\end{pmatrix}$	$\begin{pmatrix}1 & 0\\ 0 & 1\end{pmatrix}$	$\begin{pmatrix}-1 & 0\\ 0 & 1\end{pmatrix}$

Table S2 Matrices of representation U_1 and 2DPV corresponding to *Dg*43. Diperiodic plane is *xz*.

*Dg*43	$(\hat{E}\|\vec{0})$	$\left(\hat{C}_2^z\middle\|\frac{1}{2}\vec{a}_1\right)$	$\left(\hat{C}_2^y\middle\|\frac{1}{2}\vec{a}_3\right)$	$\left(\hat{C}_2^x\middle\|\frac{1}{2}\vec{a}_3-\frac{1}{2}\vec{a}_1\right)$
U_1	$\begin{pmatrix}1 & 0\\ 0 & 1\end{pmatrix}$	$\begin{pmatrix}1 & 0\\ 0 & -1\end{pmatrix}$	$\begin{pmatrix}0 & 1\\ 1 & 0\end{pmatrix}$	$\begin{pmatrix}0 & -1\\ 1 & 0\end{pmatrix}$
$\hat{h}'$	$\begin{pmatrix}1 & 0\\ 0 & 1\end{pmatrix}$	$\begin{pmatrix}-1 & 0\\ 0 & 1\end{pmatrix}$	$\begin{pmatrix}-1 & 0\\ 0 & -1\end{pmatrix}$	$\begin{pmatrix}1 & 0\\ 0 & -1\end{pmatrix}$
*Dg*43	$(\hat{\imath}\|\vec{0})$	$\left(\hat{\sigma}_{xy}\middle\|-\frac{1}{2}\vec{a}_1\right)$	$\left(\hat{\sigma}_{xz}\middle\|-\frac{1}{2}\vec{a}_3\right)$	$\left(\hat{\sigma}_{yz}\middle\|\frac{1}{2}\vec{a}_1-\frac{1}{2}\vec{a}_3\right)$
U_1	$\begin{pmatrix}0 & -i\\ i & 0\end{pmatrix}$	$\begin{pmatrix}0 & i\\ i & 0\end{pmatrix}$	$\begin{pmatrix}-i & 0\\ 0 & i\end{pmatrix}$	$\begin{pmatrix}-i & 0\\ 0 & -i\end{pmatrix}$
$\hat{h}'$	$\begin{pmatrix}-1 & 0\\ 0 & -1\end{pmatrix}$	$\begin{pmatrix}1 & 0\\ 0 & -1\end{pmatrix}$	$\begin{pmatrix}1 & 0\\ 0 & 1\end{pmatrix}$	$\begin{pmatrix}-1 & 0\\ 0 & 1\end{pmatrix}$

Table S3 Matrices of representation T_1 and 2DPV corresponding to *Dg*45. Diperiodic plane is *yz*.

*Dg*45	$(\hat{E}\|\vec{0})$	$\left(\hat{C}_2^z\middle\|\frac{1}{2}\vec{a}_3\right)$	$\left(\hat{C}_2^y\middle\|\frac{1}{2}\vec{a}_2+\frac{1}{2}\vec{a}_3\right)$	$\left(\hat{C}_2^x\middle\|\frac{1}{2}\vec{a}_2\right)$
T_1	$\begin{pmatrix}1 & 0\\ 0 & 1\end{pmatrix}$	$\begin{pmatrix}i & 0\\ 0 & -i\end{pmatrix}$	$\begin{pmatrix}-i & 0\\ 0 & -i\end{pmatrix}$	$\begin{pmatrix}1 & 0\\ 0 & -1\end{pmatrix}$
$\hat{h}'$	$\begin{pmatrix}1 & 0\\ 0 & 1\end{pmatrix}$	$\begin{pmatrix}-1 & 0\\ 0 & 1\end{pmatrix}$	$\begin{pmatrix}1 & 0\\ 0 & -1\end{pmatrix}$	$\begin{pmatrix}-1 & 0\\ 0 & -1\end{pmatrix}$
*Dg*45	$(\hat{\imath}\|\vec{0})$	$\left(\hat{\sigma}_{xy}\middle\|-\frac{1}{2}\vec{a}_3\right)$	$\left(\hat{\sigma}_{xz}\middle\|-\frac{1}{2}\vec{a}_2-\frac{1}{2}\vec{a}_3\right)$	$\left(\hat{\sigma}_{yz}\middle\|-\frac{1}{2}\vec{a}_2\right)$
T_1	$\begin{pmatrix}0 & 1\\ 1 & 0\end{pmatrix}$	$\begin{pmatrix}0 & -i\\ i & 0\end{pmatrix}$	$\begin{pmatrix}0 & -i\\ -i & 0\end{pmatrix}$	$\begin{pmatrix}0 & -1\\ 1 & 0\end{pmatrix}$
$\hat{h}'$	$\begin{pmatrix}-1 & 0\\ 0 & -1\end{pmatrix}$	$\begin{pmatrix}1 & 0\\ 0 & -1\end{pmatrix}$	$\begin{pmatrix}-1 & 0\\ 0 & 1\end{pmatrix}$	$\begin{pmatrix}1 & 0\\ 0 & 1\end{pmatrix}$

We obtain the matrices of representation $D = R \oplus R^*$ from matrices in Tables S1-S3 in the following way. If functions ψ_1 and ψ_2 belong to irreps *R* from Tables S1-S3, then ψ_1^* and ψ_2^* belong to irrep R^* so functions $\varphi_1 = (\psi_1 + \psi_1^*)/2$, $\varphi_2 = (\psi_1 - \psi_1^*)/(2i)$, $\varphi_3 = (\psi_2 + \psi_2^*)/2$ and $\varphi_4 = (\psi_2 - \psi_2^*)/(2i)$ transform according to the representation *D*. The final result is given in Tables S4-S6.

Table S4 Matrices of representation *D* corresponding to *Dg*33. Diperiodic plane is *xz*, while $\bar{1} = -1$.

*Dg*33	$(\hat{E}\|\vec{0})$	$\left(\hat{C}_2^z\middle\|\frac{1}{2}\vec{a}_3\right)$	$\left(\hat{\sigma}_{xz}\middle\|\frac{1}{2}\vec{a}_1\right)$	$\left(\hat{\sigma}_{yz}\middle\|\frac{1}{2}\vec{a}_1+\frac{1}{2}\vec{a}_3\right)$
D	$\begin{pmatrix}1 & 0 & 0 & 0\\ 0 & 1 & 0 & 0\\ 0 & 0 & 1 & 0\\ 0 & 0 & 0 & 1\end{pmatrix}$	$\begin{pmatrix}0 & \bar{1} & 0 & 0\\ 1 & 0 & 0 & 0\\ 0 & 0 & 0 & 1\\ 0 & 0 & \bar{1} & 0\end{pmatrix}$	$\begin{pmatrix}0 & 0 & \bar{1} & 0\\ 0 & 0 & 0 & \bar{1}\\ 1 & 0 & 0 & 0\\ 0 & 1 & 0 & 0\end{pmatrix}$	$\begin{pmatrix}0 & 0 & 0 & \bar{1}\\ 0 & 0 & 1 & 0\\ 0 & \bar{1} & 0 & 0\\ 1 & 0 & 0 & 0\end{pmatrix}$

Table S5 Matrices of representation *D* corresponding to *Dg*43. Diperiodic plane is *xz*, while $\overline{1} = -1$.

*Dg*43	$(\hat{E}\|\vec{0})$	$\left(\hat{C}_2^z\middle\|\frac{1}{2}\vec{a}_1\right)$	$\left(\hat{C}_2^y\middle\|\frac{1}{2}\vec{a}_3\right)$	$\left(\hat{C}_2^x\middle\|\frac{1}{2}\vec{a}_3-\frac{1}{2}\vec{a}_1\right)$
D	$\begin{pmatrix}1&0&0&0\\0&1&0&0\\0&0&1&0\\0&0&0&1\end{pmatrix}$	$\begin{pmatrix}1&0&0&0\\0&1&0&0\\0&0&\overline{1}&0\\0&0&0&\overline{1}\end{pmatrix}$	$\begin{pmatrix}0&0&1&0\\0&0&0&1\\1&0&0&0\\0&1&0&0\end{pmatrix}$	$\begin{pmatrix}0&0&\overline{1}&0\\0&0&0&\overline{1}\\1&0&0&0\\0&1&0&0\end{pmatrix}$
*Dg*43	$(\hat{\imath}\|\vec{0})$	$\left(\hat{\sigma}_{xy}\middle\|-\frac{1}{2}\vec{a}_1\right)$	$\left(\hat{\sigma}_{xz}\middle\|-\frac{1}{2}\vec{a}_3\right)$	$\left(\hat{\sigma}_{yz}\middle\|\frac{1}{2}\vec{a}_1-\frac{1}{2}\vec{a}_3\right)$
D	$\begin{pmatrix}0&0&0&\overline{1}\\0&0&1&0\\0&1&0&0\\\overline{1}&0&0&0\end{pmatrix}$	$\begin{pmatrix}0&0&0&1\\0&0&\overline{1}&0\\0&1&0&0\\\overline{1}&0&0&0\end{pmatrix}$	$\begin{pmatrix}0&\overline{1}&0&0\\1&0&0&0\\0&0&0&1\\0&0&\overline{1}&0\end{pmatrix}$	$\begin{pmatrix}0&\overline{1}&0&0\\1&0&0&0\\0&0&0&\overline{1}\\0&0&1&0\end{pmatrix}$

Table S6 Matrices of representation *D* corresponding to *Dg*45. Diperiodic plane is *yz*, while $\overline{1} = -1$.

*Dg*45	$(\hat{E}\|\vec{0})$	$\left(\hat{C}_2^z\middle\|\frac{1}{2}\vec{a}_3\right)$	$\left(\hat{C}_2^y\middle\|\frac{1}{2}\vec{a}_2+\frac{1}{2}\vec{a}_3\right)$	$\left(\hat{C}_2^x\middle\|\frac{1}{2}\vec{a}_2\right)$
D	$\begin{pmatrix}1&0&0&0\\0&1&0&0\\0&0&1&0\\0&0&0&1\end{pmatrix}$	$\begin{pmatrix}0&1&0&0\\\overline{1}&0&0&0\\0&0&0&\overline{1}\\0&0&1&0\end{pmatrix}$	$\begin{pmatrix}0&\overline{1}&0&0\\1&0&0&0\\0&0&0&\overline{1}\\0&0&1&0\end{pmatrix}$	$\begin{pmatrix}1&0&0&0\\0&1&0&0\\0&0&\overline{1}&0\\0&0&0&\overline{1}\end{pmatrix}$
*Dg*45	$(\hat{\imath}\|\vec{0})$	$\left(\hat{\sigma}_{xy}\middle\|-\frac{1}{2}\vec{a}_3\right)$	$\left(\hat{\sigma}_{xz}\middle\|-\frac{1}{2}\vec{a}_2-\frac{1}{2}\vec{a}_3\right)$	$\left(\hat{\sigma}_{yz}\middle\|-\frac{1}{2}\vec{a}_2\right)$
D	$\begin{pmatrix}0&0&1&0\\0&0&0&1\\1&0&0&0\\0&1&0&0\end{pmatrix}$	$\begin{pmatrix}0&0&0&\overline{1}\\0&0&1&0\\0&1&0&0\\\overline{1}&0&0&0\end{pmatrix}$	$\begin{pmatrix}0&0&0&\overline{1}\\0&0&1&0\\0&\overline{1}&0&0\\1&0&0&0\end{pmatrix}$	$\begin{pmatrix}0&0&\overline{1}&0\\0&0&0&\overline{1}\\1&0&0&0\\0&1&0&0\end{pmatrix}$

Group projector to the totally symmetric irreducible representation is given by:

$$\hat{P} = \frac{1}{|G(\boldsymbol{k}_0)|}\sum \hat{D}\otimes\hat{D} \otimes \hat{h}'$$

where the sum is over little group elements $G(\boldsymbol{k}_0)$. In our three cases this included the whole layer single group. Obtained projection operator is 32-dimensional. By applying $\hat{P}$ to general 32-component vector consistent with TRS-constrained matrix $\widehat{W}$:

$$\widehat{W} = i\begin{pmatrix} 0 & \langle \boldsymbol{v}_1| & \langle \boldsymbol{v}_2| & \langle \boldsymbol{v}_3| \\ -\langle \boldsymbol{v}_1| & 0 & \langle \boldsymbol{v}_4| & \langle \boldsymbol{v}_5| \\ -\langle \boldsymbol{v}_2| & -\langle \boldsymbol{v}_4| & 0 & \langle \boldsymbol{v}_6| \\ -\langle \boldsymbol{v}_3| & -\langle \boldsymbol{v}_5| & -\langle \boldsymbol{v}_6| & 0 \end{pmatrix},$$

we get symmetry constrained vectors $\boldsymbol{v}_j$. Final result is given in the Table S7.

Table S7 Form of vectors $\boldsymbol{v}_j$ $(j = 1,2,\dots,6)$ required by symmetry, for the layer single groups *Dg*33, *Dg*43 and *Dg*45. Components of vectors are along ***a***- and ***c***-axes for groups *Dg*33 and *Dg*43, and ***b***- and ***c***-axes for group Dg45 respectively. The ***a***-, ***b***- and ***c***-axes are orthorhombic axes for corresponding space groups 29, 54 and 57 respectively.

	*Dg*33	*Dg*43	*Dg*45
$\boldsymbol{v}_1$	$\begin{pmatrix} 0 \\ v_{1c} \end{pmatrix}$	$\begin{pmatrix} 0 \\ v'_{1c} \end{pmatrix}$	$\begin{pmatrix} 0 \\ 0 \end{pmatrix}$
$\boldsymbol{v}_2$	$\begin{pmatrix} v_{2a} \\ v_{2c} \end{pmatrix}$	$\begin{pmatrix} v'_{2a} \\ 0 \end{pmatrix}$	$\begin{pmatrix} v''_{2b} \\ v''_{2c} \end{pmatrix}$
$\boldsymbol{v}_3$	$\begin{pmatrix} 0 \\ v_{3c} \end{pmatrix}$	$\begin{pmatrix} v'_{3a} \\ 0 \end{pmatrix}$	$\begin{pmatrix} 0 \\ v''_{3c} \end{pmatrix}$
$\boldsymbol{v}_4$	$\begin{pmatrix} 0 \\ v_{3c} \end{pmatrix}$	$\begin{pmatrix} v'_{3a} \\ 0 \end{pmatrix}$	$\begin{pmatrix} 0 \\ v''_{3c} \end{pmatrix}$
$\boldsymbol{v}_5$	$\begin{pmatrix} v_{2a} \\ -v_{2c} \end{pmatrix}$	$\begin{pmatrix} -v'_{2a} \\ 0 \end{pmatrix}$	$\begin{pmatrix} v''_{2b} \\ -v''_{2c} \end{pmatrix}$
$\boldsymbol{v}_6$	$\begin{pmatrix} 0 \\ v_{1c} \end{pmatrix}$	$\begin{pmatrix} 0 \\ -v'_{1c} \end{pmatrix}$	$\begin{pmatrix} 0 \\ 0 \end{pmatrix}$

If we insert values for $\boldsymbol{v}_j$ into the Eq. (9) of the main text, we get the dispersion (2). Note that the form of Hamiltonian $\widehat{H}'$ required by the Table S7 is valid only in the basis that belongs to the representation *D* given in Tables S4-S6. On the other hand, eigenvalues of $\widehat{H}'$ are invariant, and are therefore the same in every basis.

The effective mass calculation

Next we show that the dispersion (2) leads to zero effective mass. We take the dispersion for $E_1(\boldsymbol{q})$, obtained from Eq. (2) of the main manuscript by taking plus signs, as an example. The proof for other bands, including Dirac-like (1) is analogous. Let us define the matrix:

$$\hat{S}(q_1, q_2) = \begin{pmatrix} \frac{\partial^2}{(\partial q_1)^2} E_1(q_1, 0) & \left[\frac{\partial^2}{\partial q_1 \partial q_2} E_1(q_1, q_2)\right]_{q_2=0} \\ \left[\frac{\partial^2}{\partial q_2 \partial q_1} E_1(q_1, q_2)\right]_{q_1=0} & \frac{\partial^2}{(\partial q_2)^2} E_1(0, q_2) \end{pmatrix}.$$

The matrix element $\left[\frac{\partial^2}{\partial q_1 \partial q_2} E_1(q_1, q_2)\right]_{q_2=0}$ means that firstly we take the derivative with respect to q_2, than take $q_2=0$, and then take derivative with respect to q_1 (and analogously for the other off-diagonal element). The matrix $\hat{S}$ in terms of Dirac delta function reads:

$$\hat{S}(q_1, q_2) = \begin{pmatrix} 2u_1\delta(q_1) & 0 \\ 0 & 2u_2\delta(q_2) \end{pmatrix}.$$

Function $E_1(q_1, q_2)$ has minimum for $q_1 = q_2 = 0$, so the effective mass tensor is:

$$\widehat{\mathrm{m}}_{\mathrm{eff}} = \hbar^2 \left[\hat{S}(q_1, q_2)\right]^{-1}|_{q_1=q_2=0}.$$

Using the interpretation of delta-function as being infinite at zero, we get $\widehat{\mathrm{m}}_{\mathrm{eff}} = \hat{0}$.

The density of states calculation

Here we show how one obtains the density of states (DOS) for FT dispersion, starting from the general definition of DOS. First we define:

$$\varepsilon_+ = \left|u_1|q_1| + u_2|q_2|\right|,$$

$$\varepsilon_- = \left|u_1|q_1| - u_2|q_2|\right|.$$

The definition for DOS reads:

$$\rho_\pm(\varepsilon) = \frac{1}{4\pi^2}\int_{-\frac{\pi}{a}}^{\frac{\pi}{a}} dq_1 \int_{-\frac{\pi}{b}}^{\frac{\pi}{b}} dq_2\, \delta(\varepsilon - \varepsilon_\pm(q_1, q_2)) =$$

$$= \frac{1}{\pi^2}\int_0^{\frac{\pi}{a}} dq_1 \int_0^{\frac{\pi}{b}} dq_2\, \delta(\varepsilon - \varepsilon_\pm(q_1, q_2)),$$

where we have reduced integration to the first quadrant. We introduce the substitution:

$$q_1 = \frac{1}{2u_1}x + \frac{1}{2u_1}y,$$

$$q_2 = \frac{1}{2u_2}x - \frac{1}{2u_2}y,$$

with the corresponding modulus of Jacobian determinant $|J| = \frac{1}{2u_1u_2}$. The range of integration in new variables becomes:

$$0 \le x \le u_1\frac{\pi}{a} + u_2\frac{\pi}{b},$$

$$-\frac{\pi u_2}{b} \le y \le \frac{\pi u_1}{a}.$$

It follows:

$$\rho_+(\varepsilon) = \frac{1}{2u_1u_2\pi^2}\int_0^{u_1\frac{\pi}{a}+u_2\frac{\pi}{b}} dx \int_{-\frac{\pi u_2}{b}}^{\frac{\pi u_1}{a}} dy\, \delta(\varepsilon - x) =$$

$$= \begin{cases} \frac{1}{2u_1u_2\pi}\left(\frac{u_1}{a}+\frac{u_2}{b}\right); 0 < \varepsilon < \frac{\pi u_1}{a}+\frac{u_2\pi}{b} \\ \frac{1}{4u_1u_2\pi}\left(\frac{u_1}{a}+\frac{u_2}{b}\right); \varepsilon = 0 \\ 0; \varepsilon < 0 \end{cases}$$

which, after taking in account the particle-hole symmetry for bands $\pm\varepsilon_+$, gives:

$$\rho_1(\varepsilon) = \frac{1}{2u_1u_2\pi}\left(\frac{u_1}{a}+\frac{u_2}{b}\right),$$

for sufficiently small $|\varepsilon|$. Similarly, we get for ε_-:

$$\rho_-(\varepsilon) = \frac{1}{2u_1u_2\pi^2}\int_0^{u_1\frac{\pi}{a}+u_2\frac{\pi}{b}} dx \int_{-\frac{\pi u_2}{b}}^{\frac{\pi u_1}{a}} dy\, \delta(\varepsilon - |y|) =$$

$$= \begin{cases} \frac{1}{u_1u_2\pi}\left(\frac{u_1}{a}+\frac{u_2}{b}\right); 0 < \varepsilon < min\left\{\frac{\pi u_1}{a}, \frac{u_2\pi}{b}\right\} \\ \frac{1}{2u_1u_2\pi}\left(\frac{u_1}{a}+\frac{u_2}{b}\right); \varepsilon = 0 \\ 0; \varepsilon < 0 \end{cases}.$$

Particle-hole symmetry for bands $\pm\varepsilon_-$ implies, for sufficiently small $|\varepsilon|$:

$$\rho_2(\varepsilon) = \frac{1}{u_1u_2\pi}\left(\frac{u_1}{a}+\frac{u_2}{b}\right).$$

After the inclusion of spin degeneracy, and using $u_1 = \hbar v_a$, $u_2 = \hbar v_b$, the total DOS for small $|\varepsilon|$ reads, in terms of Fermi velocities:

$$\rho(\varepsilon) \approx \frac{3}{\pi\hbar}\left(\frac{1}{av_b}+\frac{1}{bv_a}\right).$$

Algorithm used in ab initio search

1. **One chemical element is chosen** from the main groups of the periodic table (IIIA, IVA and VA). Particularly we considered B, C, Si or P.
2. **Setup of initial parameters.** Initial fractional coordinates of a single atom, lattice vectors and one of diperiodic groups, Dg33, Dg43 or Dg45, are chosen. The initial lattice vectors and coordinates are chosen such that bond lengths in the system are as close as possible to typical bond lengths between atoms of a given element. This is done manually. Set up the initial value of variable *current minimal energy* to a large value, i.e. DBL_MAX (predefined value in the C++ language standard). Set up the initial *scaling factors* for lattice vectors. Value of 0.8 was a usual choice.
3. Scale lattice vectors by the current *scaling factors*.
4. Atomic positions of remaining atoms in a unit cell are generated based on Wyckoff equivalent positions for the chosen group.
5. **Screening of possibly stable geometries.** The generated crystal structure (from combination of fractional coordinates and scaled lattice vectors) is checked if it is *likely* stable by analyzing eventual clustering of its atomic positions to disjoined set of clusters. The structure is assumed as unstable and disregarded for further calculations if it has more than 2 disjoined clusters. Two clusters are considered disjoined, if distance between two atoms closest to each other, but belonging to different clusters, is larger or smaller by more than n Å than the sum of their covalent radii. n = 0.3 Å was usually used for most of elements. Larger values of

n up to 0.5 Å are used for carbon, for which it is known to make a larger range of possible bond lengths. This step is done in order to speed up the search of stable structures.

6. **Symmetry-constrained geometry optimization.** If the given structure is not disregarded at the step 5 as an unsuitable initial geometry, a geometry optimization is conducted with constrained diperiodic group, i.e. its corresponding space group. Otherwise, go to the step 9. Density functional theory (DFT)-based software Siesta [S2] is used for calculations of energies and atomic forces during the group-constrained geometry optimization.
7. **Can the symmetry be preserved?** Full unconstrained structural optimization is conducted using the Siesta code. Initial geometry for the optimization is the geometry obtained at the step 6. The optimized geometry is checked for eventual breaking of the symmetry (the diperiodic group, i.e. its corresponding space group) after the full structural optimization. Also check the structural stability of the crystal using the same method described at the step 5.
8. If the symmetry is preserved and the structural stability is confirmed at the step 7, compare total energy with the *current minimal energy*. If it is a smaller one then promote it to the *current minimal energy*, and save atomic coordinates of this structure.
9. Increase scaling factors by 0.02. If they are smaller than 1.2 return to the step 3. Otherwise continue to the step 10.
10. Calculate electronic band structure for the most stable system (*current minimal*) using the Siesta code and analyze the band structure.

All *ab initio* calculations were done using DFT as implemented in the Siesta code [S2]. Space groups from Table 1 were used, which correspond to diperiodic groups, when unit cells were constructed. Lattice vector perpendicular to diperiodic plane was always 15 Å. We utilized the Perdew-Burke-Ernzerhof form of the exchange-correlation functional [S3]. The behavior of valence electrons was described by norm-conserving Troullier-Martins pseudopotential [S4]. We used a double-zeta polarized basis. The mesh cutoff energy of 250 Ry was used, which was sufficient to achieve a total energy convergence of better than 0.1 meV per unit cell during the self-consistency iterations of all calculations. Structures were considered as optimized when maximal force on atoms dropped below 0.04 eV/Å. In the search algorithm a 8 x 8 k-point Monkhorst-Pack mesh in plane of BZ corresponding to the plane of 2D materials was employed and only gamma point was used in the perpendicular direction. A denser k-point mesh of 12 x 12 was used for further optimization and calculation of band structure and density of states of the most stable structures obtained by the search algorithm.

Bands in Fig. 2(b) were obtained on 300 x 300 k-point grid around the corner of BZ (point R).

Molecular dynamics simulation, which confirmed the structural stability of P (Dg45) system, was conducted for 5 ps in 5000 steps of 1fs. Temperature was fixed at 100 K using the Nosé-Hoover thermostat. A super-cell comprising 3 x 3 x 1 repetition of a unit cell containing 36 P atoms was employed in the simulation.

ADDITIONAL REFERENCES

[S1] Wang, J.; Huang, H.; Duan, W.; Liu, Z. Identifying Dirac cones in carbon allotropes with square symmetry *J. Chem. Phys.* 2013, **139,** 184701

[S2] Soler. J. M.; Artacho, E.; Gale, J. D.; Garcia, A.; Junquera, J. P.; Ordejon, P.; Sanchez Portal. The SIESTA method for ab initio order-N materials simulation. *J. Phys. Cond. Mat.* 2002, **14**, 2745-2779.

[S3] Perdew, J. P.; Burke, K.; Ernzerhof, M. Generalized gradient approximation made simple. *Phys. Rev. Lett.* 1996, **77**, 3865-3868.

[S4] Troullier, N.; Martins, J. L. Efficient pseudopotentials for plane-wave calculations. *Phys. Rev. B* 1991, **43**, 1993-2006.

Optical and Quantum Electronics (2024) 56:1262
https://doi.org/10.1007/s11082-024-06722-y

Centrosymmetric, non-symmorphic, non-magnetic, spin–orbit coupled layers without Dirac cones

Vladimir Damljanović[1]

Received: 18 September 2023 / Accepted: 20 February 2024

Abstract
While considering the appearance of Dirac cones in spin–orbit coupled two-dimensional materials, Young and Kane (Phys Rev Lett 115:126803, 2015) have found that, in the absence of other symmetries, spatial-, time-reversal and vertical glide plane (or horizontal screw rotation) symmetry give four-fold degenerate Dirac point at the time-reversal invariant momentum along the fractional translation. Here we show in which cases additional symmetries lead to Dirac line instead of Dirac cone in the band structure. We found three centrosymmetric, non-symmorphic layer double groups with line-like degeneracies instead of nodal points. We show that besides these Dirac lines, no other band contacts occur, including the accidental ones. Our results are illustrated using a tight binding example arising from *s*-orbitals on two atoms in the primitive cell. Finally, we discussed ways towards realistic materials where such features in the electronic dispersion are expected to appear.

Keywords Dirac cones · Dirac lines · Two-dimensional materials · Spin–orbit coupling · Non-symmorphic symmetry

1 Introduction

Dirac cones near the Fermi level in the electronic band structure of two- (2D) and three-dimensional (3D) materials contribute to interesting physical properties. These include high electron mobility, well defined chirality or non-zero quantum Hall conductance in the magnetic field (Feng et al. 2021; Armitage et al. 2018; Gao et al. 2019). In that context, especially interesting are materials in which non-negligible spin–orbit coupling (SOC) does not open a gap.

Group theoretical techniques were widely applied in Quantum mechanics in the time span of almost one century and are increasingly used nowadays. Group theoretical analysis of vibrations (Wigner 1930; Dresselhaus et al. 2007), extension of spin groups concept to quasi one-dimensional systems (Lazić et al. 2013; Lazić and Damnjanović 2014; Lazić 2016) and explanation and prediction of electronic dispersions near points in the Brillouin zone (BZ) of 3D materials (Mañes 2012; Bradlyn et al. 2016) are among many

✉ Vladimir Damljanović
damlja@ipb.ac.rs

[1] Institute of Physics Belgrade, University of Belgrade, Pregrevica 118, Belgrade 11000, Serbia

examples. In that sense, it was shown that non-symmorphic symmetry leads to nodal points or lines in the band structure due to formation of hourglass dispersion (Young and Kane 2015) (n-hourglass dispersion in 3D crystals with screw symmetries greater than two Zeng et al. 2020), which (among many other things) led to complete list of band contacts in (hexagonal Zhang et al. 2018, orthorhombic Leonhardt et al. 2021 and tetragonal Hirschmann et al. 2021) 3D crystals (Wu et al. 2020). In 2D materials, *in the absence of other symmetries*, strong SOC, presence of time-reversal (TRS), space-inversion and vertical glide plane (or horizontal screw rotation) ensure Dirac cone at the BZ boundary point along the only fractional translation (Young and Kane 2015). Question remains if and in which cases additional symmetries transform the Dirac cone into something else?

Here we show that in three layer groups, Dirac lines appear instead of Dirac cones. By using non-crossing rule, we further show that no other band contacts appear, besides these Dirac lines. We use the complete set of electronic dispersions (shown graphically) in non-magnetic materials near high-symmetry BZ points (HSPs) and lines (HSLs) (Damljanović and Lazić 2023) in our search. Results of Damljanović and Lazić (2023) were not obtained by the method of Young and Kane (2015) but using allowed (co)representations (correps) of all groups of wave vector in all layer groups. Complete list for all single- and double-, ordinary or gray layer groups is available on the internet (nanolab.rs) (Nikolić et al. 2022). Results of Damljanović and Lazić (2023) are confirmed in many experimental and numerical band structures of 2D materials, such as α-Bismuthene (Kowalczyk et al. 2020) and HfB_2 (Liu et al. 2019), which corroborate their validity.

2 Method

Our method starts with the search of band structures from Damljanović and Lazić (2023) among all centrosymmetric, non-symmorphic layer double groups without horizontal glide planes. After omitting groups with Dirac cones predicted in Young and Kane (2015), the remaining groups are then analyzed for appearance of accidental band contacts. This was done in two ways: by application of the non-crossing rule (Landau and Lifshitz 1981) (von Neumann–Wigner theorem 1929, 2000) and by subducing results for 3D space groups (Leonhardt et al. 2021; Hirschmann et al. 2021) onto layers. Adding pure vertical translation to layer group gives corresponding space group. On the other hand, from corresponding space group one gets original layer group by identifying the direction in which only pure translations act (z-axis direction in the layer group notation of Kopsky and Litvin (2002)). One compares symmetry elements of corresponding space group and the original layer group and identifies crystallographic axes of space group (Hahn 2005), with the ones (including z-direction) of the original layer group (Kopsky and Litvin 2002). In some space groups (*e.g* the tetragonal ones) z-axis determination is simple, while it can be much more complicated in orthorhombic groups, where there is no preferred direction and where it can even happen that one space group corresponds to two different layer groups. Recent upgrade in C2DB database (Fu et al. 2024), gives a layer group and the corresponding space group (the space group of AA-stacking) of all 2D materials in it, which significantly simplifies application of existing abstract group theoretical results to realistic 2D materials.

For the tight-binding model we recall the fine structure Hamiltonian (Berestetskii et al. 1982):

$$\widehat{H}(\mathbf{r}) = \left(-\frac{\hbar^2}{2m}\Delta + V(\mathbf{r}) - \frac{\hbar^4}{8m^3c^2}\Delta^2 + \frac{\hbar^2}{8m^2c^2}\Delta V(\mathbf{r})\right)\widehat{\sigma}_0 + \frac{\hbar^2}{4im^2c^2}\widehat{\boldsymbol{\sigma}}\cdot[(\nabla V(\mathbf{r}))\times\nabla], \tag{1}$$

where $\widehat{\sigma}_0$ is two-dimensional, unit matrix and $\widehat{\boldsymbol{\sigma}} = \sum_{j=1}^{3}\widehat{\sigma}_j\mathbf{e}_j$ is the vector of Pauli matrices. The terms in the Hamiltonian (1) are: the kinetic energy of the electron, the potential energy of the electron, the relativistic correction to the kinetic energy, the Darwin term and the spin–orbit coupling term, respectively. The Hamiltonian (1) without SOC term has the symmetry of $V(\mathbf{r})$, while only the last term acts non-trivially in the spin space.

The Hamiltonian (1) has the following symmetry properties (Cornwell 1984):

$$\widehat{H}\left(\left\{\widehat{g}|\mathbf{R}\right\}^{-1}\mathbf{r}\right) = \widehat{u}^{\dagger}(\widehat{g})\widehat{H}(\mathbf{r})\widehat{u}(\widehat{g}), \tag{2}$$

$$\widehat{H}^{*}(\mathbf{r}) = \widehat{\sigma}_2^{\dagger}\widehat{H}(\mathbf{r})\widehat{\sigma}_2, \tag{3}$$

where $\left\{\widehat{g}|\mathbf{R}\right\}$ is an element (in Seitz notation) of the symmetry group of material and $\widehat{u}(\widehat{g}) = \begin{pmatrix} e^{i\alpha/2}e^{i\gamma/2}cos\beta/2 & e^{-i\alpha/2}e^{i\gamma/2}sin\beta/2 \\ -e^{i\alpha/2}e^{-i\gamma/2}sin\beta/2 & e^{-i\alpha/2}e^{-i\gamma/2}cos\beta/2 \end{pmatrix}$ represents proper part of the rotation $\widehat{g}$ in the spin space (α, β and γ are the Euler angles). Formulas (2) and (3) are used for finding which of the hoping integrals are mutually equal, which simplifies the tight-binding Hamiltonian.

3 Results

A closer look at Damljanović and Lazić (2023) gives that the following layer groups (without horizontal glide plane) exhibit Dirac lines rather then points: 40^D ($p\,2_1/m\,2/a\,2/m$), 44^D ($p\,2_1/b\,2_1/a\,2/m$) and 63^D ($p\,4/m\,2_1/b\,2/m$). The layer group numbers are according to Kopsky and Litvin (2002), superscript D denotes double group. To these layer groups correspond the following space groups: 51^D ($P\,2_1/m\,2/m\,2/a$, $y=0$), 55^D ($P\,2_1/b\,2_1/a\,2/m$, $z=0$) and 127^D ($P\,4/m\,2_1/b\,2/m$, $z=0$). The space group numbers are according to Hahn (2005). For each space group, plane parallel to the original layer is also given.

Next we investigate if accidental band contacts in the interior of BZ, which could lead to additional Dirac cones, are possible. Note that double degeneracy of bands across the whole BZ makes such a possibility difficult to achieve. Indeed, inspection of allowed extra representations of the little group of wave vector, for corresponding space groups at Bilbao Crystallographic Server Elcoro et al. (2017), shows that it is not possible to avoid band repulsion. In planes of symmetry, Kramers pairs are $+i, -i$ meaning that the accidental band contact should be with another such pair. The bands from each pair, that corresponds to the same extra irrep of the group C_s^D would repel each other. On the other hand, lines of symmetry contain only one two-dimensional, extra irrep which is not sufficient to support accidental band contacts. This is in agreement with the results of Zhang et al. (2023) (published simultaneously with Damljanović and Lazić (2023)), where both essential and accidental band contacts of all (magnetic) layer groups are given in the exhaustive

supplemental material in tabular form, as was done for magnetic space groups published earlier (Tang and Wan 2021; Yu et al. 2022; Liu et al. 2022; Zhang et al. 2022; Tang and Wan 2022).

The same result is obtained from the list of accidental band contacts for 3D orthorhombic (Leonhardt et al. 2021) and tetragonal (Hirschmann et al. 2021) space groups. The subduction to layer groups, from the corresponding space groups, gives only essential band contacts determined by the dimensionality of allowed correps.

Finally, to illustrate our findings, we give the tight binding model for layer group 40^D. The crystal structure of the model is shown in Fig. 1 (visualization with the help of program VESTA Momma and Izumi 2011). The Hamiltonian in the basis $\{|s_1\uparrow\rangle, |s_2\uparrow\rangle, |s_1\downarrow\rangle, |s_2\downarrow\rangle\}$ arising from *s*-orbitals and *up* and *down* spinors is:

$$\hat{H}(\mathbf{k}) = \begin{pmatrix} \hat{H}_{\uparrow}(\mathbf{k}) & \hat{0} \\ \hat{0} & \hat{H}_{\downarrow}(\mathbf{k}) \end{pmatrix}, \tag{4}$$

where

$$\begin{aligned} &\hat{H}_{\uparrow}(\mathbf{k}) = \hat{H}_{\downarrow}(\mathbf{k}) \\ &= \begin{pmatrix} c_0 + 2c_2 cos(\mathbf{k}\cdot\mathbf{b}) & 2cos(\frac{1}{2}\mathbf{k}\cdot\mathbf{a})e^{-\frac{i}{2}\mathbf{k}\cdot\mathbf{a}}(c_1 + c_3 e^{-i\mathbf{k}\cdot\mathbf{b}}) \\ 2cos(\frac{1}{2}\mathbf{k}\cdot\mathbf{a})e^{\frac{i}{2}\mathbf{k}\cdot\mathbf{a}}(c_1 + c_3 e^{i\mathbf{k}\cdot\mathbf{b}}) & c_0 + 2c_2 cos(\mathbf{k}\cdot\mathbf{b}) \end{pmatrix}, \end{aligned} \tag{5}$$

and with c_0, c_1, c_2, c_3 being the real hopping parameters between the parallel spins for the zeroth, the first, the second and the third neighbor, respectively. The electronic band structure, within this model, is:

$$\begin{aligned} &E^{\uparrow}_{1,2}(\mathbf{k}) = E^{\downarrow}_{1,2}(\mathbf{k}) = E_{1,2}(\mathbf{k}) \\ &= c_0 + 2c_2 cos(\mathbf{k}\cdot\mathbf{b}) \pm 2\left|cos\left(\frac{1}{2}\mathbf{k}\cdot\mathbf{a}\right)\right|\sqrt{c_1^2 + c_3^2 + 2c_1 c_3 cos(\mathbf{k}\cdot\mathbf{b})}. \end{aligned} \tag{6}$$

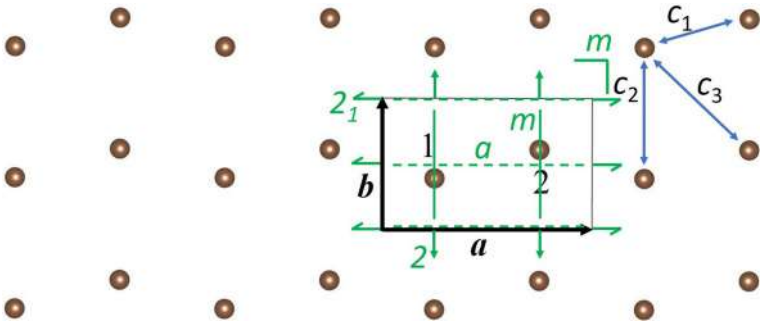

Fig. 1 The crystal structure for the tight-binding model belonging to layer group 40^D. All nuclei are of the same type, they occupy the same horizontal plane and the Wyckoff position 2*c* with $y = 0.39$. Lattice constants $|\mathbf{a}|$ and $|\mathbf{b}|$ are 6.4 and 4 Ångströms, respectively. Green symbols denote symmetry elements: 2 (2_1) - axis (screw axis) of order two, *m* (*a*) - plane (glide plane). Vertical axis of order two and spatial inversion are also present (not shown). Blue arrows illustrate hopping parameters

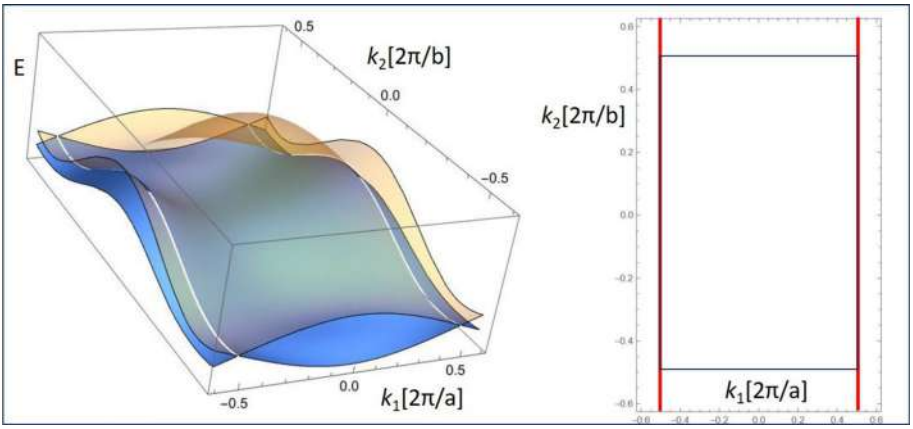

Fig. 2 Band structure of the tight-binding model for c_0, c_1, c_2 and c_3 equal to 2.1, 1.5, 1.1 and 0.8eV respectively (left panel). The positions of four-fold degenerate line nodes $E_1 = E_2$ are denoted by red lines in the reciprocal space (right panel). Black rectangle denotes BZ

Since $|c_0| > |c_1| > |c_2| > |c_3|$, the only touching of these two double degenerate bands, is for $cos\left(\frac{1}{2}\mathbf{k}\cdot\mathbf{a}\right) = 0$. This equation corresponds to nodal lines: $\pm\frac{1}{2}\mathbf{k}_a$ ($\mathbf{k}_a \cdot \mathbf{a} = 2\pi$, $\mathbf{k}_a \cdot \mathbf{b} = 0$), not to nodal points. The band structure is shown in Fig. 2 for particular values of hopping parameters. Double degeneracy of bands across the whole BZ is in accordance with Kramers theorem applied to centrosymmetric crystals.

The four-fold degeneracy of Dirac lines comes from the very construction of correps of (magnetic) little groups $G^M_{\mathbf{k}}$. For $G^M_{\mathbf{k}} = H + \theta s H$, where θ is TRS and s—a symmetry element of the layer group ($s \notin H$), correps of $G^M_{\mathbf{k}}$ are obtained from irreducible representations of H in a way that depends on the sum $S = \sum_{h\in H} \chi\left((\theta s h)^2\right)/|H|$ (χ-character of the particular irreducible representation Δ of the group H of order $|H|$) (Bradley and Cracknell 2010). For S = 1 the dimension of the correp D is as Δ. For $S \in \{-1, 0\}$, the matrices are: $\widehat{D}(h) = \begin{pmatrix} \widehat{\Delta}(h) & \widehat{0} \\ \widehat{0} & \widehat{\Delta}^*\left((\theta s)^{-1} h \theta s\right) \end{pmatrix}$, $\widehat{D}_c(\theta s h) = \begin{pmatrix} \widehat{0} & \widehat{\Delta}\left((\theta s)^2\right) \\ \widehat{I} & \widehat{0} \end{pmatrix} \cdot \widehat{D}^*(h)$. Here $\widehat{I}$ ($\widehat{0}$) are unit (zero) quadratic matrices having the same dimension as Δ, while $h \in H$ (Wigner 1959; Damnjanović 2014). In the case from Fig. 1, H is the semi-direct product of translations and C^D_{2v} and it's only extra, allowed irrep is two-dimensional: $\widehat{\Delta}(\{E|\mathbf{R}\}) = uw\widehat{\sigma}_0$, $\widehat{\Delta}\left(\left\{C_2^y|\mathbf{a}/2 + \mathbf{R}\right\}\right) = -iuw\widehat{\sigma}_2$, $\widehat{\Delta}\left(\left\{\sigma_h|\mathbf{R}\right\}\right) = -iuw\widehat{\sigma}_1$ and $\widehat{\Delta}\left(\left\{\sigma_{yz}|\mathbf{a}/2 + \mathbf{R}\right\}\right) = -iuw\widehat{\sigma}_3$ (Elcoro et al. 2017). Here $w = exp(-i\mathbf{k}\cdot\mathbf{R})$, $\mathbf{k}$ belongs to the Dirac line (away from HSP) and $u = 1$ ($u = -1$) for unbarred (barred) double group elements. One can choose $s = \left\{(\widehat{\sigma}_0, -\widehat{I}_3)|\mathbf{0}\right\}$ (unbarred spatial inversion) so that $\theta s = \left\{(\widehat{\sigma}_2 K, -\widehat{I}_3)|\mathbf{0}\right\}$ (K-complex conjugation, $\widehat{I}_3$-unit three-dimensional matrix). Since S=0, the correp is four-dimensional with $(\theta s)^{-1} h \theta s = h$ and $\widehat{\Delta}\left((\theta s)^2\right) = \widehat{\Delta}\left(\left\{(-\widehat{\sigma}_0, \widehat{I}_3)|\mathbf{0}\right\}\right) = \widehat{\Delta}\left(\left\{\overline{E}|\mathbf{0}\right\}\right) = -\widehat{\sigma}_0$. For construction of allowed irreps of little groups (without TRS) one can consult e.g. Cornwell (1984). Representation matrices of symmetry operators for 40^D in the rectangular basis can be found at the

nanolab.rs web page (Nikolić et al. 2022) and on Bilbao Crystallographic Server (via corresponding space group 51^D).

4 Discussion and conclusion

Besides layer groups treated here, groups 43^D and 45^D also possess Dirac nodal lines (Damljanović and Lazić 2023; Zhang et al. 2023), which is in accordance with Young and Kane (2015) since they have horizontal glide plane and hence are out of the scope of this paper. Additional fixed (Damljanović and Lazić 2023) and movable (Leonhardt et al. 2021) Dirac points in 43^D and 45^D are also caused by group-theoretical and topological laws. Compatibility relations near HSPs and irrep change along HSL connecting them, give the result that e.g. accidental band contacts somewhere at the XU/XS line (Zhang et al. 2023) are not only possible but are unavoidable (and movable), as explained in Hirschmann (2021), for example.

For layer groups of our investigation (40^D, 44^D and 63^D) among others, the features in the electronic band structure are caused by symmetry alone. This points towards realization by search of various materials databases (Haastrup et al. 2018; Gjerding et al. 2021; Mounet et al. 2018) according to the layer or corresponding space group. Particular attention could be payed to layered single crystals whose synthesis has already been reported (Gjerding et al. 2021; Mounet et al. 2018). The Fermi energy (E_F), on the other hand, cannot be determined by using group theory alone. Still, since nodal lines occupy a finite energy range, it should be less difficult to make them cross E_F than some nodal point. Also, the same layer group can be achieved in many different nuclear arrangements in the same primitive cell, which opens the possibility to avoid reactive, radio-active or toxic chemical elements. Future investigations could show how difficult is to realize 2D materials with prescribed symmetry in practice.

Acknowledgements Author acknowledges funding by the Ministry of Science, Technological Development and Innovation of the Republic of Serbia provided by the Institute of Physics Belgrade, University of Belgrade.

Author contributions The author of this manuscript did all steps in research presented in this manuscript and writing of this manuscript by himself.

Funding This work was supported by the Ministry of Science, Technological Development and Innovation of the Republic of Serbia.

Availability of data and materials All data generated or analyzed during this study are included in this published article.

Code availability Not applicable.

Declarations

Conflict of interest The author has no relevant financial or non-financial interests to disclose.

Ethics approval Not applicable.

Consent to participate Not applicable.

Consent for publication Not applicable.

References

Armitage, N.P., Mele, E.J., Vishwanath, A.: Weyl and Dirac semimetals in three-dimensional solids. Rev. Mod. Phys. **90**, 015001 (2018). https://doi.org/10.1103/RevModPhys.90.015001

Berestetskii, V.B., Lifshitz, E.M., Pitaevskii, L.P.: Quantum Electrodynamics. Butterworth-Heinemann, Oxford (1982)

Bradley, C.J., Cracknell, A.P.: The Mathematical Theory of Symmetry in Solids. Oxford University Press, Oxford (2010)

Bradlyn, B., Cano, J., Wang, Z., Vergniory, M.G., Felser, C., Cava, R.J., Bernevig, B.A.: Beyond Dirac and Weyl fermions: unconventional quasiparticles in conventional crystals. Science **353**(6299), 5037 (2016)

Cornwell, J.F.: Group Theory in Physics, vol. 1. Academic Press, London (1984)

Damljanović, V., Lazić, N.: Electronic structures near unmovable nodal points and lines in two-dimensional materials. J. Phys. A: Math. Theor. **56**(21), 215201 (2023). https://doi.org/10.1088/1751-8121/accf51

Damnjanović, M.: Symmetry in Quantum Nonrelativistic Physics. Faculty of Physics, University of Belgrade, Belgrade (2014)

Dresselhaus, M.S., Dresselhaus, G., Jorio, A.: Group Theory. Springer, Berlin (2007)

Elcoro, L., Bradlyn, B., Wang, Z., Vergniory, M.G., Cano, J., Felser, C., Bernevig, B.A., Orobengoa, D., Flor, G., Aroyo, M.I.: Double crystallographic groups and their representations on the Bilbao Crystallographic Server. J. Appl. Crystallogr. **50**(5), 1457–1477 (2017). https://doi.org/10.1107/S1600576717011712

Feng, X., Zhu, J., Wu, W., Yang, S.A.: Two-dimensional topological semimetals. Chin. Phys. B **30**(10), 107304 (2021). https://doi.org/10.1088/1674-1056/ac1f0c

Fu, J., Kuisma, M., Larsen, A.H., Shinohara, K., Togo, A., Thygesen, K.S.: Symmetry classification of 2Dmaterials: layer groups versus space groups. 2D Materials **11**, 035009 (2024). https://doi.org/10.1088/2053-1583/ad3e0c

Gao, H., Venderbos, J.W.F., Kim, Y., Rappe, A.M.: Topological semimetals from first principles. Annu. Rev. Mater. Res. **49**(1), 153–183 (2019). https://doi.org/10.1146/annurev-matsci-070218-010049

Gjerding, M.N., Taghizadeh, A., Rasmussen, A., Ali, S., Bertoldo, F., Deilmann, T., Knøsgaard, N.R., Kruse, M., Larsen, A.H., Manti, S., Pedersen, T.G., Petralanda, U., Skovhus, T., Svendsen, M.K., Mortensen, J.J., Olsen, T., Thygesen, K.S.: Recent progress of the computational 2D materials database (C2DB). 2D Materials **8**(4), 044002 (2021). https://doi.org/10.1088/2053-1583/ac1059

Haastrup, S., Strange, M., Pandey, M., Deilmann, T., Schmidt, P.S., Hinsche, N.F., Gjerding, M.N., Torelli, D., Larsen, P.M., Riis-Jensen, A.C., Gath, J., Jacobsen, K.W., Mortensen, J.J., Olsen, T., Thygesen, K.S.: The computational 2D materials database: high-throughput modeling and discovery of atomically thin crystals. 2D Materials **5**(4), 042002 (2018). https://doi.org/10.1088/2053-1583/aacfc1

Hahn, T.: International Tables of Crystallography Volume A: Space-Group Symmetry. Springer, Dordrecht (2005)

Hirschmann, M.: Topological band crossings in metals, magnets, and non-Hermitian systems. Ph.D. thesis, Faculty of Mathematics and Physics, University of Stuttgart (2021)

Hirschmann, M.M., Leonhardt, A., Kilic, B., Fabini, D.H., Schnyder, A.P.: Symmetry-enforced band crossings in tetragonal materials: Dirac and Weyl degeneracies on points, lines, and planes. Phys. Rev. Mater. **5**, 054202 (2021). https://doi.org/10.1103/PhysRevMaterials.5.054202

Kopsky, V., Litvin, D.B.: International Tables of Crystallography Volume E: Subperiodic Groups. Kluwer, Dordrecht (2002)

Kowalczyk, P.J., Brown, S.A., Maerkl, T., Lu, Q., Chiu, C.-K., Liu, Y., Yang, S.A., Wang, X., Zasada, I., Genuzio, F., Menteş, T.O., Locatelli, A., Chiang, T.-C., Bian, G.: Realization of symmetry-enforced two-dimensional Dirac fermions in nonsymmorphic α-Bismuthene. ACS Nano **14**(2), 1888–1894 (2020). https://doi.org/10.1021/acsnano.9b08136

Landau, L.D., Lifshitz, E.M.: Quantum Mechanics. Butterworth-Heinemann, Oxford (1981)

Lazić, N.: Quasi-classical ground states and magnons in monoperiodic spin systems. Ph.D. thesis, Faculty of Physics, University of Belgrade (2016)

Lazić, N., Damnjanović, M.: Spin ordering in RKKY nanowires: controllable phases in ^{13}C nanotubes. Phys. Rev. B **90**, 195447 (2014). https://doi.org/10.1103/PhysRevB.90.195447

Lazić, N., Milivojević, M., Damnjanović, M.: Spin line groups. Acta Crystallogr. A **69**(6), 611–619 (2013). https://doi.org/10.1107/S0108767313022642. (https://arxiv.org/abs/onlinelibrary.wiley.com/doi/pdf/10.1107/S0108767313022642)

Leonhardt, A., Hirschmann, M.M., Heinsdorf, N., Wu, X., Fabini, D.H., Schnyder, A.P.: Symmetry-enforced topological band crossings in orthorhombic crystals: classification and materials discovery. Phys. Rev. Mater. **5**, 124202 (2021). https://doi.org/10.1103/PhysRevMaterials.5.124202

Liu, Z., Wang, P., Cui, Q., Yang, G., Jin, S., Xiong, K.: Theoretical prediction of HfB_2 monolayer, a two-dimensional Dirac cone material with remarkable Fermi velocity. RSC Adv. **9**, 2740–2745 (2019). https://doi.org/10.1039/C8RA08291J

Liu, G.-B., Zhang, Z., Yu, Z.-M., Yang, S.A., Yao, Y.: Systematic investigation of emergent particles in type-III magnetic space groups. Phys. Rev. B **105**, 085117 (2022). https://doi.org/10.1103/PhysRevB.105.085117

Mañes, J.L.: Existence of bulk chiral fermions and crystal symmetry. Phys. Rev. B **85**, 155118 (2012). https://doi.org/10.1103/PhysRevB.85.155118

Momma, K., Izumi, F.: VESTA3 for three-dimensional visualization of crystal, volumetric and morphology data. J. Appl. Crystallogr. **44**(6), 1272–1276 (2011). https://doi.org/10.1107/S0021889811038970

Mounet, N., Gibertini, M., Schwaller, P., Campi, D., Merkys, A., Marrazzo, A., Sohier, T., Castelli, I.E., Cepellotti, A., Pizzi, G., Marzari, N.: Two-dimensional materials from high-throughput computational exfoliation of experimentally known compounds. Nat. Nanotechnol. **13**, 246–252 (2018). https://doi.org/10.1038/s41565-017-0035-5

Neumann, Jv., Wigner, E.: Ueber das Verhalten von Eigenwerten bei adiabatischen Prozessen. Phys. Z. **30**, 467–470 (1929)

Neumann, J., Wigner, E.: On the behaviour of eigenvalues in adiabatic processes. In: Hettema, H. (ed.) Quantum Chemistry: Classic Scientific Papers, pp. 25–31. World Scientific, Singapore (2000)

Nikolić, B., Milošević, I., Vuković, T., Lazić, N., Dmitrović, S., Popović, Z., Damnjanović, M.: Irreducible and site-symmetry-induced representations of single/double ordinary/grey layer groups. Acta Crystallogr. A **78**(2), 107–114 (2022). https://doi.org/10.1107/S205327332101322X

Tang, F., Wan, X.: Exhaustive construction of effective models in 1651 magnetic space groups. Phys. Rev. B **104**, 085137 (2021). https://doi.org/10.1103/PhysRevB.104.085137

Tang, F., Wan, X.: Complete classification of band nodal structures and massless excitations. Phys. Rev. B **105**, 155156 (2022). https://doi.org/10.1103/PhysRevB.105.155156

Wigner, E.: Ueber die elastischen Eigenschwingungen symmetrischer Systeme. Nachrichten von derGesellschaft der Wissenschaften zu Göttingen, Mathematisch-Physikalische Klasse **30**, 133–146 (1930).

Wigner, E.P.: Group Theory and Its Application to the Quantum Mechanics of Atomic Spectra. Academic Press, London (1959)

Wu, L., Tang, F., Wan, X.: Exhaustive list of topological hourglass band crossings in 230 space groups. Phys. Rev. B **102**, 035106 (2020). https://doi.org/10.1103/PhysRevB.102.035106

Young, S.M., Kane, C.L.: Dirac semimetals in two dimensions. Phys. Rev. Lett. **115**, 126803 (2015). https://doi.org/10.1103/PhysRevLett.115.126803

Yu, Z.-M., Zhang, Z., Liu, G.-B., Wu, W., Li, X.-P., Zhang, R.-W., Yang, S.A., Yao, Y.: Encyclopedia of emergent particles in three-dimensional crystals. Sci. Bull. **67**(4), 375–380 (2022). https://doi.org/10.1016/j.scib.2021.10.023

Zeng, Y., Wang, L., Yao, D.-X.: *n*-hourglass Weyl fermions in nonsymmorphic materials. Phys. Rev. B **101**, 115110 (2020). https://doi.org/10.1103/PhysRevB.101.115110

Zhang, J., Chan, Y.-H., Chiu, C.-K., Vergniory, M.G., Schoop, L.M., Schnyder, A.P.: Topological band crossings in hexagonal materials. Phys. Rev. Mater. **2**, 074201 (2018). https://doi.org/10.1103/PhysRevMaterials.2.074201

Zhang, Z., Liu, G.-B., Yu, Z.-M., Yang, S.A., Yao, Y.: Encyclopedia of emergent particles in type-IV magnetic space groups. Phys. Rev. B **105**, 104426 (2022). https://doi.org/10.1103/PhysRevB.105.104426

Zhang, Z., Wu, W., Liu, G.-B., Yu, Z.-M., Yang, S.A., Yao, Y.: Encyclopedia of emergent particles in 528 magnetic layer groups and 394 magnetic rod groups. Phys. Rev. B **107**, 075405 (2023). https://doi.org/10.1103/PhysRevB.107.075405

Electronic structures near unmovable nodal points and lines in two-dimensional materials

IOP Publishing Journal of Physics A: Mathematical and Theoretical
J. Phys. A: Math. Theor. **56** (2023) 215201 (17pp) https://doi.org/10.1088/1751-8121/accf51

Electronic structures near unmovable nodal points and lines in two-dimensional materials

V Damljanović[1,*] **and N Lazić**[2]

[1] Institute of Physics Belgrade, University of Belgrade, Pregrevica 118, 11000 Belgrade, Serbia
[2] NanoLab, Faculty of Physics, University of Belgrade, Studentski Trg 12, 11001 Belgrade, Serbia

E-mail: damlja@ipb.ac.rs

Received 22 December 2022; revised 12 April 2023
Accepted for publication 21 April 2023
Published 3 May 2023

Abstract

Unmovable nodal points (UNPs) and lines (UNLs) are band crossings whose positions in the Brillouin zone are unaltered by symmetry preserving perturbations. Not only positions but also the band structure in their vicinity are determined by the little group of wave vectors and its irreducible (co)representations. In this paper, we give the full set of electronic dispersions near all UNPs and UNLs in non-magnetic quasi two-dimensional (2D) materials, both with and without spin–orbit coupling (SOC). Analysis of all layer gray single and double groups gives nineteen different quasiparticles, the great majority of which are unavoidable for a 2D material that belongs to a certain layer group. This includes Weyl and Dirac nodal lines, dispersions with quadratic or cubic splitting, anisotropic Weyl and Dirac cones, whose orientation can be varied by e.g. strain *etc*. We indicated quasiparticles that are robust to SOC. For convenience, our results are concisely presented graphically—as a map, not in a tabular, encyclopedia form. They may be of use as checkpoints and/or for fitting experimentally (via e.g. ARPES) and numerically obtained electronic band structures data, as well as for deeper theoretical investigations.

Keywords: two-dimensional materials, linear dispersions, quadratic dispersions, cubic dispersions, symmetry

(Some figures may appear in colour only in the online journal)

* Author to whom any correspondence should be addressed.

1. Introduction

The Fermi–Dirac distribution dictates that most of the material properties depend on the electronic dispersions' shape near the Fermi energy in the Brillouin zone (BZ). On the other hand, these shapes are solely determined by the crystal symmetry and, for non-magnetic materials, the time-reversal symmetry (TRS). Presence of Dirac cones around the BZ K-points of the honeycomb lattice is the most notable example. Experimental discovery of the electric field effect in graphene, fabrication of graphene's three-dimensional (3D) analogue accompanied with the explanation of certain band structure properties using topological laws, brought topological materials into the focus of solid-state science [1–3]. Non-trivial band topology, such as the non-zero Berry phase, originates from singularities of eigenvectors in the reciprocal space. Such singularities often appear at points where two or more bands touch.

In two-dimensional (2D) materials, bands can touch at isolated points or at lines. Band touchings caused by the increased dimensionality of corepresentation (correp) of a little group do not move if the Hamiltonian parameters change, as long as the symmetry is preserved. Such touchings we call unmovable nodal points (UNPs) and lines (UNLs). Weyl/Dirac nodal lines (WNLs)/(DNLs) are examples of UNL, whose presence in a band structure leads to interesting physical properties [4–7]. These include graphene-like density of states (DOSs) [8, 9] and drumhead states whose flat bands may cause strong electron correlations [5, 10].

The explanation of band degeneracies by use of crystal symmetry and TRS appeared almost one century ago [11–13]. It was extended beyond high-symmetry points (HSPs) and lines (HSLs) in the BZ by Zak and coworkers using elementary band representations [14, 15]. Yang and Kane brought some of the band crossings in connection with the appearance of Dirac cones in 2D materials with SOC [16]. In 3D, WNL and DNL are determined by achiral gray double space groups [17], by 230 ordinary/gray single/double space groups [18], by certain black-and-white magnetic space groups [19], and in the presence and absence of spin–orbit coupling (SOC) [20]. Guo *et al* [21, 22] report DNL in the presence of SOC in 2D. On the other hand, full enumeration of layer groups' UNPs hosting fully linear dispersion in non-magnetic 2D materials is a completed task [23]. In Damljanović *et al* [23–25] the Hamiltonians are distinguished from each other by the form of their eigenvalues. The term Dirac was reserved for four-component Hamiltonians with graphene-like, isotropic or anisotropic eigenvalues [23, 26, 27]. There are several physical reasons for this distinction, e.g. the non-vanishing DOS of some dispersions [24, 25] near zero energy. On the other hand, analysis of all dispersions, besides the linear, in 2D materials has not been reported thus far [28]. Recently published reports for (3D) space groups [29–32] could be (in principle) used for layer groups, if one subduces the results for corresponding space groups to 2D BZ. This idea is indeed applied in [33], published a few months after the submission of the present paper. In [34] all massless excitations in 2D and 3D were classified.

In this paper, we calculated the exact shapes of electronic bands near all HSPs and HSLs in the BZ of all layer groups, including cases without and with SOC, in the presence of TRS. It turns out that in the Taylor expansion of Hamiltonians, the relevant terms are up to maximally third order in momentum. We found in total nineteen quasiparticles. Some of them are known (like Dirac cones in graphene), while the remaining are yet to be explored. Our results are presented graphically, as an atlas (map) rather than in a tabular, encyclopedia form, and fit into two figures and a few pages of text/formulas. For all symmetry-constrained Hamiltonians, the eigenvalues are given. We single out quasiparticles that are not destroyed by the inclusion of SOC.

2. Method

To find all possible HSPs and HSLs with multidimensional correps, one has to search through all little groups of all gray layer groups—80 for spinless and 80 for spinful cases. Correps of space groups were tabulated and made available a long time ago [35, 36]. Regarding layer groups, [37] tabulates little groups characters of layer double groups, [38] tabulates irrep matrices for generators of layer single groups, while [39] gives irrep characters of all elements of graphene's layer single group. Exhaustive information on layer groups, their little groups (both single and double, without and with TRS) and their (co)rreps, became publicly available recently [40]. Nikolić *et al* [40] was a starting point of our search.

Symmetry adapted low-energy Hamiltonians were derived from the following formula [23, 41]:

$$\hat{H}(\mathbf{k}_0+\mathbf{q}) = \hat{D}^{\dagger}(g)\,\hat{H}\left(\mathbf{k}_0+\hat{h}'\mathbf{q}\right)\hat{D}(g)\,, \tag{1}$$

where $\mathbf{k}_0$ denotes HSP or belongs to HSL, $g=\left\{\hat{h}\middle|\,\tau_{\hat{h}}\right\}$ is an element (in Seitz notation) of the little group $G_{\mathbf{k}_0}$ ($\hat{h}'\mathbf{k}_0$ is equivalent to $\mathbf{k}_0$), $\hat{h}'$ is an operator reduction of $\hat{h}$ to 2D BZ and $\hat{D}(g)$ is the irrep matrix that corresponds to g. If $-\mathbf{k}_0$ belongs to the star of $\mathbf{k}_0$, the full symmetry group of $\mathbf{k}_0$ is $G_{\mathbf{k}_0}+\theta g_0 G_{\mathbf{k}_0}$, where θ denotes time-reversal and the element $g_0=\left\{\hat{h}_0\middle|\,\tau_{\hat{h}_0}\right\}$ does not belong to $G_{\mathbf{k}_0}$, if $\mathbf{k}_0$ is not the time reversal invariant momentum ($\hat{h}_0'\mathbf{k}_0$ is equivalent to $-\mathbf{k}_0$). The additional constraint on contribution $\hat{H}'$ appearing in the Taylor expansion $\hat{H}(\mathbf{k}_0+\mathbf{q})\approx \hat{H}(\mathbf{k}_0)+\hat{H}'(\mathbf{q})$ is [23, 41]:

$$\hat{H}'^{*}(\mathbf{q}) = \hat{R}^{\dagger}(\theta g_0)\,\hat{H}'\left(-\hat{h}_0'\mathbf{q}\right)\hat{R}(\theta g_0)\,, \tag{2}$$

where $\hat{R}$ is correp matrix (linear part—without complex conjugation) that corresponds to θg_0. As opposed to dispersions, which are invariants uniquely determined by the symmetry, the Hamiltonians can be changed by a different choice of basis wave-functions. However, once the particular Hamiltonian $\hat{H}(\mathbf{q})$ in the vicinity of $\mathbf{k}_0$ is chosen, the Hamiltonian $\hat{H}_p(\mathbf{q})$ near $\mathbf{k}_p\equiv\hat{h}\mathbf{k}_0$ from the star of $\mathbf{k}_0$, is fixed by the following formula:

$$\hat{H}_p(\mathbf{q}) = \hat{R}\left(g_p^{-1}g\right)\hat{H}\left(\hat{h}^{-1}\mathbf{q}\right)\hat{R}^{\dagger}\left(g_p^{-1}g\right), \tag{3}$$

where $g_p=\left\{\hat{h}_p|\tau_p\right\}$ is the representative of the coset that contains the element $g=\left\{\hat{h}|\tau\right\}$ of the layer group, and $\hat{R}$ is the correp matrix of the little group of $\mathbf{k}_0$. In (3) one has to use the very same correp that gives $\hat{H}(\mathbf{q})$ near $\mathbf{k}_0$, not just an equivalent one. Similarly, for dispersions around $\mathbf{k}_p$:

$$E_p(\hat{h}\mathbf{q}) = E(\mathbf{q}). \tag{4}$$

Also, dispersions around two points in the reciprocal space that differ by a vector from the reciprocal lattice are identical. All necessary matrices are available in POLSym code [42] in addition to the web page [40].

Here we focus on eigenvalues of low-energy Hamiltonians, i.e. their functional dependence on $\mathbf{q}$, since they are measurable and invariant (independent on the choice of particular basis), unlike Hamiltonians themselves. The only criterion for classification is if the eigenvalues of

two Hamiltonians have identical functional dependence on $\mathbf{q}$. To avoid unnecessary complication, we do not list here all Hamiltonians that correspond to each particular corep from [40], since many of them can be transformed into each other by the similarity transformation. If two n-component Hamiltonians $\hat{H}_1$ and $\hat{H}_2$, have all eigenvalues the same, then $\hat{H}_2 = \hat{U}\hat{H}_1\hat{U}^\dagger$, with $\hat{U} = \sum_{l=1}^{n} |\Psi_l\rangle \langle\Phi_l|$ being an unitary matrix and $|\Psi_l\rangle$ ($|\Phi_l\rangle$) the normalized eigenvector of $\hat{H}_2$ ($\hat{H}_1$) that corresponds to the eigenvalue E_l, $(l = 1, 2, \ldots, n)$. The proof for this statement uses the spectral form of Hamiltonian: $\hat{U}\hat{H}_1\hat{U}^\dagger = \sum_{l=1}^{n} |\Psi_l\rangle \langle\Phi_l| \sum_{j=1}^{n} E_j |\Phi_j\rangle \langle\Phi_j| \sum_{m=1}^{n} |\Phi_m\rangle \langle\Psi_m| = \sum_{l,j,m=1}^{n} E_j |\Psi_l\rangle \delta_{l,j}\delta_{j,m} \langle\Psi_m| = \sum_{j=1}^{n} E_j |\Psi_j\rangle \langle\Psi_j| = \hat{H}_2$. Therefore, of all Hamiltonians having the same eigenvalues, only one representative is shown. In other words we proved, by exhaustion, that any $\mathbf{k}\cdot\mathbf{p}$ Hamiltonian generated by small corep of gray magnetic layer group can be reduced to one of the forms given below (with the same eigenvalues) by a proper unitary transformation.

To distinguish the anisotropic Dirac and Weyl dispersions whose orientations depend on the parameters of the model and the ones with fixed orientation, we use the following theorem. The quadratic form $f = c_1 q_1^2 + c_3 q_1 q_2 + c_2 q_2^2 = \langle \mathbf{q}| \hat{A} |\mathbf{q}\rangle$, can be reduced to $f = \lambda_1 q_1'^2 + \lambda_2 q_2'^2$, where $q_j' = \langle \lambda_j |\mathbf{q}\rangle$, while λ_j and $|\lambda_j\rangle$ are eigenvalues and eigenvectors of the matrix $\hat{A} = \begin{pmatrix} c_1 & c_3/2 \\ c_3/2 & c_2 \end{pmatrix}$, $(j = 1, 2)$. The λ_j and $|\lambda_j\rangle$ are well known and will not be presented here. The cross-section of f is an ellipse whose orientation (in principle) depends on parameters c_1, c_2 and c_3. The orientation of the ellipse is fixed if eigenvectors are independent on c_1, c_2 and c_3. This is the case if either $c_3 = 0$ or:

$$c_2 - c_1 = u c_3, \tag{5}$$

where u is a real constant, independent of c_1, c_2 and c_3.

Although in the presence of TRS, the total Chern number of a band must vanish, it can still be instructive to calculate the topological charge of a particular band crossing (more precisely, of the representative Hamiltonian). For this reason, we have calculated C, which is defined as a factor multiplying Dirac delta function in the expression for the trace of a curvature: $Tr\left(\hat{\Omega}(\mathbf{q})\right) = 2\pi C\delta(\mathbf{q})$. The trace of curvature is given by $\mathrm{Tr}(\hat{\Omega}(\mathbf{q})) = \mathrm{Tr}(\nabla_{\mathbf{q}} \times \hat{\mathbf{A}})$, where the Berry connection is $\hat{A}^{(l)}_{n,m} = i \langle n| \partial/\partial q_l |m\rangle$, $l = 1, 2$ and m, n count orthonormalized states that can be degenerate for some $\mathbf{q}$-values which belong to a contour around $\mathbf{q} = 0$ in the reciprocal space. Precisely, whenever the contour cannot be chosen to avoid these degeneracies, the eigenstates of two or more bands need to be involved in calculation. Note however, that we have calculated C for the minimal model, i.e. assuming that no other bands exist, other than the ones described by the effective Hamiltonians given below. For bigger models, the described method may give other values for C.

3. Results

All groups and all BZ points and lines hosting electronic dispersions in the absence of SOC are shown in figure 1, those with SOC are shown in figure 2. Dispersions are denoted with different symbols, as indicated in the captions and explained in the subsections below. Dispersions of the same type but with different parameters are denoted with the same symbols of different size. We used equation (4) for graphical presentation of dispersions in the whole BZ. Primitive vectors of the reciprocal lattice are $\mathbf{k}_1$ and $\mathbf{k}_2$. For oblique and rectangular-p groups with all non-symmorphic elements having fractional translations parallel to one direction (for group

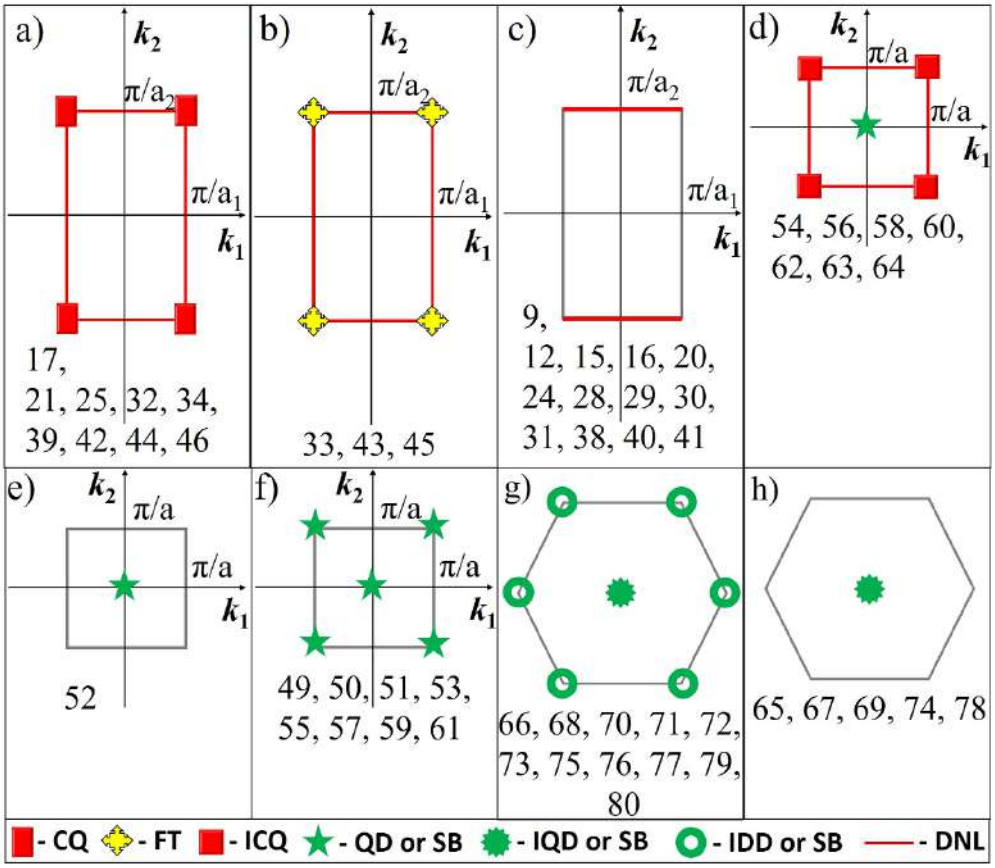

Figure 1. Dispersions near UNP and UNL in the BZ of layer groups without SOC (notation as in [43]). Dispersion acronyms in the lowest panel and the corresponding subsections in the main text are: DNL—Dirac nodal line—3.1.2, FT—fortune teller—3.2.4, IDD—isotropic Dirac—3.2.8, CQ—corner quadratic—3.3.1, ICQ—isotropic corner quadratic—3.3.2, QD—quadratic—3.3.3, IQD—isotropic quadratic—3.3.4 and SB—simple band—3.3.5. The green color denotes more than one possibility for a dispersion around a given BZ point. Other colors denote spinful degeneracy at $\mathbf{q} = 0$: red (4-fold) and yellow (8-fold).

45), $\mathbf{k}_1$ is perpendicular to that direction (to the symmorphic reflection plane). For rectangular-c groups 35^D and 36^D, WNL is along symmorphic axis of order two. For groups 27 and 34 (32, 33 and 43), $\mathbf{k}_1$ is along axis (screw axis) of order two. This convention is of use when directions along $\mathbf{k}_1$ and $\mathbf{k}_2$ differ significantly by hosted dispersions. For rectangular-c groups in figure 2, BZ is shown for the angle between primitive vectors greater than $\pi/2$. The results are equally valid if that angle is sharp, just the BZ border would be rotated. Groups not shown in figure 1 (figure 2) do not have UNP and/or UNL in the case without (with) SOC.

The studies are performed for linear, quadratic and, when it is relevant, for the third order in $\mathbf{q}$, and all together we single out 19 types of dispersions. In the following, they are described in more detail. Letters a and b denote real numbers, z denotes complex numbers, the superscript D denotes layer double group, $\hat{\sigma}_1$, $\hat{\sigma}_2$, $\hat{\sigma}_3$ ($\hat{\sigma}_0$) are Pauli matrices (is the 2D unit matrix), while q_1 and q_2 are projections of $\mathbf{q}$ along orthonormal vectors $\mathbf{e}_1$ and $\mathbf{e}_2$ respectively.

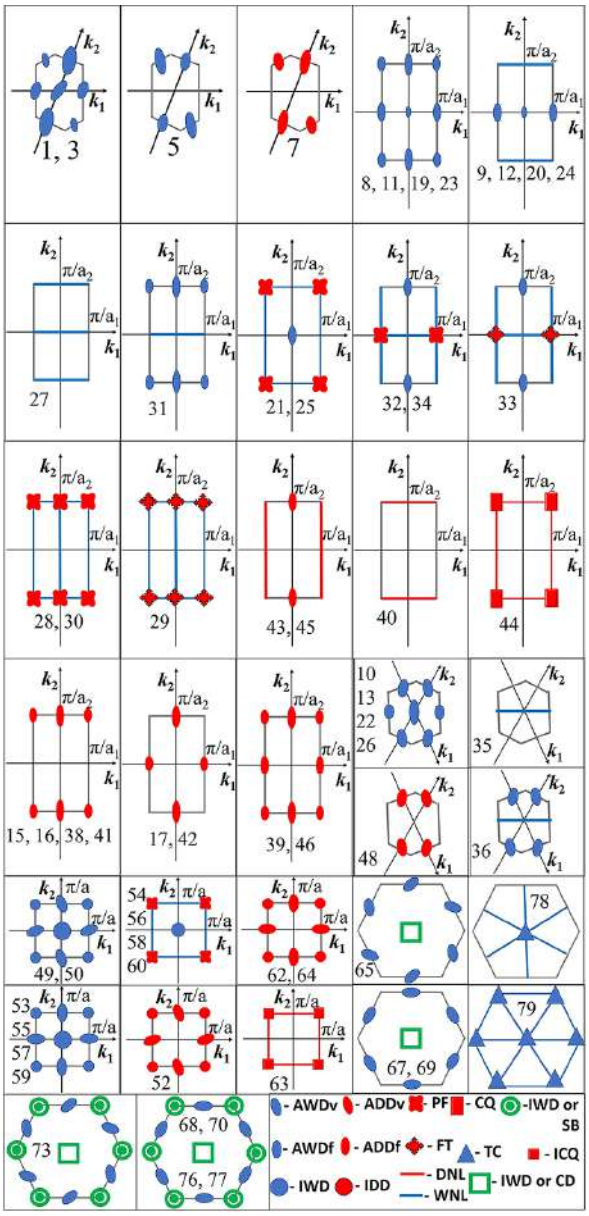

Figure 2. Dispersions near UNP and UNL in the BZ of layer groups with SOC (superscript D is omitted, notation as in [43]). Dispersion acronyms in the lowest panel and the corresponding subsections in the main text are: WNL—Weyl nodal line—3.1.1, DNL—Dirac nodal line—3.1.2, IWD—isotropic Weyl—3.2.1, AWDv-anisotropic Weyl with variable orientation—3.2.2, AWDf—anisotropic Weyl with fixed orientation—3.2.3, FT—fortune teller—3.2.4, PF-poppy flower—3.2.5, ADDv—anisotropic Dirac with variable orientation—3.2.6, ADDf -anisotropic Dirac with fixed orientation—3.2.7, IDD—isotropic Dirac—3.2.8, CQ—corner quadratic—3.3.1, ICQ—isotropic corner quadratic—3.3.2, SB—simple band—3.3.5, CD—cubic—3.4.1 and TC—triangular cubic—3.4.2. The green color denotes more than one possibility for a dispersion around a given BZ point. Other colors denote spinful degeneracy at $\mathbf{q} = 0$: blue (2-fold) and red (4-fold).

3.1. Nodal line dispersions

3.1.1. Weyl nodal line (WNL). WNL is a line of double spinful degeneracy which splits linearly in the direction perpendicular to the line. It appears only in SOC case and it is denoted with blue lines in figure 2. The dispersion and the Hamiltonian are:

$$E_{1,2} = E_0 + a_1 q_{||} \pm c\,|q_\perp|\,, \tag{6a}$$

$$\hat{H} = \left(E_0 + a_1 q_{||}\right)\hat{\sigma}_0 + q_\perp \sum_{j=1}^{3} b_j \hat{\sigma}_j, \tag{6b}$$

where $c = \sqrt{\sum_{j=1}^{3} b_j^2} > 0$ and $q_\perp$ ($q_{||}$) is projection of $\mathbf{q}$ perpendicular to (along) the line. For groups 20^D, 21^D, 24^D, 25^D, 54^D, 56^D, 58^D and 60^D, $b_3 = 0$. For groups 27^D, 28^D, 29^D(WNLs perpendicular to $\mathbf{k}_1$), 30^D, 31^D, 32^D, 33^D (WNL perpendicular to $\mathbf{k}_2$), 34^D, 35^D, 36^D, 78^D and 79^D, $b_3 = b_2 = 0$. For points in the middle and at both ends of WNL, if not occupied by any other dispersion, the following substitution should be made in the last two equations above: $E_0 + a_1 q_{||} \to E_0 + a_1 q_{||}^2$. In these points, one of the bands achieves extremum at $\mathbf{q} = 0$ with the effective mass: $\hat{m}_{\text{eff}} = \begin{pmatrix} 0 & 0 \\ 0 & m_{||} \end{pmatrix}$, which means that excitations are massless along the direction perpendicular to the WNL.

3.1.2. Dirac nodal line (DNL). DNL is a line of 4-fold spinful degeneracy, which splits into two double degenerate bands in the direction perpendicular to the line. DNL appears both in SOC and non-SOC case and it is denoted by a red line. Dispersion is:

$$E_{1,2,3,4} = E_0 + a q_{||} \pm c\,|q_\perp|\,, \tag{7a}$$

where $q_\perp$ ($q_{||}$) is projection of $\mathbf{q}$ perpendicular to (along) the line. For layer single groups, the total Hamiltonian is $\hat{H}_{\text{tot}} = \hat{\sigma}_0 \otimes \hat{H}$, with $\hat{H}$ given by (6*b*), while $E_1^{\uparrow} = E_1^{\downarrow} = E_1 = E_2$, $E_2^{\uparrow} = E_2^{\downarrow} = E_3 = E_4$ and $c = \sqrt{\sum_{j=1}^{3} b_j^2}$. For groups 15, 16, 17, 20, 21, 24, 25, 40, 43 (DNLs perpendicular to $\mathbf{k}_1$), 44, 45 (DNLs perpendicular to $\mathbf{k}_1$), 54, 56, 58, 60 and 63, $b_3 = 0$. For groups 28, 30, 31, 32, 33 (DNLs perpendicular to $\mathbf{k}_2$), 34, 38, 39, 41, 42, 43 (DNLs perpendicular to $\mathbf{k}_2$), 45 (DNLs perpendicular to $\mathbf{k}_2$), 46, 62 and 64, $b_3 = b_2 = 0$. For points in the middle and at both ends of DNL, if not occupied by any other dispersion, the following substitutions should be made in the equations for Hamiltonian (6*b*) and dispersion (7*a*): $E_0 + a_1 q_{||} \to E_0 + a_1 q_{||}^2$ and $b_2 = b_3 = 0$. For layer double groups, the Hamiltonian is:

$$\hat{H} = (E_0 + a q_{||})\hat{I}_4 + q_\perp \begin{pmatrix} b & 0 & z & 0 \\ 0 & -b & 0 & -z \\ z^* & 0 & -b & 0 \\ 0 & -z^* & 0 & b \end{pmatrix}, \tag{7b}$$

with $c = \sqrt{b^2 + |z|^2}$. For points in the middle and at both ends of DNL, if not occupied by any other dispersion, the following substitutions should be made in (7*b*): $E_0 + a_1 q_{||} \to E_0 + a_1 q_{||}^2$ (endpoints of 43^D and 45^D) and (in addition) $b = 0$ (for remaining such points).

3.2. Linear dispersions

3.2.1. Isotropic Weyl dispersion (IWD). IWD consists of two spinful non-degenerate isotropic cones touching each other at $\mathbf{q} = 0$ and it appears only in the case with SOC. IWD is

denoted by a blue circle in figure 2 (when no other dispersion is possible around that point), by a green ring with a dot inside (when simple band (SB) described latter is an alternative), or by a green square (when cubic dispersion (CD) described latter is an alternative). The dispersion and Hamiltonian are:

$$E_{1,2} = E_0 \pm |z|\,|\mathbf{q}|\,, \tag{8a}$$

$$\hat{H} = E_0\hat{\sigma}_0 + \begin{pmatrix} 0 & z(q_1 - iq_2) \\ z^*(q_1 + iq_2) & 0 \end{pmatrix}, \tag{8b}$$

for groups 54^D, 56^D, 58^D, 60^D, $z = (1-i)b_1$, for groups 67^D, 69^D, $z = (1+i\sqrt{3})b_1$, for the remaining groups $z = b_1$, except for 49^D, 50^D, 65^D, 73^D, where z remains a complex number.

3.2.2. Anisotropic Weyl dispersion with variable orientation (AWDv). AWDv consists of two anisotropic, spinful non-degenerate cones and appears only when SOC is included. The cross section of the cones is an ellipse whose orientation (major axis direction) changes when the parameters of the dispersion change. It is represented by a blue ellipse in figure 2, such that its orientation is neither strictly horizontal, nor strictly vertical nor along a BZ edge. This is just a symbol indicating that the orientation of AWDv is not pinned to any particular direction. The actual orientation can be different than the one adopted in figure 2, although equation (4) is used for presenting AWDv on the same star of the wave-vector. Dispersion and Hamiltonian are:

$$E_{1,2} = E_0 \pm \sqrt{c_1 q_1^2 + c_2 q_2^2 + c_3 q_1 q_2}, \tag{9a}$$

$$\hat{H} = E_0\hat{\sigma}_0 + \begin{pmatrix} b_1 q_1 + b_2 q_2 & z_1 q_1 + z_2 q_2 \\ z_1^* q_1 + z_2^* q_2 & -b_1 q_1 - b_2 q_2 \end{pmatrix}, \tag{9b}$$

where $c_1 = b_1^2 + |z_1|^2$, $c_2 = b_2^2 + |z_2|^2$, $c_3 = 2b_1 b_2 + z_1 z_2^* + z_1^* z_2$. For groups 3^D, 22^D, 26^D, 49^D, 50^D and 73^D, $b_1 = b_2 = 0$. The parameters c_1, c_2 and c_3 do not satisfy equation (5).

3.2.3. Anisotropic Weyl dispersion with fixed orientation (AWDf). AWDf consists of two anisotropic, spinful non-degenerate cones, whose orientation is unaltered by the symmetry preserving perturbations. It appears only when SOC is included and it is presented by a blue ellipse whose orientation is strictly vertical, strictly horizontal, along the BZ edge or perpendicular to it. Again, in actual orientation major and minor axes may interchange, and equation (4) is used for presentation in figure 2. The dispersion can be reduced to:

$$E_{1,2} = E_0 \pm \sqrt{c_1 q_1^2 + c_2 q_2^2}. \tag{10}$$

Hamiltonians of interest can be derived from (9*b*). For groups 8^D, 9^D, 10^D, 11^D, 12^D, 13^D, 31^D, 32^D, 33^D and 34^D, $b_2 = 0$ and $z_1 = 0$ so that $c_1 = b_1^2$ and $c_2 = |z_2|^2$. For groups 19^D, 20^D, 22^D, 23^D, 24^D, 26^D, 53^D, 55^D, 57^D and 59^D, $b_1 = b_2 = 0$, $z_1 = ib_3$ and $z_2 = b_4$ so that $c_1 = b_3^2$ and $c_2 = b_4^2$. For groups 21^D and 25^D, $b_2 = 0$, $z_1 = 0$ and $z_2 = ib_3$ so that $c_1 = b_1^2$ and $c_2 = b_3^2$. For groups 67^D, 68^D, 69^D and 70^D, $b_1 = \sqrt{3}b_2$ and $z_2 = -\sqrt{3}z_1$ so that $E_{1,2} = E_0 \pm \sqrt{|z_1|^2(q_1 - \sqrt{3}q_2)^2 + b_2^2(q_2 + \sqrt{3}q_1)^2}$. For groups 76^D and 77^D, $b_1 = b_2 = 0$ and $z_2 = z_1^r/\sqrt{3} - i\sqrt{3}z_1^i$ so that $E_{1,2} = E_0 \pm \sqrt{(z_1^i)^2(q_1 - \sqrt{3}q_2)^2 + (z_1^r)^2(q_1 + q_2/\sqrt{3})^2}$. Last two dispersions are examples where equation (5) applies with $u = 1/\sqrt{3}$.

3.2.4. Fortune teller dispersion (FT). FT appears both in SOC and non-SOC cases, with the degeneracies being doubled in the latter [24, 25]. It is denoted by the quad arrow, yellow for non-SOC and red for SOC case. The dispersion is:

$$E_{1,2,3,4} = E_0 \pm \left| |b_1 q_2| \pm c\,|q_1| \right|. \tag{11a}$$

For layer double groups the Hamiltonian is:

$$\hat{H} = E_0 \hat{I}_4 + \begin{pmatrix} b_2 q_1 & i b_1 q_2 & 0 & z q_1 \\ -i b_1 q_2 & b_2 q_1 & -z q_1 & 0 \\ 0 & -z^* q_1 & -b_2 q_1 & i b_1 q_2 \\ z^* q_1 & 0 & -i b_1 q_2 & -b_2 q_1 \end{pmatrix}, \tag{11b}$$

so that $c = \sqrt{|z|^2 + b_2^2} > 0$ and $\hat{I}_4$ is the unit matrix. For layer single groups the total Hamiltonian is $\hat{H}_{\text{tot}} = \hat{\sigma}_0 \otimes \hat{H}$, with $\hat{H}$ given by (11*b*) and $(\forall j \in \{1,2,3,4\})\, E_j^{\uparrow} = E_j^{\downarrow} = E_j$. For groups 43 and 45, $b_2 = 0$.

3.2.5. Poppy flower dispersion (PF). PF appears only in some non-centrosymmetric groups when SOC is included [25]. It is represented in figure 2 by a red double-ellipse. Degeneracy at $\mathbf{q} = 0$ is 4-fold (spin included) and it splits into spinful non-degenerate bands away from $q_1 = 0$ and $q_2 = 0$ lines. Dispersion and Hamiltonian are:

$$E_{1,2,3,4} = E_0 \pm \sqrt{c_1 q_1^2 + c_2 q_2^2 \pm c_3 |q_1 q_2|}. \tag{12a}$$

For groups 21^D and 25^D:

$$\hat{H} = E_0 \hat{I}_4 + \begin{pmatrix} b_1 q_1 & b_2 q_2 & z_1 q_1 & z_2 q_2 \\ b_2 q_2 & -b_1 q_1 & z_2 q_2 & -z_1 q_1 \\ z_1^* q_1 & z_2^* q_2 & -b_1 q_1 & -b_2 q_2 \\ z_2^* q_2 & -z_1^* q_1 & -b_2 q_2 & b_1 q_1 \end{pmatrix}, \tag{12b}$$

here $c_3 = \sqrt{4b_1^2|z_2|^2 + 4b_2^2|z_1|^2 - (z_1 z_2^* - z_1^* z_2)^2 - 4b_1 b_2 (z_1 z_2^* + z_1^* z_2)}$, $c_2 = b_2^2 + |z_2|^2$, $c_1 = b_1^2 + |z_1|^2$. For groups 28^D, 30^D, 32^D and 34^D:

$$\hat{H} = E_0 \hat{I}_4 + \begin{pmatrix} b_1 q_1 + b_2 q_2 & 0 & z_1 q_1 + z_2 q_2 & 0 \\ 0 & b_1 q_1 - b_2 q_2 & 0 & z_1 q_1 - z_2 q_2 \\ z_1^* q_1 + z_2^* q_2 & 0 & -b_1 q_1 - b_2 q_2 & 0 \\ 0 & z_1^* q_1 - z_2^* q_2 & 0 & -b_1 q_1 + b_2 q_2 \end{pmatrix}, \tag{12c}$$

here $c_1 = b_1^2 + |z_1|^2$, $c_2 = b_2^2 + |z_2|^2$, $c_3 = |2b_1 b_2 + z_1 z_2^* + z_1^* z_2|$. For groups 54^D, 56^D, 58^D and 60^D:

$$\hat{H} = E_0 \hat{I}_4 + \begin{pmatrix} 0 & (1-i) b_1 (q_1 - i q_2) & z^* (q_1 + i q_2) & 0 \\ (1+i) b_1 (q_1 + i q_2) & 0 & 0 & z^* (q_2 + i q_1) \\ z (q_1 - i q_2) & 0 & 0 & (1-i) b_1 (q_2 - i q_1) \\ 0 & z (q_2 - i q_1) & (1+i) b_1 (q_2 + i q_1) & 0 \end{pmatrix}, \tag{12d}$$

here $c_1 = c_2 = 2b_1^2 + |z|^2$, $c_3 = 4\sqrt{2}|b_1 z|$ (called isotropic PF in [25]).

3.2.6. Anisotropic Dirac dispersion with variable orientation (ADDv). ADDv is analogous to AWDv with degeneracy of each band doubled. It appears only in SOC case. ADDv is represented by a red ellipse with the same convention as for AWDv described in section 3.2.2. Dispersion and Hamiltonian are:

$$E_{1,2,3,4} = E_0 \pm \sqrt{c_1 q_1^2 + c_2 q_2^2 + c_3 q_1 q_2}, \tag{13a}$$

$$\hat{H} = E_0 \hat{I}_4 + \begin{pmatrix} 0 & b_1 q_1 + b_2 q_2 & z_1 q_1 + z_2 q_2 & 0 \\ b_1 q_1 + b_2 q_2 & 0 & 0 & z_1 q_1 + z_2 q_2 \\ z_1^* q_1 + z_2^* q_2 & 0 & 0 & -b_1 q_1 - b_2 q_2 \\ 0 & z_1^* q_1 + z_2^* q_2 & -b_1 q_1 - b_2 q_2 & 0 \end{pmatrix}, \tag{13b}$$

here $c_1 = b_1^2 + |z_1|^2$, $c_2 = b_2^2 + |z_2|^2$, $c_3 = 2b_1 b_2 + z_1 z_2^* + z_1^* z_2$.

3.2.7. Anisotropic Dirac dispersion with fixed orientation (ADDf). ADDf is analogous to AWDf with degeneracy of each band doubled. It appears only in SOC case and it is represented by a red ellipse. The convention follows the one for AWDf in section 3.2.3. Dispersion and Hamiltonian are:

$$E_{1,2,3,4} = E_0 \pm \sqrt{c_1 q_1^2 + c_2 q_2^2}. \tag{14a}$$

For groups 15^D, 16^D and 17^D:

$$\hat{H} = E_0 \hat{I}_4 + \begin{pmatrix} b_2 q_2 & i b_1 q_1 & z q_2 & 0 \\ -i b_1 q_1 & -b_2 q_2 & 0 & -z q_2 \\ z^* q_2 & 0 & -b_2 q_2 & i b_1 q_1 \\ 0 & -z^* q_2 & -i b_1 q_1 & b_2 q_2 \end{pmatrix}, \tag{14b}$$

here $c_1 = b_1^2$, $c_2 = b_2^2 + |z|^2$. For groups 38^D, 39^D(points $(\pm\pi/a_1, 0)$ and $(0, \pm\pi/a_2)$), 41^D, 42^D, 43^D, 45^D, 46^D (points $(\pm\pi/a_1, 0)$ and $(0, \pm\pi/a_2)$), 62^D (points $(\pm\pi/a, 0)$ and $(0, \pm\pi/a)$) and 64^D (points $(\pm\pi/a, 0)$ and $(0, \pm\pi/a)$), $b_2 = 0$. For groups 39^D (BZ-corners) and 46^D (BZ-corners), $z = 0$.

3.2.8. Isotropic Dirac dispersion (IDD). IDD is analogous to IWD with degeneracy of each band doubled. It appears in cases with and without SOC. An example of IDD is dispersion near K-points in graphene. IDD is represented by a red circle (when no other dispersions near this point are possible) or by a green ring (when SB is an alternative). Dispersion and Hamiltonian are:

$$E_{1,2,3,4} = E_0 \pm |z||\mathbf{q}|. \tag{15a}$$

For group 52^D:

$$\hat{H} = E_0 \hat{I}_4 + \begin{pmatrix} 0 & 0 & z(q_1 - i q_2) & 0 \\ 0 & 0 & 0 & z(q_1 - i q_2) \\ z^*(q_1 + i q_2) & 0 & 0 & 0 \\ 0 & z^*(q_1 + i q_2) & 0 & 0 \end{pmatrix}, \tag{15b}$$

for groups 62^D and 64^D, $z = i b_1$. For layer single groups $\hat{H}_{\text{tot}} = \hat{\sigma}_0 \otimes \hat{H}$, with $\hat{H}$ given by (8*b*) and $E_1^{\uparrow} = E_1^{\downarrow} = E_1 = E_2$, $E_2^{\uparrow} = E_2^{\downarrow} = E_3 = E_4$. For layer single groups $z = b_1$ except for 66, 73 and 75.

3.3. Quadratic dispersions

3.3.1. Corner quadratic dispersion (CQ). CQ appears at BZ corners of rectangular groups where two DNL meet. It appears both in SOC and non-SOC cases and it is denoted by a red rectangle. The 4-fold spinfull degenerate band at $\mathbf{q} = 0$, splits into two double degenerate bands for $\mathbf{q} \neq 0$ and away from DNLs. The splitting causing term is of the second order (quadratic) in $\mathbf{q}$. The dispersion is:

$$E_{1,2,3,4} = E_0 + a_1 q_1^2 + a_2 q_2^2 \pm c\,|q_1 q_2|\,. \tag{16a}$$

For layer single groups $E_1^{\uparrow} = E_1^{\downarrow} = E_1 = E_2$, $E_2^{\uparrow} = E_2^{\downarrow} = E_3 = E_4$ and the Hamiltonian is:

$$\hat{H} = \hat{\sigma}_0 \otimes \left[(E_0 + a_1 q_1^2 + a_2 q_2^2)\hat{\sigma}_0 + q_1 q_2\,(b_1\hat{\sigma}_1 + b_2\hat{\sigma}_2)\right], \tag{16b}$$

so that $c = \sqrt{b_1^2 + b_2^2}$. For groups 32, 34, 39, 42, 46, $b_2 = 0$. For layer double groups:

$$\hat{H} = (E_0 + a_1 q_1^2 + a_2 q_2^2)\hat{I}_4 + q_1 q_2 \begin{pmatrix} 0 & ib_1 & 0 & z \\ -ib_1 & 0 & -z & 0 \\ 0 & -z^* & 0 & -ib_1 \\ z^* & 0 & ib_1 & 0 \end{pmatrix}, \tag{16c}$$

so that $c = \sqrt{b_1^2 + |z|^2}$.

3.3.2. Isotropic corner quadratic dispersion (ICQ). In the BZ corners of square groups where two DNL meet, the axis of order four imposes $a_1 = a_2$ in CQ and gives ICQ. The term *isotropic* denotes that dispersions along $q_1 = 0$ and $q_2 = 0$ are identical. ICQ appears in both SOC and non-SOC cases and it is marked by a red square. The dispersion is:

$$E_{1,2,3,4} = E_0 + aq^2 \pm c\,|q_1 q_2|\,. \tag{17a}$$

For layer single groups $E_1^{\uparrow} = E_1^{\downarrow} = E_1 = E_2$, $E_2^{\uparrow} = E_2^{\downarrow} = E_3 = E_4$ and the Hamiltonian is:

$$\hat{H} = \hat{\sigma}_0 \otimes \left[(E_0 + aq^2)\hat{\sigma}_0 + q_1 q_2\,(b_1\hat{\sigma}_1 + b_2\hat{\sigma}_2)\right], \tag{17b}$$

so that $c = \sqrt{b_1^2 + b_2^2}$. For correps that remain irreducible when TRS becomes broken, $b_2 = 0$. For layer double group 63^D, $a_1 = a_2 = a$ and $b_1 = 0$ in (16*c*) so that $c = |z|$.

3.3.3. Quadratic dispersion (QD). QD appears near isolated BZ points only in non-SOC case [44]. It is denoted by the green star in figure 1, since SB can appear instead. The splitting in all directions away from the point is quadratic, as indicated by dispersion and Hamiltonian:

$$E_{1,2}^{\uparrow} = E_{1,2}^{\downarrow} = E_0 + aq^2 \pm \sqrt{[b_3(q_1^2 - q_2^2) + b_1 q_1 q_2]^2 + [b_4(q_1^2 - q_2^2) + b_2 q_1 q_2]^2}, \tag{18a}$$

$$\hat{H} = \hat{\sigma}_0 \otimes \left\{(E_0 + aq^2)\hat{\sigma}_0 + [b_3(q_1^2 - q_2^2) + b_1 q_1 q_2]\hat{\sigma}_1 + [b_4(q_1^2 - q_2^2) + b_2 q_1 q_2]\hat{\sigma}_2\right\}. \tag{18b}$$

Except for groups 49, 50, 51 and 52, in (18*a*) and (18*b*) $b_1 = b_4 = 0$. If $b_1 b_4 = b_2 b_3$, two lines of accidental degeneracy intersect at $\mathbf{q} = 0$ symmetrically under rotation by $\pi/2$, so that $\mathbf{q} = 0$ is not an isolated point any more.

3.3.4. Isotropic quadratic dispersion (IQD). IQD is QD which is fully isotropic. It appears only in non-SOC case [44] and it is indicated with a green snowflake, since the appearance of SB is other possibility. Dispersion and Hamiltonian are:

$$E^{\uparrow}_{1,2} = E^{\downarrow}_{1,2} = E_0 + \left(a \pm \sqrt{b_1^2 + b_2^2}\right) q^2, \tag{19a}$$

$$\hat{H} = \hat{\sigma}_0 \otimes \left\{(E_0 + aq^2)\hat{\sigma}_0 + [2b_2 q_1 q_2 + b_1(q_1^2 - q_2^2)]\hat{\sigma}_1 + [b_2(q_1^2 - q_2^2) - 2b_1 q_1 q_2]\hat{\sigma}_2\right\}, \tag{19b}$$

with $b_2 = 0$ except for groups 65, 66, 73, 74 and 75. Unlike QD, IQD cannot be turned into a line of degeneracies by suitable choice of non-zero parameters.

3.3.5. Simple band (SB). SB is a band (spinful non-degenerate, with SOC and double spinful degenerate in non-SOC case) which disperses quadratically near $\mathbf{q} = 0$ without any splitting (i.e. it is neither UNP nor UNL). It is introduced here only when it appears as an alternative to other dispersions. These cases are denoted by green symbols in figures 1 and 2. The dispersion and Hamiltonian are:

$$E_1 = E_0 + aq^2, \tag{20a}$$

$$\hat{H} = E_0 + aq^2. \tag{20b}$$

For layer single groups $\hat{H}_{\text{tot}} = (E_0 + aq^2)\hat{\sigma}_0$ and $E^{\uparrow}_1 = E^{\downarrow}_1 = E_1$.

3.4. Cubic dispersions

3.4.1. Cubic dispersion (CD). CD appears only when SOC is included. It consists of spinful double degenerate band at $\mathbf{q} = 0$ which splits cubically away from this point. It is denoted with a green square, since IWD is other dispersion possible at groups/BZ points form figure 2. Dispersion and Hamiltonian are:

$$E_{1,2} = E_0 + a|\mathbf{q}|^2 \pm \sqrt{\left|z_1 q_1(q_1^2 - 3q_2^2) + z_2 q_2(q_2^2 - 3q_1^2)\right|^2 + [b_1 q_1(q_1^2 - 3q_2^2) + b_2 q_2(q_2^2 - 3q_1^2)]^2}, \tag{21a}$$

$$\hat{H} = (E_0 + a|\mathbf{q}|^2)\hat{\sigma}_0 + \begin{pmatrix} b_1 q_1(q_1^2 - 3q_2^2) + b_2 q_2(q_2^2 - 3q_1^2) & z_1 q_1(q_1^2 - 3q_2^2) + z_2 q_2(q_2^2 - 3q_1^2) \\ z_1^* q_1(q_1^2 - 3q_2^2) + z_2^* q_2(q_2^2 - 3q_1^2) & -b_1 q_1(q_1^2 - 3q_2^2) - b_2 q_2(q_2^2 - 3q_1^2) \end{pmatrix}. \tag{21b}$$

If vectors $\left\{(z_1^r, z_2^r)^T, (z_1^i, z_2^i)^T\right\}$ are linearly dependent and vectors $\left\{(z_1^r, z_2^r)^T, (b_1, b_2)^T\right\}$ are also linearly dependent, then three accidental nodal lines intersect symmetrically under rotation by $\pi/3$ at $\mathbf{q} = 0$, so that $\mathbf{q} = 0$ is not an isolated point any more. For groups 67^D, 68^D, 69^D and 70^D, $b_1 = 0$ and $z_2 = 0$. For group 73^D, $b_1 = b_2 = 0$. For groups 76^D and 77^D, $b_1 = b_2 = 0$, $z_1 = ib_3$ and $z_2 = b_4$.

3.4.2. Triangular cubic dispersion (TC). TC appears only in SOC case, when three WNL intersect at a single point. It is denoted by a blue triangle in figure 2. The splitting is caused by cubic terms in the Taylor expansion of Hamiltonian. Dispersion and Hamiltonian are:

$$E_{1,2} = E_0 + aq^2 \pm |b|\left|q_2(q_2^2 - 3q_1^2)\right|, \tag{22a}$$

$$\hat{H} = (E_0 + aq^2)\hat{\sigma}_0 + bq_2(q_2^2 - 3q_1^2)\hat{\sigma}_3. \tag{22b}$$

TC appears in Hexagonal groups 78^D and 79^D.

For clarity, the results are also summarized in table 1, where dispersion description names, abbreviations, and icons are listed. In the column C, the calculated topological charge for each type (Hamiltonian) is given. Total number of bands is presented in the form $n+n$, whenever n bands (the half of the total number $2n$ of bands) touch in a way that cannot be avoided by a suitable choice of contour surrounding $\mathbf{q} = 0$. For example, both FT and PF dispersions in SOC case consist of four bands, except that for FT all four bands are connected by degeneracy lines that extend through whole BZ, while for PF two connected pairs of bands are separated from each other except at $\mathbf{q} = 0$. Thus, the contour cannot be chosen to avoid q-values for which 4, and 2 bands touch for FT and PF dispersions, respectively, while, in the case of PF, it avoids touching point $\mathbf{q} = 0$ of pairs of bands. For this reason, the number of bands involved is represented in table 1 as 4 for FT and 2+2 for PF. It turned out that in all cases of the type $n+n$, the topological charge C is equal for the two bundles.

4. Discussion and conclusions

Comparison of figures 1 and 2 allows conclusions on how e.g. inclusion of SOC affects dispersions. Dispersions in groups 40, 44 and 63 are unaltered, up to numerical values of parameters, by the inclusion of SOC. In groups 43 and 45, DNLs perpendicular to $\mathbf{k}_1$ are also preserved when SOC is included. On the other hand, SOC induces DNL to split into two WNLs in groups 9, 12, 20, 21, 24, 25, 28, 29, 30, 32 (DNL perpendicular to $\mathbf{k}_1$), 33 (DNL perpendicular to $\mathbf{k}_1$), 34 (DNL perpendicular to $\mathbf{k}_1$), 54, 56, 58 and 60. In groups 21 and 25, SOC induces transition from CQ to PF, while in square groups 54, 56, 58 and 60, SOC turns ICQ to isotropic PF. Other SOC-induced transitions are CQ to ADDf (groups 39 and 46) and ICQ to IDD in groups 62, 64. SOC induced splitting at HSP in non-magnetic layers are also discussed in [23].

Regarding topological properties, dispersions (more precisely, Hamiltonians) AWDv, AWDf, IWD, ADDv, IDD, PF (for Hamiltonian (12*d*)), QD, IQD and CD have a non-zero topological charge C. We note again that C given here is for minimal Hamiltonians required by symmetry. For bigger models, C may be different since the eigenvectors have more components. Although the Chern number of the whole band is invariant (up to a sign), this does not hold for topological charges of individual band crossings. Therefore, it may happen that in some groups the topological charges given in table 1 do not add up to an integer.

The dispersions presented in section 3 are exact, in the sense that if we knew how to solve the one-electron Schrödinger equation for a single crystal exactly, we would get the very same formulas (with the numerical values of parameters as additional results). The dispersions are unaltered as long as electron correlations are weak enough to preserve the quasiparticle picture. For these reasons, each dispersion presented here can be a research topic of its own. The synthesis of new 2D materials with the right placement of the Fermi level would likely trigger new research directions.

Besides band contacts treated here, there are accidental band contacts that appear along HSLs or away from them in the BZ. Some of these contacts are guaranteed to exist by the topological laws. Such guaranteed contacts can be moved but not removed by the symmetry preserving perturbations and are tabulated for (3D) hexagonal [45], tetragonal [46] and orthorhombic [47] space groups. These results could be used for layer groups, by subduction from corresponding space groups to 2D BZ. On the other hand, truly accidental band contacts can be destroyed by a perturbation that keeps the symmetry, which in real materials can be

Table 1. Summary of quasiparticles near UNPs and UNLs in gray layer groups. SB denotes simple band (section 3.3.5). For single groups: $C = C^{\uparrow} = C^{\downarrow}$. For dispersion consisting of two bundles of bands (+ and −), $C = C^{+} = C^{-}$.

Full name	Abbreviation	Icon	Number of bands	C	Section
Isotropic	IWD		1+1	$\frac{1}{2}$	3.2.1
Weyl		 (or CD)	1+1	$\frac{1}{2}$	3.2.1
dispersion		 (or SB)	1+1	$\frac{1}{2}$	3.2.1
Anisotropic Weyl dispersion with...					
...variable orientation	AWDv		1+1	$\frac{1}{2}\mathrm{sgn}(z_1^i z_2^r - z_1^r z_2^i)$	3.2.2
...fixed orientation	AWDf		1+1	$\frac{1}{2}\mathrm{sgn}(z_1^i z_2^r - z_1^r z_2^i)$	3.2.3
Fortune teller	FT		4	0	3.2.4
dispersion (with SOC) (without SOC)	FT		8	0	3.2.4
Poppy flower	PF		2+2	$\mathrm{sgn}(\lvert z\rvert^2 - 2b_1^2)$, (12*d*)	3.2.5
dispersion				0, (the rest)	
Anisotropic Dirac dispersion with...					
...variable orientation	ADDv		2+2	$\mathrm{sgn}(z_1^i z_2^r - z_1^r z_2^i)$	3.2.6
...fixed orientation	ADDf		2+2	0	3.2.7
Isotropic Dirac	IDD		2+2	1	3.2.8
dispersion		 (or SB)	2+2	$\frac{1}{2}$	3.2.8
Corner quadratic dispersion	CQ		4	0	3.3.1

(Continued.)

caused by a change in temperature, pressure, strain *etc*. Four-fold spinless degenerate points that belong to HSL treated in [48–50] are examples of truly accidental band contacts.

Experimental realization of a 2D material with prescribed layer symmetry is far from trivial, so one could search across a database of 3D materials that have already been synthesized and can be easily exfoliated into layers [51]. It contains materials of almost all 3D symmetries obtained by periodic repetition of layers perpendicularly. Dispersions presented in section 3 are of significance if in a 2D material, the Fermi level crosses bands near E_0. Although this

Table 1. (Continued.)

Full name	Abbreviation	Icon	Number of bands	C	Section
Isotropic corner quadratic dispersion	ICQ		4	0	3.3.2
Quadratic dispersion	QD	 (or SB)	2+2	$\mathrm{sgn}(b_2b_3 - b_1b_4)$	3.3.3
Isotropic quadratic dispersion	IQD	 (or SB)	2+2	-1	3.3.4
Cubic dispersion	CD	 (or IWD)	1+1	$\frac{3}{2}\mathrm{sgn}(z_1^r z_2^i - z_1^i z_2^r)$	3.4.1
Triangular cubic dispersion	TC		2	0	3.4.2
Weyl nodal line	WNL		2	—	3.1.1
Dirac nodal line	DNL		4	—	3.1.2

cannot be guaranteed solely by group-theoretical arguments, there are some symmetry-based results which are helpful. References [52–54] give the electron fillings necessary for a crystal belonging to a certain space or layer group to be insulating. When this condition is not fulfilled, the crystal is metallic (or insulating if the electron-electron interaction is strong). For example, if in a 2D material belonging to layer group 33, the sum of atomic numbers of all nuclei in the primitive cell is not divisible by eight, the material is a metal [52–54]. It would be possible then to dope the material with electrons or holes by e.g. gating, especially if the material belongs to a layer group that is also a symmetry of a surface (a wallpaper group).

Data availability statement

All data that support the findings of this study are included within the article (and any supplementary files).

Acknowledgments

Authors acknowledge funding by the Ministry of Science, Technological Development and Innovation of the Republic of Serbia provided by the Institute of Physics Belgrade (V D) and Faculty of Physics (N L), University of Belgrade.

ORCID iDs

V Damljanović https://orcid.org/0000-0001-7517-6439
N Lazić https://orcid.org/0000-0002-3634-0301

References

[1] Yan B and Felser C 2017 Topological materials: Weyl semimetals *Annu. Rev. Condens. Matter Phys.* **8** 337–54
[2] Armitage N P, Mele E J and Vishwanath A 2018 Weyl and Dirac semimetals in three-dimensional solids *Rev. Mod. Phys.* **90** 015001
[3] Gao H, Venderbos J W F, Kim Y and Rappe A M 2019 Topological semimetals from first principles *Annu. Rev. Mater. Res.* **49** 153–83
[4] Yang S-Y, Yang H, Derunova E, Parkin S S P, Yan B and Ali M N 2018 Symmetry demanded topological nodal-line materials *Adv. Phys.* X **3** 1414631
[5] Fang C, Weng H, Dai Xi and Fang Z 2016 Topological nodal line semimetals *Chin. Phys.* B **25** 117106
[6] Li S, Yu Z-M, Yao Y and Yang S A 2020 Type-II topological metals *Front. Phys.* **15** 43201
[7] Yang M-X, Luo W and Chen W 2022 Quantum transport in topological nodal-line semimetals *Adv. Phys.* X **7** 2065216
[8] Burkov A A, Hook M D and Balents L 2011 Topological nodal semimetals *Phys. Rev.* B **84** 235126
[9] Phillips M and Aji V 2014 Tunable line node semimetals *Phys. Rev.* B **90** 115111
[10] Volovik G E 2013 Flat band in topological matter *J. Supercond. Novel Magn.* **26** 2887–90
[11] Bouckaert L P, Smoluchowski R and Wigner E 1936 Theory of Brillouin zones and symmetry properties of wave functions in crystals *Phys. Rev.* **50** 58–67
[12] Herring C 1937 Effect of time-reversal symmetry on energy bands of crystals *Phys. Rev.* **52** 361–5
[13] Herring C 1937 Accidental degeneracy in the energy bands of crystals *Phys. Rev.* **52** 365–73
[14] Bacry H, Michel L and Zak J 1988 Symmetry and classification of energy bands in crystals *Group Theoretical Methods in Physics* ed H-D Doebner, Jorg-D Hennig and T D Palev (Berlin: Springer) pp 289–308
[15] Zak J 2002 Topologically unavoidable points and lines of crossings in the band structure of solids *J. Phys. A: Math. Gen.* **35** 6509
[16] Young S M and Kane C L 2015 Dirac semimetals in two dimensions *Phys. Rev. Lett.* **115** 126803
[17] Xie Y-M, Gao X-J, Xu X Y, Zhang C-P, Hu J-X, Gao J Z and Law K T 2021 Kramers nodal line metals *Nat. Commun.* **12** 3064
[18] Wu L, Tang F and Wan X 2021 Symmetry-enforced band nodes in 230 space groups *Phys. Rev.* B **104** 045107
[19] Yang J, Fang C and Liu Z-X 2021 Symmetry-protected nodal points and nodal lines in magnetic materials *Phys. Rev.* B **103** 245141
[20] Fang C, Chen Y, Kee H-Y and Fu L 2015 Topological nodal line semimetals with and without spin-orbital coupling *Phys. Rev.* B **92** 081201
[21] Guo D, Guo P, Tan S, Feng M, Cao L, Liu Z-X, Liu K, Lu Z-Y and Ji W 2022 Two-dimensional Dirac-line semimetals resistant to strong spin-orbit coupling *Sci. Bull.* **67** 1954–7
[22] Guo P-J, Peng C, Liu Z-X, Liu K and Lu Z-Y 2022 Symmetry-enforced two-dimensional Dirac node-line semimetals *Mater. Futures* **2** 011001
[23] Lazić N, Damljanović V and Damnjanović M 2022 Fully linear band crossings at high symmetry points in layers: classification and role of spin–orbit coupling and time reversal *J. Phys. A: Math. Theor.* **55** 325202
[24] Damljanović V, Popov I and Gajić Rš 2017 Fortune teller fermions in two-dimensional materials *Nanoscale* **9** 19337–45
[25] Damljanović V, Lazić N, Šolajić A, Pešić J, Nikolić B and Damnjanović M 2020 Peculiar symmetry-protected electronic dispersions in two-dimensional materials *J. Phys.: Condens. Matter* **32** 485501
[26] Damljanović V and Gajić R 2016 Existence of Dirac cones in the Brillouin zone of diperiodic atomic crystals according to group theory *J. Phys.: Condens. Matter* **28** 085502
[27] Damljanović V and Gajić R 2016 Addendum to 'Existence of Dirac cones in the Brillouin zone of diperiodic atomic crystals according to group theory' *J. Phys.: Condens. Matter* **28** 439401
[28] Feng X, Zhu J, Wu W and Yang S A 2021 Two-dimensional topological semimetals *Chin. Phys.* B **30** 107304
[29] Tang F and Wan X 2021 Exhaustive construction of effective models in 1651 magnetic space groups *Phys. Rev.* B **104** 085137
[30] Yu Z-M, Zhang Z, Liu G-B, Wu W, Li X-P, Zhang R-W, Yang S A and Yao Y 2022 Encyclopedia of emergent particles in three-dimensional crystals *Sci. Bull.* **67** 375–80

[31] Liu G-B, Zhang Z, Yu Z-M, Yang S A and Yao Y 2022 Systematic investigation of emergent particles in type-III magnetic space groups *Phys. Rev.* B **105** 085117
[32] Zhang Z, Liu G-B, Yu Z-M, Yang S A and Yao Y 2022 Encyclopedia of emergent particles in type-IV magnetic space groups *Phys. Rev.* B **105** 104426
[33] Zhang Z, Wu W, Liu G-B, Yu Z-M, Yang S A and Yao Y 2023 Encyclopedia of emergent particles in 528 magnetic layer groups and 394 magnetic rod groups *Phys. Rev.* B **107** 075405
[34] Tang F and Wan X 2022 Complete classification of band nodal structures and massless excitations *Phys. Rev.* B **105** 155156
[35] Aroyo M I, Kirov A, Capillas C, Perez-Mato J M and Wondratschek H 2006 Bilbao crystallographic server. II. Representations of crystallographic point groups and space groups *Acta Crystallogr.* A **62** 115–28
[36] Elcoro L, Bradlyn B, Wang Z, Vergniory M G, Cano J, Felser C, Bernevig B A, Orobengoa D, de la Flor G and Aroyo M I 2017 Double crystallographic groups and their representations on the Bilbao Crystallographic Server *J. Appl. Crystallogr.* **50** 1457–77
[37] Litvin D B and Wike T R 1991 *Character Tables and Compatibility Relations of the Eighty Layer Groups and Seventeen Plane Groups* (New York: Plenum Press)
[38] Milosevic I, Nikolic B, Damnjanovic M and Krcmar M 1998 Irreducible representations of diperiodic groups *J. Phys. A: Math. Gen.* **31** 3625
[39] Damljanović V, Kostić R and Gajić R 2014 Characters of graphene's symmetry group Dg80 *Phys. Scr.* **2014** 014022
[40] Nikolić B, Milošević I, Vuković T, Lazić N, Dmitrović S, Popović Z and Damnjanović M 2022 Irreducible and site-symmetry-induced representations of single/double ordinary/grey layer groups *Acta Crystallogr.* A **78** 107–14
[41] Mañes J L 2012 Existence of bulk chiral fermions and crystal symmetry *Phys. Rev.* B **85** 155118
[42] Damnjanović M and Milošević I 2015 Full symmetry implementation in condensed matter and molecular physics-modified group projector technique *Phys. Rep.* **581** 1–43
[43] Kopsky V and Litvin D B 2002 *International Tables of Crystallography* (*Subperiodic Groups* vol E) (London: Kluwer Academic Publishers)
[44] Yu W-W, Liu Y, Meng W, Liu H, Gao J, Zhang X and Liu G 2022 Phononic higher-order nodal point in two dimensions *Phys. Rev.* B **105** 035429
[45] Zhang J, Chan Y-H, Chiu C-K, Vergniory M G, Schoop L M and Schnyder A P 2018 Topological band crossings in hexagonal materials *Phys. Rev. Mater.* **2** 074201
[46] Hirschmann M M, Leonhardt A, Kilic B, Fabini D H and Schnyder A P 2021 Symmetry-enforced band crossings in tetragonal materials: Dirac and Weyl degeneracies on points, lines and planes *Phys. Rev. Mater.* **5** 054202
[47] Leonhardt A, Hirschmann M M, Heinsdorf N, Wu X, Fabini D H and Schnyder A P 2021 Symmetry-enforced topological band crossings in orthorhombic crystals: classification and materials discovery *Phys. Rev. Mater.* **5** 124202
[48] Guo P-J, Wei Y-W, Liu K, Liu Z-X and Lu Z-Y 2021 Eightfold degenerate fermions in two dimensions *Phys. Rev. Lett.* **127** 176401
[49] Guo P-J, Wei Y-W, Liu K, Liu Z-X and Lu Z-Y 2022 Erratum: Eightfold degenerate fermions in two dimensions [Phys. Rev. Lett. 127, 176401 (2021)] *Phys. Rev. Lett.* **129** 049901
[50] Gong J, Wang J, Yuan H, Zhang Z, Wang W and Wang X 2022 Dirac phonons in two-dimensional materials *Phys. Rev.* B **106** 214317
[51] Mounet N *et al* 2018 Two-dimensional materials from high-throughput computational exfoliation of experimentally known compounds *Nat. Nanotechnol.* **13** 246–52
[52] Watanabe H, Po H C, Zaletel M P and Vishwanath A 2016 Filling-enforced gaplessness in band structures of the 230 space groups *Phys. Rev. Lett.* **117** 096404
[53] Watanabe H, Po H C, Vishwanath A and Zaletel M 2015 Filling constraints for spin-orbit coupled insulators in symmorphic and nonsymmorphic crystals *Proc. Natl Acad. Sci.* **112** 14551–6
[54] Wieder B J and Kane C L 2016 Spin-orbit semimetals in the layer groups *Phys. Rev.* B **94** 155108

IOP Publishing Journal of Physics A: Mathematical and Theoretical
J. Phys. A: Math. Theor. **55** (2022) 325202 (22pp) https://doi.org/10.1088/1751-8121/ac7f08

Fully linear band crossings at high symmetry points in layers: classification and role of spin–orbit coupling and time reversal

N Lazić[1], V Damljanović[2,*] and M Damnjanović[1,3]

[1] NanoLab, Faculty of Physics, University of Belgrade, Studentski Trg 12, 11001 Belgrade, Serbia
[2] Institute of Physics Belgrade, University of Belgrade, Pregrevica 118, 11000 Belgrade, Serbia
[3] Serbian Academy of Sciences and Arts, Kneza Mihaila St. 35, 11000 Belgrade, Serbia

E-mail: damlja@ipb.ac.rs

Received 22 November 2021, revised 17 June 2022
Accepted for publication 6 July 2022
Published 9 August 2022

Abstract

Symmetry imposed restrictions to the Hamiltonian are systematized and applied to all of 80 clusters of single/double ordinary/gray groups (320 groups in total), to single out linear (in all directions) band crossings and corresponding effective Hamiltonians in high-symmetry Brillouin zone points of layered materials. The resulting dispersion types are isotropic or anisotropic forms of: single cone (with double degenerate crossing point and non-degenerate branches, or four-fold degenerate crossing point with double degenerate conical branches), poppy-flower (four-fold degenerate crossing point with two pairs of non-degenerate mutually rotated conical branches), and fortune teller (with nodal lines). Further, we describe the nontrivial patterns of dispersions' behavior in high symmetry points when symmetry is varied within a cluster. Namely, Clebsch–Gordan series of the products of spin representation with the integer ones are relevant when spin–orbit coupling is included, and clarify observed scenarios (gap closing, gap opening, cone preserving, cone splitting etc). Analogously, analysis of behavior of dispersions in transition from ordinary to gray group enlightens the role of time reversal symmetry. The results refine and expand data existing in literature, and interesting or even unexpected cases are singled out in discussion.

*Author to whom any correspondence should be addressed.

Keywords: two-dimensional materials, Dirac fermions, Weyl fermions, symmetry

(Some figures may appear in colour only in the online journal)

1. Introduction

Interplay between symmetry and topology of band structures is among the most attractive topics in contemporary condensed matter physics. Besides topological insulators (TIs), nodal semimetals take a notable role, being a material realization of relativistic Dirac, Weyl, and Majorana particles [1–3], or lead to the emergence of unconventional quasiparticles [4–7]. Characterized by band crossings (touching) points (lines) at Fermi level, with energies dispersing linearly, they have various interesting properties: Dirac points represent the interphases between topologically different insulating phases, Weyl points lead to semimetals with chiral anomaly, Fermi arc surface states etc. Protected by crystal symmetries [8–16], these crossing points are robust with respect to various symmetry-preserving perturbations. Energy of the crossing cannot be predicted by symmetry alone; particularly important are those on Fermi level: when placed at (special) high symmetry points (HSPs) in Brillouin zone (BZ), the material is known as a symmetry-enforced semimetal.

Leaving accidental degeneracy aside, the band crossings are within group theory related to the multi-dimensional allowed irreducible representations (IRs) of underlying symmetries. Geometrical transformations are gathered into ordinary crystallographic groups. When time reversal (TR) symmetry (either pure for paramagnetic systems, or combined with spatial symmetries for anti/ferromagnets) is included, gray or black-and-white magnetic groups [17, 18] are obtained; these are represented by irreducible corepresentations (coIRs), which have, besides unitary, additional anti-unitary operators. When spin space is included (spinfull case) to consider spin–orbit (SO) interaction, half-integer irreducible (co)representations of double groups are assigned to electron bands.

The raising interest in exploring bands topology [19–21], including its symmetry based aspects, points out the necessity to systematize numerous particular studies, and fill in existing gaps. In particular, layer groups have been intensively used to predict Dirac and beyond-Dirac topological semimetals [11, 14, 22–30], but still there is no complete overview of such symmetry-enforced band structures of layered materials, unlike space groups [31, 32]. Our thorough and systematic presentation will facilitate both numerical and experimental search for the materials with preferred symmetry and desirable band topology, as well as sub-dimensional analysis of 3D crystals [33].

In this paper all band crossings with dispersion equations linear in all BZ directions around HSPs in quasi-2D crystals are singled out, with the corresponding effective low-energy Bloch Hamiltonians. We utilize allowed (co)IRs (calculated by POLSym code [34], and recently made available online [35]) of the symmetry groups of HSPs obtained by the action of layer (LGs), double layer (DLGs), and corresponding gray magnetic groups (gray LGs and gray DLGs) in BZ. It turns out that possible dimensions of (co)IRs, and therefore of the effective Hamiltonian models, are 1, 2, and 4. Among them, two-dimensional ones may correspond to the Hamiltonians with completely linear band crossings hosting non-degenerate conical dispersion (1DC), while four-dimensional (co)IRs support two-degenerate conical (2DC), poppy flower (PF), or fortune teller (FT) shape of energy. The conical and PF dispersions may characterize semimetals, while the presence of FT indicates nodal line metal (where equienergetic lines cross in HSP). In addition, precise usage of (co)IRs (Clebsch–Gordan series, Wigner's types), enables to consider relations between single and double, or ordinary and gray groups enlightening

the impact of spin–orbit interaction or TR on the dispersions in HSPs. Results on the band crossings patterns (groups, HSPs, types, effects of spin and TR) are tabulated and discussed, stressing out the cases complementing or correcting those in literature.

The paper is structured as follows. Establishing basic concepts and notation, section 2 is a brief review of the group-theoretical apparatus within $\boldsymbol{k}\cdot\boldsymbol{p}$ theory. Then in section 3 we single out relevant HSPs in BZ of quasi-2D crystals, model Hamiltonians and the corresponding linear dispersions related to HSPs. Besides this, the robustness of the crossings (whether they are essential or not) is addressed in section 4, analyzing impact of spin and TR.

2. Symmetry of effective Bloch Hamiltonian

Following standard approach, we consider single-particle Hamiltonian H invariant under symmetry group G being one of the four types: ordinary group $G = L$, without TR symmetry θ, is either purely geometrical layer group, or its double extension (to include spin space and SO interaction), while with θ it becomes (single or double) gray layer group $G = L + \theta L$ (for nonmagnetic systems).

On momentum $\boldsymbol{k}$ from BZ L acts by isogonal point group P_I. In this way LG makes stratification of BZ, singling out generic stratum, and special lines and points, each of them being fixed by characteristic little group (stabilizer) $L_{\boldsymbol{k}}$ (a subgroup in L) of a representative momentum point $\boldsymbol{k}$. Coset representatives h from Lagrange partition $L = \bigcup_h hL_{\boldsymbol{k}}$ generate star of $\boldsymbol{k}$, and the set of representative points of all stars is irreducible domain (ID). Also, due to the trivial action of translations in BZ, all translations are in $L_{\boldsymbol{k}}$, turning it into a (double) layer group.

While TR symmetry acts trivially on a position vector, it changes the sign of a momentum. Therefore, the addition of TR to the symmetry of layered systems in general changes stratification of the BZ, and three types of stabilizers $G_{\boldsymbol{k}}$ (as subgroups in $G = L + \theta L$) may occur. For a TR invariant momentum (TRIM) $\boldsymbol{k}$ the stabilizer is (i) gray group $G_{\boldsymbol{k}} = L_{\boldsymbol{k}} + \theta L_{\boldsymbol{k}}$; otherwise, if $\boldsymbol{k}$ is not TRIM, $G_{\boldsymbol{k}}$ is either (ii) black-and-white $G_{\boldsymbol{k}} = L_{\boldsymbol{k}} + \theta h L_{\boldsymbol{k}}$ (if there is an non-identity element h such that $h\boldsymbol{k} = -\boldsymbol{k}$), or (iii) ordinary $G_{\boldsymbol{k}} = L_{\boldsymbol{k}}$ (either single or double) group. Notably, only in the latest case (iii) the star is doubled due to the TR symmetry, while otherwise it remains the same (cases (i) and (ii)).

Commuting with the translational subgroup, the Hamiltonian reduces into the Bloch spaces. If g belongs to $G_{\boldsymbol{k}}$, meaning that g stabilizes momentum $\boldsymbol{k}$ up to the vector of inverse lattice, then

$$[D(g), H(\boldsymbol{k})] = 0, \tag{1}$$

where $D(G_{\boldsymbol{k}})$ is representation of stabilizer $G_{\boldsymbol{k}}$ in the Bloch space and $H(\boldsymbol{k})$ is the Bloch Hamiltonian. The TR is antilinear operation in the state space, and therefore linear-antilinear representations $D(G_{\boldsymbol{k}})$ of magnetic little groups are considered: $D(L_{\boldsymbol{k}}) = d(L_{\boldsymbol{k}})$ are linear operators, while the other elements are represented by antilinear operators $D(\theta h L_{\boldsymbol{k}}) = d(\theta h L_{\boldsymbol{k}})\mathsf{K}$, where $d(\theta h L_{\boldsymbol{k}})$ are linear factors and K is the complex conjugation. Only matrix parts $d(L_{\boldsymbol{k}})$ and $d(\theta h)$ of all elements constitute co-representations. For gray groups, h is the identity element, and $d^2(\theta) = \omega I$, where ω is 1 for spinless, and -1 for spinfull cases (I is identity matrix). Obviously, rewritten in the terms of co-representation for the antilinear coset the relation (1) is $d(g^{-1})H(\boldsymbol{k})d(g) = H^*(\boldsymbol{k})$ (for $g \in \theta h L_{\boldsymbol{k}}$).

Consequently, symmetry provides that the corresponding Bloch Hamiltonian and the stabilizer representation are reduced in $|\alpha|$-dimensional subspaces, where $|\alpha|$ is the dimension of

the allowed irreducible linear(-antilinear) representation $D^{(\boldsymbol{k},\alpha)}(G_{\boldsymbol{k}})$. Eigenvectors $|\boldsymbol{k},\alpha;\ \mathrm{a}\rangle$ of Bloch Hamiltonian:

$$H(\boldsymbol{k})|\boldsymbol{k},\alpha;\mathrm{a}\rangle = \varepsilon_\alpha(\boldsymbol{k})|\boldsymbol{k},\alpha;\mathrm{a}\rangle, \tag{2}$$

are assigned by quantum numbers $(\boldsymbol{k},\alpha)$ of linear(-antilinear) IRs (and allowed representations), meaning [36] that:

$$D(g)|\boldsymbol{k},\alpha;\mathrm{a}\rangle = \sum_{\mathrm{a}'} D^{(\boldsymbol{k},\alpha)}_{\mathrm{a}'\mathrm{a}}(g)|\boldsymbol{k},\alpha;\mathrm{a}'\rangle. \tag{3}$$

Expansion of the Bloch Hamiltonian in the vicinity of HSP $\boldsymbol{k}_0$ is

$$\begin{aligned} H(\boldsymbol{k}_0+\boldsymbol{k}) &= \sum_{n\geqslant 0} H^{(n)}(\boldsymbol{k}_0+\boldsymbol{k}),\\ H^{(n)}(\boldsymbol{k}_0+\boldsymbol{k}) &= \frac{1}{n!}\sum_{p_1,\ldots,p_n} \frac{\partial^n H(\boldsymbol{k}_0)}{\partial k_{p_1}\ldots\partial k_{p_n}} k_{p_1}\ldots k_{p_n}, \end{aligned} \tag{4}$$

where $p_i = 1,2$. Gathering terms with $n>0$ within perturbation $H'(\boldsymbol{k}_0+\boldsymbol{k})$, an effective Hamiltonian is obtained with help of projector $P_\alpha = \sum_{\mathrm{a}=1}^{|\alpha|} |\ \boldsymbol{k}_0,\alpha;\mathrm{a}\ \rangle\langle\ \boldsymbol{k}_0,\alpha;\mathrm{a}\ |$ composed of the eigenvectors of unperturbed Hamiltonian $H^{(0)}(\boldsymbol{k}_0) = H(\boldsymbol{k}_0)$ (matrix with zero order term $n=0$). In the first perturbation order, the effective Hamiltonian is $H'_\alpha(\boldsymbol{k}) = P_\alpha H'(\boldsymbol{k}) P_\alpha$, and the symmetry conditions (1) for each effective term $H^{(n)}_\alpha$ of the expansion (4) becomes:

$$D^{(\boldsymbol{k}_0,\alpha)}(g) H^{(n)}_\alpha(\boldsymbol{k}_0+\boldsymbol{k}) D^{(\boldsymbol{k}_0,\alpha)}(g^{-1}) = H^{(n)}_\alpha(\boldsymbol{k}_0+g\boldsymbol{k}). \tag{5}$$

As before, depending on the type of a considered system, $D^{(\boldsymbol{k}\alpha)} = d^{(\boldsymbol{k}\alpha)}$ is a unitary integer (spinless) or a half-integer (spinfull) IR of a (double) layer group, or, a linear-antilinear representation composed of the unitary matrix of coIR $d^{(\boldsymbol{k}\alpha)}$ (multiplied by operator of complex-conjugation on the coset accompanied by TR) for a magnetic little group. In all these cases of layer groups the dimensions of IRs are 1, 2 or 4.

Stabilizer $G_{\boldsymbol{k}_0+\boldsymbol{k}}$ of a representative momentum $\boldsymbol{k}_0+\boldsymbol{k}$ from the generic stratum (dense in BZ) is a subgroup of $G_{\boldsymbol{k}_0}$, and the subduced (co)representation obeys compatibility relations

$$d^{(\boldsymbol{k}_0\alpha)}(G_{\boldsymbol{k}_0})\downarrow G_{\boldsymbol{k}_0+\boldsymbol{k}} = \oplus_i f_i d^{(\boldsymbol{k}_0+\boldsymbol{k},\alpha_i)}(G_{\boldsymbol{k}_0+\boldsymbol{k}}), \tag{6}$$

where f_i is frequency number of the irreducible component $d^{(\boldsymbol{k}_0+\boldsymbol{k},\alpha_i)}$. For the elements of $G_{\boldsymbol{k}_0+\boldsymbol{k}}$ the symmetry condition (5) becomes commutation causing that the energy branches in the vicinity of $\boldsymbol{k}_0$ have degeneracies (1 or 2) of (co)representations $d^{(\boldsymbol{k}_0+\boldsymbol{k},\alpha_i)}(G_{\boldsymbol{k}_0+\boldsymbol{k}})$, while the degeneracy of the energy at crossing point $\boldsymbol{k}_0$ coincides with the dimension (2 or 4) of (co)representation $d^{(\boldsymbol{k}_0\alpha)}(G_{\boldsymbol{k}_0})$.

3. Linear dispersions

3.1. Effective Hamiltonian

At first, the forms of the effective Hamiltonians having completely linear dispersions in BZ around HSPs will be derived. According to (4), the matrix elements of the effective low-energy Hamiltonian linear ($n=1$) in momentum are $[H^{(1)}_\alpha(\boldsymbol{k}_0+\boldsymbol{k})]_{ab} = \sum_p w^p_{ab} k_p$, where parameters

$w^p_{ab} = \partial[H_\alpha(\boldsymbol{k}_0)]_{ab}/\partial k_p$ are constrained by symmetry conditions (5) and hermiticity ($w^p_{ab} = w^{p*}_{ba}$). The conditions (5) can be rewritten in the super-operator form as:

$$\left[d^{(\boldsymbol{k}_0,\alpha)}(g) \otimes d^{(\boldsymbol{k}_0,\alpha)^*}(g) \otimes v(g)\right] w = w, \quad \text{for } g \in L_{k_0} \tag{7}$$

$$\left[d^{(\boldsymbol{k}_0,\alpha)}(g) \otimes d^{(\boldsymbol{k}_0,\alpha)^*}(g) \otimes I_2\right] w^* = w, \quad \text{for } g = \theta h, \tag{8}$$

where w is a column of parameters w^p_{ab}, which is looked for. The group action in 2D BZ is introduced by usual two-dimensional polar-vector representation $v(L_{k_0})$ of subgroup, and $v(\theta h) = I_2$. Since a linear effective Hamiltonian is bi-uniquely related to a non-vanishing column w, from (7) it follows that w is a fixed point for subgroup representation $d^{(\boldsymbol{k}_0,\alpha)} \otimes d^{(\boldsymbol{k}_0,\alpha)^*} \otimes v$, i.e. linear terms exist if [21] vector representation $v(L_{k_0})$ appears in $d^{(\boldsymbol{k}_0,\alpha)} \otimes d^{(\boldsymbol{k}_0,\alpha)^*}(L_{k_0})$; for magnetic groups there is additional condition (8) for the antiunitary coset.

Linearly independent columns $w_{ab} = \left(w^1_{ab}, w^2_{ab}\right)^{\mathrm{T}}$ define *linearity rank*: number of BZ directions along which energies are linear in $\boldsymbol{k}$. Obviously, completely linear dispersions have linearity rank 2. Since it is beyond the scope of the paper, herein the details about the dispersions are not studied, we only note in section 4 which groups have linearity rank 1 (the vanishing linear term could be either nodal line when all higher order terms cancel, or of higher order dispersion). Linearity rank 0 refers to Hamiltonians without linear terms.

Instead of using absolute basis and parameters w^p_{ab}, it is more convenient to give the effective Hamiltonians in the basis of Hermitian matrices. With Pauli matrices σ_i $(i = 1, 2, 3)$ and identity matrix $\sigma_0 = I_2$, the effective 2D and 4D Hamiltonians (1D does not yield band crossing) are:

$$H_2 = \sum_{i=0}^{3} \sum_{p=1}^{2} v^p_i k_p \sigma_i, \tag{9}$$

$$H_4 = \sum_{i,j=0}^{3} \sum_{p=1}^{2} v^p_{ij} k_p (\sigma_i \otimes \sigma_j). \tag{10}$$

Clearly, real parameters v^p_i and v^p_{ij} are bi-uniquely related to w^p_i and w^p_{ij}, respectively. For each HSP and its allowed (co)IRs [35] of dimension 2 and 4, the symmetry allowed parameters v^p_i and v^p_{ij} are to be found. The task is performed assuming that layer is perpendicular to the z-axis. All calculations follow notation from [34, 35] (labels of HSPs, IDs), including (co)IRs.

Orthogonal part of any Euclidean transformation from arbitrary layer group leaves both the xy-plane and the z-axis invariant, having thus block-diagonal $2 \times 2 + 1 \times 1$ form. Action in 2D BZ is defined by the upper block. As a result, there is 10 different isogonal groups [35] composed of these 2×2 matrices, which, due to torus topology, yield 14 IDs of 2D BZ. IDs are the same for LG and DLG, while adding TR changes ID of noncentrosymmetric groups. Ordinals of the IDs are associated to the ordinary (gray) groups in the row ID (ID') in figure 2.

There are seven special points (figure 1): $\Gamma = (0, 0)$, $X = (1/2, 0)$, $Y = (0, 1/2)$, $S = (1/2, 1/2)$, $M = (1/2, 0)$, $K = (1/3, 1/3)$ and $L = (2/3, -1/3)$, with coordinates given in primitive basis $\{\boldsymbol{b}_1, \boldsymbol{b}_2\}$. They are distributed over 10 IDs: ID1 and ID3-ID5 have no HSPs; ID2 and ID8 have Γ, X, Y, and S; ID9 has Γ, Y, and S; ID7 and ID13 have Γ, X, and S; ID6 and ID12 have Γ, K, and L; ID10 and ID14 have Γ, M, and K; ID11 has Γ and K. For oblique and rectangular-p groups with all non-symmorphic elements having fractional translations parallel

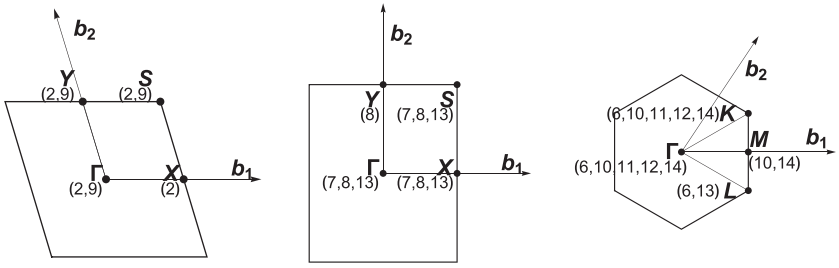

Figure 1. HSPs. Each point is shown only in ID (equivalent copies from BZ are missing). Ordinals of IDs [35] are listed in brackets; IDs are associated to groups in figure 2. Left panel: oblique and c-centered rectangular ($|\boldsymbol{b}_1| = |\boldsymbol{b}_2|$) groups; middle panel: rectangular-p and square ($|\boldsymbol{b}_1| = |\boldsymbol{b}_2|$) groups; right panel: hexagonal groups.

to one direction (for group 45), $\boldsymbol{b}_1$ is perpendicular to that direction (to the symmorphic reflection plane). For group 34 (32, 33, 43) $\boldsymbol{b}_1$ is along axis (screw axis) of order two. This notation differs from [37] in the following way (notation in brackets corresponds to [37]): for oblique groups $X(Y)$, $Y(B)$, $S(A)$; for rectangular-c $Y(S)$, $S(Y)$; for square $Y(X)$, $S(M)$; for rectangular-p groups 8, 11, 12, 16, 17, 20, 24, 31, 32, 33, 34, 38, 40, 41, 43, 45 $X(Y)$, $Y(X)$. For other cases the two notations are the same.

All of the HSPs are TRIM except K and L. Therefore, the stabilizer of Γ, X, Y, S, M is a gray group, while for K it is either a black-and-white (in hexagonal gray LGs: 66, 67, 69, 71–73, 75–78, 80) or an ordinary group (in the hexagonal gray LGs: 65, 68, 70, 74, 79). Stabilizers of L are ordinary, as it is the HSP only in ordinary groups (68, 70 and 79). In the most of the cases the stabilizer is the whole group, exceptions are points Y in ID9, K in ID11 and ID14, and X in ID13 where it is a halving subgroup, and point M in ID14 where the stabilizer is index-three subgroup.

Altogether we found 42 different effective Hamiltonians with completely linear dispersions at HSPs: 21 for 2D and 21 for 4D Hamiltonians are presented in tables 1 and 2. Number of nonzero coefficients v_i^p and v_{ij}^p may be 6, 4, 3, 2 or 1, as emphasized; the other vanish due to the symmetry. In particular, this includes those responsible for slope, which manifests that neither of the dispersions is tilted.

The results for all of 80 layer group clusters are summarized in figure 2. All HSPs hosting linearity rank 2 dispersions are listed, once for each of the associated allowed representations assigning/supporting such dispersions, with indicated effective model (subscript). The list of linear dispersions systematized in this way may be used for various analyzes, and in the following sections some of them will be performed.

3.2. Dispersion types

Band crossings of the presented Hamiltonian models have linearity rank 2 with conical, PF (both can be realized in isotropic or anisotropic forms) or FT shape of dispersion. A conical dispersion corresponds to compatibility relations (6) with dimensions $2 \to 1 \oplus 1$ (1DC), or $4 \to 2 \oplus 2$ (2DC), while the both PF and FT are related to splitting dimensions $4 \to 1 \oplus 1 \oplus 1 \oplus 1$. The cases with 1DC and 2DC are usually referred to as Weyl and Dirac fermions respectively. PF consists of two mutually rotated non-degenerate anisotropic cones (some authors consider PF as generalized Dirac dispersion [25, 39]), while FT is composed of locally flat bands, with equienergetic nodal lines.

Table 1. Two-dimensional effective Hamiltonian forms. Non-vanishing symmetry adapted parameters v_i^p in (9) are defined in terms of independent constants c_i (obtaining values in concrete problems). Symbol in column S is used in figure 2 to identify model, while the number of the independent parameters, and corresponding dispersion equation are in columns Par. and equation; all energy branches are non-degenerate. Two coefficients v_0^1 and v_0^2, vanishing in all models, are omitted.

S	v_1^1	v_2^1	v_3^1	v_1^2	v_2^2	v_3^2	Par.	Equation
a	0	0	c_1	0	c_2	0	2	(11b)
b	0	0	c_1	c_2	0	0	2	(11b)
c	0	0	c_1	c_2	c_3	0	3	(11b)
d	0	$-c_1$	0	c_1	0	0	1	(11c)
e	0	c_1	0	c_1	0	0	1	(11c)
f	0	c_2	0	0	0	c_1	2	(11b)
g	0	c_2	0	c_1	0	0	2	(11b)
h	c_1	0	0	0	c_1	0	1	(11c)
i	c_1	0	0	0	c_2	0	2	(11b)
j	c_1	$-c_1$	0	$-c_1$	$-c_1$	0	1	(11c)
k	c_1	c_1	0	$-c_1$	c_1	0	1	(11c)
l	$\sqrt{3}c_1$	$-c_1$	0	c_1	$\sqrt{3}c_1$	0	1	(11c)
m	c_1	$-\sqrt{3}c_1$	0	$-\sqrt{3}c_1$	$-c_1$	0	1	(11c)
n	$\sqrt{3}c_1$	$-\sqrt{3}c_2$	0	c_1	$3c_2$	0	2	(11a)
o	c_1	$-c_2$	0	c_2	c_1	0	2	(11c)
p	c_1	c_2	0	c_2	$-c_1$	0	2	(11c)
q	c_1	c_3	0	c_2	c_4	0	4	(11a)
r	c_2	c_3	0	0	0	c_1	3	(11b)
s	$\sqrt{3}c_2$	$\sqrt{3}c_3$	$\sqrt{3}c_1$	c_2	c_3	$-3c_1$	3	(11a)
t	$\sqrt{3}c_2$	$-\sqrt{3}c_3$	$\sqrt{3}c_1$	$-3c_2$	$3c_3$	c_1	3	(11a)
u	c_3	c_5	c_1	c_4	c_6	c_2	6	(11a)

For completeness, a brief overview of all types of dispersions (of linearity rank 2) are given, despite some of them have been already studied [11, 23, 24, 28, 29]. For each model (row of the tables 1 and 2) the Hamiltonian matrix is formed according to (9) or (10) with non-vanishing v_i^p and v_{ij}^p; it is expressed in terms of independent coefficients $c_1, \ldots, c_6$ (given in the row). As eigenvalues of these $\boldsymbol{k}$-dependent matrices, the obtained dispersions are parametrized by coefficients c_i. For example $c_1(\sqrt{3}k_1 + k_2)\sigma_1 - c_2(\sqrt{3}k_1 - 3k_2)\sigma_2$ is the matrix for the two dimensional Hamiltonian in 14th row in table 1 (symbol *n*).

General anisotropic 1DC dispersion is

$$\varepsilon_{\pm}(k_1, k_2) = \pm\sqrt{ak_1^2 + bk_1k_2 + ck_2^2}, \tag{11a}$$

where a, b, c are c_i-related parameters with ranges providing real energies. Equienergetic curves on this cone are ellipses with semi-axes a' and c' ($\frac{a}{\varepsilon^2} = \frac{\cos^2\varphi}{a'^2} + \frac{\sin^2\varphi}{c'^2}$, $\frac{c}{\varepsilon^2} = \frac{\sin^2\varphi}{a'^2} + \frac{\cos^2\varphi}{c'^2}$, $\frac{b}{\varepsilon^2} = 2\cos\varphi\sin\varphi\left(\frac{1}{a'^2} - \frac{1}{c'^2}\right)$), which are rotated with respect to the k_1k_2-coordinate system for the angle φ between axes a' and k_1. To illustrate, the Hamiltonian *n* (table 1) from the above example has dispersion (11a), with $a = 3(c_1^2 + c_2^2)$, $b = \sqrt{12}(c_1^2 - 3c_2^2)$ and $c = c_1^2 + 9c_2^2$. For $b = 0$ the dispersion is still an anisotropic 1DC (but not rotated)

$$\varepsilon_{\pm}(k_1, k_2) = \pm\sqrt{ak_1^2 + ck_2^2}, \tag{11b}$$

Table 2. Four-dimensional effective Hamiltonian forms. Non-vanishing symmetry adapted parameters v_{ij}^{p} in (10) are defined in terms of independent constants c_i (obtaining values in concrete problems). Symbol in column S is used in figure 2 to identify model, while the number of the independent parameters, corresponding dispersion equation, and the degeneracy of the branches are in columns Par, equation, and Deg. Ten coefficients v_{00}^{1}, v_{01}^{1}, v_{03}^{1}, v_{32}^{1}, v_{00}^{2}, v_{01}^{2}, v_{03}^{2}, v_{12}^{2}, v_{22}^{2} and v_{32}^{2}, vanishing in all models, are omitted.

S	v_{02}^{1}	v_{10}^{1}	v_{11}^{1}	v_{12}^{1}	v_{13}^{1}	v_{20}^{1}	v_{21}^{1}	v_{22}^{1}	v_{23}^{1}	v_{30}^{1}	v_{31}^{1}	v_{33}^{1}	v_{02}^{2}	v_{10}^{2}	v_{11}^{2}	v_{13}^{2}	v_{20}^{2}	v_{21}^{2}	v_{23}^{2}	v_{30}^{2}	v_{31}^{2}	v_{33}^{2}	Par.	Equation	Deg.
A	0	0	0	0	0	0	0	0	0	0	0	c_1	0	0	0	c_2	0	0	c_3	0	0	0	3	(11b)	2
B	0	0	0	0	0	0	0	0	0	0	0	c_1	0	c_2	0	0	c_3	0	0	0	0	0	3	(11b)	2
C	0	0	0	0	0	0	0	0	0	0	0	c_1	0	c_3	0	0	c_4	0	0	0	c_2	0	4	(11b)	2
D	0	0	0	0	0	0	0	0	0	0	c_1	0	0	c_2	0	0	c_3	0	0	0	0	0	3	(11b)	2
E	0	0	0	0	0	$-c_1$	0	0	0	0	0	0	0	c_1	0	0	0	0	0	0	0	0	1	(11c)	2
F	0	0	0	0	0	$-\frac{c_1+c_2}{2}$	0	0	$\frac{c_1-c_2}{2}$	0	0	0	0	$\frac{c_1+c_2}{2}$	0	$\frac{c_1-c_2}{2}$	0	0	0	0	0	0	2	(12d)	1
G	0	0	0	0	c_2	0	0	0	$-c_3$	0	0	0	0	0	0	0	0	0	0	0	0	c_1	3	(11b)	2
H	0	0	0	0	c_2	0	0	0	c_4	0	0	c_1	c_3	0	0	0	0	0	0	0	0	0	4	(11b)	2
I	0	0	0	0	c_3	0	0	0	c_5	0	0	c_1	0	0	c_4	0	0	c_6	0	0	c_2	0	6	(12a)	1
J	0	0	0	c_3	0	0	0	c_1	0	0	0	0	c_2	0	0	0	0	0	0	0	0	0	3	(12c)	1
K	0	0	0	c_4	0	0	0	c_2	0	c_1	0	0	c_3	0	0	0	0	0	0	0	0	0	4	(12c)	1
L	0	0	c_4	0	0	0	c_6	0	0	0	c_2	0	0	c_3	0	0	c_5	0	0	c_1	0	0	6	(12a)	1
M	0	c_1	0	0	0	$-c_2$	0	0	0	0	0	0	0	c_2	0	0	c_1	0	0	0	0	0	2	(11c)	2
N	0	c_2	0	0	0	c_3	0	0	0	0	0	0	0	0	0	0	0	0	0	0	c_1	0	3	(11b)	2
O	0	c_2	0	0	0	c_4	0	0	0	c_1	0	0	c_3	0	0	0	0	0	0	0	0	0	4	(12c)	1
P	0	c_3	0	0	0	c_5	0	0	0	0	c_1	0	0	c_4	0	0	c_6	0	0	0	c_2	0	6	(11a)	2
Q	0	c_3	0	0	0	c_5	0	0	0	c_1	0	0	0	0	0	c_4	0	0	c_6	0	0	c_2	6	(12a)	1
R	c_1	c_2	0	0	c_3	$-c_3$	0	0	c_2	0	c_1	0	c_1	c_2	0	$-c_3$	$-c_3$	0	$-c_2$	0	$-c_1$	0	3	(12b)	1
S	c_2	0	0	0	0	0	0	0	0	0	0	0	0	0	0	0	0	0	0	0	c_1	0	2	(11b)	2
T	c_3	0	0	0	0	0	0	0	0	0	0	0	0	0	0	c_2	0	0	c_4	0	0	c_1	4	(11b)	2
U	c_3	0	0	0	0	0	0	0	0	0	0	0	0	c_2	0	0	c_4	0	0	c_1	0	0	4	(12c)	1

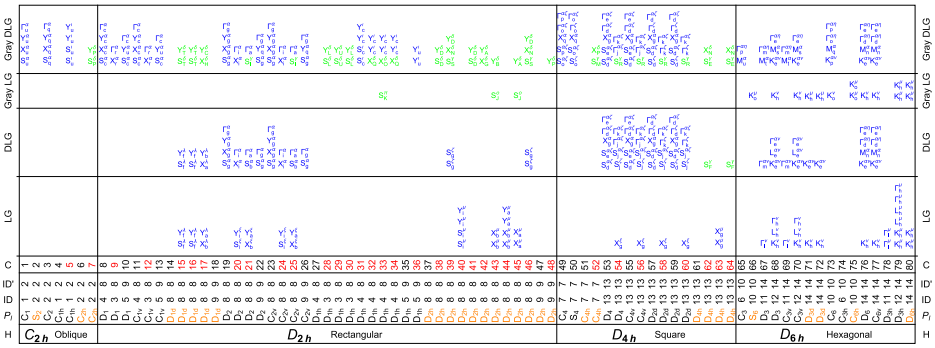

Figure 2. HSPs (see figure 1) hosting completely linear dispersions obtained by action of LG, DLG, and their gray extensions in 2D BZ for each cluster C; ordinals are according to [38]. Dimensions of the allowed (co)IRs are distinguished by colors: blue stands for 2D, while green corresponds to 4D (co)IRs. The subscript is the label of the Hamiltonian model in tables 1 and 2. The superscripts correspond to the labels of SO transitions from the tables 3 and 4. Also, the first column *H* is holoedry (with lattice type) and isogonal groups P_I are given in the second one. Those groups with inversion symmetry included are orange colored, while non-symmorphic groups are singled out by red in column C. In the column ID and ID' are ordinals of IDs of (gray) LGs according to [35].

which isohypses are ellipses with semi-axes $\varepsilon/\sqrt{a}$ and $\varepsilon/\sqrt{c}$. Finally, *isotropic 1DC* is obtained by $a = c$:

$$\varepsilon_{\pm}(k_1, k_2) = \pm a|\boldsymbol{k}|. \tag{11c}$$

As for 4D, *general anisotropic PF* dispersion [29] is:

$$\varepsilon_{\pm,u}(k_1, k_2) = \pm\sqrt{ak_1^2 + ub|k_1k_2| + ck_2^2}, \quad u = \pm 1. \tag{12a}$$

Substituting $a = c$ the *isotropic PF* is obtained:

$$\varepsilon_{\pm,u}(k_1, k_2) = \pm\sqrt{ak^2 + ub|k_1k_2|}, \quad u = \pm 1, \tag{12b}$$

while (12a) for $b^2 = 4ac$ becomes nodal line *FT dispersion* [28]:

$$\varepsilon_{\pm,u}(k_1, k_2) = \pm\left|\sqrt{a}|k_1| + u\sqrt{c}|k_2|\right|, \quad u = \pm 1. \tag{12c}$$

Effective model Hamiltonian F from table 2 describes also isotropic PF but slightly modified:

$$\varepsilon_{\pm,u}(k_1, k_2) = \pm\sqrt{\frac{(c_1^2 + c_2^2)(k_1^2 + k_2^2) + u|c_1^2 - c_2^2||k_1^2 - k_2^2|}{2}}, \quad u = \pm 1; \tag{12d}$$

substitution $k_1 \pm k_2 \to k_\pm$ reduces it to the form (12b). Here, positive $\varepsilon_{+,u}$ (as well as negative $\varepsilon_{-,u}$) branches are touched along the lines $k_1 = \pm k_2$. The rest of the 4D Hamiltonians result in 2DC (double degenerate cones described by equations discussed in 2D case). All dispersions are given in figure 3.

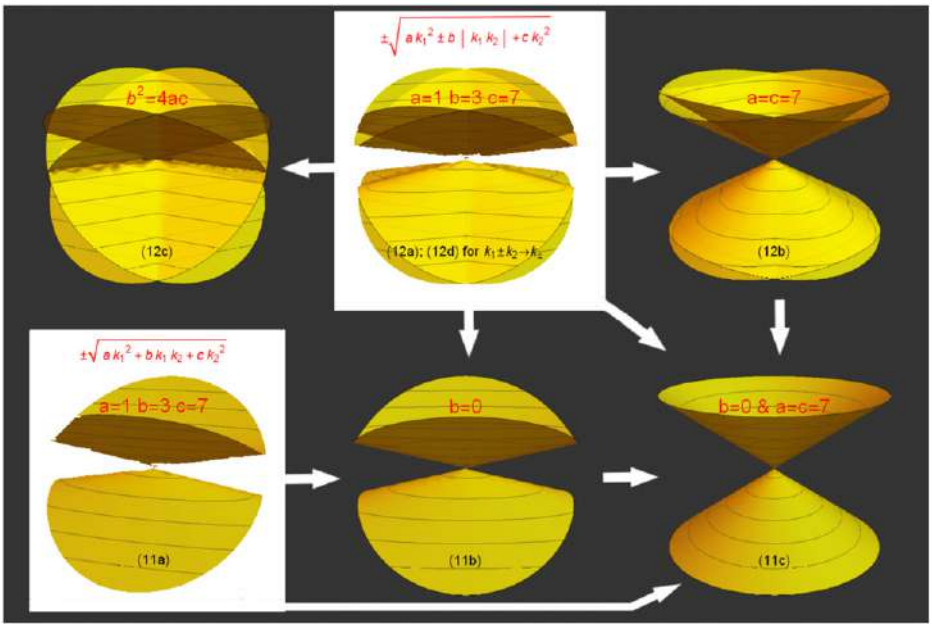

Figure 3. Fully linear dispersions in the vicinity of HSPs in quasi-2D systems. For each type the equation number is given; the value of parameters are set to $a = 1, b = 3, c = 7$, unless it is specified otherwise. All the cases can be obtained from the two most general marked cases; this is denoted by the arrows.

4. Analysis

Having at disposal all possible completely linear dispersions in the HSPs of layered systems, we analyze their interrelations. In this context the roles of SO coupling and TR symmetry are examined. In the group-theoretical language inclusion of spin can be seen as transition from single to double group, while TR relates ordinary and gray group.

4.1. Spin–orbit interaction

SO interaction is taken into account through the relation between integer and half-integer representations. Total space is tensor product of the orbital space with two-dimensional spin-half space, the later carrying spin representation $u(G_{\boldsymbol{k}_0}) \in \mathrm{SU}(2)$. Since composed of SU(2) matrices, u can be either irreducible or reducible $u = u_1 \oplus u_2$ (u_i are irreducible). Hence, each integer irreducible (allowed) co-representation $d^{(\boldsymbol{k}_0,\alpha)}(G_{\boldsymbol{k}_0})$ is multiplied by $u(G_{\boldsymbol{k}_0})$, yielding a half-integer representation, either irreducible itself $d^{(\boldsymbol{k}_0,\tilde{\alpha})}(G_{\boldsymbol{k}_0})$ (with frequency number $f^{\tilde{\alpha}} = 1$ in the decomposition below), or decomposed onto irreducible components (associated to $\boldsymbol{k}_0$ and counted by $\tilde{\alpha}$):

$$d^{(\boldsymbol{k}_0,\alpha)}(G_{\boldsymbol{k}_0}) \otimes u(G_{\boldsymbol{k}_0}) = \oplus_{\tilde{\alpha}} f^{\tilde{\alpha}} d^{(\boldsymbol{k}_0,\tilde{\alpha})}(G_{\boldsymbol{k}_0}). \tag{13}$$

However, not all completely linear band crossings remain such when spin space is added. Besides (13), this depends also on compatibility relation (6) between HSP and generic point stabilizer (co)IRs. Namely, the tensor product of the both sides of (6) by the spin representation

u can be found: obvious rule $u(G_{\boldsymbol{k}_0}{\downarrow}G_{\boldsymbol{k}_0+\boldsymbol{k}}) = u(G_{\boldsymbol{k}_0+\boldsymbol{k}})$ gives $(d^{(\boldsymbol{k}_0\alpha)}(G_{\boldsymbol{k}_0}) \otimes u(G_{\boldsymbol{k}_0})){\downarrow}G_{\boldsymbol{k}_0+\boldsymbol{k}} = \oplus_i f_i(d^{(\boldsymbol{k}_0+\boldsymbol{k},\alpha_i)}(G_{\boldsymbol{k}_0+\boldsymbol{k}}) \otimes u(G_{\boldsymbol{k}_0+\boldsymbol{k}}))$. Then right and left sides are reduced in Clebsch–Gordan series.

As an illustration of mechanism how band splitting (the degeneracy of branches around a crossing point) is changed after the SO inclusion, let us consider the u-reducible case. The components u_j ($j = 1, 2$) are one-dimensional, and remain irreducible when subduced onto generic domain. Clearly, following the relation (13), each integer (orbital) (co)IR is decomposed onto two half-integer (co)IRs $d^{(\boldsymbol{k}_0,\tilde{\alpha}_j)}(G_{\boldsymbol{k}_0})$ of the same dimension, equivalent to $d^{(\boldsymbol{k}_0,\alpha)}(G_{\boldsymbol{k}_0}) \otimes u_j(G_{\boldsymbol{k}_0})$, giving essentially two independent energies. Applying further the compatibility relation leads to $(d^{(\boldsymbol{k}_0,\alpha)}(G_{\boldsymbol{k}_0}) \otimes u_j(G_{\boldsymbol{k}_0})){\downarrow}G_{\boldsymbol{k}_0+\boldsymbol{k}} = \sum_i f_i^j(d^{\boldsymbol{k}_0+\boldsymbol{k},\alpha_i}(G_{\boldsymbol{k}_0+\boldsymbol{k}}) \otimes u_j(G_{\boldsymbol{k}_0+\boldsymbol{k}}))$, which determines the degeneracy of branches around HSP for each group of bands counted by j when SO is considered.

We calculated the decompositions (13) for the both cases without and with TR symmetry. Results with crossing bands are presented in the table 3 for ordinary groups and table 4 for gray groups, together with linearity rank. Extracting the data from these tables, i.e. analyzing (13) for all possible dimensions (1, 2, and 4) of (co)IRs, different ways how SO may affect band crossings are listed below, where notation $|\alpha| \xrightarrow{\text{SO}} \oplus_{\tilde{\alpha}}|\tilde{\alpha}|$ is used to explicate the dimensions of the allowed representations in spinless and spinful cases. Non-crossing cases correspond to linearity rank 0.

- $1 \xrightarrow{\text{SO}} 2$. SO induces transition from an orbital nondegenerate band (no crossing) to a band crossing, with one of the following dispersions:
  - (α) 1DC;
  - (β) Linearity rank 1.
- $2 \xrightarrow{\text{SO}} 4$. Transitions from 2D integer (co)IR are:
  - (γ) A two-fold orbital band (no crossing) becomes four-degenerate point with (modified) PF or 2DC;
  - (δ) 2D crossing point of linearity rank 1 yields four-degenerate band crossing with PF, FT or 2DC;
  - (ϵ) 2D crossing point of linearity rank 1 becomes 4D crossing with linearity rank 1.
- $2 \xrightarrow{\text{SO}} 2 \oplus 2$. When 2D integer (co)IR produces two 2D half-integer (co)IRs, possible patterns are:
  - (ζ) Single two-fold orbital band (no crossing) yields two 1DC (differing in energy);
  - (η) Single two-fold orbital band (no crossing) becomes a 1DC and a two-fold band (without crossing);
  - (θ) Single two-fold orbital band (no crossing) gives two two-degenerate crossings of linearity rank 1;
  - (ι) Two-degenerate point of linearity rank 1 gives two 1DC;
  - (κ) Two-degenerate point of linearity rank 1 gives two two-degenerate linearity rank 1 crossings;
  - (λ) Spinless 1DC yields two 1DC;
  - (μ) Spinless 1DC transforms into two two-fold band (gap opening pattern).
- $2 \xrightarrow{\text{SO}} 2 \oplus 1 \oplus 1$. Transition from a spinless 1DC crossing to:
  - (ν) 1DC and two non-degenerate bands (cone preserving).

Table 3. Influence of SO coupling to the type of the splitting without TR symmetry: each row denotes a particular type (label in the column T is used as superscript in figure 2) of transition from spinless case (described s by degeneracy $|\alpha|$ at the crossing point and linearity rank L_α) to the spinfull case (characterized by frequency $f^{\tilde{\alpha}}$ in decomposition (13), crossing point degeneracy $|\tilde{\alpha}|$, and linearity rank $L_{\tilde{\alpha}}$). In the last column are corresponding groups with hosting HSPs (also specified in figure 2).

T	$\lvert\alpha\rvert$	L_α	$f^{\tilde{\alpha}}$	$\lvert\tilde{\alpha}\rvert$	$L_{\tilde{\alpha}}$	…, Group HSP_1 HSP_2…, …
α	1	0	1	2	2	19*SXY*Γ, 20*X*Γ, 21*S*Γ, 22*S*Γ, 23*SXY*Γ, 24*X*Γ, 25*S*Γ, 26*S*Γ, 53*SX*Γ, 54*S*Γ, 55*SX*Γ, 57*SX*Γ, 58*S*Γ, 59*SX*Γ, 60*S*Γ, 67Γ, 68*KL*Γ, 69Γ, 70*KL*Γ, 71*K* 72*K*, 76*KM*Γ, 77*KM*Γ 56*S*Γ
γ	2	0	1	4	2	62*S*, 64*S*
ζ	2	0	1 1	2 2	2 2	39*S*, 46*S*, 53*S*Γ, 54*S*Γ, 55*S*Γ, 56*S*Γ, 57*S*Γ, 58*S*Γ, 59*S*Γ, 60*S*Γ
η	2	0	$\begin{smallmatrix}1\\1\end{smallmatrix}$	$\begin{smallmatrix}2\\2\end{smallmatrix}$	$\begin{smallmatrix}0\\2\end{smallmatrix}$	76Γ, 77Γ
κ	2	1	2	2	1	7*S*, 7*Y*, 48*Y*, 52*X*
	2	1	1 1	2 2	1 1	38*SY*, 39*XY*, 41*SY*, 42*XY* 43*SY*, 45*SY*, 46*XY*, 62*X*, 64*X*
λ	2	2	2	2	2	15*SY*, 16*SY*, 17*XY*
μ	2	2	1 1	2 2	0 0	40*SY*, 43*X*, 44*XY*, 45*X*, 63*X*, 78Γ, 79*KL*Γ, 80*K*
ν	2	2	1 1 1	1 1 2	0 0 2	67Γ, 68*KL*Γ, 69Γ, 70*KL*Γ, 71*K*, 72*K*, 76*K*, 77*K*
ξ	2	2	1 1 1 1	1 1 1 1	0 0 0 0	20*SY*, 21*XY*, 24*SY*, 25*XY*, 54*X*, 56*X*, 58*X*, 60*X*

- $2 \xrightarrow{\text{SO}} 1 \oplus 1 \oplus 1 \oplus 1$: another gap opening pattern, where a spinless 1DC splits into

  (ξ) Four non-degenerate bands (no crossing).

- $4 \xrightarrow{\text{SO}} 4 \oplus 4$: one way to split spinless FT dispersion (4D allowed integer representation) is to

  (o) Two four-fold crossings of the linearity rank 1.

- $4 \xrightarrow{\text{SO}} 2 \oplus 2 \oplus 2 \oplus 2$: also, spinless FT dispersion may be transformed into

  (π) Four 2D crossings of linearity rank 1.

Table 4. Influence of SO coupling to the type of the splitting with TR symmetry: each row is a particular type (label in the column T is used as superscript in figure 2) of transition from spinless case (described by degeneracy $|\alpha|$ at the crossing point, linearity rank L_α, and a number W_α of the subgroup IR) to the spinfull case (characterized by frequency $f^{\tilde{\alpha}}$ in decomposition (13), crossing point degeneracy $|\tilde{\alpha}|$, linearity rank $L_{\tilde{\alpha}}$ and Wigner's kind of subgroup IR $W_{\tilde{\alpha}}$). In the last column are corresponding groups with hosting HSPs (also specified in figure 2).

T	$\lvert\alpha\rvert$	L_α	W_α	$f^{\tilde{\alpha}}$	$\lvert\tilde{\alpha}\rvert$	$L_{\tilde{\alpha}}$	$W_{\tilde{\alpha}}$	…, Group HSP_1 HSP_2…, …
α	1	0	1	1	2	2	−1	1*SXY*Γ, 10*Y*, 13*Y*, 65*M*
α	1	0	1	1	2	2	0	3*SXY*Γ, 8*SXY*Γ, 9*X*Γ, 10*S*Γ, 11*SXY*Γ, 12*X*Γ, 13*S*Γ, 22*Y*, 26*Y*, 49*SX*Γ, 50*SX*Γ, 65Γ, 67*M*, 68*M*, 69*M*, 70*M*, 73*KM*Γ
α	1	0	1	1	2	2	1	19*SXY*Γ, 20*X*Γ, 21Γ, 22*S*Γ, 23*SXY*Γ, 24*X*Γ, 25Γ, 26*S*Γ, 53*SX*Γ, 54Γ, 55*SX*Γ, 56Γ, 58Γ, 59*SX*Γ, 60Γ, 67Γ, 68*K*Γ, 69Γ, 70*K*Γ, 76*KM*Γ, 77*KM*Γ 57*SX*Γ
β	1	0	1	1	2	1	0	4*SXY*Γ, 5*X*Γ, 35*Y*, 74*M*
β	1	0	1	1	2	1	1	27*SXY*Γ, 28*X*Γ, 29*X*Γ, 30*X*Γ, 31*X*Γ, 32Γ, 33Γ, 34Γ, 35*S*Γ, 36*S*Γ, 78*M* 79*M*
γ	2	0	0	1	4	2	−1	21*S*, 25*S*
γ	2	0	0	1	4	2	0	54*S*, 56*S*, 58*S*, 60*S*
γ	2	0	1	1	4	2	0	39*S*, 46*S*, 52*S*, 54*S*, 56*S*, 58*S*, 60*S*
γ	2	0	1	1	4	2	1	62*S*, 64*S*
δ	2	1	0	1	4	2	−1	28*SY*, 29*SY*, 30*SY*, 32*X*, 33*X*, 34*X*
δ	2	1	1	1	4	2	−1	7*SY*, 15*SY*, 16*SY*, 17*XY*, 48*Y*, 52*X*
δ	2	1	1	1	4	2	0	38*SY*, 39*XY*, 41*SY*, 42*XY*, 43*Y*, 45*Y*, 46*XY*, 62*X*, 64*X*
ϵ	2	1	1	1	4	1	0	40*SY*, 43*X*, 44*XY*, 45*X*, 63*X*
ζ	2	0	0	1 1	2 2	2 2	0 0	49*S*Γ, 50*S*Γ
ζ	2	0	1	1 1	2 2	2 2	1 1	53*S*Γ, 54Γ, 55*S*Γ, 56Γ, 57*S*Γ, 58Γ, 59*S*Γ, 60Γ
η	2	0	0	1 1	2 2	0 2	−1 0	65Γ
η	2	0	0	1 1	2 2	0 2	0 0	73Γ

(*continued on next page*)

Table 4. Continued.

T	$\lvert\alpha\rvert$	L_α	W_α	$f^{\tilde{\alpha}}$	$\lvert\tilde{\alpha}\rvert$	$L_{\tilde{\alpha}}$	$W_{\tilde{\alpha}}$	..., Group HSP_1 HSP_2..., ...
η	2	0	1	1	2	0	0	67Γ, 68Γ, 69Γ, 70Γ
				1	2	2	1	
η	2	0	1	1	2	0	1	76Γ, 77Γ
				1	2	2	1	
θ	2	0	1	1	2	1	0	32*S*, 34*S*
				1	2	1	0	
ι	2	1	0	1	2	2	−1	5*SY*, 36*Y*
				1	2	2	−1	
ι	2	1	1	1	2	2	0	31*SY*, 32*Y*, 33*Y*, 34*Y*
				1	2	2	0	
κ	2	1	0	1	2	1	−1	9*SY*, 12*SY*
				1	2	1	−1	
κ	2	1	1	1	2	1	0	20*SY*, 21*XY*, 24*SY*, 25*XY*, 54*X*, 56*X*, 58*X*, 60*X*
				1	2	1	0	
μ	2	2	0	1	2	0	−1	66*K*
				1	2	0	0	
μ	2	2	0	1	2	0	0	75*K*
				1	2	0	0	
μ	2	2	1	1	2	0	0	71*K*, 72*K*
				1	2	0	1	
μ	2	2	1	1	2	0	1	79*K*, 80*K*
				1	2	0	1	
ν	2	2	0	1	2	2	0	73*K*
				2	1	0	1	
ν	2	2	1	1	1	0	1	68*K*, 70*K*, 76*K*, 77*K*
				1	1	0	1	
				1	2	2	1	
o	4	2	0	1	4	1	−1	43*S*, 45*S*
				1	4	1	−1	

(*continued on next page*)

Table 4. Continued.

T	$\lvert\alpha\rvert$	L_α	W_α	$f^{\tilde{\alpha}}$	$\lvert\tilde{\alpha}\rvert$	$L_{\tilde{\alpha}}$	$W_{\tilde{\alpha}}$	…, Group HSP_1 HSP_2…, …
				1	2	1	−1	
π	4	2	−1	1	2	1	−1	33*S*
				1	2	1	−1	
				1	2	1	−1	

4.2. Time-reversal symmetry

The role of TR symmetry is clarified through the transition from ordinary L to gray groups G. This involves magnetic (black-and-white, as well) little groups, and possibly new strata (with change of the ID), including HSPs of G not characterizing the corresponding L. An enlarged stabilizer of a momentum $\boldsymbol{k}$ may give rise to an enlarged degeneracy of the energy in $\boldsymbol{k}$, while enlarged star necessarily enlarges the dimension of the associated coIR. In fact, the impact of TR symmetry is essentially encoded in the algorithm for co-representations construction. Irreducible co-representations [17, 18] of $G_{\boldsymbol{k}}$ are derived from IRs of $L_{\boldsymbol{k}}$: each real IR (Wigner's I kind) of $L_{\boldsymbol{k}}$ is extended to co-IR of $G_{\boldsymbol{k}}$, a quaternion IR (II kind, equivalent to its conjugate, but without equivalent real IR) gives co-IR of the double dimension, while two mutually conjugate complex IRs give one co-IR of the double dimension. Hence, besides the case of an ordinary stabilizer $G_{\boldsymbol{k}} = L_{\boldsymbol{k}}$, TR symmetry preserves the HSP degeneracy also for crossings hosted by HSP invariant under magnetic group, but with allowed coIR determined by a real subgroup IR. On the other hand, the HSP degeneracy may be doubled for magnetic stabilizers with quaternion or complex subgroup IR. However, even when HSP degeneracy remains the same, the dispersion need not stay completely linear, and its shape may be not preserved. The enlarged group by TR imposes new conditions on Hamiltonian parameters and also affect the compatibility relations.

For this purpose to each of the stabilizer's (co)IR we assign the number [18] $W = \frac{1}{L_{\boldsymbol{k}}}\sum_{\ell\in L_{\boldsymbol{k}}}\chi\left((\theta h\ell)^2\right)$, which shows whether it is composed of two (mutually non-equivalent $W = 0$, kind III, or equivalent $W = -1$, kind II) or one ($W = 1$, kind I) subgroup IR. It is given as the last entry in the tables 3 and 4 to enable tracking the role of TR symmetry. To illustrate, let us consider, for example, the transition $1 \xrightarrow{\mathrm{SO}} 2\ (\alpha)$ to 1DC described in the subsection 4.1. In the table 4 this appears in 3 rows mutually differing by the last entry (column $W_{\tilde{\alpha}}$). In the third case, when both integer and half-integer coIRs carry the value $W_\alpha = W_{\tilde{\alpha}} = 1$, the corresponding groups appear also in table 3; this means that this type of transition is preserved under TR symmetry. On the contrary, the remaining two cases (with last entries 0 and −1 for half-integer coIRs) do not appear in table 3. This is expected since herein a conical dispersion in gray DLG is hosted by the half-integer coIR composed of two 1D subgroup half-integer IRs. Thus, breaking TR symmetry in these cases leads to non-crossing bands. The both situations are sketched in figure 4.

One can further similarly analyze relations between ordinary and gray groups case-by-case. In this way, combining the results from the both tables 4 and 3, different cluster processes can be found. Some of them are illustrated in figure 4; recall that all the crossings are symmetry enforced (thus no avoided crossing can appear). The skipped cases are with linearity rank 1 either in spinless or in spinfull case.

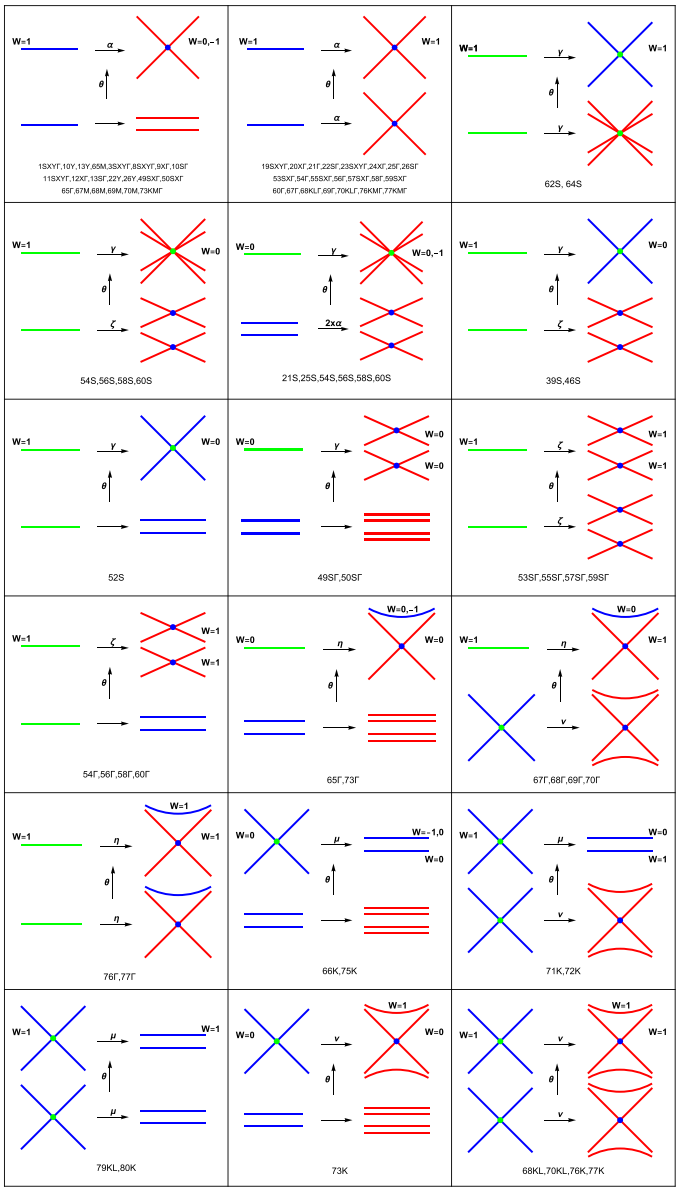

Figure 4. Manifestations of SO coupling and TR symmetry. Each figure describes transitions within a cluster at HSP (cluster and HSP are indicated at the bottom): horizontal arrows are for transitions from single to double groups (with the Greek letter indicating type from tables 3 and 4), while vertical ones are from ordinary to gray (with indicated kind of hosting coIR from table 4). Color of the bands is degeneracy in orbital-spin space: red, blue and green are for degeneracy 1, 2 and 4.

5. Discussion and conclusions

The linear dispersions at HSPs and underlying effective models allowed by integer and half-integer 2D and 4D (co)IRs are studied. Different dispersion types linear in all directions are classified and listed, completing thus the results existing in literature. Having these data at disposal, it was possible to analyze influence of SO coupling and TR symmetry to interrelate dispersions within the same cluster of the single/double ordinary/gray layer groups.

Obtained classification of the effective Hamiltonians may give some insight to band topology. One natural invariant is winding number, along paths around HSP hosting linear dispersion, as this point is a sort of singularity. For illustration, we calculated it for Hamiltonian (9), with result for each of the two bands $w = \mathrm{sgn}(v_1^1 v_2^2 - v_1^2 v_2^1)$.

Summarizing results, firstly note that the LG clusters 2, 6, 14, 18, 37, 47, 51, 61, all of them being centrosymmetric, do not support linear band crossing in HSPs at all, while 4, 27, 35 and 74 do not support fully linear (with linearity rank 2), but have linearity rank 1 band crossings (see table 4). Further, as visible in table 2, the only fully linear 2D band crossing model in HSPs is 1DC. Notably, these are hosted at TRIM and non-TRIM points in ordinary single, as well as in ordinary and gray double groups in both symmorphic and non-symmorphic cases. In the remaining (gray single) groups, 1DC occurs only in *K* (thus not TRIM) point of some (symmorphic) groups [23, 24].

As for 4D models, inclusion of spin gives four-fold degenerate point with PF in two double groups (LG 62 and LG 64), while TR gives rise to FT dispersion [28] in 3 gray LGs. The presence of both spin and TR give rise to 4D coIRs in 27 gray double layer groups. Only 3 of them (7, 48, 52) are without special lines; their special points are surrounded by generic points with 2D allowed coIRs, enabling only 2DC dispersions. In all other 4D cases, besides 2DC cases (for 2D generic allowed coIRs), nondegenerate generic coIRs enable also four-band dispersion structures, but special lines with degenerate coIRs impose touching of pairs of bands, restricting linear rank 2 dispersions to PF and FT types. PF and FT types appear in noncentrosymmetric gray DLGs with a non-symmorphic symmetry: FT in 2 groups, and PF in 10 groups in total [29]. Degeneracy of the generic allowed representations in centrosymmetric gray DLGs admits 2DC dispersions, as it was proposed [11]; actually, this is realized in 15 of these groups, as in the remaining 3 (40, 44 and 63, nonsymmorphic) the dispersion is linear along a single direction, while the second one is special line (at BZ edge) with single 4D allowed coIR, thus becoming four-fold degenerate nodal line. In particular, concerning IDs, 2DC is found in three HSPs *X*, *Y*, *S* (gray DLGs 39, 46), in two HSPs *X*, *S* (52, 62, 64), in two HSPs *Y*, *S* (7, 15, 16, 38, 41), in two HSPs *X*, *Y* (17, 42), and single point *Y* (gray DLGs 43, 45, 48). In the groups 43 and 45 additional HSPs with four-fold band crossings, as required by fermion doubling theorem [15], are at *X* and *S*, but have linearity rank 1 (table 4). Concerning the whole BZ, note that for the groups 48, 52, 62, and 64 points *X* and *Y* are symmetry related. Thus, for engineering Dirac semimetals, it is particularly important to single out group 48, since effectively one need to tune band contacts only at a single point, i.e. for filling $4n + 2$, both (symmetry related) cones in BZ are on the Fermi level, if there are no additional electron or hole pockets.

It is interesting that simultaneously 2D and 4D completely linear dispersions are hosted only by the gray DLGs 21, 25, 32, 33, 34, 54, 56, 58, 60 (note that in these groups there are also HSPs with linearity rank 1). Note further, our results indicate that fermion doubling is not a general rule; namely, in some groups FT (e.g. gray LG33, LG43, LG45) and 2DC (e.g. double gray LG39 and LG46) are the only linear dispersions and appear in odd number of HSPs. More complex situation is with 1DC and PF, since whenever there are odd number of these dispersion, there are also other dispersion types.

Inclusion of the spin–orbit interaction causes various effects on the HSPs' dispersions, including gap closing (α, γ, η), gap opening (ξ), cone preserving (ν), cone splitting (λ) scenarios (discussion about the cases with the linearity rank 1 is skipped). For example, an isotropic 1DC in gray LGs [23, 24], which is preserved (ν) by SO perturbation also in gray DLG, is at *K* point in symmorphic cluster 68, 70, 73, 76, 77. Similar analysis reported in [30] omitted symmorphic gray DLG 73. Concerning the TR symmetry breaking, we found also that the cone persists at *K* point in corresponding LGs and DLGs 68, 70, 76, 77, except in the group LG and DLG 73, where the vanishing TR symmetry opens a gap.

Besides spinless to spinfull transition, we examined influence of TR symmetry to dispersion at crossing point. Addition of TR symmetry may preserve or double the degeneracy in HSP. Concerning the preserved double degeneracy, our results single out the cases where 1DC appears both with and without TR symmetry, as well as those when TR even prevent linearity of dispersion. On the other hand, TR symmetry in centrosymmetric groups 62 and 64, although does not change four-fold degeneracy, modifies the dispersion type: in ordinary double groups two generic nondegenerate allowed IRs enable two positive (and two negative) bands touching along special lines (with single degenerate allowed IR); TR symmetry joins these IRs in a single 2D allowed coIR, transforming PF to 2DC dispersion.

Focusing on TR symmetric materials without and with SO from the literature, we further discuss applicability of our results. The frequently elaborated honeycomb lattice belongs to LG 80 with *K* point hosting Dirac cone being gaped by SO. That is symmetry prediction confirmed by DFT calculations in honeycomb lattices of C, Si, Ge, Sn or Pb elements [40, 41]. Buckled honeycomb lattice belongs to LG 72 with the same behavior of bands near *K* as in LG 80. Tight binding model on Si, Ge and Se elemental lattices [42] and DFT band structure of As_2X_2 ($X = Cl, F, I, Br$) monolayers [43] confirm our predictions. Similarly, Dirac cones split by SO near *K* point shows LG 66 with nonmagnetic high buckled $Co_2C_{18}H_{12}$ as DFT-example [44]. On the other hand LG 77 supports Dirac cones at *K* both without and with SO, with monolayer FeB_2 [45] and HfB_2 [46] as DFT-examples. Square LG 64 supports Dirac cones at *X* and *S* only in the presence of SO interaction; this is confirmed by DFT band structure of MX compounds ($M = Sc, Y$; $X = S, Se, Te$) [47] as well as in *X* point (*S* point was not discussed since the corresponding energies are too far from the Fermi level) in ARPES experiments and DFT calculations in synthesized layered 3D ZrSiS [48] and numerically in monolayer HfGeTe [49]. Experimentally synthesized α-bismuthene belongs to LG 42 and hosts spinfull Dirac cones at *X* and *Y* points, as confirmed by micro-ARPES technique and DFT calculations [50].

Among already reported structures with PF or FT dispersions are monolayer GaXY ($X = Se, Te$; $Y = Cl, Br, I$), with non-centrosymmetric symmetry LG 32 providing SO caused Dirac cones at *X* point and PF at *Y* point. Indeed, fourfold degeneracy at *Y* point (called Dirac point in [51]) splits linearly away from it, as justified numerically [51] (dispersion near *X* point was not discussed more closely). DFT band structure of monolayer Ta_3SiTe_6 and Nb_3SiTe_6 [52] requires some attention. Corresponding structure with space group $Pmc2_1$ (SG 26 in notation [53]) is obtained by periodic distribution of monolayers along vertical axis. The monolayers may be of the symmetry either LG 28 or LG 29; these two groups are similar, both with the horizontal screw axis of order two, and two planes, the vertical one is mirror and the horizontal glide in LG 28, while in LG 29 the vertical is glide and the horizontal is mirror. LG 28 should host PF dispersions at the points *Y* and *S*, with low energy effective six-parameters Hamiltonian. However, monolayers Ta_3SiTe_6 and Nb_3SiTe_6 have horizontal symmorphic mirror plane [52], and their symmetry group is LG 29, with FT dispersions (special case of PF) at *Y* and *S* points, and effective Hamiltonian having four independent real parameters. Indeed, linear dispersion in *Y* and *S* points are reported [52] (instead of minimal 4 parameters authors use 6 as for LG 28, which can not affect the result).

Since surfaces of (semi-infinite) 3D single crystals are also periodic in two directions, some layer groups are also wallpaper groups being the symmetries of surfaces. Those contain symmetry elements that do not flip the surface-normal: perpendicular (to the surface) rotational axes of order two, three, four, or six, and perpendicular mirror, or glide planes. It may happen that surface reconstruction or adding atoms at surface in regular manner can lower the symmetry. Such is the case for thin layer consisting of odd number of silicon (110)-sheets, where FT dispersion was found experimentally [54]. FT dispersion was caused by the Coulomb interaction (described by gray LGs) rather than by the relativistic corrections (described by gray DLGs) so linear dispersion is maintained over wide energy range. In addition, BZ of reconstructed surface shrinks, so that another FT dispersion at the center of rectangular surface BZ might be obtained by intersection from FT bands originating from the corners. This might explain why FT dispersion at $\overline{X}$ of Si(110)-surface BZ, seen in ARPES [54], remained intact by different surface reconstruction types.

3D TIs are known [19] to have large SO coupling that causes Dirac cones at surface states. Our results apply also to TIs with the remark that only surface states that fall within the bulk gap are investigated in the literature, since they give rise to surface conductivity. The surface states with the energy within the bulk gap, are identified by analysis of topological properties of bulk bands (via bulk-boundary correspondence) and cannot be predicted by group theory alone. 3D compounds Bi_2Se_3, Bi_2Te_3, Sb_2Te_3 and Sb_2Se_3 belong to the SG 166 ($R\bar{3}m$) with (111) surface with symmetry gray DLG 69 so Dirac cones are expected in $\overline{\Gamma}$ and $\overline{M}$ of the surface BZ. DFT calculations show that first three materials have surface Dirac cone at $\overline{\Gamma}$ within the bulk gap, while states near $\overline{M}$ fall far out of the bulk gap and were not shown. On the other hand the last compound Sb_2Se_3 does not have surface states in the gap and it is not TI [55]. Surface low energy effective Hamiltonian near $\overline{\Gamma}$ has one real parameter, in accordance with our results. Surface Dirac cone in $\overline{\Gamma}$ has been seen in ARPES experiments in Bi_2Te_3 and Sb_2Te_3 [56]. Similarly, 3D compound LaBi crystallizes in SG 225 ($Fm\bar{3}m$) with (001) surface having symmetry LG 55. SOC Dirac cones are expected to appear on $\overline{S}$, $\overline{\Gamma}$, and $\overline{X}$ points of the BZ. ARPES experiments supported by DFT calculations show Dirac cones at $\overline{\Gamma}$ and $\overline{S}$ in the bulk gap, while bands near $\overline{X}$ were outside the gap [57]. Theoretically proposed 3D compound Sr_2Pb_3, that belongs to SG 127 ($P4/mbm$) and its (001) surface to LG 56 (wallpaper group 12 in notation [53]), is expected to be non-symmorphic TI [15]. Our result show that SO causes Dirac cone at $\overline{\Gamma}$ and PF at $\overline{M}$ point for LG 56. DFT band structure show linear dispersions from fourfold degenerate energy at $\overline{M}$ [15]. Their effective low energy Hamiltonian has two independent real parameters and suggests that the dispersion is Dirac-like (2DC in our notation). Necessary splitting that causes bands along $\overline{M}$–$\overline{\Gamma}$ to be non-degenerate (as required by symmetry) was attributed to quadratic corrections to the effective Hamiltonian [15]. Our analysis indicates that the dispersion at $\overline{M}$ should be PF, with three-parameters Hamiltonian and with bands along $\overline{M}$–$\overline{\Gamma}$ being non-degenerate already in the linear approximation.

The presented theoretical framework is straightforwardly extendable to (ferro/anti-ferro) magnetic systems invariant under black-and-white ordinary or double groups. Also, it can be used on an equal footing to analyze higher order dispersion terms, dispersions in the vicinity of special lines which occur in 2D BZ of layer materials, as well as to clarify the cases with single linear direction in energy.

Acknowledgments

Authors acknowledge funding by the Ministry of Education, Science and Technological Development of the Republic of Serbia provided by the Institute of Physics Belgrade (VD), Faculty of Physics (NL and MD) and Serbian Academy of Sciences and Arts (MD).

Data availability statement

All data that support the findings of this study are included within the article (and any supplementary files).

ORCID iDs

N Lazić https://orcid.org/0000-0002-3634-0301
V Damljanović https://orcid.org/0000-0001-7517-6439
M Damnjanović https://orcid.org/0000-0003-2806-253X

References

[1] Yan B and Felser C 2017 Topological materials: Weyl semimetals *Annu. Rev. Condens. Matter Phys.* **8** 337–54
[2] Armitage N P, Mele E J and Vishwanath A 2018 Weyl and Dirac semimetals in three-dimensional solids *Rev. Mod. Phys.* **90** 015001
[3] Gao H, Venderbos J W F, Kim Y and Rappe A M 2019 Topological semimetals from first principles *Annu. Rev. Mater. Res.* **49** 153–83
[4] Wieder B J, Kim Y, Rappe A M and Kane C L 2016 Double Dirac semimetals in three dimensions *Phys. Rev. Lett.* **116** 186402
[5] Barry B, Cano J, Wang Z, Vergniory M G, Felser C, Cava R J and Andrei Bernevig B 2016 Beyond Dirac and Weyl fermions: unconventional quasiparticles in conventional crystals *Science* **353** aaf5037
[6] Zhu Z, Winkler G W, Wu Q, Ju L and Soluyanov A A 2016 Triple point topological metals *Phys. Rev.* X **6** 031003
[7] Wang Z, Alexandradinata A, Cava R J and Andrei Bernevig B 2016 Hourglass fermions *Nature* **532** 189–94
[8] Abrikosov A A and Beneslavskii S D 1971 Possible existence of substances intermediate between metals and dielectrics *Sov. Phys. JETP* **32** 699–708
[9] Mañes J L 2012 Existence of bulk chiral fermions and crystal symmetry *Phys. Rev.* B **85** 155118
[10] Fang C, Gilbert M J, Dai X and Andrei Bernevig B 2012 Multi-Weyl topological semimetals stabilized by point group symmetry *Phys. Rev. Lett.* **108** 266802
[11] Young S M and Kane C L 2015 Dirac semimetals in two dimensions *Phys. Rev. Lett.* **115** 126803
[12] van Miert G and Morais Smith C 2016 Dirac cones beyond the honeycomb lattice: a symmetry-based approach *Phys. Rev.* B **93** 035401
[13] Kim J, Baik S S, Jung S W, Sohn Y, Ryu S H, Choi H J, Yang B-J and Kim K S 2017 Two-dimensional Dirac fermions protected by space-time inversion symmetry in black phosphorus *Phys. Rev. Lett.* **119** 226801
[14] Park S and Yang B-J 2017 Classification of accidental band crossings and emergent semimetals in two-dimensional noncentrosymmetric systems *Phys. Rev.* B **96** 125127
[15] Wieder B J, Barry B, Wang Z, Cano J, Kim Y, Kim H-S D, Rappe A M, Kane C L and Andrei Bernevig B 2018 Wallpaper fermions and the nonsymmorphic Dirac insulator *Science* **361** 246–51
[16] Yang J, Fang C and Liu Z-X 2021 Symmetry-protected nodal points and nodal lines in magnetic materials *Phys. Rev.* B **103** 245141

[17] Dimmock J O and Wheeler R G 1962 Irreducible representations of magnetic groups *J. Phys. Chem. Solids* **23** 729–41
[18] Bradley C J and Davies B L 1968 Magnetic groups and their corepresentations *Rev. Mod. Phys.* **40** 359–79
[19] Hasan M Z and Kane C L 2010 Colloquium: topological insulators *Rev. Mod. Phys.* **82** 3045–67
[20] Qi X-L and Zhang S-C 2011 Topological insulators and superconductors *Rev. Mod. Phys.* **83** 1057–110
[21] Kruthoff J, de Boer J, van Wezel J, Kane C L and Slager R-J 2017 Topological classification of crystalline insulators through band structure combinatorics *Phys. Rev.* X **7** 041069
[22] Asano K and Hotta C 2011 Designing Dirac points in two-dimensional lattices *Phys. Rev.* B **83** 245125
[23] Damljanović V and Gajić R 2016 Existence of Dirac cones in the Brillouin zone of diperiodic atomic crystals according to group theory *J. Phys.: Condens. Matter* **28** 085502
[24] Damljanović V and Gajić R 2016 Addendum to 'existence of Dirac cones in the Brillouin zone of diperiodic atomic crystals according to group theory' *J. Phys.: Condens. Matter* **28** 439401
[25] Wieder B J and Kane C L 2016 Spin–orbit semimetals in the layer groups *Phys. Rev.* B **94** 155108
[26] Wang J 2017 Antiferromagnetic Dirac semimetals in two dimensions *Phys. Rev.* B **95** 115138
[27] Young S M and Wieder B J 2017 Filling-enforced magnetic Dirac semimetals in two dimensions *Phys. Rev. Lett.* **118** 186401
[28] Damljanović V, Popov I and Gajić R 2017 Fortune teller fermions in two-dimensional materials *Nanoscale* **9** 19337–45
[29] Damljanović V, Lazić N, Šolajić A, Pešić J, Nikolić B and Damnjanović M 2020 Peculiar symmetry-protected electronic dispersions in two-dimensional materials *J. Phys.: Condens. Matter* **32** 485501
[30] Luo W, Ji J, Lu J, Zhang X and Xiang H 2020 Two-dimensional topological semimetals protected by symmorphic symmetries *Phys. Rev.* B **101** 195111
[31] Tang F and Wan X 2021 Exhaustive construction of effective models in 1651 magnetic space groups *Phys. Rev.* B **104** 085137
[32] Yu Z-M, Zhang Z, Liu G-B, Wu W, Li X-P, Zhang R-W, Yang S A and Yao Y 2022 Encyclopedia of emergent particles in three-dimensional crystals *Sci. Bull.* **67** 375–80
[33] Bouhon A, Lange G F and Slager R-J 2021 Topological correspondence between magnetic space group representations and subdimensions *Phys. Rev.* B **103** 245127
[34] Damnjanović M and Milošević I 2015 Full symmetry implementation in condensed matter and molecular physics—modified group projector technique *Phys. Rep.* **581** 1–43
[35] Nikolić B, Milošević I, Vuković T, Lazić N, Dmitrović S, Popović Z and Damnjanović M 2022 Irreducible and site-symmetry-induced representations of single/double ordinary/grey layer groups *Acta Crystallogr.* A **78** 107–14
[36] Jansen L and Boon M 1967 *Theory of Finite Groups. Applications in Physics* (Amsterdam: North-Holland)
[37] de la Flor G, Souvignier B, Madariaga G and Aroyo M I 2021 Layer groups: Brillouin-zone and crystallographic databases on the Bilbao crystallographic server *Acta Crystallogr.* A **77** 559–71
[38] Kopsky V and Litvin D B 2002 *International Tables of Crystallography Volume E: Subperiodic Groups* (Dordrecht: Kluwer)
[39] Jin Y J, Zheng B B, Xiao X L, Chen Z J, Xu Y and Xu H 2020 Two-dimensional Dirac semimetals without inversion symmetry *Phys. Rev. Lett.* **125** 116402
[40] Yakovkin I N 2017 Spin–orbit band gaps and destruction of Dirac cones *Surf. Sci.* **662** 1–5
[41] Gutzler R and Christian Schön J C 2017 Two-dimensional silicon-carbon compounds: structure prediction and band structures *Z. Anorg. Allg. Chem.* **643** 1368–73
[42] Liu C-C, Jiang H and Yao Y 2011 Low-energy effective Hamiltonian involving spin–orbit coupling in silicene and two-dimensional germanium and tin *Phys. Rev.* B **84** 195430
[43] Tang W, Sun M, Ren Q, Wang S and Yu J 2016 Halogenated arsenenes as Dirac materials *Appl. Surf. Sci.* **376** 286–9
[44] Ma Y, Dai Y, Li X, Sun Q and Huang B 2014 Prediction of two-dimensional materials with half-metallic Dirac cones: $Ni_2C_{18}H_{12}$ and $Co_2C_{18}H_{12}$ *Carbon* **73** 382–8
[45] Zhang H, Li Y, Hou J, Du A and Chen Z 2016 Dirac state in the FeB_2 monolayer with graphene-like boron sheet *Nano Lett.* **16** 6124–9
[46] Liu Z, Wang P, Cui Q, Yang G, Jin S and Xiong K 2019 Theoretical prediction of HfB_2 monolayer, a two-dimensional Dirac cone material with remarkable Fermi velocity *RSC Adv.* **9** 2740–5

[47] Guo H, Zhao J, Chen C, Li S, Jiang W, Fan H, Tian X and Yang S A 2020 Nonsymmorphic nodal-line metals in the two-dimensional rare earth monochalcogenides MX (M = Sc, Y; X = S, Se, Te) *J. Mater. Sci.* **55** 14883–92
[48] Schoop L M *et al* 2016 Dirac cone protected by non-symmorphic symmetry and three-dimensional Dirac line node in ZrSiS *Nat. Commun.* **7** 11696
[49] Guan S, Liu Y, Yu Z-M, Wang S-S, Yao Y and Yang S A 2017 Two-dimensional spin–orbit Dirac point in monolayer HfGeTe *Phys. Rev. Materials* **1** 054003
[50] Kowalczyk P J *et al* 2020 Realization of symmetry-enforced two-dimensional Dirac fermions in nonsymmorphic α-bismuthene *ACS Nano* **14** 1888–94
[51] Wu W, Jiao Y, Li S, Sheng X-L, Yu Z-M and Yang S A 2019 Hourglass Weyl loops in two dimensions: theory and material realization in monolayer GaTeI family *Phys. Rev. Mater.* **3** 054203
[52] Li S, Liu Y, Wang S-S, Yu Z-M, Guan S, Sheng X-L, Yao Y and Yang S A 2018 Nonsymmorphic-symmetry-protected hourglass Dirac loop, nodal line, and Dirac point in bulk and monolayer X_3SiTe_6 (X = Ta, Nb) *Phys. Rev.* B **97** 045131
[53] Hahn T 2005 *International Tables of Crystallography Volume A: Space-Group Symmetry* (Berlin: Springer)
[54] Kopciuszyński M, Krawiec M, Żurawek L and Zdyb R 2020 Experimental evidence of a new class of massless fermions *Nanoscale Horiz.* **5** 679–82
[55] Zhang H, Liu C-X, Qi X-L, Dai X, Fang Z and Zhang S-C 2009 Topological insulators in Bi_2Se_3, Bi_2Te_3 and Sb_2Te_3 with a single Dirac cone on the surface *Nat. Phys.* **5** 438–42
[56] Hsieh D *et al* 2009 Observation of time-reversal-protected single-Dirac-cone topological-insulator states in Bi_2Te_3 and Sb_2Te_3 *Phys. Rev. Lett.* **103** 146401
[57] Nayak J *et al* 2017 Multiple Dirac cones at the surface of the topological metal LaBi *Nat. Commun.* **8** 13942

Physica E 170 (2025) 116224

Contents lists available at ScienceDirect

Physica E: Low-dimensional Systems and Nanostructures

journal homepage: www.elsevier.com/locate/physe

Existence of Mexican-hat dispersion and symmetry group of a layer

Vladimir Damljanović

Institute of Physics Belgrade, University of Belgrade, Pregrevica 118, Belgrade, 11000, Serbia

ARTICLE INFO

Editor: Ming-Wei Wu

Keywords:
Simple bands
Layer groups
Spin–orbit coupling

ABSTRACT

Increased interest in physics of graphene and other two-dimensional materials boosted investigations of band structure near nodal points and lines. In contrast, group theoretical explanation of simple bands (that do not touch other bands), is sporadically present in the literature. This paper presents electronic dispersions up to fourth order in momentum, near Brillouin zone (BZ) high symmetry points of all eighty layer groups. The method applies to non magnetic materials both with or without spin–orbit coupling. Particular attention is devoted to Mexican-hat dispersion, showing that it can appear only at BZ center of hexagonal layer groups. Presented symmetry adapted Taylor expansion of bands can be used to fit ab-initio or experimental band structures, or for analytical calculation of crystal properties. The results presented here might serve also as a guiding tool for design of new two-dimensional materials.

1. Introduction

Discovery of electric field effect in atomically thin graphene increased investigations on two-dimensional (2D) materials. When placed in a vertical magnetic field topological properties of bands become physically measurable. In that sense, most attention is devoted to various type of band crossings, many of which are imposed by symmetry laws [1–4].

On the other hand, simple bands (SB), *i.e.* parts of band structure that do not contain nodal points or lines, also lead to fascinating physics. Two dimensional materials having Mexican-hat dispersion (MHD) are predicted to be multiferroic due to presence of van Hove singularity of the $1/\sqrt{E}$ - type [5]. Furthermore, MHD gives that effective mass on two bands extrema changes sign so that originally repulsive electron–electron interaction becomes attractive, giving quasi-bound electron states [6,7]. In addition, materials with MHD have large figure of merit, which makes them suitable for thermoelectric applications [8,9]. For these reasons it would be useful if a general prescription on how to search materials with MHD would exist, and group theory is a powerful tool in this respect.

In 2D, no publications deal with exhaustive symmetry treatment of SB, to best of author knowledge, although three of them treat low-energy Hamiltonians and dispersions [10], *i.e.* effective Hamiltonians without dispersions [11,12], in the vicinity of nodal points and lines. On the other hand, encyclopedia type papers on dispersions in 3D [13–18] cannot be used easily for 2D in many cases. While it is straightforward task in crystals with axis of order three, four or six, going back from AA stacking to original layer can be complicated in orthorhombic crystals. Fortunately, recent upgrade in C2DB base [19] helps in solving this problem.

In this paper, we have used group-theoretical tools to find dispersions of SB in the vicinity of high-symmetry points (HSPs) in the reciprocal space. We have adapted the Taylor expansion to the underlying symmetry up to polynomial of fourth degree. All HSPs of all eighty layer groups, both without and with spin–orbit coupling (SOC) are covered. The results are applicable to non-magnetic layers where the time-reversal (TRS) alone is symmetry of the system. We have illustrated our results using one-band tight-binding model on a structure having the same symmetry as graphene (which belongs to layer group 80).

2. Method

Let $\mathbf{k}_0$ be a HSP in the BZ. For $\mathbf{k}=\mathbf{k}_0+\mathbf{q}$ ($|\mathbf{q}|$ is small), the electronic dispersion $E(\mathbf{q})$ has the following properties: $E(\hat{g}\mathbf{q})=E(\mathbf{q})$ and, if $\mathbf{k}_0$ is time-reversal invariant momentum (TRIM), $E(-\mathbf{q})=E(\mathbf{q})$. Here $\hat{g}$ is rotation/improper rotation from the point group of the wave vector $\underline{G}_0(\mathbf{k}_0)$ reduced to two-dimensional reciprocal space ($\hat{g}\mathbf{k}_0$ differs from $\mathbf{k}_0$ by a reciprocal lattice vector). In that sense, *e.g.* spatial inversion is represented by $-\hat{\sigma}_0$, while the Pauli matrix $\hat{\sigma}_3$, represents xz-(symmorphic or glide) reflection plane. TRS in the reciprocal space acts as spatial inversion $\hat{\imath}$, so that the effective little group is $\underline{G}_0(\mathbf{k}_0)+\hat{\imath}\underline{G}_0(\mathbf{k}_0)$, if $\underline{G}_0(\mathbf{k}_0)$ does not already contain $\hat{\imath}$. The point groups obtained from $\underline{G}_0(\mathbf{k}_0)$ by adding $\hat{\imath}$ are given in Table 1.

In other words, $\underline{G}_0^{eff}(\mathbf{k}_0)$ is equal to $\underline{G}_0(\mathbf{k}_0)$ if $-\mathbf{k}_0$ does not differ from $\mathbf{k}_0$ by a reciprocal lattice vector ($\mathbf{k}_0$ is not TRIM), or if $\mathbf{k}_0$ is TRIM

E-mail address: damlja@ipb.ac.rs.

https://doi.org/10.1016/j.physe.2025.116224
Received 20 January 2025; Received in revised form 17 February 2025; Accepted 26 February 2025
Available online 10 March 2025

Table 1
Correspondence between group $\underline{G}_0(\mathbf{k}_0)$ and the one with spatial inversion added.

$\underline{G}_0(\mathbf{k}_0)$	$\underline{G}_0(\mathbf{k}_0)\otimes\underline{C}_i$	$\underline{G}_0(\mathbf{k}_0)$	$\underline{G}_0(\mathbf{k}_0)\otimes\underline{C}_i$	$\underline{G}_0(\mathbf{k}_0)$	$\underline{G}_0(\mathbf{k}_0)\otimes\underline{C}_i$
$\underline{C}_1$	$\underline{C}_i$	$\underline{C}_4$	$\underline{C}_{4h}$	$\underline{D}_{2h}$	$\underline{D}_{2h}$
$\underline{C}_s$	$\underline{C}_{2h}$	$\underline{C}_6$	$\underline{C}_{6h}$	$\underline{D}_{4h}$	$\underline{D}_{4h}$
$\underline{C}_2$	$\underline{C}_{2h}$	$\underline{D}_2$	$\underline{D}_{2h}$	$\underline{D}_{6h}$	$\underline{D}_{6h}$
$\underline{C}_3$	$\underline{S}_6$	$\underline{D}_4$	$\underline{D}_{4h}$	$\underline{D}_{2d}$	$\underline{D}_{4h}$
$\underline{D}_3$	$\underline{D}_{3d}$	$\underline{D}_6$	$\underline{D}_{6h}$	$\underline{D}_{3d}$	$\underline{D}_{3d}$
$\underline{C}_{2v}$	$\underline{D}_{2h}$	$\underline{C}_{4v}$	$\underline{D}_{4h}$	$\underline{S}_4$	$\underline{C}_{4h}$
$\underline{C}_{3v}$	$\underline{D}_{3d}$	$\underline{C}_{6v}$	$\underline{D}_{6h}$	$\underline{S}_6$	$\underline{S}_6$
$\underline{C}_{3h}$	$\underline{C}_{6h}$	$\underline{C}_{2h}$	$\underline{C}_{2h}$	$\underline{C}_i$	$\underline{C}_i$
$\underline{D}_{3h}$	$\underline{D}_{6h}$	$\underline{C}_{4h}$	$\underline{C}_{4h}$	$\underline{C}_{6h}$	$\underline{C}_{6h}$

but $\underline{G}_0(\mathbf{k}_0)$ contains spatial inversion. In the case $\mathbf{k}_0$ is TRIM and $\underline{G}_0(\mathbf{k}_0)$ is not centrosymmetric then $\underline{G}_0^{eff}(\mathbf{k}_0)=\underline{G}_0(\mathbf{k}_0)+\hat{i}\underline{G}_0(\mathbf{k}_0)$.

If $E(\mathbf{q})$ is simple band, one can expand $E(\mathbf{q})$ in Taylor series. The coefficients of the expansion (partial derivatives of E) are obtained by Wigner method of group projectors ($\otimes$ denotes the Kronecker product):

$$\hat{P}_n=\frac{1}{|\underline{G}_0^{eff}(\mathbf{k}_0)|}\sum_{g\in\underline{G}_0^{eff}(\mathbf{k}_0)}\underbrace{\hat{g}\otimes\cdots\otimes\hat{g}}_{n}.$$

One acts with the projector $\hat{P}_n$ on trial vector of dimension 2^n ($n=1,2,3,\ldots$). The trial vector must be general but has to reflect symmetry under permutation of coordinates in partial derivatives. For example trial vector for second order derivatives is $|\text{trial2}\rangle=(\partial^2E/\partial q_1^2,\partial^2E/\partial q_1\partial q_2,\partial^2E/\partial q_2\partial q_1,\partial^2E/\partial q_2^2)^T=(u,v,v,w)^T$. In *e.g.* group $\underline{C}_3$ elements are identity ($\hat{E}$), rotation by $2\pi/3$ ($\hat{C}_3$) and rotation by $4\pi/3$ ($\hat{C}_3^2$). In two-dimensional, orthonormal basis those elements are represented in the following way:

$$\hat{E}\leftrightarrow\begin{pmatrix}1&0\\0&1\end{pmatrix},\hat{C}_3\leftrightarrow\frac{1}{2}\begin{pmatrix}-1&-\sqrt{3}\\\sqrt{3}&-1\end{pmatrix},\hat{C}_3^2\leftrightarrow\frac{1}{2}\begin{pmatrix}-1&\sqrt{3}\\-\sqrt{3}&-1\end{pmatrix}.$$

From here we found the group projector for second order derivatives:

$$\hat{P}_2=\frac{1}{2}\begin{pmatrix}1&0&0&1\\0&1&-1&0\\0&-1&1&0\\1&0&0&1\end{pmatrix},$$

which acts on trial vector in the following way:

$$\frac{1}{2}\begin{pmatrix}1&0&0&1\\0&1&-1&0\\0&-1&1&0\\1&0&0&1\end{pmatrix}\begin{pmatrix}u\\v\\v\\w\end{pmatrix}=\frac{1}{2}\begin{pmatrix}u+w\\0\\0\\u+w\end{pmatrix}.$$

Going back to polynomial, we get for the second order: $aq_1^2+0q_1q_2+0q_2q_1+aq_2^2=a(q_1^2+q_2^2)=a\mathbf{q}^2$, where we have included the factor 1/2 arising from second order Taylor expansion into coefficients u, v and w, while $a=(1/2)(u+w)$ is a new real constant.

We have applied the method for all HSPs of all eighty layer groups to find invariant Taylor polynomials up to fourth order in q_1,q_2. The results are shown in the following section. The HSPs of layer groups hosting simple bands are derived by omitting unmovable nodal lines and points given in [10] and movable but unavoidable nodal lines through BZ HSPs given in [20]. When little group of a wave vector contains both one-dimensional and multidimensional allowed irreps, both simple bands and band crossings are possible at this HSP. All types of essential band crossings are described in [10] and here they will be given only by dispersion, where may appear instead of simple bands. Reader interested in band crossings can consult [10] for more detailed description.

In the case of band contacts in two dimensions, minimal cutoff order that induces splitting is equal to two (three) for the case without (with) SOC in non-magnetic case (type II/gray magnetic layer single or double groups) [10,11]. This is smaller than for three-dimensional magnetic space groups where the cutoff order is at most six [11]. For expansion beyond these orders no additional splittings occur. In addition, the existence of SBs near HSPs is governed by the dimensionality of little group's correps. Simple bands are belonging to one-dimensional correps or, in case with SOC, two-dimensional correps if the crystal is invariant under spatial inversion. In the latter case, Kramers' theorem ensures that the two bands stick together across the whole BZ. Therefore, we are sure that expansion of SBs beyond fourth order would not induce splitting.

3. Results

We found in total seven dispersion formulas. For effective little groups $\underline{C}_6$, $\underline{D}_6$, $\underline{C}_{6v}$, $\underline{C}_{6h}$, $\underline{D}_{6h}$, $\underline{S}_6$ and $\underline{D}_{3d}$ one gets the following dispersion (a, b, c, E_0 are real parameters, q_1, q_2 are coordinates of rectangular system):

$$E(\mathbf{q})\approx E_0+a\mathbf{q}^2+b\mathbf{q}^4. \tag{1}$$

For $ab<0$, Eq. (1) presents the MHD for $a<0$, *i.e.* inverted MHD for $a>0$. Groups $\underline{D}_{2d}$, $\underline{C}_{4v}$, $\underline{D}_4$ and $\underline{D}_{4h}$ give (q_1 is along horizontal axis of order two, *i.e.* vertical reflection plane):

$$E(\mathbf{q})\approx E_0+a\mathbf{q}^2+b_1(q_1^4+q_2^4)+b_2q_1^2q_2^2, \tag{2}$$

groups $\underline{C}_4$, $\underline{C}_{4h}$ and $\underline{S}_4$ give:

$$E(\mathbf{q})\approx E_0+a\mathbf{q}^2+b_1(q_1^4+q_2^4)+b_2q_1^2q_2^2+b_3(q_1^3q_2-q_1q_2^3), \tag{3}$$

groups $\underline{D}_2$, $\underline{D}_{2h}$, $\underline{C}_{2v}^z$ and $\underline{C}_{2h}^{\text{horizontal}}$ give (q_1 is along horizontal axis of order two, *i.e.* vertical reflection plane):

$$E(\mathbf{q})\approx E_0+a_1q_1^2+a_2q_2^2+b_1q_1^4+b_3q_2^4+b_2q_1^2q_2^2, \tag{4}$$

groups $\underline{C}_i$, $\underline{C}_2^z$ and $\underline{C}_{2h}^z$ give:

$$E(\mathbf{q})\approx E_0+\sum_{j,l=1}^{2}a_{j,l}q_jq_l+\sum_{j,l,n,m=1}^{2}b_{j,l,n,m}q_jq_lq_nq_m, \tag{5}$$

groups $\underline{C}_3$ and $\underline{C}_{3h}$ give:

$$E(\mathbf{q})\approx E_0+a\mathbf{q}^2+c_1(q_1^3-3q_1q_2^2)+c_2(q_2^3-3q_1^2q_2)+b\mathbf{q}^4, \tag{6}$$

while groups $\underline{D}_3$, $\underline{C}_{3v}$ and $\underline{D}_{3h}$ give (q_1 is along horizontal axis of order two, *i.e.* vertical reflection plane):

$$E(\mathbf{q})\approx E_0+a\mathbf{q}^2+c_1(q_1^3-3q_1q_2^2)+b\mathbf{q}^4. \tag{7}$$

With these knowledge we obtain dispersions in all layer gray (single and double) groups. The results are shown in Fig. 1, for SOC not included and Fig. 2, for the case with SOC. The orientation of the basis vectors in the reciprocal space is the following: for all oblique and rectangular groups having fractional translations parallel to one direction, the vector $\mathbf{k}_1$ is orthogonal to that direction.

Inclusion of SOC gives the same form of SBs with just altered coefficients, provided that SB appears both without and with SOC at a given point of the BZ. With inclusion of SOC four possibilities exist: nodal structure splits into two SBs, as at K-points of graphene; SB remains doubly degenerate SB/splits into two non-degenerate SBs; SB becomes nodal point/line or finally, SB is absent both without and with SOC. Since all HSPs are at the same time TRIM, except for the K-points

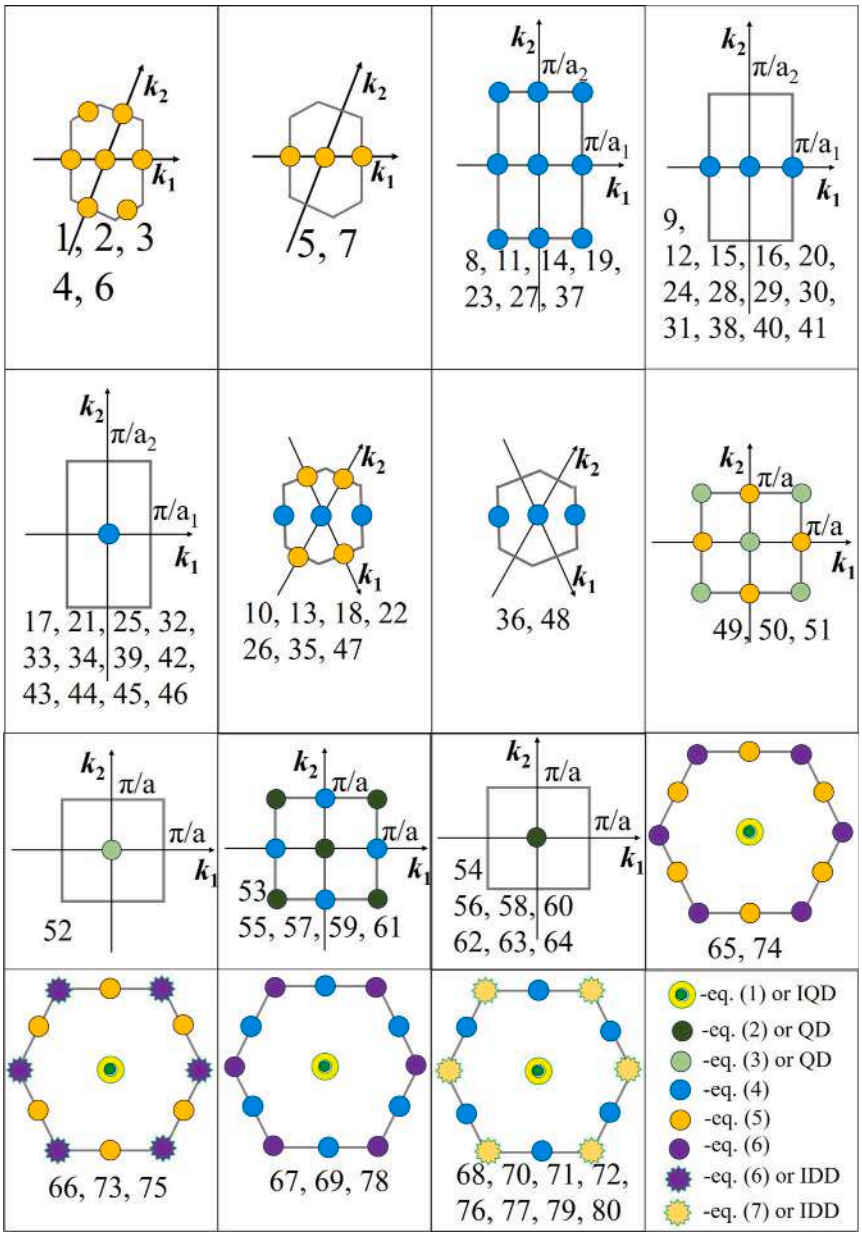

Fig. 1. Positions of simple bands in k-space for all gray layer groups without SOC. IDD — isotropic Dirac dispersion: $E_{1,2,3,4}(\mathbf{q}) = E_0 \pm a|\mathbf{q}|$, QD — quadratic dispersion: $E_{1,2,3,4}(\mathbf{q}) = E_0 + a\mathbf{q}^2 \pm \left\{ \left[b_3(q_1^2 - q_2^2) + b_1 q_1 q_2\right]^2 + \left[b_4(q_1^2 - q_2^2) + b_2 q_1 q_2\right]^2 \right\}^{1/2}$, IQD — isotropic quadratic dispersion: $E_{1,2,3,4}(\mathbf{q}) = E_0 + (a \pm b)\mathbf{q}^2$. See [10] for more detailed description of these dispersions.

of hexagonal groups, SB would split into nodal point/line with inclusion of SOC except if the system is centrosymmetric. Indeed, all groups given in Fig. 2 include spatial inversion except for hexagonal groups 65, 67–70, 73–74, 76–79. For centrosymmetric systems, Kramers' theorem ensures that spin up and spin down coefficients in SBs are mutually equal, giving rise to double (spinful) degeneracy.

As an example we consider layer group 80 at the Γ-point for SOC included. Group of the wave vector is $\underline{D}_{6h}^{D}$ which has six extra irreducible representations [21]. All six of them are pseudoreal [21], which means that TRS does not induce additional degeneracy. Since all six of them are two-dimensional and the group is centrosymmetric we conclude that SB exists around the Γ-point. Calculation by group projectors described in section Method gives that the simple band is given by Eq. (1).

For further illustration we consider one site tight-binding model belonging to gray single layer group 80. The crystal structure is shown in Fig. 3 (visualization by use of VESTA [22]). The Hamiltonian is one dimensional and the band structure is:

$$E(\mathbf{k}) = E_0 + 2t\left\{\cos(\mathbf{k}\cdot\mathbf{a}_1) + \cos(\mathbf{k}\cdot\mathbf{a}_2) + \cos[\mathbf{k}\cdot(\mathbf{a}_1 + \mathbf{a}_2)]\right\}. \tag{8}$$

Near BZ center (point group of the wave vector D_{6h}) we have $\mathbf{k} = 0 + \mathbf{q}$ so that the dispersion is:

$$E_\Gamma(\mathbf{q}) \approx E_0 + 6t - \frac{3}{2}ta^2\mathbf{q}^2 + \frac{3}{32}ta^4\mathbf{q}^4. \tag{9}$$

For $t > 0$ ($t < 0$) Eq. (9) presents MHD (inverted MHD).

Around M-point (point group of the wave vector D_{2h}) we have $\mathbf{k} = \mathbf{b}_1/2 + \mathbf{q}$ so that:

$$E_M(\mathbf{q}) \approx E_0 - 2t + \frac{1}{2}ta^2(3q_1^2 - q_2^2) - \frac{1}{96}ta^4(9q_1^4 + 18q_1^2q_2^2 - 7q_2^4). \tag{10}$$

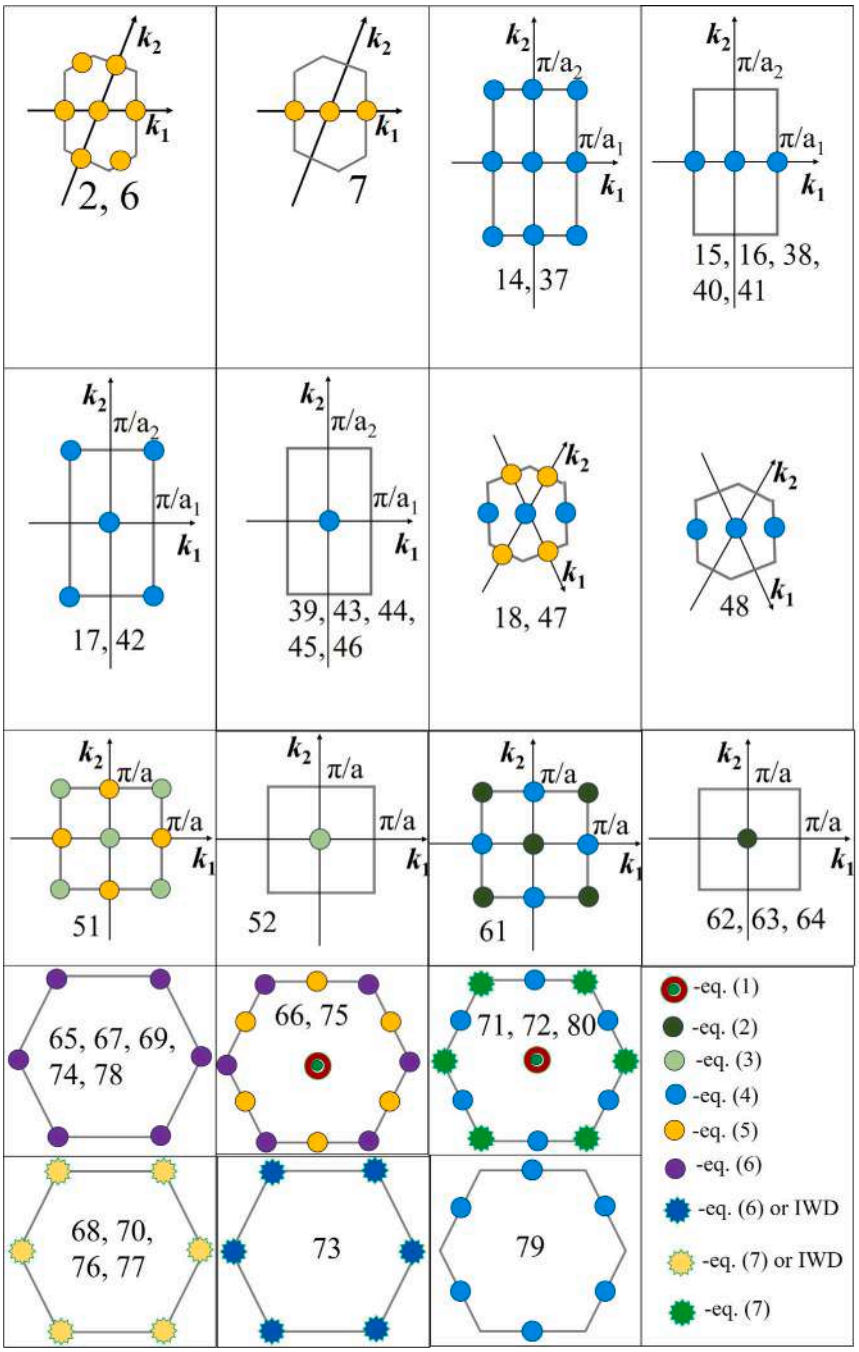

Fig. 2. Positions of simple bands in k-space for all gray layer groups with SOC. Superscript D for double groups is omitted. IWD — isotropic Weyl dispersion: $E_{1,2} = E_0 \pm a|\mathbf{q}|$. See [10] for more detailed description of this dispersion.

Around K-point (point group of the wave vector D_{3h}) we have ($\mathbf{k} = (\mathbf{b}_1 + \mathbf{b}_2)/3 + \mathbf{q}$):

$$E_K(\mathbf{q}) \approx E_0 - 3t + \frac{3}{4}ta^2\mathbf{q}^2 - \frac{\sqrt{3}}{8}ta^3(q_1^3 - 3q_1q_2^2) - \frac{3}{64}ta^4\mathbf{q}^4. \quad (11)$$

The Eqs. (9), (10) and (11) are another confirmations of the theory presented here. Note that inclusion of SOC would give the same results with just altered coefficients E_0 and t.

4. Discussion

The signs of parameters in formulas (1)–(7) cannot be determined using group theory alone, so *e.g.* in formula (1) it is not guaranteed that $ab < 0$, the necessary condition for MHD/inverted MHD. However, in multiband cases, for the lowest lying band, the second order perturbation theory gives $a < 0$, which is the first prerequisite for MHD. Also, if in some 2D material, it turns out that $ab > 0$, application of symmetry preserving strain may give $ab < 0$. In addition, Figs. 1 and 2 show that the symmetry forbids appearance of MHD outside of BZ centers of hexagonal groups. Existence of MHD at the Γ-point is experimentally confirmed in hexagonal GaSe grown on GaAs by molecular beam epitaxy [23]. The MHD and high electron mobility are numerically predicted in single layers of γ – SnX (X = O, S, Se, Te), which are also hexagonal materials, by first principles investigation [24]. Similarly, hexagonal lattices of group-VA elements, having symmetry of graphene, are shown analytically to exhibit MHD with magnetic instability and unique thermoelectric properties [25]. First principle calculations show

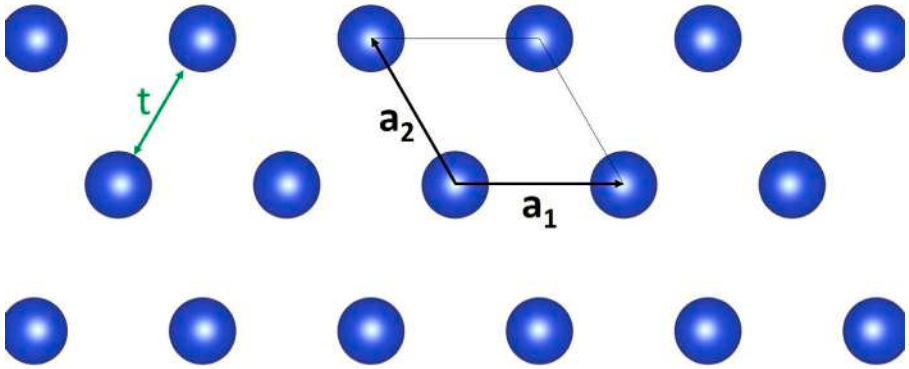

Fig. 3. Lattice structure for the tight-binding model. Black parallelogram denotes primitive unit cell. Hopping parameter t between nearest neighbors is indicated in green color.

inverted MHD at BZ center in Janus $\gamma - \mathrm{Ge_{2XY}}$ (X/Y = S, Se, Te) monolayers having symmetry $p3m1$ (layer group 69) [26]. The inverted MHD remains feature in the band structure also when vertical electric field is applied. This effect can be explained having in mind that group $p3m1$ is also a wallpaper group, so it does not contain elements that flip the surface of 2D material. When homogeneous electric field is applied perpendicularly to the sample, the symmetry group remains the same.

Formulas other then (1) are also used in the literature for fitting. Penta-graphene belongs to layer group $p\bar{4}2_1m$ (layer group 58), so that its isogonal group is $\underline{D}_{2d}$ which is non-centrosymmetric [27]. After adding spatial inversion the group becomes $\underline{D}_{4h}$, which requires Eq. (2) for fitting bands around BZ center. This exact equation is used in [27] under the name tetragonal MHD.

Sometimes it is necessary to go beyond fourth order invariant polynomials. Hexagonal gallium chalcogenides belong to layer group 78 ($p\bar{6}m2$) and the band structure is fitted with polynomial of order six in [28]. Instead of giving full polynomial of order six, for comparison with the results of [28] here we only calculate the number of real coefficients. Using general formula for symmetrized nth power of a representation [29], we get: $\left[\Gamma^{\otimes 6}_{2DPV}\right] = 2A_{1g} + A_{2g} + 2E_{2g}$ in the group $\underline{D}_{6h}$ (Γ_{2DPV} is the operator reduction of polar vector representation to 2D reciprocal space). The number of parameters is equal to two, which is in accordance with formula for fitting in [28]. On the other hand, the formula four in [30], used for fitting of hexagonal GaS band structure around Γ-point, cannot be justified by symmetry since it is anisotropic already in quadratic approximation. Deviations from completely isotropic dispersion in the vicinity of BZ center are due to higher order terms in the Taylor expansion of electronic energy, as already suggested by [28]. On the other hand, truncation of electronic energy to first few terms in Taylor expansion has physical origin in Fermi–Dirac distribution which, even around room temperature, deviates only slightly from its step-like form at absolute zero. States around Fermi momenta are important in investigations of *e.g.* charge transport properties. In the case of graphene, electronic energy obeying massless Dirac dispersion is a good approximation although higher order terms induce anisotropy.

5. Conclusions

In summary we have determined dispersions of simple bands in the vicinity of special points in the reciprocal space for non-magnetic two-dimensional materials without and with spin–orbit coupling. Our results can be used for fitting of experimental (*e.g.* via ARPES) or numerical band structures and for deeper theoretical analysis. Application to real materials requires only layer group determination which can be done using freely available program [19], once the crystal structure is known. Further research is necessary to clarify cases when TRS alone is broken. This can be the case of magnetic layers, where extension of spin group concepts from *e.g.* quasi one-dimensional materials [31–33], would be appropriate.

Our results are presented in graphical form, not in encyclopedia manner, which might ensure easier usage. The problem of finding new materials is reduced, in this particular case of simple bands, to problem of synthesis of 2D materials with prescribed symmetry. In that sense, available data bases of numerically stable and real materials might be useful [34–36]. The last point for crystal growers would be the right placement of the Fermi level, which cannot be addressed using symmetry alone, although electron filling conditions for symmetry groups of insulating systems can be helpful [37–39]. If the total atomic number of all nuclei in the primitive cell does not satisfy criteria given in [37–39], some bands will cross the Fermi level for systems with weak electronic correlations. Although originally given for electronic dispersions, the results in non-SOC case given in Fig. 1 can be used for analyzing phononic bands too.

CRediT authorship contribution statement

Vladimir Damljanović: Writing – review & editing, Writing – original draft, Visualization, Validation, Supervision, Resources, Project administration, Methodology, Investigation, Funding acquisition, Formal analysis, Data curation, Conceptualization.

Declaration of competing interest

The authors declare that they have no known competing financial interests or personal relationships that could have appeared to influence the work reported in this paper.

Acknowledgment

Author acknowledges funding by the Ministry of Science, Technological Development and Innovation of the Republic of Serbia provided by the Institute of Physics Belgrade.

Data availability

No data was used for the research described in the article.

References

[1] Xiaolong Feng, Jiaojiao Zhu, Weikang Wu, Shengyuan A. Yang, Two-dimensional topological semimetals, Chin. Phys. B 30 (10) (2021) 107304.
[2] N.P. Armitage, E.J. Mele, Ashvin Vishwanath, Weyl and Dirac semimetals in three-dimensional solids, Rev. Modern Phys. 90 (2018) 015001.
[3] V. Damljanović, R. Gajić, Existence of Dirac cones in the Brillouin zone of diperiodic atomic crystals according to group theory, J. Phys.: Condens. Matter. 28 (8) (2016) 085502.

[4] V. Damljanović, R. Gajić, Addendum to 'Existence of Dirac cones in the Brillouin zone of diperiodic atomic crystals according to group theory', J. Phys.: Condens. Matter. 28 (43) (2016) 439401.
[5] L. Seixas, A.S. Rodin, A. Carvalho, A.H. Castro Neto, Multiferroic two-dimensional materials, Phys. Rev. Lett. 116 (2016) 206803.
[6] Vladimir A. Sablikov, Aleksei A. Sukhanov, Quasi-bound states and resonant skew scattering in two-dimensional materials with a Mexican-hat dispersion, Phys. E: Low- Dimens. Syst. Nanostructures 145 (2023) 115492.
[7] Vladimir A. Sablikov, Aleksei A. Sukhanov, Quasi-bound electron pairs in two-dimensional materials with a Mexican-hat dispersion, Phys. Lett. A 481 (2023) 129006.
[8] M. Nurhuda, A.R.T. Nugraha, M.Y. Hanna, E. Suprayoga, E.H. Hasdeo, Thermoelectric properties of Mexican-hat band structures, Adv. Nat. Sci. Nanosci. Nanotechnol. 11 (1) (2020) 015012.
[9] Cong Wang, Zhiyuan Xu, Ke Xu, Guoying Gao, Excellent room-temperature thermoelectricity of 2D GeP_3: Mexican-hat-shaped band dispersion and ultralow lattice thermal conductivity, Molecules 26 (21) (2021).
[10] V. Damljanović, N. Lazić, Electronic structures near unmovable nodal points and lines in two-dimensional materials, J. Phys. A 56 (21) (2023) 215201.
[11] Feng Tang, Xiangang Wan, Complete classification of band nodal structures and massless excitations, Phys. Rev. B 105 (2022) 155156.
[12] Zeying Zhang, Weikang Wu, Gui-Bin Liu, Zhi-Ming Yu, Shengyuan A. Yang, Yugui Yao, Encyclopedia of emergent particles in 528 magnetic layer groups and 394 magnetic rod groups, Phys. Rev. B 107 (2023) 075405.
[13] Feng Tang, Xiangang Wan, Exhaustive construction of effective models in 1651 magnetic space groups, Phys. Rev. B 104 (2021) 085137.
[14] Zhi-Ming Yu, Zeying Zhang, Gui-Bin Liu, Weikang Wu, Xiao-Ping Li, Run-Wu Zhang, Shengyuan A. Yang, Yugui Yao, Encyclopedia of emergent particles in three-dimensional crystals, Sci. Bull. 67 (4) (2022) 375–380.
[15] Gui-Bin Liu, Zeying Zhang, Zhi-Ming Yu, Shengyuan A. Yang, Yugui Yao, Systematic investigation of emergent particles in type-III magnetic space groups, Phys. Rev. B 105 (2022) 085117.
[16] Zeying Zhang, Gui-Bin Liu, Zhi-Ming Yu, Shengyuan A. Yang, Yugui Yao, Encyclopedia of emergent particles in type-IV magnetic space groups, Phys. Rev. B 105 (2022) 104426.
[17] Zeying Zhang, Zhi-Ming Yu, Gui-Bin Liu, Zhenye Li, Shengyuan A. Yang, Yugui Yao, MagneticKP: A package for quickly constructing kp models of magnetic and non-magnetic crystals, Comput. Phys. Comm. 290 (2023) 108784.
[18] João Victor V. Cassiano, Augusto de Lelis Araújo, Paulo E. Faria Junior, Gerson J. Ferreira, DFT2kp: Effective kp models from ab-initio data, SciPost Phys. Codebases (2024) 25.
[19] Jingheng Fu, Mikael Kuisma, Ask Hjorth Larsen, Kohei Shinohara, Atsushi Togo, Kristian S. Thygesen, Symmetry classification of 2D materials: layer groups versus space groups, 2D Mater. 11 (3) (2024) 035009.
[20] Vladimir Damljanović, Movable but unavoidable nodal lines through high-symmetry points in 2D materials, Prog. Theor. Exp. Phys. 2023 (4) (2023) 043I02.
[21] L. Elcoro, B. Bradlyn, Z. Wang, M.G. Vergniory, J. Cano, C. Felser, B.A. Bernevig, D. Orobengoa, G. de la Flor, M.I. Aroyo, Double crystallographic groups and their representations on the Bilbao Crystallographic Server, J. Appl. Crystallogr. 50 (5) (2017) 1457–1477.
[22] Koichi Momma, Fujio Izumi, *VESTA3* for three-dimensional visualization of crystal, volumetric and morphology data, J. Appl. Crystallogr. 44 (6) (2011) 1272–1276.
[23] Ming-Wei Chen, HoKwon Kim, Dmitry Ovchinnikov, Agnieszka Kuc, Thomas Heine, Olivier Renault, Andras Kis, Large-grain MBE-grown GaSe on GaAs with a Mexican hat-like valence band dispersion, Npj 2D Mater. Appl. 2 (2018) 2.
[24] Vu V. Tuan, A.A. Lavrentyev, O.Y. Khyzhun, Nguyen T.T. Binh, Nguyen V. Hieu, A.I. Kartamyshev, Nguyen N. Hieu, Mexican-hat dispersions and high carrier mobility of $\gamma-$SnX (X = O, S, Se, Te) single-layers: a first-principles investigation, Phys. Chem. Chem. Phys. 24 (2022) 29064–29073.
[25] Hâldun Sevinçli, Quartic dispersion, strong singularity, magnetic instability, and unique thermoelectric properties in two-dimensional hexagonal lattices of group-VA elements, Nano Lett. 17 (2017) 2589–2595.
[26] Tuan V. Vu, Huynh V. Phuc, Le C. Nhan, A.I. Kartamyshev, Nguyen N. Hieu, Predicted novel Janus $\gamma-Ge_2XY$ (X/Y = S, Se, Te) monolayers with Mexican-hat dispersions and high carrier mobilities, J. Phys. D: Appl. Phys. 56 (13) (2023) 135302.
[27] Ningning Jia, Yongting Shi, Zhiheng Lv, Junting Qin, Jiangtao Cai, Xue Jiang, Jijun Zhao, Zhifeng Liu, Tetragonal Mexican-hat dispersion and switchable half-metal state with multiple anisotropic Weyl fermions in penta-graphene, New J. Phys. 25 (3) (2023) 033033.
[28] V. Zólyomi, N.D. Drummond, V.I. Fal'ko, Band structure and optical transitions in atomic layers of hexagonal gallium chalcogenides, Phys. Rev. B 87 (2013) 195403.
[29] G.Ya. Lyubarskii, The Application of Group Theory in Physics, Pergamon Press, New York, 1960.
[30] Dmitry V. Rybkovskiy, Alexander V. Osadchy, Elena D. Obraztsova, Transition from parabolic to ring-shaped valence band maximum in few-layer GaS, GaSe, and InSe, Phys. Rev. B 90 (2014) 235302.
[31] Nataša Lazić, Marko Milivojević, Milan Damnjanović, Spin line groups, Acta Crystallogr. Sect. A 69 (6) (2013) 611–619.
[32] Nataša Lazić, Milan Damnjanović, Spin ordering in RKKY nanowires: Controllable phases in ^{13}C nanotubes, Phys. Rev. B 90 (2014) 195447.
[33] Nataša Lazić, Quasi-classical ground states and magnons in monoperiodic spin systems, in: Faculty of Physics (Ph.D. thesis), University of Belgrade, 2016.
[34] Sten Haastrup, Mikkel Strange, Mohnish Pandey, Thorsten Deilmann, Per S. Schmidt, Nicki F. Hinsche, Morten N. Gjerding, Daniele Torelli, Peter M. Larsen, Anders C. Riis-Jensen, Jakob Gath, Karsten W. Jacobsen, Jens Jørgen Mortensen, Thomas Olsen, Kristian S. Thygesen, The computational 2D materials database: high-throughput modeling and discovery of atomically thin crystals, 2D Mater. 5 (4) (2018) 042002.
[35] Morten Niklas Gjerding, Alireza Taghizadeh, Asbjørn Rasmussen, Sajid Ali, Fabian Bertoldo, Thorsten Deilmann, Nikolaj Rørbæk Knøsgaard, Mads Kruse, Ask Hjorth Larsen, Simone Manti, Thomas Garm Pedersen, Urko Petralanda, Thorbjørn Skovhus, Mark Kamper Svendsen, Jens Jørgen Mortensen, Thomas Olsen, Kristian Sommer Thygesen, Recent progress of the computational 2D materials database (C2DB), 2D Mater. 8 (4) (2021) 044002.
[36] Nicolas Mounet, Marco Gibertini, Philippe Schwaller, Davide Campi, Andrius Merkys, Antimo Marrazzo, Thibault Sohier, Ivano Eligio Castelli, Andrea Cepellotti, Giovanni Pizzi, Nicola Marzari, Two-dimensional materials from high-throughput computational exfoliation of experimentally known compounds, Nature Nanotechnology 13 (2018) 246–252.
[37] Haruki Watanabe, Hoi Chun Po, Michael P. Zaletel, Ashvin Vishwanath, Filling-enforced gaplessness in band structures of the 230 space groups, Phys. Rev. Lett. 117 (2016) 096404.
[38] Haruki Watanabe, Hoi Chun Po, Ashvin Vishwanath, Michael Zaletel, Filling constraints for spin–orbit coupled insulators in symmorphic and nonsymmorphic crystals, Proc. Natl. Acad. Sci. 112 (47) (2015) 14551–14556.
[39] Benjamin J. Wieder, C.L. Kane, Spin–orbit semimetals in the layer groups, Phys. Rev. B 94 (2016) 155108.

LETTER

Non-magnetic layers with a single symmetry-protected Dirac cone: Which additional dispersions must appear?

To cite this article: V. Damljanović 2024 *EPL* **147** 56003

A Letters Journal Exploring the Frontiers of Physics

September 2024

EPL, **147** (2024) 56003
doi: 10.1209/0295-5075/ad7317

www.epljournal.org

Non-magnetic layers with a single symmetry-protected Dirac cone: Which additional dispersions must appear?

V. Damljanović[(a)]

Institute of Physics Belgrade, University of Belgrade - Pregrevica 118, 11000 Belgrade, Serbia

received 17 March 2024; accepted in final form 23 August 2024
published online 13 September 2024

Abstract – In two-dimensional (2D), non-magnetic materials, a single Dirac cone at high-symmetry point (HSP) of the Brillouin zone (BZ), akin to the one in graphenes' band structure, cannot appear as the only quasiparticle at the Fermi level. Here we found two layer groups with time-reversal symmetry, among all possible both without and with spin-orbit coupling, that host one Dirac cone at HSP and we show which additional dispersions appear: a pair of Dirac lines on opposite BZ edges and a pair of Dirac cones that can be moved but not removed by symmetry preserving perturbations, on the other two BZ edges. We illustrate our theory by a tight-binding band structure and discuss real 2D materials that belong to one of the two symmetry groups. Finally, we single out smaller or bigger discrepancies among the published papers on the same or related topic.

Introduction. – Two-dimensional (2D) materials became focal point of intensive research due to their mechanical and electrical properties suitable for both fundamental research and applications. Materials' 2D Brillouin zone (BZ) allows application of topology in the explanation of their physical properties. Electron wave functions near band contacts, like Dirac cones in graphene, gain additional significance when a 2D material is placed in the vertical magnetic field. The absence of back-scattering and the high electron conductivity near materials edges giving rise to Quantum Hall effect, are some of the examples [1,2].

The crystal and time-reversal symmetry (TRS) explain both band contacts and dispersion in their vicinity. Group-theoretical methodology relies on tables of irreducible (co)representations ((co)reps) of underlying symmetry groups. For dispersions in three-dimensional (3D) crystals, space group representations are firstly used for prediction of bulk chiral fermions [3], and finalized in a complete list of excitations near high-symmetry points (HSPs) and lines (HSLs) in gray and black-and-white space groups [4–7].

Regarding subperiodic groups, computer program POLSym [8] contains (co)reps for all families of line- and layer groups and was used by [9–11] to develop spin-group theory for quasi–one-dimensional systems. On the other hand, all types of (co)reps of all gray and ordinary layer groups are available recently [12]. Dispersions near all HSPs and HSLs in non-magnetic 2D materials are reported in [13], which explained published numerical and experimental band structures (*e.g.*, in [14,15]), and can be used as a starting point in designing new 2D materials with physical properties given in advance. Magnetic layer and rod groups are treated in [16] (without dispersions —Hamiltonian eigenvalues), which was published at about the same time as [13].

Topological laws forbid one twofold Dirac cone (also called Weyl fermion, since it arises by the crossing of two non-degenerate bands), like those in spinless band structure of graphene, to be the only feature at a given energy (including the Fermi level) in non-magnetic 2D materials. This is a consequence of fermion doubling due to condensed-matter realization of parity anomaly in magnetic field [17] and also in zero field [18]. In the spin-orbit coupling (SOC) case for materials with C_n vertical rotation axis ($n = 2, 4, 6$), the number of twofold Dirac cones must be a multiple of $2n$, which gives even stronger restriction on the number of twofold Dirac cones [19]. A fourfold Dirac cone, obtained by the crossing of two, spinful doubly degenerate bands also cannot appear as the only feature at a given energy in the presence of TRS [20,21]. Fermion doubling for fourfold Dirac fermions is analyzed in the context of a half 2D topological insulator state [22,23], but explanation presumably originating from quantum field

[(a)]E-mail: damlja@ipb.ac.rs (corresponding author)

theoretic concepts is still lacking. In that respect the question arises: in a given symmetry group, if it imposes a fourfold Dirac cone at one BZ HSP, what other band contacts must appear? Are those contacts essential degeneracies or are there also accidental band contacts (ABCs)? If so, are these ABCs protected by topology or are they truly accidental (can be gapped by symmetry preserving perturbations)? The present paper aims to give answers to these questions.

Method. – A list of UNPs and UNLs is given in [13], for spinless and spinful electrons in the presence of TRS. The position of UNPs and UNLs is given by the dimensionality of the allowed correp of the little group. The matrices of correps can be used to find an effective Hamiltonian in the vicinity of UNPs and UNLs, and hence the dispersions (Hamiltonian eigenvalues). We search band structures near unmovable nodal points published in [13], to identify layer groups having one fourfold Dirac cone in the BZ. Next, additional dispersions near UNPs and UNLs that must be present are identified. For investigation of accidental band contacts the non-crossing rule is applied [24–26]. Although there are exceptions from the non-crossing rule [27], we will work with centrosymmetric groups with SOC, thus avoiding theories for crossings of two bands [19] and linked nodal lines in centrosymmetric groups without SOC [28–30]. For the tight-binding model, we use the fine structure Hamiltonian $\hat{H}_{\rm fs}(\mathbf{r})$, obtained from the Dirac equation by expansion up to $(1/c)^2$ [31]. More precisely, the following symmetry properties are used [32]: $\hat{H}_{\rm fs}(g^{-1}\mathbf{r}) = \hat{u}^{\dagger}(g_0)\hat{H}_{\rm fs}(\mathbf{r})\hat{u}(g_0)$, where $\hat{u}(g_0)$ represents the rotational part of the layer symmetry element g in the spin space and can be found at Bilbao Crystallographic Server [33]. In addition, TRS implies $\hat{H}^{*}_{\rm fs}(\mathbf{r}) = \hat{\sigma}_2\hat{H}_{\rm fs}(\mathbf{r})\hat{\sigma}_2$, with $\hat{\sigma}_2$ being the Pauli matrix. These symmetry properties of $\hat{H}_{\rm fs}(\mathbf{r})$ significantly simplify the tight-binding Hamiltonian in highly symmetric layers, allowing an analytical solution of the eigenvalues problem.

Results. – A closer look at dispersions near all HSPs and HSLs [13] for the SOC case gives that centrosymmetric layer double groups 43^D ($p\ 2/b\ 2_1/a\ 2/a$) and 45^D ($p\ 2_1/b\ 2_1/m\ 2/a$) host one fourfold Dirac point at BZ HSP. To these groups corresponds the following space groups: 54^D ($P\ 2_1/c\ 2/c\ 2/a$; $y = 0$) and 57^D ($P\ 2/b\ 2_1/c\ 2_1/m$; $x = 0$), respectively (plane parallel to the diperiodic one is also given, the notation for layer and space groups is according to [34] and [35], respectively). Besides the fourfold Dirac point there is also a fourfold Dirac line at one edge of the BZ for each of the two groups [13].

We next investigate if additional band contacts are possible or even unavoidable. We use allowed, extra irreps from the Bilbao Crystallographic Server [33] for corresponding space groups. For group 57^D, the high-symmetry line H has four one-dimensional irreps being paired by TRS in the following way: $(\overline{H}_2, \overline{H}_5)$ and $(\overline{H}_4, \overline{H}_3)$. The screw axis of order two is represented by $(-ie^{i\pi u}, ie^{i\pi u})$ for both pairs of irreps ($u = 1/2$ corresponds to BZ corner). Near end points of line H both pairs are $(-i, i)$ and $(1, -1)$, respectively. However, at the point Y ($u = 0$) irreps $(\overline{Y}_3, \overline{Y}_4)$ are $(-2i, 2i)$, while those

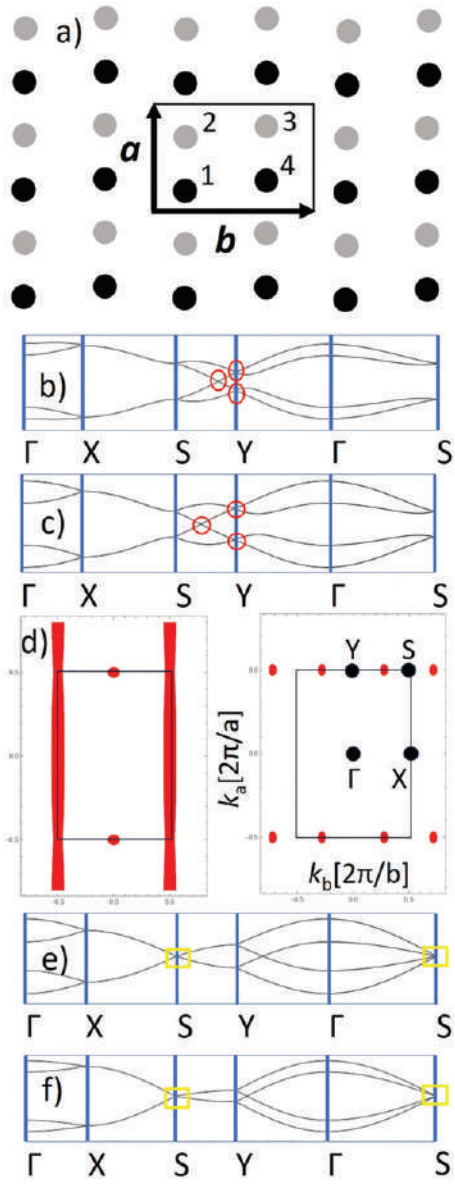

Fig. 1: (a) Crystal structure adopted for the tight-binding model. Black (white) nuclei are above (below) the drawing plane; (b), (c): band structure along high-symmetry lines. Fourfold Dirac cones are enclosed with red ellipses; (d) areas in the reciprocal space (indicated in red color) where $E_2 - E_1 <$ 0.6 eV (left panel; the same picture is for $E_4 - E_3 < 0.6$ eV), *i.e.*, $E_3 - E_2 < 0.6$ eV (right panel). Black rectangles denote BZ. Parameters f_0, f_1, f_2, c_1, c_2 are equal to 2.1, 1.6, 1.1, 1.4, 0.9 eV ((c) and (d)), *i.e.*, 1.8, 1.6, 0.7, 1.8, 1.4 eV (b), respectively; (e), (f): band structure without SOC. Yellow rectangles enclose fortune teller dispersion at the point S. $\widetilde{f}_0$, $\widetilde{f}_1$ and $\widetilde{f}_2$ are 1.7, 1.8 and 0.8 eV (e), *i.e.*, 1.4, 2.1 and 0.4 eV (f), respectively.

$$\hat{A}(\mathbf{k}) = \begin{pmatrix} f_0 & f_1\left(1+e^{-i\mathbf{k}\cdot\mathbf{a}}\right) & 0 & f_2\left(1+e^{-i\mathbf{k}\cdot\mathbf{b}}\right) \\ f_1\left(1+e^{i\mathbf{k}\cdot\mathbf{a}}\right) & f_0 & f_2\left(1+e^{-i\mathbf{k}\cdot\mathbf{b}}\right) & 0 \\ 0 & f_2\left(1+e^{i\mathbf{k}\cdot\mathbf{b}}\right) & f_0 & f_1\left(1+e^{i\mathbf{k}\cdot\mathbf{a}}\right) \\ f_2\left(1+e^{i\mathbf{k}\cdot\mathbf{b}}\right) & 0 & f_1\left(1+e^{-i\mathbf{k}\cdot\mathbf{a}}\right) & f_0 \end{pmatrix},$$
$$\hat{B}(\mathbf{k}) = \begin{pmatrix} 0 & c_1\left(1+e^{-i\mathbf{k}\cdot\mathbf{a}}\right) & 0 & ic_2\left(1-e^{-i\mathbf{k}\cdot\mathbf{b}}\right) \\ -c_1\left(1+e^{i\mathbf{k}\cdot\mathbf{a}}\right) & 0 & -ic_2\left(1-e^{-i\mathbf{k}\cdot\mathbf{b}}\right) & 0 \\ 0 & ic_2\left(1-e^{i\mathbf{k}\cdot\mathbf{b}}\right) & 0 & c_1\left(1+e^{i\mathbf{k}\cdot\mathbf{a}}\right) \\ -ic_2\left(1-e^{i\mathbf{k}\cdot\mathbf{b}}\right) & 0 & -c_1\left(1+e^{-i\mathbf{k}\cdot\mathbf{a}}\right) & 0 \end{pmatrix}. \quad (2)$$

$$E_{1,2,3,4} = f_0 \pm 2\sqrt{c_1^2\cos^2\left(\frac{\mathbf{k}\cdot\mathbf{a}}{2}\right) + \left[\sqrt{c_2^2\sin^2\left(\frac{\mathbf{k}\cdot\mathbf{b}}{2}\right) + f_1^2\cos^2\left(\frac{\mathbf{k}\cdot\mathbf{a}}{2}\right)} \pm \left|f_2\cos\left(\frac{\mathbf{k}\cdot\mathbf{b}}{2}\right)\right|\right]^2}, \quad (3)$$

at the BZ corner are $(\overline{T}_3, \overline{T}_4) = (0, 0)$. Since compatibility relations near point Y are not satisfied, two double degenerate zones must touch an odd number of times somewhere on the line H (most probably once). For the remaining parts of the Brillouin zone, accidental band contacts are forbidden by the non-crossing rule. A similar analysis applies to space group 54^D with the same result. The main conclusion of this paragraph is that, for layer groups 43^D and 45^D, there are $2(2n-1)$ additional fourfold Dirac cones somewhere at the BZ edge (the one that does not host the fourfold Dirac line), with n most probably being one. These additional fourfold Dirac cones can be moved along the BZ edge, but cannot be gapped by symmetry preserving perturbations.

We illustrate our findings using a tight-binding example on the structure having symmetry 45^D, shown in fig. 1 (visualization by VESTA [36]). The eight-dimensional tight-binding Hamiltonian in the basis of s-orbitals and up and down spinors $\{|s_1\uparrow\rangle, |s_2\uparrow\rangle, |s_3\uparrow\rangle, |s_4\uparrow\rangle, |s_1\downarrow\rangle, |s_2\downarrow\rangle, |s_3\downarrow\rangle, |s_4\downarrow\rangle\}$ is

$$\hat{H}(\mathbf{k}) = \begin{pmatrix} \hat{A}(\mathbf{k}) & \hat{B}(\mathbf{k}) \\ \hat{B}^\dagger(\mathbf{k}) & \hat{A}(\mathbf{k}) \end{pmatrix}, \quad (1)$$

with $\hat{A}$ and $\hat{B}$ given by

see eq. (2) *above*

Here f_0, f_1, f_2 are real hopping parameters between zeroth, the first and the second neighbors (parallel spins), *i.e.,* c_1, c_2 are real hopping parameters between the first and the second neighbors (antiparallel spins). The electronic band structure, within this model is

see eq. (3) *above*

with each of the four bands from (3) being doubly degenerate, as expected from Kramers' theorem for centrosymmetric systems with SOC. Four doubly degenerate bands are obtained by four possible combinations of $+$ and $-$ in (3). Bands E_1, E_2, E_3, E_4 are ordered according to non-decreasing energy for each $\mathbf{k}$ in the following way: $(-,+) \leq (-,-) \leq (+,-) \leq (+,+)$. The fourfold degeneracy is obtained for

$$c_2^2\sin^2(\mathbf{k}\cdot\mathbf{b}) + 4f_1^2\cos^2\left(\frac{\mathbf{k}\cdot\mathbf{a}}{2}\right)\cos^2\left(\frac{\mathbf{k}\cdot\mathbf{b}}{2}\right) = 0, \quad (4)$$

which is valid at $\mathbf{k}\cdot\mathbf{b} = \pm\pi$ (unmovable fourfold Dirac lines).

Along lines $\mathbf{k}\cdot\mathbf{a} = \pm\pi$ dispersions (3) become

$$E_{1,2,3,4} = f_0 \pm 2\left|\left|f_2\cos\left(\frac{\mathbf{k}\cdot\mathbf{b}}{2}\right)\right| \pm \left|c_2\sin\left(\frac{\mathbf{k}\cdot\mathbf{b}}{2}\right)\right|\right|, \quad (5)$$

which gives $\mathbf{k}\cdot\mathbf{b} = 0$ (unmovable fourfold Dirac points) and $\mathbf{k}\cdot\mathbf{b} = \pm 2\mathrm{arctg}(f_2/c_2)$, as positions of movable fourfold Dirac points from touching of two inner, doubly degenerate bands.

To investigate dispersions near touching points closer, we write $\mathbf{k} = \mathbf{k}_0 + \mathbf{q}$ and expand (3) for small $|\mathbf{q}|$. Dispersions become

$$E_{1,2,3,4}(\mathbf{q}) \approx f_0 \pm 2|f_2| \pm \sqrt{f_1^2(\mathbf{q}\cdot\mathbf{a})^2 + c_2^2(\mathbf{q}\cdot\mathbf{b})^2}, \quad (6)$$

near unmovable fourfold Dirac points, *i.e.,*

$$E_{3,2}(\mathbf{q}) \approx f_0 \pm \sqrt{c_1^2(\mathbf{q}\cdot\mathbf{a})^2 + (c_2^2+f_2^2)(\mathbf{q}\cdot\mathbf{b})^2}, \quad (7)$$

near movable fourfold Dirac points. The absence of other contacts between bands across the reciprocal space is illustrated in fig. 1, which is in accordance with the non-crossing rule. It also follows from fig. 1 that all four, doubly degenerate bands are tangled together so that an insulator with such a band structure must have a total number of electrons per primitive cell divisible by eight. This is in accordance with the filling factor for layer group 45^D [37], *i.e.,* its corresponding space group [38,39]. The same filling factor is reported for layer groups 43^D and 33^D [37–39]. In the case of strong electron correlations,

for filling factors other than $8n$, systems with these three layer groups will either remain gapless for all strengths of electronic correlations (even if the band structure picture is no longer valid), become gapped by spontaneously breaking the symmetry, or become gapped with the same symmetry achieving spin-orbital liquid with long-range entanglement and topological order [37–39].

Discussion and conclusions. – We discuss our results in relations to the existing literature and in a broader context of this research area. The positions of movable nodal points and lines published for 3D hexagonal [40], orthorhombic [41] and tetragonal [42] space groups could be used for layer groups, too, via corresponding space groups. Movable band contacts for groups 43^D and 45^D found here are reported for their 3D analogs 54^D and 57^D [41]. When the third dimension to k-space is added, the band contacts remain point-like for 54^D, but become part of a movable nodal line for 57^D [41].

Using a tight-binding model, the authors of [20] classify band touchings in non-magnetic materials into four possible cases. All four cases are obtained by breaking symmetry elements in layer group 64^D [20]. The groups 43^D and 45^D arise by further breaking symmetry of case I (two symmetry equivalent fourfold Dirac points), from [20]. The group-subgroup chain is $43^D < 48^D < 64^D$ and $45^D < 48^D < 64^D$, so these groups are not maximal subgroups of 64^D [43,44]. This case is not included in the classification of [20]. The same holds for centrosymmetric, non-symmorphic groups 40^D, 44^D and 63^D, hosting fourfold Dirac lines instead of cones.

Regarding physical properties expected for 2D materials belonging to groups 43^D and 45^D, the most prominent feature is that they are anisotropic. Anisotropy in, *e.g.*, graphene can be achieved by applying uniaxial strain or periodically modulated potential. The crystal structure of 2D materials belonging to 43^D and 45^D itself, liberates researchers of additional efforts to artificially induce anisotropy as in the case of graphene. Anisotropy leads not only to renormalization of tensor components (of, *e.g.*, electrical conductivity) but also to new effects, like hyperbolic plasmons and excitons [45]. On the other hand, it is predicted that the appearance of fourfold Dirac lines might lead to light-induced anomalous Hall conductivity with applications in phototransistors [46]. In groups 43^D and 45^D, the shift of the Fermi level E_F can switch between properties arising from fourfold Dirac lines and anisotropic fourfold Dirac cones.

For experimental realization of materials belonging to layer groups given in advance, one can search the database of 2D materials [47,48] and layered 3D materials which were synthesized in the past [49]. Recent upgrade of C2DB database includes the layer and corresponding space group (obtained from the layer group by AA stacking) of 2D materials in it, which makes closer connections between abstract group-theoretical results and realistic 2D materials [50]. Material $KAsO_2$ belongs to the layer group 45, with synthesis of its 3D layered analog described before [51]. The 2D version is a non-magnetic insulator with a band gap of around 4 eV [47]. Further investigations would be necessary to show if it would be possible to shift its Fermi level by, *e.g.*, doping. On the other hand, band connectivity of groups 43^D and 45^D (and their common subgroup 33^D), which is the highest among all layer groups, forbids their realization by small deformations of a material belonging to any of their supergroups. Deformations, however small they may be, are supposed to close a finite gap at some BZ point, which we think is unlikely.

Groups 40^D, 43^D and 45^D are reported [52] to host semi-Dirac fermions (SDF), which disperse linearly in one direction in k-space and quadratically in the orthogonal direction. Indeed, tight binding dispersions (3) become $E_{1,2,3,4} \approx h_\pm + h_1^\pm(\mathbf{q}\cdot\mathbf{a})^2 \pm h_2|(\mathbf{q}\cdot\mathbf{b})|$, with $h_\pm = f_0 \pm 2\sqrt{c_1^2+c_2^2+f_1^2}$, $h_1^\pm = \mp(c_1^2+f_1^2)/(4\sqrt{c_1^2+c_2^2+f_1^2})$, $h_2 = |f_2|\sqrt{c_2^2+f_1^2}/\sqrt{c_1^2+c_2^2+f_1^2}$ (near points $(0,\pm\pi/b)$), *i.e.,* $h_\pm = f_0 \pm 2|c_2|$, $h_1^\pm = \pm(c_1^2+f_1^2)/(4|c_2|)$, $h_2 = |f_2|$ (near points $(\pm\pi/a,\pm\pi/b)$); only upper (only lower) signs are combined in $h_\pm$, $h_1^\pm$. However, the list of groups and BZ points hosting SDF in [52] is incomplete. As shown in [13], SDFs appear also at the midpoints of BZ borders of groups 44^D and 63^D and at the BZ corners of group 43^D. Also, the symmetry-adapted low-energy Hamiltonian derived in [52], gives point-like, instead of line-like degeneracies required by symmetry. The term SDF is used for line-nodes extrema (as found in [53]), which differs from semi-Dirac dispersion around point-like degeneracy as introduced in [54,55]. In other words, SDF have the following dispersion: $E_{1,2} = E_0 + aq_1^2 \pm b|q_2|$, while semi-Dirac cones have $E_{1,2} = E_0 \pm \sqrt{aq_1^2+bq_2^4}$. SDF treated in [52], [13] and [53] and also discussed here, are pinned to HSP and are intact by symmetry preserving perturbations, in a similar manner as fourfold Dirac dispersion at HSP treated in this paper.

When SOC is neglected, the hopping parameters between states with opposite spins vanish, while those with the parallel spins slightly change. The dispersions (3) become $\widetilde{E}_{1,2,3,4} = \widetilde{f}_0 \pm 2||\widetilde{f}_1\cos(\mathbf{k}\cdot\mathbf{a}/2)| \pm |\widetilde{f}_2\cos(\mathbf{k}\cdot\mathbf{b}/2)||$, which give fortune teller states (FT) near BZ corners $\widetilde{E}_{1,2,3,4} = \widetilde{f}_0 \pm ||\widetilde{f}_1(\mathbf{q}\cdot\mathbf{a})| \pm |\widetilde{f}_2(\mathbf{q}\cdot\mathbf{b})||$, as predicted before for layer (single) groups 33, 43 and 45 [56]. Nonzero density of states (DOS) of $2/(\pi\max\{b|\widetilde{f}_1|, a|\widetilde{f}_2|\})$ near bands contact, distinguish FT dispersion from other linear dispersions. The formula for DOS presented here does not include doubly degeneracy of bands and corrects the inessential numerical error in [56]. Eightfold spinful degeneracy for electrons (*i.e.,* fourfold degeneracy for, *e.g.*, phonons) at BZ corners, together with FT dispersion, is guaranteed by mere belonging of a 2D material to one of these three groups [56]. Later it was pointed out that in some layer single groups, fourfold degeneracy (eightfold, for electrons with spin) might appear also on some high-symmetry lines [57,58] by truly accidental band contacts (TABC). Although being an interesting idea, such TABC

can be destroyed by symmetry preserving perturbations and are assumed to appear rarely in real materials in [56]. In other words, even if present by chance, TABC could be gapped by change of temperature, pressure, humidity etc., which could cause a potential device designed by use of TABC to malfunction. The absence of (eightfold degenerate) TABC on BZ edges in our tight-binding model without SOC (shown in fig. 1(e) and (f)), in *ab initio* band structure of a silicone monolayer in [56] and measured by ARPES [59], is another confirmation of our statements. Note that part of table I of [60] (apart from the materials mentioned in it) that deals with Dirac phonons at HSPs, repeats group-theoretical results published five years before in table I of [56] for unmovable, fourfold (spinless) degenerate band contacts. The other part (Dirac phonons on HSLs [60]), contains seven groups that might host TABC, six of which were reported and one originally omitted in [57,58].

Reference [61] study phonons in PtI_4 and $LiBiO_2$ monolayers belonging to layer groups 33 and 45, respectively. The $\mathbf{k}\cdot\mathbf{p}$ Hamiltonian derived in [61] around the BZ corner of group 45, does not reduce to zero at BZ corner and has four real parameters, instead of three required by symmetry [56]. The number of real independent parameters in a low-energy Hamiltonian derived from symmetry is invariant, unlike its form which depends on the basis, and could be used as a crosscheck. Group theory was used for finding which gray layer groups host Dirac cones both without and with SOC [62]. Group 73 is missing in the results of [62], as can be seen by comparing cases with and without SOC in [13]. Gray layer groups without SOC hosting Dirac cones listed much earlier in [63,64], might be a useful starting point of analysis performed in [62]. Here we add that eleven groups being the main group-theoretical result summarized in table I of [65], are the exact eleven groups published seven years before in [63,64]. The group-theoretical treatment of Dirac points of electrons without SOC (treated in [63,64]) and that of linear Weyl points of phonons (treated in [65]) are identical. Similarly, the group-theoretical results of [66], reporting electronic dispersions near fourfold degeneracies in non-centrosymmetric materials with SOC, are repeated without citation in [67]. The $\mathbf{k}\cdot\mathbf{p}$ Hamiltonian near the $\overline{M}$ point of the wallpaper group $p4g$ (which is also the layer group 56) has two real parameters and leads to doubly degenerate bands as if the group was centrosymmetric [68]. This is not in accordance with the earlier publication [66], where the Hamiltonian near BZ corners of layer group 56 has three parameters and gives doubly degeneracy only along HSLs, as required by symmetry.

Finally, we mention that our group-theoretical treatment of dispersions holds for fixed nuclei and should not be transferred directly to dynamical Hamiltonians, such as the electron-phonon Hamiltonian relevant for the explanation of conventional superconductivity. For dynamical problems, symmetry analysis of phonons (like the one for graphene [69]), could be useful. Also, a single fourfold Dirac cone at HSP as the only quasiparticle at the Fermi level, appears in some black-and-white layer groups describing antiferromagnetic ordering [70], where time reversal alone is not a symmetry.

* * *

VD acknowledges funding by the Ministry of Science, Technological Development and Innovation of the Republic of Serbia provided by the Institute of Physics Belgrade.

Data availability statement: All data that support the findings of this study are included within the article (and any supplementary files).

REFERENCES

[1] Feng X., Zhu J., Wu W. and Yang S. A., *Chin. Phys. B*, **30** (2021) 107304.
[2] Armitage N. P., Mele E. J. and Vishwanath A., *Rev. Mod. Phys.*, **90** (2018) 015001.
[3] Mañes J. L., *Phys. Rev. B*, **85** (2012) 155118.
[4] Tang F. and Wan X., *Phys. Rev. B*, **104** (2021) 085137.
[5] Yu Z.-M., Zhang Z., Liu G.-B., Wu W., Li X.-P., Zhang R.-W., Yang S. A. and Yao Y., *Sci. Bull.*, **67** (2022) 375.
[6] Liu G.-B., Zhang Z., Yu Z.-M., Yang S. A. and Yao Y., *Phys. Rev. B*, **105** (2022) 085117.
[7] Zhang Z., Liu G.-B., Yu Z.-M., Yang S. A. and Yao Y., *Phys. Rev. B*, **105** (2022) 104426.
[8] Damnjanović M. and Milošević I., *Phys. Rep.*, **581** (2015) 1.
[9] Lazić N., Milivojević M. and Damnjanović M., *Acta Crystallogr. Sect. A*, **69** (2013) 611.
[10] Lazić N. and Damnjanović M., *Phys. Rev. B*, **90** (2014) 195447.
[11] Lazić N., *Quasi-classical Ground States and Magnons in Monoperiodic Spin Systems*, PhD Thesis, Faculty of Physics, University of Belgrade (October 2016).
[12] Nikolić B., Milošević I., Vuković T., Lazić N., Dmitrović S., Popović Z. and Damnjanović M., *Acta Crystallogr. Sect. A*, **78** (2022) 107.
[13] Damljanović V. and Lazić N., *J. Phys. A: Math. Theor.*, **56** (2023) 215201.
[14] Kowalczyk P. J., Brown S. A., Maerkl T., Lu Q., Chiu C.-K., Liu Y., Yang S. A., Wang X., Zasada I., Genuzio F., Menteş T. O., Locatelli A., Chiang T.-C. and Bian G., *ACS Nano*, **14** (2020) 1888.
[15] Liu Z., Wang P., Cui Q., Yang G., Jin S. and Xiong K., *RSC Adv.*, **9** (2019) 2740.
[16] Zhang Z., Wu W., Liu G.-B., Yu Z.-M., Yang S. A. and Yao Y., *Phys. Rev. B*, **107** (2023) 075405.
[17] Semenoff G. W., *Phys. Rev. Lett.*, **53** (1984) 2449.
[18] Haldane F. D. M., *Phys. Rev. Lett.*, **61** (1988) 2015.
[19] Fang C. and Fu L., *Sci. Adv.*, **5** (2019) eaat2374.
[20] Young S. M. and Kane C. L., *Phys. Rev. Lett.*, **115** (2015) 126803.
[21] Wieder B. J., Bradlyn B., Wang Z., Cano J., Kim Y., Kim H.-S. D., Rappe A. M., Kane C. L. and Bernevig B. A., *Science*, **361** (2018) 246.

[22] Schindler F., Tsirkin S. S., Neupert T., Andrei Bernevig B. and Wieder B. J., *Nat. Commun.*, **13** (2022) 5791.

[23] Lin K.-S., Palumbo G., Guo Z., Hwang Y., Blackburn J., Shoemaker D. P., Mahmood F., Wang Z., Fiete G. A., Wieder B. J. and Bradlyn B., *Nat. Commun.*, **15** (2024) 550.

[24] Landau L. D. and Lifshitz E. M., *Quantum Mechanics* (Butterworth-Heinemann, Oxford) 1981.

[25] Neumann J. v. and Wigner E., *Phys. Z.*, **30** (1929) 467.

[26] Neumann J. v. and Wigner E., *On the behaviour of eigenvalues in adiabatic processes*, in *Quantum Chemistry: Classic Scientific Papers*, edited by Hettema H. (World Scientific, Singapore) 2000, pp. 25–31.

[27] Owusu H. K., Wagh K. and Yuzbashyan E. A., *J. Phys. A: Math. Theor.*, **42** (2008) 035206.

[28] Yu R., Weng H., Fang Z., Dai X. and Hu X., *Phys. Rev. Lett.*, **115** (2015) 036807.

[29] Kim Y., Wieder B. J., Kane C. L. and Rappe A. M., *Phys. Rev. Lett.*, **115** (2015) 036806.

[30] Ahn J., Kim D., Kim Y. and Yang B.-J., *Phys. Rev. Lett.*, **121** (2018) 106403.

[31] Berestetskii V. B., Lifshitz E. M. and Pitaevskii L. P., *Quantum Electrodynamics* (Butterworth-Heinemann, Oxford) 1982.

[32] Cornwell J. F., *Group Theory in Physics,* Vol. **1** (Academic Press, London) 1984.

[33] Elcoro L., Bradlyn B., Wang Z., Vergniory M. G., Cano J., Felser C., Bernevig B. A., Orobengoa D., de la Flor G. and Aroyo M. I., *J. Appl. Crystallogr.*, **50** (2017) 1457.

[34] Kopsky V. and Litvin D. B., *International Tables of Crystallography Volume E: Subperiodic Groups* (Kluwer Academic Publishers, Dordrecht) 2002.

[35] Hahn T., *International Tables of Crystallography Volume A: Space-Group Symmetry* (Springer, Dordrecht) 2005.

[36] Momma K. and Izumi F., *J. Appl. Crystallogr.*, **44** (2011) 1272.

[37] Wieder B. J. and Kane C. L., *Phys. Rev. B*, **94** (2016) 155108.

[38] Watanabe H., Po H. C., Zaletel M. P. and Vishwanath A., *Phys. Rev. Lett.*, **117** (2016) 096404.

[39] Watanabe H., Po H. C., Vishwanath A. and Zaletel M., *Proc. Natl. Acad. Sci. U.S.A.*, **112** (2015) 14551.

[40] Zhang J., Chan Y.-H., Chiu C.-K., Vergniory M. G., Schoop L. M. and Schnyder A. P., *Phys. Rev. Mater.*, **2** (2018) 074201.

[41] Leonhardt A., Hirschmann M. M., Heinsdorf N., Wu X., Fabini D. H. and Schnyder A. P., *Phys. Rev. Mater.*, **5** (2021) 124202.

[42] Hirschmann M. M., Leonhardt A., Kilic B., Fabini D. H. and Schnyder A. P., *Phys. Rev. Mater.*, **5** (2021) 054202.

[43] Ivantchev S., Kroumova E., Madariaga G., Pérez-Mato J. M. and Aroyo M. I., *J. Appl. Crystallogr.*, **33** (2000) 1190.

[44] de la Flor G., Souvignier B., Madariaga G. and Aroyo M. I., *Acta Crystallogr. Sect. A*, **77** (2021) 559.

[45] Rudenko A. N. and Katsnelson M. I., *2D Mater.*, **11** (2024) 042002.

[46] Yang S.-Y., Yang H., Derunova E., Parkin S. S. P., Yan B. and Ali M. N., *Adv. Phys.: X*, **3** (2018) 1414631.

[47] Haastrup S., Strange M., Pandey M., Deilmann T., Schmidt P. S., Hinsche N. F., Gjerding M. N., Torelli D., Larsen P. M., Riis-Jensen A. C., Gath J., Jacobsen K. W., Mortensen J. J., Olsen T. and Thygesen K. S., *2D Mater.*, **5** (2018) 042002.

[48] Gjerding M. N., Taghizadeh A., Rasmussen A., Ali S., Bertoldo F., Deilmann T., Knøsgaard N. R., Kruse M., Larsen A. H., Manti S., Pedersen T. G., Petralanda U., Skovhus T., Svendsen M. K., Mortensen J. J., Olsen T. and Thygesen K. S., *2D Mater.*, **8** (2021) 044002.

[49] Mounet N., Gibertini M., Schwaller P., Campi D., Merkys A., Marrazzo A., Sohier T., Castelli I. E., Cepellotti A., Pizzi G. and Marzari N., *Nat. Nanotechnol.*, **13** (2018) 246.

[50] Fu J., Kuisma M., Larsen A. H., Shinohara K., Togo A. and Thygesen K. S., *2D Mater.*, **11** (2024) 035009.

[51] Emmerling F. and Röhr C., *Z. Naturforsch. B*, **58** (2003) 620.

[52] Meng W., Liu Y., Zhang X., He Z., Yu W.-W., Zhang H., Tian L. and Liu G., *Phys. Rev. B*, **107** (2023) 115167.

[53] Damljanović V. and Gajić R., *J. Phys.: Condens. Matter*, **29** (2017) 185503.

[54] Pardo V. and Pickett W. E., *Phys. Rev. Lett.*, **102** (2009) 166803.

[55] Banerjee S., Singh R. R. P., Pardo V. and Pickett W. E., *Phys. Rev. Lett.*, **103** (2009) 016402.

[56] Damljanović V., Popov I. and Gajić R., *Nanoscale*, **9** (2017) 19337.

[57] Guo P.-J., Wei Y.-W., Liu K., Liu Z.-X. and Lu Z.-Y., *Phys. Rev. Lett.*, **127** (2021) 176401.

[58] Guo P.-J., Wei Y.-W., Liu K., Liu Z.-X. and Lu Z.-Y., *Phys. Rev. Lett.*, **129** (2022) 049901(E).

[59] Kopciuszyński M., Krawiec M., Żurawek L. and Zdyb R., *Nanoscale Horiz.*, **5** (2020) 679.

[60] Gong J., Wang J., Yuan H., Zhang Z., Wang W. and Wang X., *Phys. Rev. B*, **106** (2022) 214317.

[61] Wang C., Yu W.-W., Liu Y., Zhang X., Jin L., Liu C. and Liu G., *J. Phys.: Condens. Matter*, **35** (2023) 425702.

[62] Luo W., Ji J., Lu J., Zhang X. and Xiang H., *Phys. Rev. B*, **101** (2020) 195111.

[63] Damljanović V. and Gajić R., *J. Phys.: Condens. Matter*, **28** (2016) 085502.

[64] Damljanović V. and Gajić R., *J. Phys.: Condens. Matter*, **28** (2016) 439401.

[65] Zhong M., Liu H., Wang J., Xie C., Yuan H., Zhang Z., Ding G., Wang X. and Zhang G., *Phys. Rev. B*, **107** (2023) 205406.

[66] Damljanović V., Lazić N., Šolajić A., Pešić J., Nikolić B. and Damnjanović M., *J. Phys.: Condens. Matter*, **32** (2020) 485501.

[67] Meng W., Liu Y., Yu W.-W., Zhang X. and Liu G., *Mater. Today Phys.*, **27** (2022) 100774.

[68] Mao N., Wang H., Dai Y., Huang B. and Niu C., *npj Comput. Mater.*, **8** (2022) 154.

[69] Dresselhaus M. S., Dresselhaus G. and Jorio A., *Group Theory* (Springer, Berlin) 2007.

[70] Young S. M. and Wieder B. J., *Phys. Rev. Lett.*, **118** (2017) 186401.

Journal of Physics: Condensed Matter

PAPER

Peculiar symmetry-protected electronic dispersions in two-dimensional materials

To cite this article: V Damljanovi *et al* 2020 *J. Phys.: Condens. Matter* **32** 485501

IOP Publishing Journal of Physics: Condensed Matter
J. Phys.: Condens. Matter **32** (2020) 485501 (8pp) https://doi.org/10.1088/1361-648X/abaad1

Peculiar symmetry-protected electronic dispersions in two-dimensional materials

V Damljanović[1,3], N Lazić[2], A Šolajić[1], J Pešić[1], B Nikolić[2] and M Damnjanović[2]

[1] Institute of Physics Belgrade, University of Belgrade, Pregrevica 118, 11080 Belgrade, Serbia
[2] NanoLab, Faculty of Physics, University of Belgrade, PO Box 44, Belgrade 11001, Serbia

E-mail: damlja@ipb.ac.rs

Received 16 June 2020, revised 23 July 2020
Accepted for publication 30 July 2020
Published 8 September 2020

Abstract

Symmetry indicates that low energy spectra of materials could be richer than well-known Dirac, semi-Dirac, or quadratic, hosting some unusual quasiparticles. Performing the systematic study of exact forms of low energy effective Hamiltonians and dispersions in high-symmetry points with fourfold degeneracy of bands, we found new, previously unreported dispersion, which we named poppy flower (PF) after its shape. This massless fermion exists in non-magnetic two-dimensional (2D) crystals with spin–orbit coupling (SOC), which are invariant under one of the proposed ten noncentrosymmetric layer groups. We suggest real three-dimensional (3D) layered materials suitable for exfoliation, having layers that belong to these symmetry groups as candidates for realization of PF fermions. In 2D systems without spin–orbit interaction, fortune teller (FT)-like fermions were theoretically predicted, and afterward experimentally verified in the electronic structure of surface layer of silicon. Herein, we show that such fermions can also be hosted in 2D crystals with SOC, invariant under additional two noncentrosymmetric layer groups. This prediction is confirmed by density functional based calculation: layered $BiIO_4$, which has been synthesized already as a 3D crystal, exfoliates to stable monolayer with symmetry $pb2_1a$, and FT fermion is observed in the band structure. Analytically calculated density of states (DOS) of the PF shows semimetallic characteristic, in contrast to metallic nature of FT having non-zero DOS at the bands contact energy. We indicate possibilities for symmetry breaking patterns which correspond to the robustness of the proposed dispersions as well as to the transition from Dirac centrosymmetric semimetal to PF.

Keywords: electronic dispersions, spin–orbit coupling, symmetry, new fermions

(Some figures may appear in colour only in the online journal)

1. Introduction

Electronic dispersion essentially determines crystal properties and it is well known that it is assigned by quantum numbers of the underlying symmetry group. These are space, layer (including wallpaper) or line groups, referring respectively to dimensionality of crystals: 3D, quasi-2D (Q2D), or quasi-1D. Probably the most famous example of a low-dimensional material is graphene (there are also related single layers, such as borophene [1], borophosphene [2], graphynes [3], etc), which hosts Dirac like (linear in quasi-momentum) dispersion in the vicinity of high symmetry Dirac points. Such shape of energy bands, besides being responsible for some intriguing phenomena, provides material realization of relativistic electron. This triggered numerous investigations of the connection between symmetry of materials and appearance of Dirac and Weyl points in their band structures. These points are attributed to existence of rotational [4], nonsymmorphic [5], mirror [6], space-time inversion [7, 8], time-reversal plus fractional translation [9], and generalized chiral symmetry [10]. There are also results on the search for Weyl and Dirac

[3] Author to whom any correspondence should be addressed.

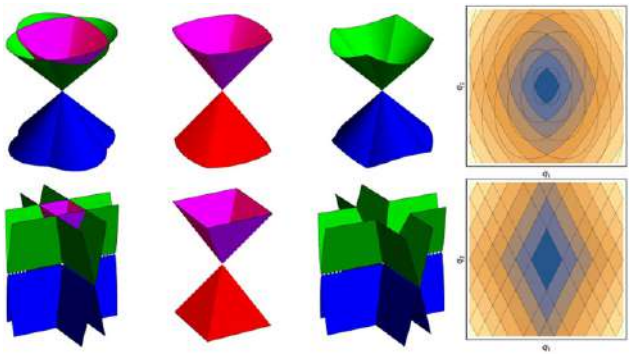

Figure 1. PF (up) and FT (bottom) dispersions (given by equations (3.1)): from left to right are all bands, bands $E_{\pm1,+1}$, bands $E_{\pm1,-1}$ and horizontal sections of the bands (iso-energetic lines).

points according to group theoretical criteria in Brillouin zones (BZs) of all space [11], layer [12–14] or wallpaper groups [15].

In addition, geometrical symmetries impose conditions that lead to the emergence of unconventional quasiparticles in condensed matter systems. In 3D materials, enforced by space groups, double Dirac points [16], three-component [17, 18] or hourglass fermions [19] are found, inspiring further theoretical and experimental research [20–25]. Concerning Q2D systems, besides Dirac (as in graphene [26]), there are also semi-Dirac (Dirac-like in one direction, and quadratic in the orthogonal one, as in black phosphorus [27]), quadratic (as in molybdenum disulphide [28]), and fortune teller (FT) dispersions [29], which corresponds to the coexistence of a nodal point and lines. Namely, symmetry analysis of the possible completely linear dispersions in non-magnetic, Q2D materials with negligible spin–orbit coupling (SOC) has shown that only completely massless fermions appearing in layers are Dirac and FT [29]. Recently, FT dispersion has been experimentally confirmed in a surface layer of silicon [30].

A question arises whether new types of fermions are possible in Q2D materials by inclusion of SOC? With help of layer double groups (LDGs) and time-reversal symmetry (TRS) (i.e. gray LDG), we made a quite general search for linear dispersions in the vicinity of high symmetry points (HSPs); since no reference to nonsymmorphic symmetries is made, the topological (hour-glass like) band crossing mechanisms are not *a priori* assumed, as it is usual. Indeed, it turns out that there are two peculiar types (figure 1) featuring twelve nonsymmorphic and noncentrosymmetric groups: two groups support previously predicted FT, and the remaining ones poppy flower (PF) dispersion (generalizing both FT and Dirac types).

After a brief overview of necessary group-theoretical methods, the obtained results are discussed on the basis of effective low-energy model, calculated densities of states and symmetry breaking patterns. Also, a list of material candidates supporting the new dispersions is provided. The predicted effect is justified by density functional based relaxation and band structure calculation in $BiIO_4$ monolayer. Synthesis of this layered 3D material was reported around a decade ago [31]. Numerical band structure confirms our group theoretical prediction, which may be the motivation for future laboratory synthesis of this material as monolayer.

2. Method

Symmetry determines Bloch Hamiltonian in the vicinity of high-symmetry BZ wave vector through the allowed irreducible representations (IRs) of the little group [32]. Allowed IRs of LDGs are subduced from the corresponding space groups IRs (found on Bilbao Crystallographic Server [33]), and also independently constructed by POLSym code [34]. Concerning LDGs with TRS, the dimensions [33, 35] of the allowed IRs (actually co-representations) are 1, 2 or 4, and for generic ones, giving bands degeneracy, this is 1 or 2. Here we focus on the band structures near quadruple points at high-symmetry momenta. Further, we do not consider generically degenerate bands, giving double degenerate Dirac dispersion (precisely, it consists of two double spinfull degenerate cones meeting at one fourfold degenerate point); this automatically excludes centrosymmetric crystals, as Kramers degeneracy in them forbids nondegenerate bands [36]. Among the remaining groups, only twelve are with special points with four-dimensional allowed (co)representation.

Analysis of all allowed IRs R of little groups $G(\boldsymbol{k}_0)$ of HSPs $\boldsymbol{k}_0$ in LDG lacking the inversion symmetry gives the following conditions for quadruple point: $\boldsymbol{k}_0$ is time-reversal invariant momentum, R is two-dimensional, either real or complex IR. Therefore, we consider $\hat{H}(\boldsymbol{k})$ being Hamiltonian of the system $\hat{H}_0$ (including spin–orbit) in the basis $\{|\Psi_1\rangle, |\Psi_2\rangle, |\theta\Psi_1\rangle, |\theta\Psi_2\rangle\}$, where the spinors $|\Psi_i\rangle = |\Psi_i(\boldsymbol{k})\rangle$ ($i = 1, 2$ counts two bands touching each other at $\boldsymbol{k}_0$ also in the absence of TRS) belong to R at $\boldsymbol{k}_0$ and θ is an anti-unitary operator of TRS, for which we used $\theta^2 = -\hat{\sigma}_0$, since spinfull case is considered. Throughout the text $\hat{\sigma}_0$ is two-by-two unit matrix, and $\hat{\sigma}_1, \hat{\sigma}_2, \hat{\sigma}_3$ are Pauli matrices. Denoting the little group elements by $\ell = (h|\boldsymbol{r}_{\hat{h}} + \boldsymbol{b})$, where h is crystallographic double point group element, while $\boldsymbol{r}_{\hat{h}}$ and $\boldsymbol{b}$ are fractional and lattice translation, respectively, one gets the conditions imposed by time-reversal and geometrical symmetries on $\hat{H}(\boldsymbol{k}_0 + \boldsymbol{q})$ in the vicinity of $\boldsymbol{k}_0$ (therefore, the wavevector $\boldsymbol{q}$ is small):

$$\hat{H}^*(\boldsymbol{k}_0 + \boldsymbol{q}) = \hat{T}^\dagger \hat{H}(\boldsymbol{k}_0 - \boldsymbol{q})\hat{T}, \tag{2.1}$$

$$\hat{H}(\boldsymbol{k}_0 + \boldsymbol{q}) = \hat{D}^\dagger(\ell)\hat{H}(\boldsymbol{k}_0 + \hat{h}'\boldsymbol{q})\hat{D}(\ell). \tag{2.2}$$

Here, $\hat{D} = \mathrm{diag}(\hat{R}, \hat{R}^*)$, and $\hat{h}'$ is an operator reduction of vector representation $\hat{h}$ to 2D BZ, while $\hat{T} = -\mathrm{i}\hat{\sigma}_2 \otimes \hat{\sigma}_0$ represents the action of θ on the basis of spinors.

To focus on the terms linear in $\boldsymbol{q}$, Hamiltonian is expanded in the form $\hat{H}(\boldsymbol{k}_0 + \boldsymbol{q}) \approx \sum_{i=1,2} q_i \frac{\partial \hat{H}(\boldsymbol{k}_0+\boldsymbol{q})}{\partial q_i}|_{\boldsymbol{q}=0}$ (energy scale is conveniently shifted such that $\hat{H}(\boldsymbol{k}_0) = 0$). To incorporate symmetry, the matrix elements of the Hamiltonian gradient are arranged into the four-by-eight matrix $\hat{W}$, which entries $w_{pq} = \left(w^1_{pq}\ w^2_{pq}\right)$ are pairs $w^i_{pq} = \frac{\partial H_{pq}(\boldsymbol{k}_0+\boldsymbol{q})}{\partial q_i}|_{\boldsymbol{q}=0}$. The form

Table 1. Groups providing dispersions (3.1). Notations for layer (columns 1 and 2) and space groups (columns 4, 5 and 6) are according to [37, 38] respectively. IR notation in the eighth column is as in Bilbao Crystallographic Server [33]. Effective Hamiltonian is indicated in the last column by the nonzero parameters (and their interrelations) of (2.5). For the last four groups $a = c$ while $\bar{M}_6$ and $\bar{M}_7$ are conjugated pair of IRs.

Layer double group			Corresponding space double group						
Group		IR	Group			Plane	IR	Dispersion	Nonzero v^i_{pq}
21	$p2_12_12$	$\bar{S}_5$	18	$P2_12_12$	D^3_2	$z=0$	$\bar{S}_5$	(3.1a)	$v^1_{13}, v^1_{23}, v^1_{33}, v^2_{11}, v^2_{21}, v^2_{31}$
25	$pba2$	$\bar{S}_5$	32	$Pba2$	C^8_{2v}	$z=0$	$\bar{S}_5$	(3.1a)	$v^1_{13}, v^1_{23}, v^1_{33}, v^2_{11}, v^2_{21}, v^2_{31}$
28	$pm2_1b$	$\bar{Y}_5, \bar{S}_5$	26	$Pmc2_1$	C^2_{2v}	$y=0$	$\bar{Z}_5, \bar{U}_5$	(3.1a)	$v^1_{11}, v^1_{21}, v^1_{31}, v^2_{10}, v^2_{20}, v^2_{30}$
29	$pb2_1m$	$\bar{Y}_5, \bar{S}_5$	26	$Pmc2_1$	C^2_{2v}	$x=0$	$\bar{Z}_5, \bar{T}_5$	(3.1b)	$v^1_{02}, v^2_{10}, v^2_{20}, v^2_{30}$
30	$pb2b$	$\bar{Y}_5, \bar{S}_5$	27	$Pcc2$	C^3_{2v}	$x=0$	$\bar{Z}_5, \bar{T}_5$	(3.1a)	$v^1_{11}, v^1_{21}, v^1_{31}, v^2_{10}, v^2_{20}, v^2_{30}$
32	$pm2_1n$	$\bar{Y}_5$	31	$Pmn2_1$	C^7_{2v}	$y=0$	$\bar{Z}_5$	(3.1a)	$v^1_{13}, v^1_{23}, v^1_{33}, v^2_{10}, v^2_{20}, v^2_{30}$
33	$pb2_1a$	$\bar{Y}_5$	29	$Pca2_1$	C^5_{2v}	$y=0$	$\bar{Z}_5$	(3.1b)	$v^1_{33}, v^2_{11}, v^2_{21}, v^2_{30}$
34	$pb2n$	$\bar{Y}_5$	30	$Pnc2$	C^6_{2v}	$x=0$	$\bar{Z}_5$	(3.1a)	$v^1_{13}, v^1_{23}, v^1_{33}, v^2_{10}, v^2_{20}, v^2_{30}$
54	$p42_12$	$(\bar{M}_6, \bar{M}_7)$	90	$P42_12$	D^2_4	$z=0$	$(\bar{M}_6, \bar{M}_7)$	(3.1a)	$\left\{\begin{array}{l} v^1_{02}=v^2_{02}=v^1_{31}=-v^2_{31} \\ v^1_{10}=v^2_{10}=v^1_{23}=-v^2_{23} \\ v^1_{13}=-v^2_{13}=-v^1_{20}=-v^2_{20} \end{array}\right\}$
56	$p4bm$	$(\bar{M}_6, \bar{M}_7)$	100	$P4bm$	C^2_{4v}	$z=0$	$(\bar{M}_6, \bar{M}_7)$	(3.1a)	
58	$p\bar{4}2_1m$	$(\bar{M}_6, \bar{M}_7)$	113	$P\bar{4}2_1m$	D^3_{2d}	$z=0$	$(\bar{M}_6, \bar{M}_7)$	(3.1a)	
60	$p\bar{4}b2$	$(\bar{M}_6, \bar{M}_7)$	117	$P\bar{4}b2$	D^7_{2d}	$z=0$	$(\bar{M}_6, \bar{M}_7)$	(3.1a)	

$$\hat{W} = \begin{pmatrix} w_{11} & w_{12} & w_{13} & w_{14} \\ w^*_{12} & w_{22} & w_{14} & w_{24} \\ w^*_{13} & w^*_{14} & -w_{11} & -w^*_{12} \\ w^*_{14} & w^*_{24} & -w_{12} & -w_{22} \end{pmatrix} \tag{2.3}$$

follows from the relation (2.1), together with $w^i_{pq} = w^{i*}_{qp}$ corresponding to the requirement that Hamiltonian $\hat{H}$ is a Hermitian operator. Note that the form (2.3) of $\hat{W}$ leads to the traceless Hamiltonian: it excludes the scalar term (which imposes the tilt of the bands). The geometrical symmetries are incorporated by (2.2), which is rewritten [11, 29] as an efficient fixed point condition

$$\left|\widehat{W}\right\rangle = \hat{D} \otimes \hat{D}^* \otimes \hat{h}' \left|\widehat{W}\right\rangle, \tag{2.4}$$

on the column vector (32×1) form $\left|\widehat{W}\right\rangle$ of $\hat{W}$. The equation (2.4) is solved with help of the group projection operators for all of the twelve noncentrosymmetric groups hosting quadruple points at high symmetry momenta; in this way, the symmetry determines form of $\hat{W}$. To explicate this, it is more convenient to use another general expansion of the effective low energy Hamiltonian,

$$\hat{H}(\boldsymbol{q}) = \sum_{p,q=0}^{3} \sum_{i=1}^{2} q_i v^i_{pq}\, \hat{\sigma}_p \otimes \hat{\sigma}_q, \tag{2.5}$$

and find the constraints imposed by symmetry on the real coefficients v^i_{pq} (simply interrelated with w^i_{pq}).

3. Results and discussion

3.1. Symmetry adapted Hamiltonians and dispersions

Groups hosting new dispersions are listed in table 1. Besides intrinsic layer group notation (the first part), the space group of the system obtained by periodic repetition of the layer along axis perpendicular to it (column plane) according to Bilbao Crystallographic Server is also given (second part), where the directions x, y and z are along axes of orthorombic/tetragonal 3D primitive unit cell. On the other hand, in POLSym approach we used convention that layers are in xy-plane. Orthogonal lattice vectors $\boldsymbol{a}_1$ and $\boldsymbol{a}_2$ span primitive rectangular/square 2D unit cell, while reciprocal lattice vectors $\boldsymbol{k}_1$ and $\boldsymbol{k}_2$ satisfy $\boldsymbol{a}_j \cdot \boldsymbol{k}_l = 2\pi\delta_{j,l}$ and q_1, q_2 are projections of $\boldsymbol{q}$ along $\boldsymbol{k}_1$ and $\boldsymbol{k}_2$. Relevant BZs are in figure 2.

Effective Hamiltonians allowed by symmetry group in the special points of Brillouin's zone are presented in the last column of the table 1: the nonzero real coefficients v^i_{pq} in the expansion (2.5) are specified, together with the constraints among them. The listed forms correspond to the group settings (lattice vectors and coordinate origin) and double valued irreducible co-representations obtained by POLSym code. In fact, this enabled flexibility in the choice of generators (coordinate system and translational periods), which finally results in the form of irreducible co-representations. These are chosen such to get the same form of the effective Hamiltonian whenever it is possible (for different groups). Equivalent (but different) settings (and co-representations) produce different (still equivalent with respect to dispersions) Hamiltonian forms. Clearly, the exact values of the nonzero coefficients v^i_{pq} (listed in the last column of the table 1) are material dependent. The groups' generators and their representative matrices in the allowed co-representations associated to the specified high-symmetry points are in the table 2. It should be remarked that in all the considered cases this point is fixed by the whole gray group, i.e. the little group is the gray (double) group, and the allowed co-representations of the little group are simultaneously the irreducible co-representations of the gray group. The matrices of the relevant co-representations are four-dimensional. In all the cases time-reversal corresponds to the matrix $\hat{T}$; all other generators are represented by the block-diagonal

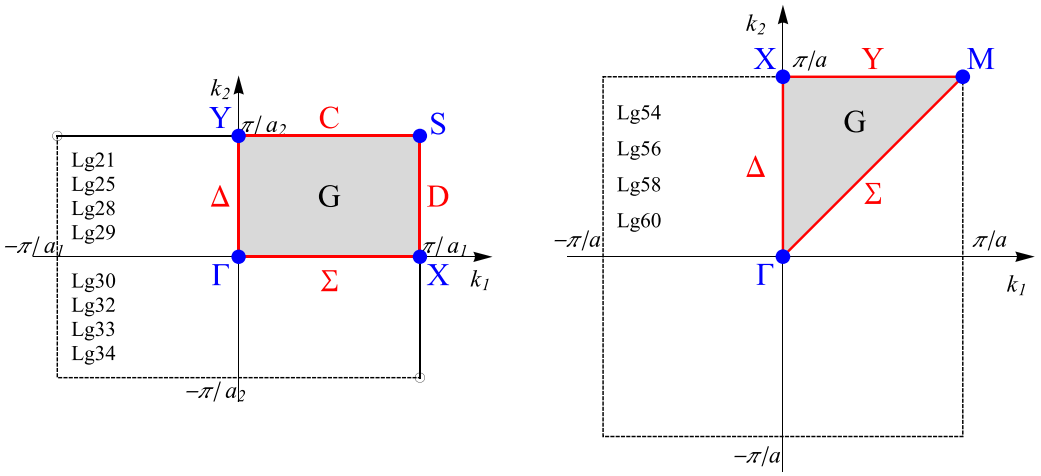

Figure 2. BZs of the groups (listed in table 1) supporting dispersions (3.1). For layer groups 28, 29, 30, 32, 33 and 34 vector $\boldsymbol{k}_2$ is along (screw) axis of order two.

matrices $\hat{D} = \mathrm{diag}(\hat{R}, \hat{R}^*)$, with mutually conjugated 2×2 blocks. Therefore, only this block, $\hat{R}$, is given in the table 2.

The described technique leads to two new types of dispersions (figure 1; crossings are taken at $E = 0$). The first one is PF, with four bands (obtained for $u, v = \pm 1$):

$$E_{v,u}(\boldsymbol{q}) = v\sqrt{aq_1^2 + cq_2^2 + u\,b\,|q_1 q_2|}. \tag{3.1a}$$

The expression under the square root is non-negative since a, b and c are positive quantities (functions of v^i_{pq}) such that $b^2 - 4ac < 0$. For quadratic layer groups (54, 56, 58, 60) $c = a$, and above dispersion degenerates to the isotropic one $E_{v,u} = v\sqrt{a\boldsymbol{q}^2 + u\,b\,|q_1 q_2|}$. Two groups, 29 and 33, enforce $b^2 - 4ac = 0$, hosting thus FT dispersions (with bands counted by $u, v = \pm 1$):

$$E_{v,u}(\boldsymbol{q}) = v\,|f\,|q_1| + u\,g\,|q_2|\,|, \tag{3.1b}$$

with f, g positive quantities, also functions of v^i_{pq}. Note that on the other side, the limit $b \to 0^+$ gives Dirac dispersion.

3.2. Density of states

Dispersions (3.1), differing from the well-known Dirac, semi-Dirac or quadratic, impose specific physical properties. In this context, one must take into account the range of validity of these forms, describing the realistic band structures only in the vicinity of high-symmetry point. In particular, corresponding density of states (DOS) near $E = 0$ are:

$$\rho^{\mathrm{SOC}}_{\mathrm{PF}} = \frac{2|E|}{\pi\sqrt{4ac - b^2}}, \tag{3.2a}$$

$$\rho^{\mathrm{SOC}}_{\mathrm{FT}} \approx \frac{L}{4\pi^2\sqrt{f^2 + g^2}}. \tag{3.2b}$$

Unlike to PF, but similarly to 3D nodal semimetals [39], exact calculation of DOS of FT is prevented due to the non-circular iso-energetic lines (figure 1). Thus, the last expression corresponds to realistic situations where the horizontal parts of band crossing lines are of the length L (this is an effective range of approximation). In non-SOC case calculation of DOS gives doubled results (3.2), since each energy is spin degenerate, which is then decoupled from the orbital one. Non zero DOS of FT near $E = 0$ is in contrast to DOS of Dirac or PF dispersions being proportional to $|E|$, as well as to semi-Dirac which is proportional to $\sqrt{|E|}$. This affects many properties, to mention only charge and spin transport. Further, it can be shown that the electron effective mass, obtained from band curvatures, for all dispersions (3.1) vanishes. Let us emphasize that the higher order terms, neglected in derivation cannot change the obtained band topology (figure 1), though may distort bands slightly.

3.3. Symmetry breaking

Despite the obtained dispersions are essential, i.e. resistant to symmetry preserving perturbation, an interesting additional insight is gained by considering symmetry breaking. Herein, taking into account group–subgroup relations, we discuss the possibilities of robustness or switching between various dispersions at the same BZ-point by lowering the symmetry, e.g. due to strain. It is expected that decreasing the number of symmetry elements leads to relaxing the constraints imposed on Hamiltonians, and consequently increasing (or preserving) the number of independent parameters. In this context, taking into account the number of non-zero parameters v^i_{pq} of (2.5) given in table 1, it is meaningful to consider the transitions from FT to anisotropic PF, as well as from isotropic PF to FT, when the symmetry is lowered. Precisely, the allowed four-band model Hamiltonian diagonalizing in PF dispersion have six real independent parameters, which are reduced to three for quadratic groups; similarly, there are 4 real independent Hamiltonian parameters for FT. Before proceeding, let us take a brief look into the robustness of FT and PF.

Regarding groups 29 and 33 supporting FT dispersion, symmetry reduction in which either nonsymmorphic glide plane or screw axis (but not both) is retained causes that FT at the Y point splits into two non-degenerate conical dispersions. Opposite out-of-plane shifts of the adjacent nuclei positioned

Table 2. Allowed irreducible co-representations: for each group and corresponding HSP, the generators are listed, and the block-diagonal part $\hat{R}$ of double valued co-representation $\hat{D}$ representing these generators (in the same order). Here, $C_{n\hat{n}}$ is rotation for $2\pi/n$ around axis $\hat{n}$ (which is $\hat{x}$, $\hat{y}$, $\hat{z}$, or $\hat{c} = \frac{1}{\sqrt{2}}(\hat{x} + \hat{y})$), $m_{\hat{n}}$ is vertical mirror plane which contains $\hat{n}$ axis, m_{h} is horizontal mirror plane, and $S_n = C_{n\hat{z}} m_{\mathrm{h}}$.

Group	HSP	Generators			$\hat{R}$			
21	S	$(C_{2\hat{x}}\|\frac{1}{2}0)$	$(C_{2\hat{y}}\|0\frac{1}{2})$		$\hat{\sigma}_3$	$\hat{\sigma}_1$		
25	S	$(m_{\hat{x}}\|\frac{1}{2}0)$	$(m_{\hat{y}}\|0\frac{1}{2})$		$\hat{\sigma}_3$	$\hat{\sigma}_1$		
28	Y	$(I\|10)$	$(C_{2\hat{y}}\|0\frac{1}{2})$	$m_{\hat{y}}$	$\hat{\sigma}_0$	$-\hat{\sigma}_3$	$-\mathrm{i}\hat{\sigma}_2$	
28	S	$(I\|10)$	$(C_{2\hat{y}}\|0\frac{1}{2})$	$m_{\hat{y}}$	$-\hat{\sigma}_0$	$-\hat{\sigma}_3$	$-\mathrm{i}\hat{\sigma}_2$	
29	Y	$(I\|10)$	$(C_{2\hat{y}}\|0\frac{1}{2})$	m_{h}	$\hat{\sigma}_0$	$-\hat{\sigma}_3$	$-\mathrm{i}\hat{\sigma}_2$	
29	S	$(I\|10)$	$(C_{2\hat{y}}\|0\frac{1}{2})$	m_{h}	$-\hat{\sigma}_0$	$-\hat{\sigma}_3$	$-\mathrm{i}\hat{\sigma}_2$	
30	Y	$(I\|10)$	$(m_{\hat{y}}\|0\frac{1}{2})$	$C_{2\hat{y}}$	$\hat{\sigma}_0$	$-\hat{\sigma}_3$	$-\mathrm{i}\hat{\sigma}_2$	
30	S	$(I\|10)$	$(m_{\hat{y}}\|0\frac{1}{2})$	$C_{2\hat{y}}$	$-\hat{\sigma}_0$	$-\hat{\sigma}_3$	$-\mathrm{i}\hat{\sigma}_2$	
32	Y	$(I\|10)$	$(m_{\mathrm{h}}\|\frac{1}{2}\frac{1}{2})$	$m_{\hat{y}}$	$\hat{\sigma}_0$	$-\hat{\sigma}_3$	$-\mathrm{i}\hat{\sigma}_2$	
33	Y	$(m_{\mathrm{h}}\|\frac{1}{2}0)$	$(C_{2\hat{y}}\|0\frac{1}{2})$		$\mathrm{i}\hat{\sigma}_3$	$\hat{\sigma}_1$		
34	Y	$(I\|10)$	$(m_{\mathrm{h}}\|\frac{1}{2}\frac{1}{2})$	$C_{2\hat{y}}$	$\hat{\sigma}_0$	$-\hat{\sigma}_3$	$-\mathrm{i}\hat{\sigma}_2$	
54	M	$(I\|10)$	$(C_{2\hat{c}}\|\frac{1}{2}\frac{1}{2})$	$C_{4\hat{z}}$	$-\hat{\sigma}_0$	$-\mathrm{i}\hat{\sigma}_2$	$\mathrm{e}^{-\mathrm{i}\frac{3\pi}{4}}$	$\mathrm{diag}(1,\mathrm{i})$
56	M	$(I\|10)$	$(m_{\hat{c}}\|\frac{1}{2}\frac{1}{2})$	$C_{4\hat{z}}$	$-\hat{\sigma}_0$	$-\mathrm{i}\hat{\sigma}_2$	$\mathrm{e}^{-\mathrm{i}\frac{3\pi}{4}}$	$\mathrm{diag}(1,\mathrm{i})$
58	M	$(I\|10)$	$(m_{\hat{c}}\|\frac{1}{2}\frac{1}{2})$	S_4	$-\hat{\sigma}_0$	$-\mathrm{i}\hat{\sigma}_2$	$\mathrm{e}^{-\mathrm{i}\frac{3\pi}{4}}$	$\mathrm{diag}(1,\mathrm{i})$
60	M	$(I\|10)$	$(C_{2\hat{c}}\|\frac{1}{2}\frac{1}{2})$	S_4	$-\hat{\sigma}_0$	$-\mathrm{i}\hat{\sigma}_2$	$\mathrm{e}^{-\mathrm{i}\frac{3\pi}{4}}$	$\mathrm{diag}(1,\mathrm{i})$

in the mirror plane, transforms mirror into a glide plane, while doubling the lattice constant; this in turn halves primitive vector $\boldsymbol{k}_1$ of the reciprocal lattice. Group 29 reduces to 33 and the S point in 29 becomes Y point in 33. Consequently, FT in Y and S points in 29 are robust against lowering the symmetry to group 33. Similarly, concerning the PF, any homogenous stretching along $\boldsymbol{a}_1$ or $\boldsymbol{a}_2$ axis deforms square primitive cell to rectangular, reducing the symmetries of layer groups 54 and 58 (56 and 60) to the group 21 (25) and causes PF to change from isotropic to anisotropic form, which implies direction-dependent electronic and related properties.

Since PF is a generalized form of FT, one could expect that the parameters of these dispersions can be interrelated by tuning. However, continuous transformation from FT to PF at the same point of the BZ is not possible, since neither of groups supporting FT is a subgroup of any of groups allowing PF, nor vice-versa. The expression (3.2a) for DOS of PF shows that the changing parameters such that PF approaches to FT results in a singularity at zero energy. In the other words, if opposite would hold, arbitrarily small displacements of nuclei, being sufficient to lower the symmetry, would cause a jump of (graphene-like) negligible DOS of PF to a finite and constant DOS of FT, which we found unlikely. At the same time, such obstruction from DOS does not forbid the transition between Dirac (double degenerate cones with four-fold degenerate point) and PF, nor it forbids splitting of FT and PF into two non-degenerate conical dispersions (with double degenerate point).

Following the above arguments, it is expected that transition from Dirac cone to PF may be realized by lowering the symmetry, since Dirac dispersions has less independent parameters than PF. According to [5] Dirac semimetals in time-reversal invariant two-dimensional systems with strong SOC are possible in nonsymmorphic groups with inversion symmetry. E.g. let us consider the layer group 46 (*pmmn*), hosting Dirac cones at X, Y and S HSPs (the BZ is the same as this one given on the left panel in figure 2). It is expected that the violation of the inversion symmetry leads to Weyl points or node [5]. However, listing all subgroups, it turns out that the two of the subgroups, 32 and 21, actually host PF in the points Y and S, respectively. Indeed, in [46], using spinfull tight-binding model with four sites (with s-orbitals) per unit cell, authors show that at fillings 2, 6, system invariant under double layer group 21 is semimetal, which hosts one fourfold degenerate and four Weyl points. A plethora of such cases, where groups allowing PF from the table 1 are subgroups of symmetry groups of Dirac semimetals, indicates candidates for transitions between centrosymmetric and noncentrosymmetric crystals with protected four-fold band crossing point. Moreover, the existence of such essential fourfold degenerate point simultaneously with double degenerate Weyl points in the same system, makes that the layers from our list represent possible two-dimensional materials suitable for the study of their interplay.

3.4. Material realization

Despite the fabrication of freestanding layers is not always feasible, the above theoretical predictions required material realizations, or at least numerical simulations. To find realistic material with layer groups from table 1 we searched the list [41] of 3D layered materials, synthesis of which has been reported in the literature. In the table 3 we listed potential material candidates with symmetry groups allowing the predicted peculiar dispersions. These are laboratory fabricated 3D crystals with layered structures, which could be easily or potentially exfoliated into layers.

It is interesting to single out our group-theoretical findings indicated that dispersions (3.1) are not preserved when SOC is neglected, except for the LDG 33, which supports FT dispersion also in that case [29]. Inclusion of SOC moves FT from

Table 3. Material candidates: layered systems with symmetry groups hosting the dispersions (3.1). Layer and corresponding space groups are listed for materials given by a formula and materials project ID. Abbreviations EE and PE stand for easily and potentially exfoliable, respectively, according to [41].

Layer group		Space group		Formula	ID	EE/PE
21	$p2_12_12$	18	$P2_12_12$	As_2SO_6	mp-27230	EE
				$MgMoTeO_6$	mp-1210722	EE
25	$pba2$	32	$Pba2$	$Au_2Se_2O_7$	mp-28095	EE
				$Re_2S_2O_{13}$–I	mp-974650	EE
28	$pm2_1b$	26	$Pmc2_1$	TlP_5	mp-27411	EE
				KO_2H_4F	mp-983327	PE
				$NaGe_3P_3$	mp-1104707	PE
29	$pb2_1m$	26	$Pmc2_1$	WO_2Cl_2	mp-32539	EE
32	$pm2_1n$	31	$Pmn2_1$	CuCOCl	mp-562090	EE
33	$pb2_1a$	29	$Pca2_1$	$BiIO_4$	mp-1191266	PE
				$KPSe_6$	mp-18625	EE
58	$p\bar{4}2_1m$	113	$P\bar{4}2_1m$	$LiReO_2F_4$	mp-554108	EE

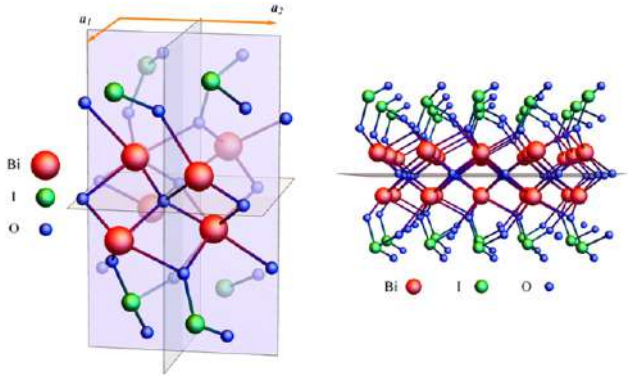

Figure 3. Crystal structure of $BiIO_4$ mono-layer: elementary cell (left) and a part of layer (right).

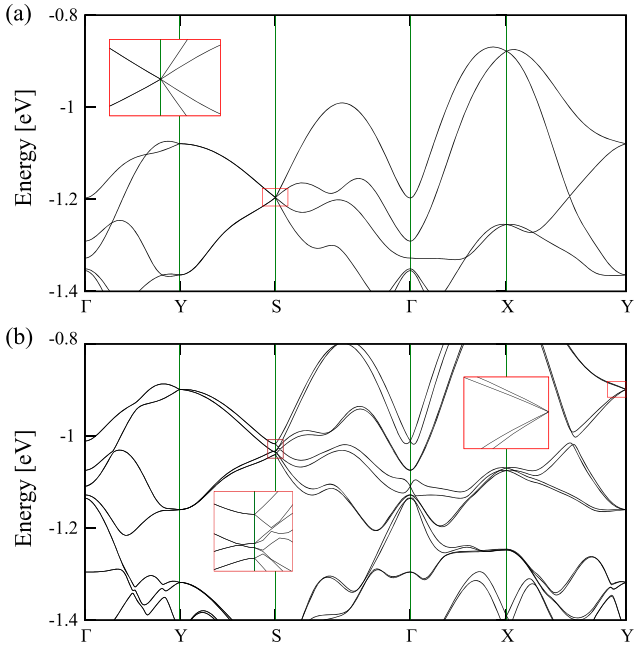

Figure 4. Band structure of $BiIO_4$ mono-layer without SOC (top) and with SOC (bottom), with insets showing magnified FT and split FT dispersions. The Fermi level is set to zero eV.

BZ corners to the Y-point. The material $BiIO_4$ belongs to corresponding space group 29 and has layers parallel to the $y = 0$ plane. Consequently, it should exfoliate to layer group 33 so we choose it for further DFT investigations, as an example of achievements of our theory. Since IRs from table 1 are the only extra IRs in these BZ points, the dispersions (3.1) are unavoidable for crystals with symmetry of these groups. On the other hand, the position of Fermi level cannot be determined solely by symmetry arguments, nor it can be guaranteed that no other bands cross or touch the Fermi level.

We determined crystal (figure 3) and band structure (figure 4) of $BiIO_4$ mono-layer configuration using DFT calculations: full relaxation and bands calculations were performed by QUANTUM ESPRESSO software package [42], full relativistic PAW pseudopotentials [43, 44], with the Perdew–Burke–Ernzerhof exchange–correlation functional [45]. The energy cutoff for electron wavefunction and charge density of 47 Ry and 476 Ry were chosen, respectively. The band structures were found in 500 k-points on selected path, and 2500 k-points for 2D band structure plots in the vicinity of HSPs.

Crystal structure of mono-layer is shown in figure 3. It belongs to rectangular lattice of the group 33, with nearly equal $a_1 = 0.566\,\text{nm}$ and $a_2 = 0.575\,\text{nm}$. Band structure of $BiIO_4$ mono-layer with and without SOC is shown in figure 4. It turns out that the system is insulating in undoped and ungated regime. The closest to Fermi level FT state is at -0.9 eV. When SOC is neglected energy at the point S is eightfold degenerate (including spin), which gives electron filling of $8n$ that is necessary for insulating systems [40]. With inclusion of SOC the eightfold spinfull degeneracy at S is lifted, but sets of eight non-degenerate bands each, form *cat's cradle* structure along ΓX line, as predicted in reference [46]. This gives again electron filling of $8n$ [46, 47]. Our electron filling of 184, derived from DFT calculations, is indeed divisible by 8. Electron filling for DLG 33 prevents FT to be the only dispersion at the Fermi level, while for remaining groups in table 1 the filling condition necessary for Fermi surface consisting of isolated points is $\nu = 4n + 2$.

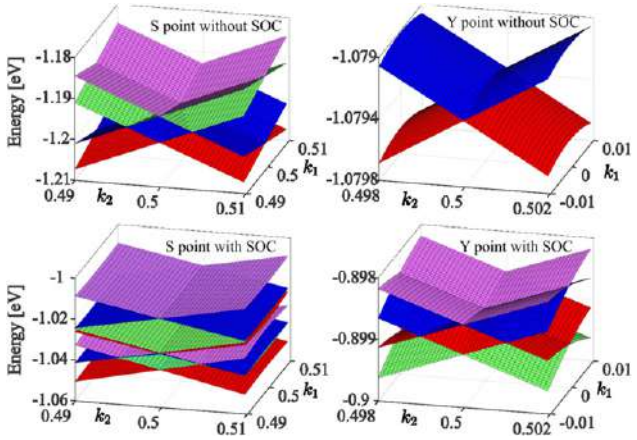

Figure 5. Band structures of $BiIO_4$ mono-layer without and with SOC near points *S* and *Y*. Inclusion of SOC turns FT dispersion into nodal lines in *S*, and degenerate Dirac line into FT in *Y*.

Behavior of FT states with inclusion of SOC is shown in figure 5. In non-SOC case, two pairs of Dirac lines meet at the point *S* and form the FT states. SOC splits eightfold degenerate band at *S* into four double degenerate ones. Near point *Y*, SOC splits fourfold spinfull degenerate Dirac line into one FT state. Since SOC strength is proportional to the fourth power of the atomic number [48], heavy elements in the material induced observable splitting.

4. Conclusions

Characterized by band crossings (touching) points (lines) at Fermi level from which energies disperse linearly, nodal metals/semimetals take an important role in investigations of various topological properties of crystals. Among them, symmetry-enforced ones represent a class of materials hosting such dispersions in HSPs due to increased degeneracy. In the language of group theory, while the spinless case is described by the ordinary group of geometrical transformations, the spinfull situation, when system is robust on spin–orbit perturbation, needs double groups. Additional inclusion of TRS leads to gray magnetic ordinary or double group. The increased degeneracy of energy is enabled by higher dimensional allowed irreducible (co)representations of the corresponding underlying crystal symmetry.

New fermions in 2D materials revealed by application of full gray double layer group symmetry contribute to the interesting physical phenomena of layered systems: two new types of dispersions beyond Dirac, PF and FT, accompany the fourfold degeneracy of bands in high-symmetry points. Our findings single out list of twelve nonsymmorphic and noncentrosymmetric layer groups that support such unusual linear electronic dispersions. As the method is not based on the topological mechanism (invoking nonsymmorphic symmetry), the result is general, verifying *a posteriori* the necessity of nonsymmorphic elements for the considered dispersions. Providing this list, numerical simulations aimed to find material realizations of the peculiar dispersions are facilitated, which is of a great importance to achieve corresponding physical properties. PF dispersion occurs in ten groups; in particular, there are single isolated HSP hosting it in the groups $p2_12_12$, $pba2$ (point *S*), $pm2_1n$, $pb2n$ (*Y*), and $p42_12$, $p4bm$, $p\bar{4}2_1m$, $p\bar{4}b2$ (*M*), while the groups $pm2_1b$ and $pb2b$ have two such points (*Y*, *S*). On the other hand, the FT type of dispersion in the group $pb2_1a$ is hosted in single (*Y*), and in the group $pb2_1m$ in two HSPs (*Y*, *S*).

Particularly interesting are groups $pb2_1a$, supporting FT dispersion both with and without SOC, as well as $pba2$ and $p4bm$, which are also wallpaper groups, preserved even when perpendicular, homogenous electric field is applied (e.g. due to gating). Moreover, coexistence of degenerate point and lines at the same energy in FT dispersion may lead to some new phenomena. FT dispersion has constant contribution to DOS, manifested as a plateau nearby zero energy in FT. This may be important in technological applications, especially when electron and/or spin transport are looked for, like materials for solar cells [49], spintronic etc. On the contrary, PF dispersion, similarly to Dirac ones, contributes by linear DOS with no states on zero energy. It has both isotropic and anisotropic forms which may be continuously transformed into each other by crystal deformations.

Our numerical calculations show that layered $BiIO_4$ 3D crystal, exfoliates to stable mono-layer having a symmetry group from our list. Band structure of $BiIO_4$ mono-layer confirms theoretical prediction, but further efforts are necessary in order to place the Fermi level at right energy.

Acknowledgments

Authors VD, AŠ and JP acknowledge funding provided by the Institute of Physics Belgrade, through the Grant by the Ministry of Education, Science and Technological Development of the Republic of Serbia. NL, BN and MD were supported by the Serbian Ministry of Education, Science and Technological Development under Project Number OI171035. DFT calculations were performed using computational resources at Johannes Kepler University, Linz, Austria.

ORCID iDs

V Damljanović https://orcid.org/0000-0001-7517-6439
N Lazić https://orcid.org/0000-0002-3634-0301
A Šolajić https://orcid.org/0000-0002-0553-0858
J Pešić https://orcid.org/0000-0002-8600-7187
B Nikolić https://orcid.org/0000-0002-7241-3248
M Damnjanović https://orcid.org/0000-0003-2806-253X

References

[1] Gupta S, Kutana A and Yakobson B I 2018 Dirac cones and nodal line in borophene *J. Phys. Chem. Lett.* **9** 2757–62
[2] Zhang Y, Kang J, Zheng F, Gao P-F, Zhang S-L and Wang L-W 2019 Borophosphene: a new anisotropic Dirac cone monolayer with a high Fermi velocity and a unique self-doping feature *J. Phys. Chem. Lett.* **10** 6656–63
[3] Zhang L Z, Wang Z F, Wang Z M, Du S X, Gao H-J and Liu. F 2015 Highly anisotropic Dirac fermions in square graphynes *J. Phys. Chem. Lett.* **6** 2959–62

[4] Fang C, Gilbert M J, Dai X and Andrei Bernevig B 2012 Multi-Weyl topological semimetals stabilized by point group symmetry *Phys. Rev. Lett.* **108** 266802

[5] Young S M and Kane C L 2015 Dirac semimetals in two dimensions *Phys. Rev. Lett.* **115** 126803

[6] van Miert G and Smith C M 2016 Dirac cones beyond the honeycomb lattice: a symmetry-based approach *Phys. Rev.* B **93** 035401

[7] Wang J 2017 Antiferromagnetic Dirac semimetals in two dimensions *Phys. Rev.* B **95** 115138

[8] Kim J, Baik S S, Jung S W, Sohn Y, Ryu S H, Choi H J, Yang B-J and Kim K S 2017 Two-dimensional Dirac fermions protected by space-time inversion symmetry in black phosphorus *Phys. Rev. Lett.* **119** 226801

[9] Young S M and Wieder B J 2017 Filling-enforced magnetic Dirac semimetals in two dimensions *Phys. Rev. Lett.* **118** 186401

[10] Kawarabayashi T, Aoki H and Hatsugai Y 2019 Topologically protected doubling of tilted Dirac fermions in two dimensions *Phys. Status Solidi* B **256** 1970025

[11] Mañes J L 2012 Existence of bulk chiral fermions and crystal symmetry *Phys. Rev.* B **85** 155118

[12] Damljanović V and Gajić R 2016 Existence of Dirac cones in the Brillouin zone of diperiodic atomic crystals according to group theory *J. Phys.: Condens. Matter* **28** 085502

[13] Damljanović V and Gajić R 2016 Addendum to existence of Dirac cones in the Brillouin zone of diperiodic atomic crystals according to group theory *J. Phys.: Condens. Matter* **28** 439401

[14] Park S and Yang B-J 2017 Classification of accidental band crossings and emergent semimetals in two-dimensional noncentrosymmetric systems *Phys. Rev.* B **96** 125127

[15] Wieder B J, Bradlyn B, Wang Z, Cano J, Kim Y, Kim H-S D, Rappe A M, Kane C L and Andrei Bernevig B 2018 Wallpaper fermions and the nonsymmorphic Dirac insulator *Science* **361** 246–51

[16] Wieder B J, Kim Y, Rappe A M and Kane C L 2016 Double Dirac semimetals in three dimensions *Phys. Rev. Lett.* **116** 186402

[17] Bradlyn B, Cano J, Wang Z, Vergniory M G, Felser C, Cava R J and Andrei Bernevig B 2016 Beyond Dirac and Weyl fermions: unconventional quasiparticles in conventional crystals *Science* **353** aaf5037

[18] Zhu Z, Winkler G W, Wu QuanS, Ju L and Alexey A 2016 Soluyanov. Triple point topological metals *Phys. Rev.* X **6** 031003

[19] Wang Z, Alexandradinata A, Cava R J and Andrei Bernevig B 2016 Hourglass fermions *Nature* **532** 189–94

[20] Lv B Q *et al* 2017 Observation of three-component fermions in the topological semimetal molybdenum phosphide *Nature* **546** 627–31

[21] Barik R K, Shinde R and Singh A K 2018 Multiple triple-point fermions in Heusler compounds *J. Phys.: Condens. Matter* **30** 375702

[22] Yang Y *et al* 2019 Topological triply degenerate point with double Fermi arcs *Nat. Phys.* **15** 645–9

[23] Ma J *et al* 2017 Experimental evidence of hourglass fermion in the candidate nonsymmorphic topological insulator KHgSb *Sci. Adv.* **3** e1602415

[24] Wang S-S, Liu Y, Yu Z-M, Sheng X-L and Yang S A 2017 Hourglass Dirac chain metal in rhenium dioxide *Nat. Commun.* **8** 1844

[25] Singh B, Ghosh B, Su C, Lin H, Agarwal A and Bansil A 2018 Topological hourglass Dirac semimetal in the nonpolar phase of Ag_2BiO_3 *Phys. Rev. Lett.* **121** 226401

[26] Novoselov K S, Geim A K, Morozov S V, Jiang D, Zhang Y, Dubonos S V, Grigorieva I V and Firsov A A 2004 Electric field effect in atomically thin carbon films *Science* **306** 666–9

[27] Kim J *et al* 2015 Observation of tunable band gap and anisotropic Dirac semimetal state in black phosphorus *Science* **349** 723–6

[28] Wang Z M 2014 *MoS_2 Materials, Physics and Devices* (Berlin: Springer)

[29] Damljanović V, Popov I and Gajić R 2017 Fortune teller fermions in two-dimensional materials *Nanoscale* **9** 19337–45

[30] Kopciuszyński M, Krawiec M, Żurawek L and Zdyb R 2020 Experimental evidence of a new class of massless fermions *Nanoscale Horiz.* **5** 679–82

[31] Nguyen S D, Yeon J, Kim S-H and Shiv Halasyamani P 2011 $BiO(IO_3)$: a new polar iodate that exhibits an Aurivillius-type $(Bi_2O_2)^{2+}$ layer and a large SHG response *J. Am. Chem. Soc.* **133** 12422–5

[32] Cornwell J F 1984 *Group Theory in Physics* (New York: Academic)

[33] Elcoro L *et al* 2017 Double crystallographic groups and their representations on the Bilbao Crystallographic Server *J. Appl. Crystallogr.* **50** 1457–77

[34] Damnjanović M and Milošević I 2015 Full symmetry implementation in condensed matter and molecular physics—modified group projector technique *Phys. Rep.* **581** 1–43

[35] Litvin D B and Wike T R 1991 *Character Tables and Compatibility Relations of the Eighty Layer Groups and Seventeen Plane Groups* (New York: Plenum)

[36] Dresselhaus M S, Dresselhaus G and Jorio A 2008 *Group Theory* (Berlin: Springer)

[37] Kopsky V and Litvin D B 2002 *International Tables of Crystallography Volume E: Subperiodic Groups* (Dordrecht: Kluwer)

[38] Hahn T 2005 *International Tables of Crystallography Volume A: Space-Group Symmetry* (Berlin: Springer)

[39] Burkov A A, Hook M D and Leon B 2011 Topological nodal semimetals *Phys. Rev.* B **84** 235126

[40] Watanabe H, Po H C, Zaletel M P and Vishwanath A 2016 Filling-enforced gaplessness in band structures of the 230 space groups *Phys. Rev. Lett.* **117** 096404

[41] Mounet N *et al* 2018 Two-dimensional materials from high-throughput computational exfoliation of experimentally known compounds *Nat. Nanotechnol.* **13** 246–52

[42] Giannozzi P *et al* 2009 QUANTUM ESPRESSO: a modular and open-source software project for quantum simulations of materials *J. Phys.: Condens. Matter* **21** 395502

[43] Blöchl P E 1994 Projector augmented-wave method *Phys. Rev.* B **50** 17953–79

[44] Kresse G and Joubert D 1999 From ultrasoft pseudopotentials to the projector augmented-wave method *Phys. Rev.* B **59** 1758–75

[45] Perdew J P, Burke K and Ernzerhof M 1996 Generalized gradient approximation made simple *Phys. Rev. Lett.* **77** 3865–8

[46] Wieder B J and Kane C L 2016 Spin–orbit semimetals in the layer groups *Phys. Rev.* B **94** 155108

[47] Watanabe H, Po H C, Vishwanath A and Zaletel M 2015 Filling constraints for spin-orbit coupled insulators in symmorphic and nonsymmorphic crystals *Proc. Natl Acad. Sci.* **112** 14551–6

[48] Yang S A 2016 Dirac and Weyl materials: fundamental aspects and some spintronics applications *SPIN* **06** 1640003

[49] Boriskina S, Zhou J, Ding Z and Chen G 2018 Efficiency limits of solar energy harvesting via internal photoemission in carbon materials *Photonics* **5** 4

Optical and Quantum Electronics (2018) 50:272
https://doi.org/10.1007/s11082-018-1543-8

An example of diperiodic crystal structure with semi-Dirac electronic dispersion

V. Damljanović[1]

Received: 30 October 2017 / Accepted: 14 June 2018

Abstract
In the physics of two-dimensional materials, notion semi-Dirac dispersion denotes electronic dispersion which is Dirac-like along one direction in the reciprocal space, and quadratic along the orthogonal direction. In our earlier publication (Damljanović and Gajić in J Phys Condens Matter 29:185503, 2017) we have shown that certain layer groups are particularly suitable for hosting semi-Dirac dispersion in the vicinity of some points in the Brillouin zone (BZ). In the present paper we have considered tight-binding model up to seventh nearest neighbors, on a structure belonging to layer group $Dg5$. According to our theory, this group should host semi-Dirac dispersion at A and B points in the BZ. The structure has four atoms per primitive cell, and it is isostructural with sublattice occupied by phosphorus atoms in the layered material $SnPSe_3$. While the first order perturbation theory of double degenerate level gives two pairs of semi-Dirac cones and correctly reproduces dispersion in the Dirac-like direction, exact diagonalisation of four-by-four tight-binding Hamiltonian shows node lines caused by accidental degeneracy in the band structure. We discuss these degeneracies in the context of von Neumann–Wigner theorem, and conclude that although dispersion remains semi-Dirac in the exact diagonalisation method, the band structure does not necessarily form cones. In order to get full picture of behavior of bands in the vicinity of semi-Dirac points, first order perturbation theory may not be sufficient and one may need higher order corrections.

Keywords Semi-Dirac dispersion · Two-dimensional materials · Layer groups · Tight-binding model

This article is part of the Topical Collection on Focus on Optics and Bio-photonics, Photonica 2017.

Guest Edited by Jelena Radovanovic, Aleksandar Krmpot, Marina Lekic, Trevor Benson, Mauro Pereira, Marian Marciniak.

✉ V. Damljanović
damlja@ipb.ac.rs

[1] Institute of Physics Belgrade, University of Belgrade, Pregrevica 118, Belgrade, Serbia

1 Introduction

Two-dimensional (2D) materials are materials that are periodic in two spatial directions but finite in the third, orthogonal direction. These materials gain particular attention after discovery of graphene, a one atom thick layer of carbon atoms arranged in a honeycomb lattice. In contrast to graphene, in which all atoms belong to a single plane, buckled silicene and germanene for example, occupy Wyckoff positions with unequal z-coordinates. Existence of massless electrons whose dynamics is described by Dirac (Weyl) equation is among notable properties of graphene and related, so called Dirac, materials.

Besides Dirac materials, there is another class of 2D materials in which electronic dispersion is Dirac-like (linear) along some direction in the 2D Brillouin zone (BZ), and quadratic along the orthogonal direction. Such semi-Dirac dispersion supports both massless and massive electrons at the same point of the BZ, thus giving rise to highly anisotropic material properties. Using density functional theory (DFT), semi-Dirac dispersion has been predicted in TiO_2/VO_2 nanostructures (Pardo and Pickett 2009, 2010), in silicene oxide (Zhong et al. 2017) and in square selenene and tellurene (Xian et al. 2017). A tight-binding model show semi-Dirac dispersion in phosphorene under strain for certain critical values of hopping parameters (Duan et al. 2016). First experimental realization of material with semi-Dirac dispersion was reported in 2015. It was demonstrated that few-layer black phosphorus doped with potassium posses semi-Dirac dispersion at the BZ center for certain level of doping (Kim et al. 2015). The behavior of semi-Dirac fermions in external magnetic field and consequences that this dispersion imposes on Klein tunneling is examined in more detail in Banerjee et al. (2009) and Banerjee and Pickett (2012). Evolution of Hofstadter spectrum on a square lattice with the application of an on-site uniaxial staggered potential shows merging of two Dirac points into a semi-Dirac one (Deplace and Montambaux 2010). Analysis of semi-Dirac systems based on DFT show that in some cases, spin-orbit coupling (SOC) can open a small gap and can lead to topologically non-trivial bands, which contribute to non-zero total Chern number (Huang et al. 2015). Such systems are then suitable for demonstration of quantum Hall effect. Analogous conclusion is derived for semi-Dirac systems under laser light illumination (Saha 2016). On the other hand, Narayan (2015) concluded that for semi-Dirac semimetals circularly polarized light does not open a band gap. The influence of electronic correlations on semi-Dirac systems was also investigated. It was found by renormalization group theory, that interplay of Coulomb interaction between electrons and disorder can drive the semi-Dirac system to non-Fermi-liquid behavior (Zhao et al. 2016). Similarly, approximate solution of Schwinger–Dyson equation show that moderate Coulomb interaction can induce excitonic gap opening in semi-Dirac band structure (Wang et al. 2017). Anisotropic properties of semi-Dirac materials have potential applications in electronics (Mannhart and Schlom 2010). For example, a p–n junction made from such material would have negative differential conductance for certain bias voltage (Saha et al. 2017).

Group theory is a powerful tool in predicting various types of electronic dispersions. In some cases mere belonging of a crystal to some space groups, leads unavoidably to certain dispersion. For example, Mañes (2012) has found sufficient conditions for existence of bulk chiral fermions in 3D single crystals and has provided a list of space groups that host such dispersion in the vicinity of given points of the BZ. The non-symmorphic space group $P2_12_12_1$ (No. 19 in notation of Hahn 2005) belongs to Mañes list. Geilhufe et al. (2017) have searched the Organic Materials Database and have found six compounds that belong to this space group and in addition have only Dirac points at the Fermi level.

Another search was performed within reported DFT crystal structures collected in Materials Project database (Cheon et al. 2017). This search was for 3D crystal structures that consist of weakly interacting layers and hence, are suitable for obtaining 2D forms by e.g. exfoliation. Recently a list of four layer (diperiodic) groups that host semi-Dirac dispersion was given (Damljanović and Gajić 2017). The corresponding theory was formulated for non-magnetic, 2D materials with negligible SOC.

In this paper we have searched a list of layered 3D materials (Cheon et al. 2017), for structures that consist of layers belonging to layer group $p11b$ ($Dg5$ in notation of Kopsky and Litvin 2002), with layers periodically repeated along the z-axis. The layer group $p11b$ hosts semi-Dirac dispersion at A and B points of the BZ (Damljanović and Gajić 2017). In what follows, we have considered a tight-binding model from s-orbitals on a system isostructural to phosphorus sublattice in the single layer of material $SnPSe_3$ that belongs to the list (Cheon et al. 2017).

2 Method and results

Space group $P1c1$ (No. 7) is obtained by periodic repetition of layer group $Dg5$ along the axis that is perpendicular to diperiodic plane. On the other hand, diperiodic plane is perpendicular to the y-axis in the space group $P1c1$. For these reasons we have searched 3D layered materials given in Cheon et al. (2017), belonging to the space group $P1c1$, such that layers are parallel to the unique glide plane. We have found following five materials whose structures satisfy these requirements: Al_2CdCl_8 (Materials Project No. mp-28361 Bergerhoff et al. 1983; Staffel and Mayer 1987), $Cr(PO_3)_5$ (mp-705019 Bergerhoff et al. 1983; Jain et al. 2011; Hautier et al. 2011; El-Horr and Bagieu Beucher 1986), $LiTi(PO_3)_5$ (mp-684059 Bergerhoff et al. 1983; Jain et al. 2011; Hautier et al. 2011; El-Horr and Bagieu Beucher 1986), $SnPSe_3$ (mp-570370 Bergerhoff et al. 1983; Israel et al. 1998) and $SnPS_3$ (mp-13923 Bergerhoff et al. 1983; Dittmar and Schaefer 1974). If one would neglect SOC one would get semi-Dirac dispersion in these materials, irrespectively of the method used to calculate the band structure, as long as the approximation used is sufficiently fine (Damljanović and Gajić 2017). The inclusion of SOC would require analysis of double groups and it may be a topic of future research.

As an illustration, we will investigate electronic dispersion within a tight-binding model on a structure that belongs to layer group $Dg5$. In order to make the structure more realistic, we choose it to be isostructural with the sublattice of phosphorus ions in $SnPSe_3$, a material whose stability was confirmed by DFT calculations (Bergerhoff et al. 1983; Israel et al. 1998). The crystal structure and corresponding BZ is shown on Fig. 1. The lattice parameters are 6.996 and 12.006 Å, while the oblique angle is 124.6°. The Wyckoff position $2a$ is occupied twice, with nuclei having (fractional) coordinates (0.12600, 0.56620, 2.83 Å) and (0.87540, 0.43600, 1.17 Å). The positions of other nuclei are determined by symmetry (Kopsky and Litvin 2002). Although our system is isostructural with phosphorus sublattice of $SnPSe_3$, we do not assume that it is made from phosphorus atoms. We consider a tight-binding (LCAO MO) model from s-orbitals, in order to make the model simple. The internuclear distances and hopping integrals are given in the Table 1. The tight-binding Hamiltonian is ($*$ denotes complex conjugation):

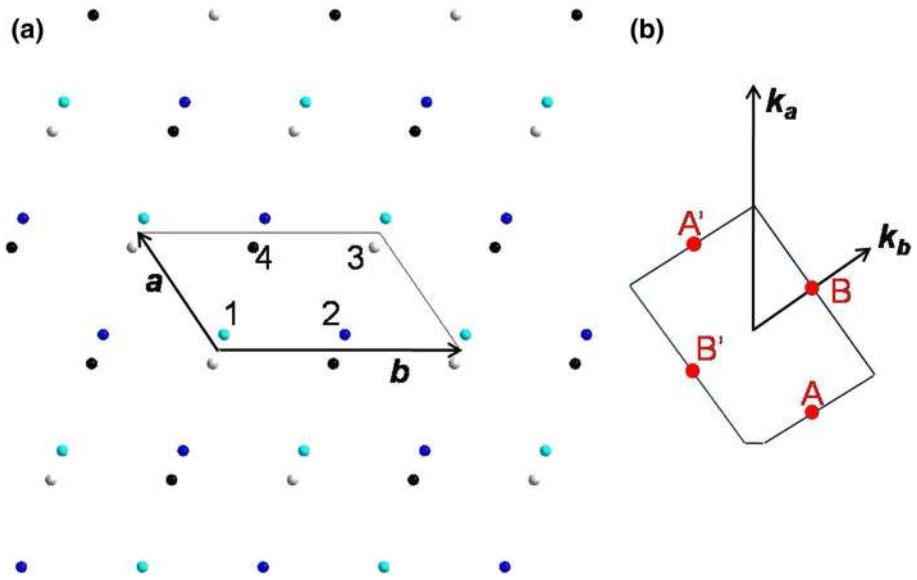

Fig. 1 **a** Crystal structure belonging to *Dg*5 for the tight-binding model. Black parallelogram denotes primitive unit cell. All nuclei are of the same type. Height of nuclei above the drawing plane is denoted by colors: blue + 2.83 Å, black + 1.17 Å, gray − 1.17 Å, turquoise − 2.83Å. **b** Corresponding Brillouin zone with basis vectors of the reciprocal lattice and positions of *A* and *B* points that host semi-Dirac dispersion. (Color figure online)

Table 1 Internuclear distances and corresponding hopping parameters for the structure from Fig. 1

Pair of nuclei	Internuclear distance (Å)	Hopping integral
$\mathbf{r}_1, \mathbf{r}_1$	0	γ_{11}
$\mathbf{r}_3, \mathbf{r}_3$	0	γ_{33}
$\mathbf{r}_1, \mathbf{r}_3 - \mathbf{b} - \mathbf{a}$	2.2677	γ_{13}
$\mathbf{r}_1, \mathbf{r}_4$	6.0619	γ_{14}
$\mathbf{r}_3, \mathbf{r}_4$	6.4446	γ_{34}
$\mathbf{r}_3, \mathbf{r}_4 + \mathbf{b}$	6.4446	γ_{34}
$\mathbf{r}_1, \mathbf{r}_3 - \mathbf{b}$	6.4794	γ'_{13}
$\mathbf{r}_3, \mathbf{r}_4 - \mathbf{a}$	6.5389	γ'_{34}
$\mathbf{r}_3, \mathbf{r}_4 + \mathbf{a} + \mathbf{b}$	6.5389	γ'_{34}
$\mathbf{r}_1, \mathbf{r}_4 - \mathbf{a}$	6.9012	γ'_{14}
$\mathbf{r}_1, \mathbf{r}_1 + \mathbf{a}$	6.9960	γ'_{11}
$\mathbf{r}_1, \mathbf{r}_1 - \mathbf{a}$	6.9960	γ'_{11}
$\mathbf{r}_3, \mathbf{r}_3 + \mathbf{a}$	6.9960	γ'_{33}
$\mathbf{r}_3, \mathbf{r}_3 - \mathbf{a}$	6.9960	γ'_{33}

Other distances (higher neighbors of $\mathbf{r}_1$ or $\mathbf{r}_3$) are bigger than 7.8 Å

$$\mathsf{H}(\mathbf{k}) = \begin{pmatrix} \gamma_{11} + 2\gamma'_{11}\cos(\mathbf{k}\cdot\mathbf{a}) & 0 & \gamma_{13}e^{-i\mathbf{k}\cdot(\mathbf{a}+\mathbf{b})} + \gamma'_{13}e^{-i\mathbf{k}\cdot\mathbf{b}} & \gamma_{14} + \gamma'_{14}e^{-i\mathbf{k}\cdot\mathbf{a}} \\ 0 & \gamma_{11} + 2\gamma'_{11}\cos(\mathbf{k}\cdot\mathbf{a}) & \gamma_{14} + \gamma'_{14}e^{-i\mathbf{k}\cdot\mathbf{a}} & \gamma'_{13} + \gamma_{13}e^{-i\mathbf{k}\cdot\mathbf{a}} \\ \gamma_{13}e^{i\mathbf{k}\cdot(\mathbf{a}+\mathbf{b})} + \gamma'_{13}e^{i\mathbf{k}\cdot\mathbf{b}} & \gamma_{14} + \gamma'_{14}e^{i\mathbf{k}\cdot\mathbf{a}} & \gamma_{33} + 2\gamma'_{33}\cos(\mathbf{k}\cdot\mathbf{a}) & h_{34} \\ \gamma_{14} + \gamma'_{14}e^{i\mathbf{k}\cdot\mathbf{a}} & \gamma'_{13} + \gamma_{13}e^{i\mathbf{k}\cdot\mathbf{a}} & h^*_{34} & \gamma_{33} + 2\gamma'_{33}\cos(\mathbf{k}\cdot\mathbf{a}) \end{pmatrix}, \quad (1)$$

$$h_{34} = \gamma_{34}\left(1 + e^{i\mathbf{k}\cdot\mathbf{b}}\right) + \gamma'_{34}\left(e^{-i\mathbf{k}\cdot\mathbf{a}} + e^{i\mathbf{k}\cdot(\mathbf{a}+\mathbf{b})}\right). \quad (2)$$

We are interested in the electronic band structure in the vicinity of points $\mathbf{k}_A = (-\mathbf{k_a} + \mathbf{k_b})/2$ and $\mathbf{k}_B = \mathbf{k_b}/2$. The band structure for certain ratios of hopping integrals is shown on Fig. 2. We can see in the vicinity of point (0, 0) the presence of dispersion which is Dirac-like along one direction in the BZ and quadratic along the perpendicular direction. In addition, we see that the band structure contains double spinless degenerate line (one line per each pair of bands) which is not caused by the TRS nor crystal symmetry.

To determine more precisely the exact type of dispersion in the vicinity of given BZ points, we calculate analytically the band structure, first by the perturbation theory of degenerate energy level and later exactly, by solving quartic equation. In order to simplify calculations we assume $\gamma'_{11} = \gamma'_{33} = \gamma'_{13} = \gamma'_{14} = \gamma'_{34} = 0$ and, although not required by symmetry, $\gamma_{11} = \gamma_{33} (= \gamma_1)$. The energies at both A and B points are $E_0 = \gamma_1 - \sqrt{\gamma_{13}^2 + \gamma_{14}^2}$ and $E'_0 = \gamma_1 + \sqrt{\gamma_{13}^2 + \gamma_{14}^2}$. Both E_0 and E'_0 are doubly degenerate. For the A-point we write $\mathsf{H}(\mathbf{k}_A + \mathbf{q}) = \mathsf{H}(\mathbf{k}_A) + \mathsf{H}'$ and apply first order perturbation theory of degenerate levels E_0

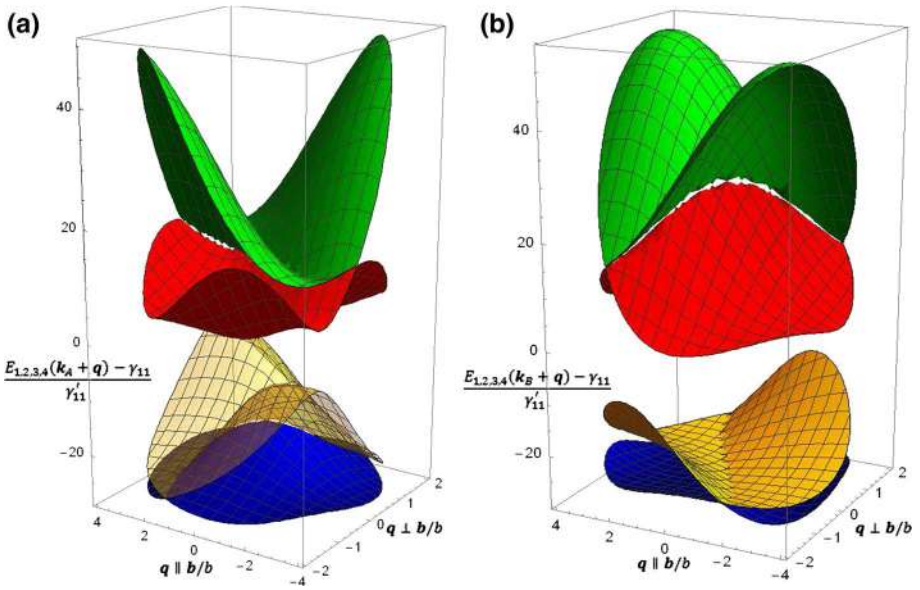

Fig. 2 The electronic band structure in the vicinity of A (**a**) and B (**b**) points of the BZ for $\gamma_{13}/\gamma'_{11} = 18$, $\gamma_{14}/\gamma'_{11} = 10.5$, $\gamma_{34}/\gamma'_{11} = 8$, $\gamma'_{13}/\gamma'_{11} = 6.5$, $\gamma'_{34}/\gamma'_{11} = 4.5$, $\gamma'_{14}/\gamma'_{11} = 2.5$, $\gamma'_{33}/\gamma'_{11} = 0.5$ and $(\gamma_{33} - \gamma_{11})/\gamma'_{11} = -0.5$. $\mathbf{q}$ is in units $1\ /\ b$ in the direction parallel to $\mathbf{b}/b$, and in units $1/(acos(34.6°))$ in the direction perpendicular to $\mathbf{b}/b$. Coordinates of the A point in panel a, i.e. B point in panel b, are (0, 0)

and E_0', with $\mathsf{H}' = \mathsf{H}(\mathbf{k}_A + \mathbf{q}) - \mathsf{H}(\mathbf{k}_A)$ being perturbation. We do the same for the B-point. The final result for the B-point is:

$$E_{1,2} \approx E_0' - \frac{1}{2}C_2 q_2'^2 \pm \frac{1}{2}\sqrt{u_2 q_1'^2 + v_2 q_2'^4}, \tag{3}$$

$$E_{3,4} \approx E_0 + \frac{1}{2}C_1 q_2^2 \pm \frac{1}{2}\sqrt{u_1 q_1^2 + v_1 q_2^4}, \tag{4}$$

while for the A-point we obtain:

$$E_{1,2} \approx E_0' - \frac{1}{2}C_1 q_2^2 \pm \frac{1}{2}\sqrt{u_1 q_1^2 + v_1 q_2^4}, \tag{5}$$

$$E_{3,4} \approx E_0 + \frac{1}{2}C_2 q_2'^2 \pm \frac{1}{2}\sqrt{u_2 q_1'^2 + v_2 q_2'^4}. \tag{6}$$

Here $\mathbf{q}$ is a vector of small modulus, q_1, q_2, q_1' and q_2' are the projections of $\mathbf{q}$ along vectors $\mathbf{e}_1$, $\mathbf{e}_2$, $\mathbf{e}_3$ and $\mathbf{e}_4$, respectively. In addition:

$$u_{1,2} = \left[2\frac{\gamma_{13}\gamma_{14}}{\sqrt{\gamma_{13}^2 + \gamma_{14}^2}}\mathbf{a} + \left(\frac{\gamma_{13}\gamma_{14}}{\sqrt{\gamma_{13}^2 + \gamma_{14}^2}} \mp \gamma_{34} \right)\mathbf{b} \right]^2, \tag{7}$$

$$v_{1,2} = 4\frac{(\mathbf{a}\times\mathbf{b})^4 \gamma_{13}^6 \gamma_{14}^2 \gamma_{34}^2}{u_{1,2}^2 (\gamma_{13}^2 + \gamma_{14}^2)^2}, \tag{8}$$

$$C_{1,2} = \frac{(\mathbf{a}\times\mathbf{b})^2 \gamma_{13}^2}{u_{1,2}\sqrt{\gamma_{13}^2 + \gamma_{14}^2}} \left(\frac{\gamma_{13}^2 \gamma_{14}^2}{\gamma_{13}^2 + \gamma_{14}^2} + \gamma_{34}^2 \right), \tag{9}$$

$$\mathbf{e}_1 = \frac{2}{\sqrt{u_1}} \frac{\gamma_{13}\gamma_{14}}{\sqrt{\gamma_{13}^2 + \gamma_{14}^2}}\mathbf{a} + \frac{1}{\sqrt{u_1}} \left(\frac{\gamma_{13}\gamma_{14}}{\sqrt{\gamma_{13}^2 + \gamma_{14}^2}} - \gamma_{34} \right)\mathbf{b}, \tag{10}$$

$$\mathbf{e}_3 = \frac{2}{\sqrt{u_2}} \frac{\gamma_{13}\gamma_{14}}{\sqrt{\gamma_{13}^2 + \gamma_{14}^2}}\mathbf{a} + \frac{1}{\sqrt{u_2}} \left(\frac{\gamma_{13}\gamma_{14}}{\sqrt{\gamma_{13}^2 + \gamma_{14}^2}} + \gamma_{34} \right)\mathbf{b}, \tag{11}$$

$$\mathbf{e}_{2,4} = \frac{\mathbf{e}_{1,3} \times (\mathbf{a}\times\mathbf{b})}{|\mathbf{a}\times\mathbf{b}|}. \tag{12}$$

Since u_1, u_2, v_1 and v_2 are all greater than zero, the obtained dispersion is of semi-Dirac type as predicted by Damljanović and Gajić (2017), but the accidental double degeneracy is missed.

Exact solution, based on solving quartic characteristic equation, gives the following condition for double degeneracy:

$$\left(\gamma_{13}^2+\gamma_{14}^2\right)\gamma_{34}^2 sin^2(\mathbf{q}\cdot\mathbf{b}/2)=\gamma_{13}^2\gamma_{14}^2 sin^2(\mathbf{a}\cdot\mathbf{q}+\mathbf{b}\cdot\mathbf{q}/2), \tag{13}$$

which has solution for sufficiently small $|\mathbf{q}|$, irrespectively of relations between γ_{13}, γ_{14} and γ_{34}. The Taylor expansion of the exact energy around $\mathbf{q}=0$ (B-point) gives $E_{1,2}\approx E_0'\pm(1/2)\sqrt{u_2}\left|q_1'\right|$, in the direction $\mathbf{e}_3$, and $E_{1,2}\approx E_0'\pm(1/2)w_2\left|q_2'\right|^3$, in the direction perpendicular to $\mathbf{e}_3$. Similarly, $E_{3,4}\approx E_0\pm(1/2)\sqrt{u_1}|q_1|$ in the direction $\mathbf{e}_1$ and $E_{3,4}\approx E_0\pm(1/2)w_1|q_2|^3$, in the direction perpendicular to $\mathbf{e}_1$. Here:

$$w_{1,2}=\frac{|\mathbf{a}\times\mathbf{b}|^3}{3u_{1,2}^{3/2}}\frac{\gamma_{13}\gamma_{14}\gamma_{34}}{\sqrt{\gamma_{13}^2+\gamma_{14}^2}}\left(\frac{\gamma_{13}^2\gamma_{14}^2}{\gamma_{13}^2+\gamma_{14}^2}-\gamma_{34}^2\right). \tag{14}$$

For the A-point we make substitution $\gamma_{13}\rightarrow-\gamma_{13}$ in the above formulas. It follows that the first order perturbation theory gives correct BZ-direction of Dirac-like dispersion and correct behavior of band structure in this direction. For the orthogonal direction as well as behavior of bands in complete vicinity of A, B-points the first order perturbation theory is not sufficient and higher order corrections are needed.

Regarding line of accidental spinless degeneracy found in exact solution of four-component Hamiltonian, one has to note that similar degeneracy occurs in the tight-binding example for layer group $Dg48$ of Damljanović and Gajić (2017). In this case the degeneracy is a consequence of the fact that model Hamiltonian is two-component and that third order polynomial has at least one real zero. By studding the compatibility relations of all four layer single groups found in Damljanović and Gajić (2017) in the vicinity of $\mathbf{k}_0$ we get that two-dimensional irrep decomposes into two nonequivalent, one-dimensional irreps: $\Gamma_{2D}(G(\mathbf{k}_0))=\Gamma_{1D}(G(\mathbf{k}_0+\mathbf{q}))+\Gamma_{1D}'(G(\mathbf{k}_0+\mathbf{q}))$, where $\mathbf{q}$ is small, jet non-zero wave vector. According to von Neumann–Wigner theorem, two bands touching at $\mathbf{k}_0$ do not repel each other at nearby points and may cross there too (Landau and Lifshitz 1981).

3 Conclusions

In summary, we have investigated electronic dispersion on a structure belonging to layer group $Dg5$, using tight-binding model from s-orbitals. We applied two methods for obtaining electronic dispersion: the first order perturbation theory of doubly degenerate level and exact diagonalization based on solving quartic equation. The first order perturbation method gives correct behavior in the Dirac-dispersion direction, while for other directions one needs higher order corrections. Accidental node line present in the exact method does not appear in the first order perturbation method. Further investigation should show if e.g. band topology cause these lines to always appear in four groups from Damljanović and Gajić (2017).

In addition, we have pointed out that in the literature there have already been reported numerically stable 3D structures, which consist of weakly interacting layers belonging to $Dg5$. Closer ab initio electronic band structure investigations of single layers of these structures, could give more insight into the particular types of semi-Dirac dispersion that are expected to appear.

Acknowledgements This work was supported by the Serbian Ministry of Education, Science and Technological Development under Project Nos. OI 171005 and III 45016.

References

Banerjee, S., Pickett, W.E.: Phenomenology of a semi-Dirac semi-Weyl semimetal. Phys. Rev. B **86**, 075124 (2012)

Banerjee, S., Singh, R.R.P., Pardo, V., Pickett, W.E.: Tight-binding modeling and low-energy behavior of the semi-Dirac point. Phys. Rev. Lett. **103**, 016402 (2009)

Bergerhoff, G., Hundt, R., Sievers, R., Brown, I.D.: The inorganic crystal structure data base. J. Chem. Inf. Comput. Sci. **23**, 66–69 (1983)

Cheon, G., Duerloo, K.-A.N., Sendek, A.D., Porter, C., Chen, Y., Reed, E.J.: Data mining for new two- and one-dimensional weakly bonded solids and lattice-commensurate heterostructures. Nano Lett. **17**, 1915–1923 (2017)

Damljanović, V., Gajić, R.: Existence of semi-Dirac cones and symmetry of two-dimensional materials. J. Phys. Condens. Matter **29**, 185503 (2017)

Deplace, P., Montambaux, G.: Semi-Dirac point in the Hofstadter spectrum. Phys. Rev. B **82**, 035438 (2010)

Dittmar, G., Schaefer, H.: Die Struktur des Di-Zinn-Hexathiohypodiphosphats $Sn_2P_2S_6$. Z. Naturforschung B **29**, 312–317 (1974)

Duan, H., Yang, M., Wang, R.: Electronic structure and optic absorption of phosphorene under strain. Phys. E **81**, 177–181 (2016)

El-Horr, N., Bagieu Beucher, M.: Structure d'un polyphosphate mixte de plomb et de lithium, $Pb_2Li(PO_3)_5$. Acta Crystallogr. C **42**, 647–651 (1986)

Geilhufe, R.M., Borysov, S.S., Bouhon, A., Balatsky, A.V.: Data mining for three-dimensional organic Dirac materials: focus on space group 19. Sci. Rep. **7**, 7298 (2017)

Hahn, T. (ed.): International Tables for Crystallography Volume A: Space-Group Symmetry. Springer, Dordreht (2005)

Hautier, G., Jain, A., Ong, S.P., Kang, B., Moore, C., Doe, R., Ceder, G.: Phosphates as lithium-ion battery cathodes: an evaluation based on high-throughput ab initio calculations. Chem. Mater. **23**, 3495–3508 (2011)

Huang, H., Liu, Z., Zhang, H., Duan, W., Vanderbilt, D.: Emergence of a Chern-insulating state from a semi-Dirac dispersion. Phys. Rev. B **92**, 161115 (2015)

Israel, R., de Gelder, R., Smits, J.M.M., Beurskens, P.T., Eijt, S.W.H., Rasing, T., van Kempen, H., Maior, M.M., Motrija, S.F.: Crystal structure of di-tin-hexa(seleno)hypodiphosphate, $Sn_2P_2Se_6$, in the ferroelectric and paraelectric phase. Z. Krist. Cryst. Mater. **213**, 34–41 (1998)

Jain, A., Hautier, G., Moore, C.J., Ong, S.P., Fischer, C.C., Mueller, T., Persson, K.A., Ceder, G.: A high-throughput infrastructure for density functional theory calculations. Comput. Mater. Sci. **50**, 2295–2310 (2011)

Kim, J., Baik, S.S., Ryu, S.H., Sohn, Y., Park, S., Park, B.-G., Denlinger, J., Yi, Y., Choi, H.J., Kim, K.S.: Observation of tunable band gap and anisotropic Dirac semimetal state in black phosphorus. Science **349**, 723–726 (2015)

Kopsky, V., Litvin, D.B. (eds.): International Tables for Crystallography Volume E: Subperiodic Groups. Kluwer, Dordreht (2002)

Landau, L.D., Lifshitz, L.M.: Quantum Mechanics: Non-Relativistic Theory. Butterworth-Heinemann, London (1981)

Mañes, J.L.: Existence of bulk chiral fermions and crystal symmetry. Phys. Rev. B **85**, 155118 (2012)

Mannhart, J., Schlom, D.G.: Oxide interfaces—an opportunity for electronics. Science **327**, 1607–1611 (2010)

Narayan, A.: Floquet dynamics in two-dimensional semi-Dirac semimetals and three-dimensional Dirac semimetals. Phys. Rev. B **91**, 205445 (2015)

Pardo, V., Pickett, W.E.: Half-metallic semi-Dirac-point generated by quantum confinement in TiO_2/VO_2 nanostructures. Phys. Rev. Lett. **102**, 166803 (2009)

Pardo, V., Pickett, W.E.: Metal–insulator transition through a semi-Dirac point in oxide nanostructures: VO_2 (001) layers confined within TiO_2. Phys. Rev. B **81**, 035111 (2010)

Saha, K.: Photoinduced Chern insulating states in semi-Dirac materials. Phys. Rev. B **94**, 081103 (2016)

Saha, K., Nandkishore, R., Parameswaran, S.A.: Valley-selective Landau–Zener oscillations in semi-Dirac p–n junctions. Phys. Rev. B **96**, 045424 (2017)

Staffel, T., Mayer, G.: Synthesis and crystal structures of $Cd(AlCl_4)_2$ and $Cd_2(AlCl_4)_2$. Z. Anorg. Allg. Chem. **548**, 45–54 (1987)

Wang, J.-R., Liu, G.-Z., Zhang, C.-J.: Excitonic pairing and insulating transition in two-dimensional semi-Dirac semimetals. Phys. Rev. B **95**, 075129 (2017)

Xian, L., Paz, A.P., Bianco, E., Ajayan, P.M., Rubio, A.: Square selenene and tellurene: novel group VI elemental 2D materials with nontrivial topological properties. 2D Mater. **4**, 041003 (2017)

Zhao, P.-L., Wang, J.-R., Wang, A.-M., Liu, G.-Z.: Interplay of Coulomb interaction and disorder in a two-dimensional semi-Dirac fermion system. Phys. Rev. B **94**, 195114 (2016)

Zhong, C., Chen, Y., Xie, Y., Sun, Y.-Y., Zhang, S.: Semi-Dirac semimetal in silicene oxide. Phys. Chem. Chem. Phys. **19**, 3820–3825 (2017)

Opt Quant Electron (2018) 50:195
https://doi.org/10.1007/s11082-018-1461-9

Bifurcation in reflection spectra of holographic diffraction grating recorded on dicromated pullulan

Svetlana Savić-Šević[1] · Dejan Pantelić[1] · Vladimir Damljanović[1] · Branislav Jelenković[1]

Received: 6 November 2017 / Accepted: 3 April 2018

Abstract Volume diffraction gratings were created holographically on a dichromated pullulan (polysaccharide doped with chromium). Specific and very rare multi-peak structure in the reflection spectra is observed. It was found that multiple peaks are consequence of non-ideal structure of volume diffraction grating. Theoretical analysis and numerical simulations confirm that the observed behavior arise from a slight randomness of grating parameters: refractive index, grating period, film thickness. The results of calculation are in agreement with experimental results.

Keywords Holographic diffraction grating · Reflection spectra · Bifurcation · Polysaccharide

1 Introduction

Reflection volume hologram gratings, fabricated using a single-beam method, usually have only one Bragg peak in the spectrum. Wang et al. (2006) noted the appearance of multiple peaks in the spectrum of volume diffraction grating recorded in dichromated gelatin, phenomenon that looks like bifurcation within the Bragg plateau. We also observed bifurcation phenomena in the reflection spectrum of diffraction gratings recorded in dichromated pullulan (DCP), which is a polysaccharide doped with chromium. Compared to dichromated gelatin, the DCP material is simpler to prepare and process, it is weakly sensitive to humidity, thus retaining high resolution and diffraction

This article is part of the Topical Collection on Focus on Optics and Bio-photonics, Photonica 2017.

Guest Edited by Jelena Radovanovic, Aleksandar Krmpot, Marina Lekic, Trevor Benson, Mauro Pereira, Marian Marciniak.

✉ Svetlana Savić-Šević
savic@ipb.ac.rs

[1] Institute of Physics, University of Belgrade, Pregrevica118, 11080 Zemun, Belgrade, Serbia

efficiency (Pantelic et al. 1998; Savic et al. 2002; Savic-Šević and Pantelic 2007). The typical number of peaks in the spectrum is between two and four. We have extended the research presented in (Wang et al. 2006) by taking into account that the grating parameters depend also on x, y coordinates.

In order to understand multi-peak structure of diffraction gratings, experimental results were compared with theory. The corresponding model investigates effects of several important parameters: absorption of radiation within the photosensitive layer, non-uniform thickness of layers, refractive index modulation and non-uniform spatial period of the grating. Reflection spectra of volume Bragg gratings were calculated using method of characteristic matrix (Born and Wolf 1980). Our model suggests that multi peak structures are produced by uneven modulation of Bragg layers inside the volume hologram. The results of calculation are in agreement with experimental results. Such behavior of reflection spectra is important for effect of broadening bandgaps of photonic crystals. Understanding mechanism of their formations and appearance can help us to establish standard procedure for fabrications of such spatially non uniform volume gratings.

2 Fabrication and optical characterization of volume holographic gratings

The results presented below were obtained by the following preparation procedure for DCP. Holographic photosensitive material was prepared by mixing 10% aqueous solution of pullulan (from Sigma–Aldrich) and 10% of the ammonium dichromate. DCP solution was stirred and warmed to 50 °C to achieve homogeneity. The solution was coated onto a thoroughly cleaned glass slides placed on the flat horizontal surface. Film was dried overnight under normal laboratory conditions. The thicknesses of the dried layers, was 14 μm.

The experimental setup is shown in Fig. 1. Periodic structures in a DCP were fabricated using a single-beam method schematically shown in Fig. 1a. Hologram recording was achieved by exposing DCP to a single longitudinal mode, diode pumped Nd-YAG laser (Verdi) at 532 nm. The laser beam was expanded and pullulan layer was exposed at normal incidence with 200 mW/cm^2 of optical power, for 120 s. After propagation through emulsion, the beam was reflected back from a mirror behind the holographic plate. The two counter-propagating beams interfere, creating a standing wave pattern within an emulsion.

Plates were chemically processed, after the exposure. Processing involves washing the plates in a mixture of water and isopropyl alcohol (3:1 ratio) for 120 s, and drying for 60 s in pure isopropyl alcohol. Periodic structure formed below the surface during the processing is revealed in cross-sectional view of the DCP grating, Fig. 2.

To measure reflection, and transmission spectra, of the DCP, light from the halogen lamp was collimated and directed onto the DCP plate using set-ups given in Fig. 1b, c, respectively. Spectra were measured using fiber type spectrometer (Ocean Optics).

The photonic structure obtained under usual experimental conditions looks uniform, as in Fig. 3a. However, magnified part of the same sample shows that the structure is not ideally uniform across the layer of the DCP, Fig. 3b. In Fig. 3c we show several transmission spectra of the same DCP grating. Spectra were measured using the microscope attached to the spectrometer, as schematically presented in Fig. 1c. Transmission spectra were measured at several positions and each spectrum corresponds to area which is approximately 50 μm in diameter, with 1 mm distance between two adjacent areas.

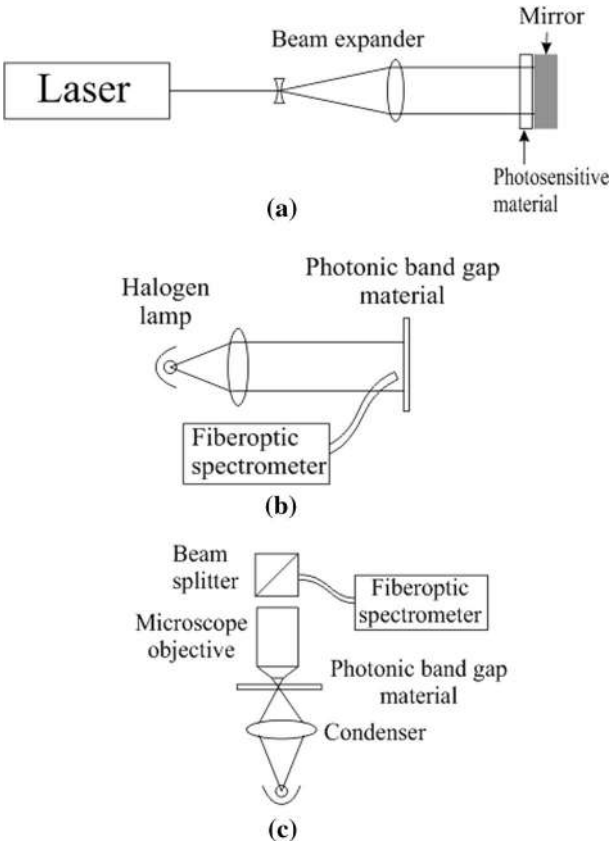

Fig. 1 Experimental setup for **a** generating holographic diffraction gratings in DCP; and for measuring reflection and transmission spectra **b** macroscopically; and **c** microscopically

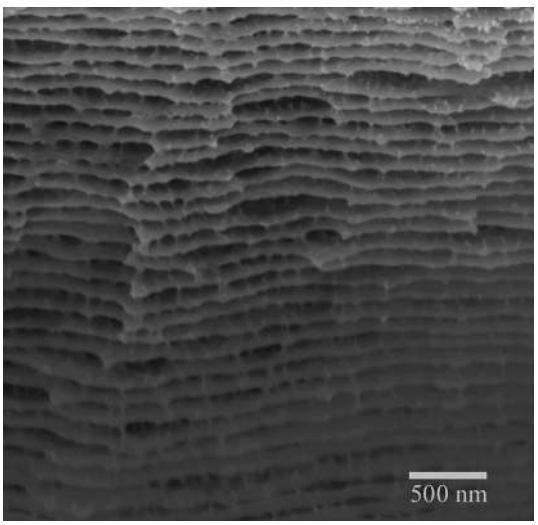

Fig. 2 SEM picture of the cross - section of DCP volume diffraction grating

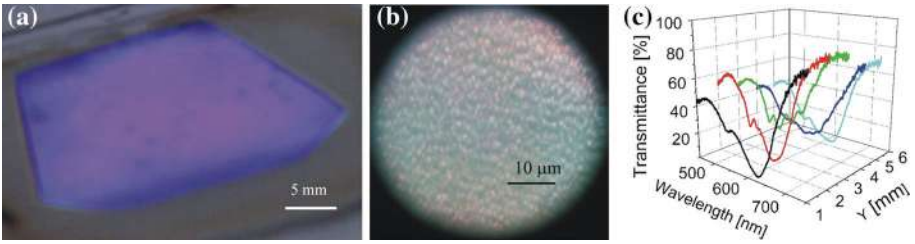

Fig. 3 **a** Image of the DCP sample, the scale bar is 5 mm; **b** zoomed part of the image **a** obtained using ×40 objectives, and microscopic set-up shown in Fig. 1c. The scale bar is 10 µm; **c** transmission spectra obtained from different areas (each of diameter of 50 µm) of the DCP sample, with 1 mm distance between two adjacent areas

3 Numerical simulations

We have calculated reflection spectra of a volume Bragg gratings by the method of characteristic matrix (Born and Wolf 1980). First, we approximated the refractive index variation along the direction perpendicular to the DCP surface, with a function whose mathematical expression is as follows (Wang et al. 2006, 2008; Liu and Zhou 1994):

$$n(z) = n_0 + \Delta n_1 \exp(-\alpha_g T) ch\left\{ \alpha_g \left[(N - j + 1)\Lambda - \frac{z}{M_j} \right] \right\} + \Delta n_2 \exp(-\alpha_g T) \cos\left(\frac{2\pi \times z}{\Lambda \times M_j} \right) \tag{1}$$

Graphical presentation of the function is given in Fig. 4. As can be seen from Eq. (1), z-dependence of the refractive index $n(z)$ incorporates three terms. The first one is the average refractive index of the material n_0, indicated by the dashed line in Fig. 4.

The second term describes the effects of attenuation of two counter-propagating beams leading to global variation of the refractive index Δn_1 (described by hyperbolic cosine). The last term describes a sinusoidal modulation (with amplitude Δn_2) of the index of refraction. Additional parameters are: α_g—absorption coefficient, T—the material thickness, Λ—grating period, N—the number of grating layers. We assume that the grating period is not constant, due to uneven expansion of the material during processing. Instead, each period of the grating (defined by parameter j; $1 \leq j \leq N$) is slightly changed, as defined by random variable M_j:

$$M_j = 1.262 - \frac{0.26}{N - 1} j + \frac{R_j}{45} \tag{2}$$

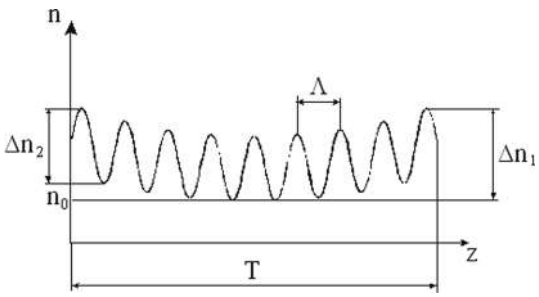

Fig. 4 Refractive index variation of a Bragg grating recorded in DCP, used in theoretical calculations

where R_j is a random number with Gaussian statistics, zero mean value and the standard deviation of 1.5. Variation of the layer thickness is small, however, consequences on optical properties are significant, leading to the band gap broadening.

With the above assumptions, the method of characteristic matrix produces rapidly oscillating spectra. This is different from experimentally recorded smooth spectra. Therefore, we had to modify the theoretical model. In previous research (Wang et al. 2006), it was assumed that grating parameters vary only along z-axis (i.e. depth of material). As we have found from microscope images (Fig. 3b, c) transmission or reflection spectra depend on the location on the material surface (x and y coordinates). This means that the grating parameters depend on x, y coordinates too. The resulting spectrum (as measured by any finite aperture optical device) is an average value of many spectra integrated along the aperture.

Therefore, we introduced an additional random factor $r_{k,j}$ into Eq. (2):

$$M_j \rightarrow M_j + \frac{r_{k,j}}{45} = 1.262 - \frac{0.26}{N-1} j + \frac{R_j}{45} + \frac{r_{k,j}}{45} \tag{3}$$

here $r_{k,j}$ is also Gaussian random number with mean value 0 and standard deviation of 1.5. The meaning of other parameters is the same as in Eq. (2).

First we use Eq. (2) to calculate spectrum by the characteristic matrix method. This calculation is repeated several times giving typically reflection spectra with 2, 3 and 4 peaks. The following values for parameters were used: n_0= 1.45, Λ = 184 nm, N = 78, $\Delta n_1 \exp(-\alpha_g T) = \Delta n_2 \exp(-\alpha_g T) = 0.08$, $T = 14$ μm, and $\alpha_g = 0.02(\mu m)^{-1}$ (measured value). Then we fixed R_j and generate arrays $r_{k,j}$ where k is from 1 to 15 and j from 1 to 78. These way k different spectra were calculated and the result is obtained by averaging individual spectra.

The results of the model given in (Wang et al. 2006) show that appearance of multi peak band gap can be due to uneven spatial modulation of interference pattern recorded inside the material. There are two reasons for uneven modulation, irregular swelling of material during processing, and attenuation of radiation inside the emulsion.

The results of our calculations are shown in Fig. 5. We can see that for different variations of layer thickness after processing, different number of peaks appear. Since differences in the variations in the layer thickness are exclusively due to presence of random parameter with Gaussian distribution, we can assign appearance of peaks to this parameter, which is in agreement with (Wang et al. 2006).

Results presented in the upper row in Fig. 5, calculated assuming that thickness of layers varies (middle row) according to Eq. (2), contain noise-like, rapidly oscillating part. The bottom row in Fig. 5 presents resulting spectra obtained by lateral averaging defined by Eq. (3). Averaging over spectrums from several neighboring points eliminates rapidly oscillating part. In the bottom row of Fig. 5 we compare reflection spectra obtained experimentally using set-up shown in Fig. 1b (black dotted curves) and by numerical simulation (red solid curves). The results of calculation are in agreement with experimental results.

4 Discussion of fabrication of structured band gaps in DCP

Structured reflection spectra under the usual chemical processing are very rare [0.5% probability (Wang et al. 2006)]. In order to investigate how special techniques in processing volume holograms lead to more frequent appearance of structured reflection spectra, we prepared 250 samples of DCP photonic crystals with different concentration of ammonium

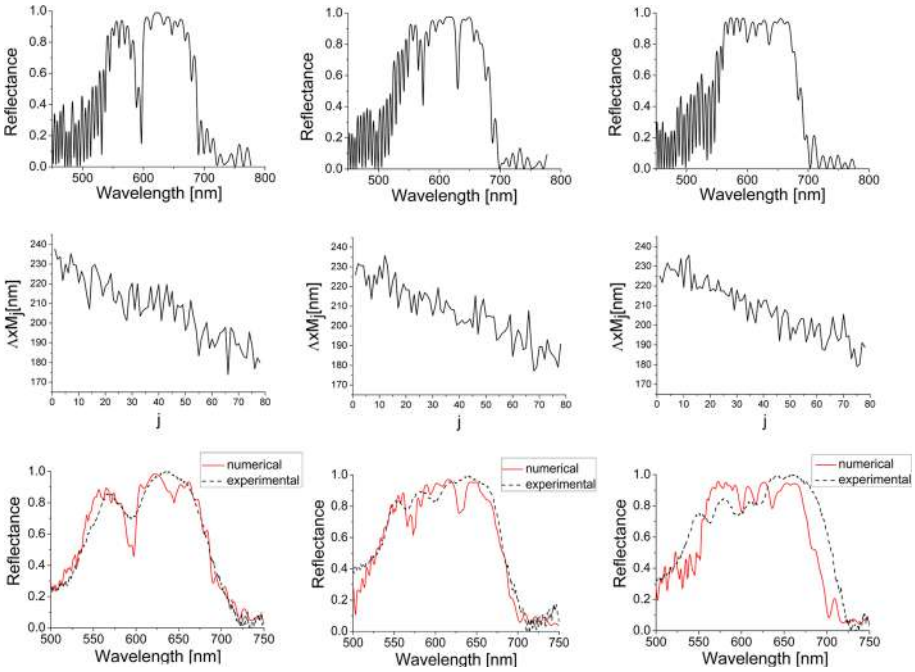

Fig. 5 Calculated reflection spectra of photonic structures in DCP showing multiple peaks as result of the layer thickness variation (upper row). Layer thickness variation (middle row). Averaged results taking into account the different thickness variation of layers in adjacent lateral regions of the film (red solid curve) and reflection spectra obtained experimentally (black dotted curve) using set-up shown in Fig. 1b (bottom row). (Color figure online)

dichromate (from 10 to 50% by weight of pullulan), different thickness of DCP (6–30 μm) and use various chemical processing. Samples were developed in mixture of water and isopropyl alcohol. We noticed that probability of obtaining multi peak and wider band gap photonic crystals is higher (although by only a few percent), by increasing the water to isopropyl ratio. If water to isopropyl ratio is 3:1 or more, analysis of our samples shows that probability of obtaining two peak photonic crystals is about 10 and 1.5% for three or more peaks.

5 Conclusions

In this paper we investigated bifurcation in the reflection spectra of the holographic DCP gratings. Volume holograms in DCP were made using simple, single-beam holographic technique. Although these types of diffraction spectra of volume hologram are usually rare, there are exact ways to increase the frequency of appearance of multi peak structure by using certain techniques in processing of DCP, as described in Sect. 2. Our simulation model suggests that multi peak structures are produced by uneven modulation of interference pattern inside the volume hologram. In addition, smoothness of reflectivity function is due to the difference in layer thickness in neighboring regions of the grating.

Acknowledgements This work was funded by the Ministry of Education, Science and Technological Development of the Republic of Serbia, under Grants Number OI 171038 and III 45016.

References

Born, M., Wolf, E.: Priciples of Optics. Pergamon, New York (1980)
Liu, D., Zhou, J.: Nonlinear analysis for a reflection hologram. Opt. Commun. **107**, 471–479 (1994)
Pantelić, D., Savić, S., Jakovljević, D.: Dichromated pullulan as a novel photosensitive holographic material. Opt. Lett. **23**, 807–809 (1998)
Savić, S., Pantelić, D., Jakovljević, D.: Real-time and postprocessing holographic effects in dichromated pullulan. Appl. Opt. **41**, 4484–4488 (2002)
Savić-Šević, S., Pantelić, D.: Dichromated pullulan diffraction gratings: influence of environmental conditions and storage time on their properties. Appl. Opt. **46**, 287–291 (2007)
Wang, Z., Liu, D., Zhou, J.: Investigation of a peculiar bifurcation phenomenon in diffraction spectra of volume holograms. Opt. Lett. **31**, 3270–3272 (2006)
Wang, Z., Zhai, T., Zhao, R., Liu, D.: The influence of asymmetric expansion properties and random fluctuation on the bandwidth of a hologram. J. Opt. A Pure Appl. Opt. **10**, 085205 (2008)

condensed matter

MDPI

Article

Ab Initio Study of the Electronic, Vibrational, and Mechanical Properties of the Magnesium Diboride Monolayer

Jelena Pešić [1,*], Igor Popov [1,2], Andrijana Šolajić [1], Vladimir Damljanović [1], Kurt Hingerl [3], Milivoj Belić [4] and Radoš Gajić [1]

1 Laboratory for graphene, other 2D materials and ordered nanostructures, Center for Solid State Physics and New Materials, Institute of Physics Belgrade, University of Belgrade, 11080 Belgrade, Serbia; popov@ipb.ac.rs (I.P.); solajic@ipb.ac.rs (A.Š.); damlja@ipb.ac.rs (V.D.); rgajic@ipb.ac.rs (R.G.)
2 Institute for Multidisciplinary Research, University of Belgrade, Kneza Višeslava 1, 11030 Belgrade, Serbia
3 Center for Surface and Nanoanalytics, Johannes Kepler University, 4040 Linz, Austria; Kurt.Hingerl@jku.at
4 Science Program, Texas A&M University at Qatar, P.O. Box 23874, Doha, Qatar; milivoj.belic@qatar.tamu.edu
* Correspondence: yelena@ipb.ac.rs

Received: 15 March 2019; Accepted: 1 April 2019; Published: 2 April 2019

Abstract: Magnesium diboride gained significant interest in the materials science community after the discovery of its superconductivity, with an unusually high critical temperature of 39 K. Many aspects of the electronic properties and superconductivity of bulk MgB_2 and thin sheets of MgB_2 have been determined; however, a single layer of MgB_2 has not yet been fully theoretically investigated. Here, we present a detailed study of the structural, electronic, vibrational, and elastic properties of monolayer MgB_2, based on ab initio methods. First-principles calculations reveal the importance of reduction of dimensionality on the properties of MgB_2 and thoroughly describe the properties of this novel 2D material. The presence of a negative Poisson ratio, higher density of states at the Fermi level, and a good dynamic stability under strain make the MgB_2 monolayer a prominent material, both for fundamental research and application studies.

Keywords: magnesium diboride; 2D materials; density functional theory

PACS: 71.15.Mb; 74.70.Ad

1. INTRODUCTION

Magnesium diboride was first synthesized and had its structure confirmed in 1953 [1]. An interest in its properties has grown ever since 2001, when it was discovered that MgB_2 exhibits the highest superconducting transition temperature T_c of all metallic superconductors. It is an inter-metallic s-wave compound superconductor with a quasi-two dimensional character [2] and a critical temperature of superconductive transition at T_c = 39 K. The experimental confirmation of the isotope effect [3] in MgB_2 indicated that it is a phonon-mediated BCS superconductor. A better definition would describe MgB_2 as self-doped semimetal with a crucial σ-bonding band that is nearly filled [4]. The basic aspects of the electronic structure and pairing is in a rather strong coupling of high frequency boron–boron stretch modes to the bonding electronic boron–boron states at the Fermi surface. The phonon-mediated mechanism with different coupling strengths between a particular phonon mode and selected electronic bands, boron σ- and π-bands [5–13], results in the presence of two superconducting gaps at the Fermi level. MgB_2 has already been fabricated in bulk, as single crystals, and as a thin film, and shows potential for practical applications.

The discovery of graphene in 2004 [14] sparked an interest in 2D materials and their properties. A variety of new properties, which distinguished graphene from graphite [14–22], inspired a search for other low-dimensional limits of layered materials and possibilities they offered. Interest in a low-dimensional limit of MgB_2 has arisen in past years, showing that it is superconductive even in a monolayer [23,24].

MgB_2 has a distinct layer structure, where boron atoms form a honeycomb layer and magnesium atoms are located above the center of the hexagons, between every boron plane. The boron layers alternate with a triangular lattice of magnesium layers. There is a noticeable structural similarity of MgB_2 to graphite-intercalated compounds (GICs), some of which also exhibit superconductivity [25–29]. Both monolayer and two-layer graphene, decorated/intercalated with atoms of alkali and alkaline earth metals, exhibit superconductivity and have been thoroughly studied using ab initio methods and isotropic and anisotropic Eliashberg theory [30–32].

Furthermore, a similarity in the electronic structure between GICs and MgB_2 exists. The peculiar and unique property of MgB_2 is a consequence of the incomplete filling of two σ bands corresponding to strongly covalent sp^2-hybrid bonding within the graphite-like boron layers [33].

Here, we present a comprehensive study of the electronic, vibrational, and mechanical properties of MgB_2 using ab initio methods, in order to provide its detail description.

2. Computational Details

MgB_2 has a hexagonal unit cell and consists of graphite-like B_2 layers stacked with the Mg atoms in between, as shown in Figure 1. The first-principles calculations were performed within the density functional theory (DFT) formalism, using a general gradient approximation (GGA) to calculate the electronic structure. For all electronic and phonon structure, the Quantum Espresso software package [34] was used with ultra-soft pseudopotentials and a plane-wave cutoff energy of 30 Ry. All calculated structures are relaxed to their minimum energy configuration, following the internal force on atoms and stress tensor of the unit cell. We used the Monkhorst-Pack $48 \times 48 \times 48$ and $40 \times 40 \times 1$ k-meshes, for the calculations of the electronic structure of the MgB_2 bulk and MgB_2 monolayer, respectively. The phonon frequencies are calculated using Density Functional Perturbation Theory (DPFT) on the $12 \times 12 \times 12$ and $20 \times 20 \times 1$ phonon wave vector mesh for the bulk and monolayer structures, respectively. In two-dimensional systems, the van der Waals (vdW) interaction was found to play an important role on the electronic structure [35]; however, as this is study on monolayer MgB_2, we do not treat vdW interactions, especially since, in this case, the effects are minor and including them would add additional computational costs but would not yield more accurate results.

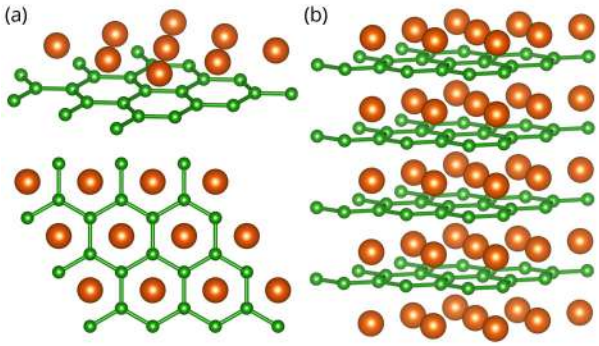

Figure 1. Crystal structure of the MgB_2 monolayer (**a**) and bulk MgB_2 (**b**), with a hexagonal unit cell. Green (orange) spheres represent Boron (Magnesium) atoms. Color online.

The crystal structure of MgB_2 and the MgB_2 monolayer are presented in Figure 1. The lattice parameters for the bulk MgB_2 are in agreement with the experimental results, $a = 3.083$ Å and $c/a = 1.142$ [9]. In order to avoid an interlayer interaction due to the periodicity and to simulate a 2D

material, an artificial vacuum layer was set to be 25 Å. When the monolayer is modelled, the structure is geometrically optimized, allowing the atoms to reach a minimum potential energy state. The bond length between neighbouring atoms remained to be 1.78 Å, but the distance from the boron layer to the Mg atoms changed from $h = 1.76$ Å to $h = 1.60$ Å.

For the molecular dynamics (MD) study, the Siesta code was utilized [36]. The super-cell is built by repeating the unit cell three times in both in-plane directions, whereas the lattice vector in the perpendicular direction is 15 Å, providing a large enough vacuum space between the 2D material and its periodic replica in order to avoid their mutual interaction. The lattice parameters and the geometry of the unit cell are initially optimized using the conjugate gradient method. The Perdew-Burke-Ernzerhof form of the exchange-correlation functional [37], the double-zeta polarized basis set, and the Troulier-Martins pseudopotentials [38] were used in all MD calculations.

The second-order elastic constants were calculated using the ElaStic software package [39]. First, the direction is projected from the strain tensor and total energies for each deformation are calculated. Elastic constants are then calculated using the second derivatives of the energy curves, dependent on the parameter η. In our calculations, the maximum positive and negative amplitudes of 5% Lagrangian strain were applied, with a step of 0.1%.

For the 2D square, rectangular, or hexagonal lattices, the non-zero second-order elastic constants, in Voigt notation, are c_{11}, c_{22}, c_{12}, and c_{66}. Due to symmetry, in hexagonal structures $c_{11} = c_{22}$ and $c_{66} = \frac{1}{2}(c_{11} - c_{12})$; so, we have 2 independent elastic constants. The layer modulus, which represents the resistance of a 2D material to stretching, is given as

$$\gamma = \frac{1}{4}(c_{11} + c_{22} + 2c_{12}).$$

The 2D Young modulus Y for strains in the (10) and (01) directions, Poisson's ratio ν and the shear modulus G are obtained from the following relations,

$$Y = \frac{c_{11}^2 - c_{12}^2}{c_{11}}, \ \nu = \frac{c_{12}}{c_{22}}, \ G = c_{66}.$$

Units for elastic constants and those parameters are N/m.

3. Results and Discussion

In order to determine the stability of a single layer of MgB_2, we perform MD simulations based on DFT and the super-cell approach. Besides the system with optimized (pristine) lattice parameters, we also consider a biaxially stretched system (up to 3% of tensile strain) and biaxially compressed system (up to 5% of compressive strain). The MD simulations are conducted in the range of temperatures between 50–300 K, with a step of 50 K, using the Nosé–Hoover thermostat [40].

Figure 2a shows the average distance between Mg and B atomic layers, as evolved over a time of 1 ps. Throughout the simulation time, there is no further evolution of the z-coordinate and the Mg atom shows only oscillatory movement around the equilibrium positions (as is shown in Figure 2) Importantly, the separation indicates that the Mg atoms do not leave the surface of the MgB_2 crystal. The plane in which the Mg atoms reside shifts away from the plane of the B atoms on average by 0.09 Å in a compressed crystal, while the distance between the planes decreases on average by 0.42 Å in the stretched system. This (relatively larger) shift in the latter case can be understood by analysing the details of the MgB_2 atomic structure. When the crystal is biaxially stretched, its Mg–B bond lengths increase, which is partially compensated by the nesting of the Mg atoms in the hollow sites closer to the B sublattice. Despite these atomic shifts, the MD simulations show the structural stability of the system. The stability from the MD simulations can be further quantitatively derived from the global Lindemann index, the dependence of which on temperature is shown in Figure 2b. It is calculated

for the pristine crystal, with a compressive strain of 5% and a tensile strain of 3%, from the local Lindemann indices, given by the formula

$$q_i = \frac{1}{N-1} \sum_{j \neq i} \frac{\sqrt{\langle r_{ij}^2 \rangle - \langle r_{ij} \rangle^2}}{\langle r_{ij} \rangle},$$

by averaging over all atoms. Here q_i is the local Lindemann index of atom i, N is number of atoms, r_{ij} is a separation between atoms i and j, and the angle brackets denote averaging over time (i.e., MD steps) [41]. The linear behaviour of the Lindemann indices indicate that systems are stable, at least up to room temperature.

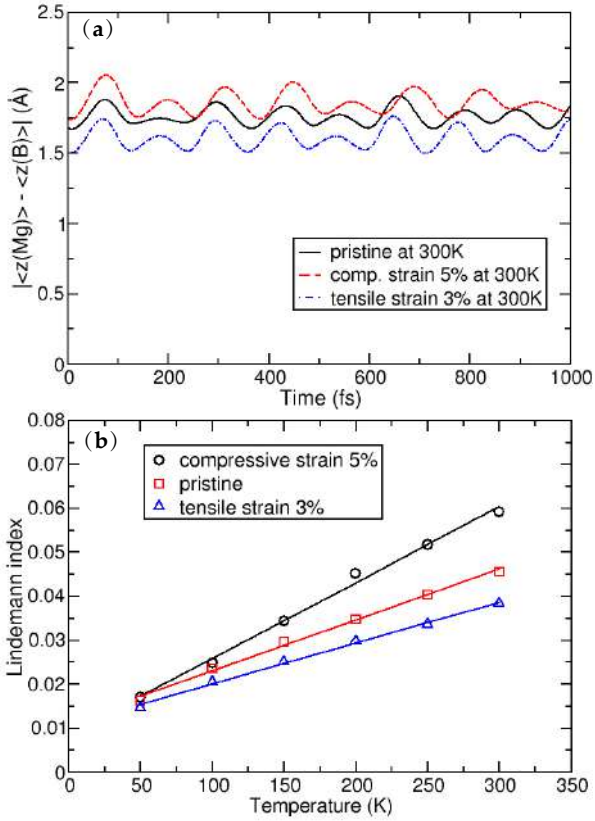

Figure 2. (**a**): Average distance between the Mg and B atomic layers; and (**b**): the dependence of the global Lindemann index as a function of temperature.

The calculated second-order elastic constants and other structural parameters for monolayer MgB_2 are given in Table 1. All elastic constants related to the bulk material (those that have 3, 4, or 5 in their subscripts), are calculated close to zero, as is expected for the monolayer. Compared to similar 2D materials, the layer modulus of MgB_2 of 30.18 N/m is relatively small (in the range of Silicene and Germanene), roughly five times smaller than that of graphene or h–BN, for example [42,43]. Similar results are obtained for the Young modulus. Compared to borophene (two-dimensional boron sheets with rectangular structures) [44], which is a hard and brittle 2D material that exhibits an extremely large Young's modulus of 398 N/m along the a direction [45], the MgB_2 monolayer has a significantly smaller value of 63.29 N/m. The most interesting observation in the elastic properties of the MgB2 monolayer is that the c_{12} constant is negative, which gives a negative Poisson ratio in the a and b directions, too—although, with a very small negative value of -0.05. However, compared to 2D borophene, which has an out-of-plane negative Poisson's ratio (that effectively holds the strong boron bonds lying along the a direction and makes the boron sheet show superior mechanical flexibility

along the b direction [46]), we obtain similar values [45]. For comparison, graphene has a Young modulus of 352.2 N/m and a Poisson ratio of 0.185 [42]. After confirming its stability and determining the elastic properties of the MgB_2 monolayer, we study its electronic properties. In Figure 3, the electronic structures of bulk MgB_2 and the MgB_2 monolayer are presented. The band structures for the bulk along the high-symmetry points Γ-K-M-Γ-A-L, and for the monolayer along Γ-K-M-Γ were calculated. The Fermi level is set to zero. The band structure of the bulk is in full agreement with previous studies [10,47–49]. The two bands crossing the Fermi level play a crucial role in the electronic properties of MgB_2. The density of the states around E_f are predominantly related to the B atoms and their p-orbitals, whereas the Mg atom contribution is negligible in this region. Previous studies described Mg as fully ionized and showed that the electrons donated to the system are not localized on the anion but, rather, are distributed over the whole crystal [6]. A similarity to graphite can be observed, with three σ bands, corresponding to the in-plane sp_xp_y (sp^2) hybridization in the boron layer and two π-bands of boron p_z orbitals [33]. Boron $p_{x(y)}$ and p_z orbitals contribute as σ and π states. Analysing projected DOS, one concludes that the σ states are considerably involved in the total density of states at the Fermi level, while the π states have only a partial contribution. It is worth emphasizing that the bulk bands of this material at the K-point above the Fermi level present a formation similar to the Dirac cones in graphene.

In the monolayer, there is an increase in the total density of states at the Fermi level from $N(E_f)_{bulk}$ = 0.72 states/eV to $N(E_f)_{mono}$ = 0.97 states/eV. In the same manner as in the bulk, the monolayer Mg atoms negligibly contribute to the density of states at the Fermi level, and the main contribution comes from the B p-orbitals. The characteristic Dirac cone-like structure is still present and closer to the Fermi level. Dg77, as the symmetry group of the MgB_2 monolayer, hosts a Dirac-like dispersion in the vicinity of the K-point in the hexagonal Brillouin zone, if the orbital wave functions belong to the 2D representation E of the C_{3v} point group of the wave vector [50,51]. In the tight-binding case, the p_x and p_y orbitals of two boron ions give rise to one E-representation (and to two one-dimensional representations), while the s-orbitals form a basis for one E-representation and p_z-orbitals form a basis for one E-representation as well. This explains the presence of the Dirac cones at the K-point in the band structure of the MgB_2 monolayer (as shown in Figure 3b).

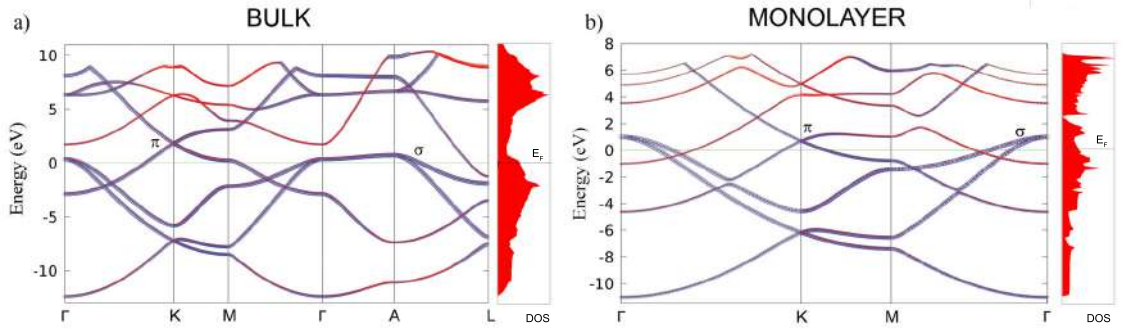

Figure 3. The electronic band structure and total density of states in bulk MgB_2 (**a**) and the MgB_2 monolayer (**b**). The blue and red colors represent the B and Mg atoms contributions to the electronic dispersion, respectively.

Table 1. The calculated elastic stiffness constants, layer modulus γ, Young's modulus Y, Poisson's ratio ν, and shear modulus G for the MgB_2 monolayer. All parameters are in units of N/m.

c_{11}	c_{12}	c_{66}	γ	Y	ν	G
63.4	−3.1	33.3	30.18	63.29	−0.05	33.3

Figure 4 shows the phonon dispersions for both the bulk and monolayer. For the bulk (in Figure 4a), there are four optical modes at the Γ point. Due to the light atomic mass of the B

atoms and the strong B–B coupling, the two high-frequency modes almost have a pure boron character. The in-plane stretching mode E_{2g} and the out-of-plane mode (where the atoms move in opposite directions B_{1g}) are the boron atom modes. E_{2g} is a doubly-degenerate Raman active mode and experimental studies [6,9] showed that this mode is very sensitive to structural changes and it has a strong electron-phonon coupling. The low-frequency modes (A_{2u}) and double degenerate (E_{1u}) are infrared active and they do not involve changes on in-plane bonds. In Figure 4b, the phonon dispersion of the MgB_2 monolayer is presented. In the phonon spectrum there are no imaginary frequencies, which confirms, once again, the dynamical stability of the system (also demonstrated earlier by the MD calculations).

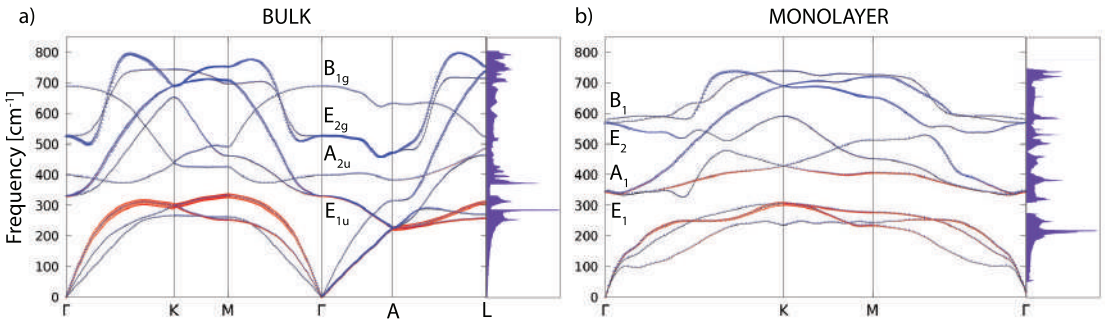

Figure 4. The phonon dispersion and the phonon density of states for the MgB_2 bulk (**a**) and monolayer (**b**). The blue and red colours represent the B and Mg atom contributions in the phonon dispersion, respectively.

At the Γ point, there are three acoustic and six optical modes (from which two pairs are doubly degenerate). The optical modes A_1, B_1, E_1, and E_2 are related to the optical modes of the parent material. Two significant differences between the bulk and monolayer spectrum can be observed: The E_1 and A_1 mode become energy degenerate in the monolayer, resulting in either a slight softening (hardening) of the modes which leads to nearly equal frequencies, which opens a gap in the phonon density of states (DOS) between the acoustic and optical modes. A more significant effect concerns the softening of the B_1 mode and hardening of the E_2 mode. As in the bulk E_{2g} mode, the monolayer E_2 mode is strongly coupled to electrons, causing the superconductivity in the monolayer in a similar fashion as in the bulk. In Figure 5, the vibrational frequencies and normal coordinates for the MgB_2 monolayer are presented. The symmetry group is C_{6v}, and the acoustic modes are A_1 and E_1. The optical modes at the Γ point are A_1, B_1, E_1, and E_2, where the infrared-active ones are A_1 and E_1. The Raman-active modes are A_1, E_1, and E_2, and B_1 is silent. In Table 2, the Raman tensor for the MgB_2 monolayer is presented [52]. Similar to graphene, the phonon eigenvectors and the normal coordinates at the Γ-point are determined by symmetry rules and, therefore, are a model independent.

Table 2. Raman tensor of the MgB_2 monolayer.

	Raman Tensors				
MgB_2-mono $Dg77 = TC_{6v}$ $O_z \,\|\|\, C_6$ $O_x \,\|\|\, \sigma_v$	A_1 $\begin{pmatrix} a & 0 & 0 \\ 0 & a & 0 \\ 0 & 0 & b \end{pmatrix}$	E_1 $\begin{pmatrix} 0 & 0 & c \\ 0 & 0 & 0 \\ c & 0 & 0 \end{pmatrix}$	$\begin{pmatrix} 0 & 0 & 0 \\ 0 & 0 & c \\ 0 & c & 0 \end{pmatrix}$	E_2 $\begin{pmatrix} d & 0 & 0 \\ 0 & -d & 0 \\ 0 & 0 & 0 \end{pmatrix}$	$\begin{pmatrix} 0 & -d & 0 \\ -d & 0 & 0 \\ 0 & 0 & 0 \end{pmatrix}$

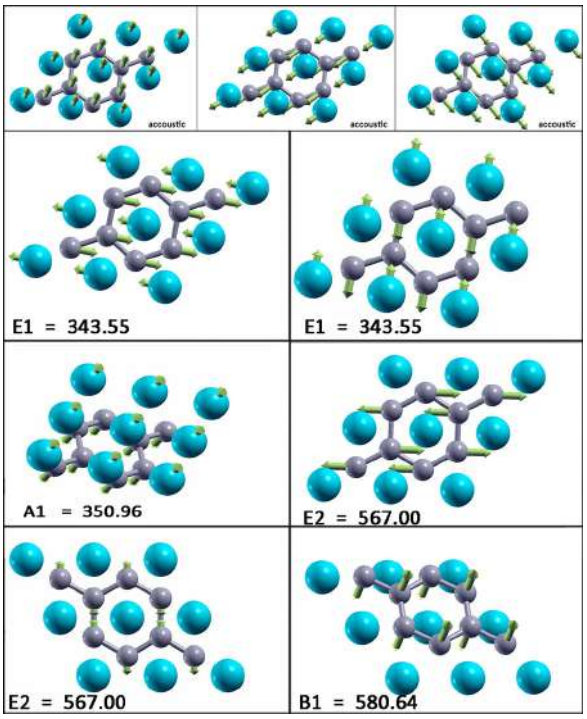

Figure 5. Vibrational frequencies (in wavenumbers) and the vibration normal coordinates at Γ for the MgB_2 monolayer.

4. Conclusions

The electronic band structure, density of states, phonon dispersion, and elastic constants have been calculated for the MgB_2 monolayer and compared to the bulk material, using first-principles calculations within the DFT framework. We demonstrated an increase of electronic density of states at the Fermi level in the monolayer (compared to the bulk) and determined its stability under various strains. These two features are crucial for the enhancement of electron–phonon coupling and they enable significant mechanical modification that increases the critical superconducting temperature. Establishing stability and offering insight into this novel 2D material, we focus on the effects of ultimate lowering of the dimensionality. The question of reduction of dimensionality to its limit, a truly atomic-scale 2D system, and the consequences of this [53–61] are highly relevant, not only to fundamental science but also to applications in nanotechnology.

Author Contributions: Conceptualization, J.P. and R.G.; Validation, K.H., M.B., R.G.; Investigation, J.P., I.P., A.Š. and V.D.; Writing—Original Draft Preparation, J.P., I.P., A.Š. and V.D.; Writing—Review & Editing, J.P.; Supervision, R.G.; Funding Acquisition, K.H., M.B. and R.G.

Funding: This research is supported by Serbian Ministry of Education, Science and Technological Development under projects OI 171005, III 45018, and III 45016 and by the Qatar National Research Fund, cycle 11, under grant number NPRP 11S-1126-170033. K. H. acknowledges the support of the European Commission under the H2020 grant TWINFUSYON.GA692034.

Acknowledgments: The DFT calculations were performed using the computational resources at Johannes Kepler University, Linz, Austria. This work was supported by the Serbian Ministry of Education, Science and Technological Development under projects OI 171005, III 45018, and III 45016.

Conflicts of Interest: The authors declare no conflict of interest.

References

1. Jones, M.E.; Marsh R.E. The preparation and structure of magnesium boride, MgB_2. *J. Am. Chem. Soc.* **1953**, *76*, 5.
2. Nagamatsu, J.; Nakagawa, N.; Muranaka, T.; Zenitani, Y.; Akimitsu, J. Superconductivity at 39 K in magnesium diboride. *Nature* **2001**, *410*, 63.
3. Bud'ko, S.L.; Lapertot, G.; Petrovic, C.; Cunningham, C.E.; Anderson, N.; Canfield, P.C. Boron Isotope Effect in Superconducting MgB_2. *Phys. Rev. Lett.* **2001**, *86*, 1877.
4. Pickett, W. Superconductivity: 2D Physics, Unknown Mechanisms, Current Puzzles. *Emerg. Phenom. Correl. Matter Lect. Notes Autumn School Corr. Electron.* **2013**, *2013*, 45.
5. Choi, H.J.; Roundy, D.; Sun, H.; Cohen, M.L.; Steven Louie, G. The origin of the anomalous superconducting properties of MgB_2. *Nature* **2002**, *418*, 758.
6. Kortus, J.; Mazin, I.I.; Belaachenko, K.D.; Antropov, V.P.; Boyer, L.L. Superconductivity of Metallic Boron in MgB_2. *Phys. Rev. Lett.* **2001**, *86*, 4656.
7. An, J.M.; Pickett, W.E. Superconductivity of MgB_2: Covalent Bonds Driven Metallic. *Phys. Rev. Lett.* **2001**, *86*, 4366.
8. Liu, A.Y.; Mazin, I.I.; Kortus, J. Beyond Eliashberg Superconductivity in MgB_2: Anharmonicity, Two-Phonon Scattering, and Multiple Gaps. *Phys. Rev. Lett.* **2001**, *87*, 087005.
9. Kong, Y.; Dolgov, O.V.; Jepsen, O.; Andersen, O.K. Electron-phonon interaction in the normal and superconducting states of MgB_2. *Phys. Rev. B* **2001**, *64*, 020501.
10. Bohnen, K.-P.; Heid, R.; Renker, B. Phonon Dispersion and Electron-Phonon Coupling in MgB_2 and AlB_2. *Phys. Rev. Lett.* **2001**, *86*, 5771.
11. Kunc, K.; Loa, I.; Syassen, K.; Kremer, R.K.; Ahn, K. MgB_2 under pressure: phonon calculations, Raman spectroscopy, and optical reflectance. *J. Phys. Condens. Matter* **2001**, *13* , 9945.
12. Choi, H.J.; Roundy, D.; Sun, H.; Cohen, M.L.; Louie, S.G. First-principles calculation of the superconducting transition in MgB2 within the anisotropic Eliashberg formalism. *Phys. Rev. B* **2002**, *66*, 020513.
13. Canfield, P.C.; Crabtree, G.W. Magnesium Diboride: Better Late than Never. *Phys. Today* **2003**, *56*, 34.
14. Novoselov, K.S.; Geim, A.K.; Morozov, S.V.; Jiang, D.; Zhang, Y.; Dubonos, S.V.; Grigorieva, I.V.; Firsov, A.A. Electric Field Effect in Atomically Thin Carbon Films. *Science* **2004**, *306*, 666–669.
15. Katsnelson, M.I.; Novoselov, K.S.; Geim, A.K. Chiral tunnelling and the Klein paradox in graphene. *Nat. Phys.* **2006**, *2*, 620–625.
16. Katsnelson, M.I. Zitterbewegung, chirality, and minimal conductivity in graphene. *Eur. Phys. J. B* **2006**, *51*, 157–160.
17. Rusin, T.M.; Zawadzki, W. Zitterbewegung of electrons in graphene in a magnetic field. *Phys. Rev. B* **2008**, *78*, 125419.
18. Pisana, S.; Lazzeri, M.; Casiraghi, C.; Novoselov, K.S.; Geim, A.K.; Ferrari, A.C.; Mauri, F. Breakdown of the adiabatic Born-Oppenheimer approximation in graphene. *Nat. Mater.* **2007**, *6*, 198–201.
19. Piscanec, S.; Lazzeri, M.; Mauri, F.; Ferrari, A.C.; Robertson, J. Kohn Anomalies and Electron-Phonon Interactions in Graphite. *Phys. Rev. Lett.* **2004**, *93*, 85503.
20. Novoselov, K.S.; Jiang, Z.; Zhang, Y.; Morozov, S.V.; Stormer, H.L.; Zeitler, U.; Maan, J.C.; Boebinger, G.S.; Kim, P.; Geim, A.K. Room-temperature quantum Hall effect in graphene. *Science* **2007**, *315*, 1379.
21. Zhou, S.Y.; Gweon, G.-H.; Fedorov, A.V.; First, P.N.; de Heer, W.A.; Lee, D.-H.; Guinea, F.; Castro Neto, A.H.; Lanzara, A.; et al. Substrate-induced bandgap opening in epitaxial graphene. *Nat. Mater.* **2007**, *6*, 770–775.
22. Zhang, Y.; Tan, Y.; Stormer, H.L.; Kim, P. Experimental observation of the quantum Hall effect and Berry's phase in graphene. *Nature* **2005**, *438*, 201–204.
23. Bekaert, J.; Aperis, A.; Partoens, B. Oppeneer, P.M.; Milošević, M.V. Evolution of multigap superconductivity in the atomically thin limit: Strain-enhanced three-gap superconductivity in monolayer MgB2 *Phys. Rev. B* **2017**, *96*, 094510.
24. Morshedloo, T.; Roknabadi, M.R.; Behdani, M. First-principles study of the superconductivity in MgB_2 bulk and in its bilayer thin film based on electron–phonon coupling. *Physica C* **2015**, *509*, doi:10.1016/j.physc.2014.11.006.
25. Calandra, M.; Profeta, G.; Mauri, F. Superconductivity in metal-coated graphene. *Phys. Status Solidi (b)* **2012**, *249*, 2544.

26. Ludbrook, B.M.; Levy, G.; Nigge, P.; Zonno, M.; Schneider, M.; Dvorak, D.J.; Veenstra, C.N.; Zhdanovich, S.; Wong, D.; Dosanjh, P.; et al. Evidence for superconductivity in Li-decorated monolayer graphene. *Proc. Natl. Acad. Sci. USA* **2015**, *112*, 11795.
27. Profeta, G.; Calandra, M.; Mauri, F. Phonon-mediated superconductivity in graphene by lithium deposition. *Nat. Phys.* **2012**, *8*, 131–134.
28. Pešić, J.; Gajić, R.; Hingerl, K.; Belić, M. Strain-enhanced superconductivity in Li-doped graphene. *Europhys. Lett.* **2014**, *108*, 67005.
29. Szczesniak, D.; Durajski, A.P.; Szczesniak, R. Influence of lithium doping on the thermodynamic properties of graphene based superconductors. *J. Phys-Condens. Mat.* **2014**, *26*, 255701.
30. Durajski, A.; Skoczylas, K.; Szczesniak, R. Superconductivity in bilayer graphene intercalated with alkali and alkaline earth metals. *Phys. Chem. Chem. Phys.* **2019**, *21*, 5925.
31. Zheng, J.-J.; Margine, E.R. First-principles calculations of the superconducting properties in Li-decorated monolayer graphene within the anisotropic Migdal-Eliashberg formalism. *Phys. Rev. B* **2016**, *94*, 064509.
32. Margine, E.R.; Lambert, H.; Giustino, F. Electron-phonon interaction and pairing mechanism in superconducting Ca-intercalated bilayer graphene. *Sci. Rep.* **2016**, *6*, 21414.
33. Mazin, I.I.; Antropov, V.P. Electronic structure, electron–phonon coupling, and multiband effects in MgB_2. *Phys. C Supercond.* **2003**, *385*, 49–65.
34. Giannozzi, P.; Andreussi, O.; Brumme, T.; Bunau, O.; Buongiorno, N.M.; Calandra, M.; Car, R.; Cavazzoni, C.; Ceresoli, D.; Cococcioni, M. et al. Quantum espresso: A modular and open-source software project for quantum simulations of materials. *J. Phys. Condensed Matter* **2009**, *21*, 395502.
35. Lu, N.; Guo, H.; Zhuo, Z.; Wang, L.; Wu, X.; Zeng, X.C. Twisted MX_2/MoS_2 heterobilayers: effect of van der Waals interaction on the electronic structure. *Nanoscale* **2017**, *9*, 19131–19138.
36. Soler, J.M.; Artacho, E.; Gale, J.D.; García, A.; Junquera, J.; Ordejón, P.; Sánchez-Portal, D. The SIESTA method for ab initio order-N materials simulation. *J. Phys. Condens. Matter.* **2002**, *14*, 2745.
37. Perdew, J.P.; Burke, K.; Ernzerhof, M. Generalized Gradient Approximation Made Simple. *Phys. Rev. Lett.* **1996**, *77*, 3865–3868.
38. N. Troullier; Martins, J.L. Efficient pseudopotentials for plane-wave calculations. *Phys. Rev. B* **1991**, *43*, 1993–2006, doi:10.1103/PhysRevB.43.1993.
39. Golesorkhtabar, R.; Pavone, P.; Spitaler, J.; Puschnig, P.; Draxl, C.ElaStic: A tool for calculating second-order elastic constants from first principles. *Comput. Phys. Commun.* **2013**, *184*, 1861–1873.
40. Nosé, S. A unified formulation of the constant temperature molecular dynamics methods. *J. Chem. Phys.* **1984**, *81*, 511.
41. Lindemann, F.A. The calculation of molecular vibration frequencies. *Phys. Z.* **1910**, *11*, 609.
42. Andrew, R.C.; Mapasha, R.E.; Ukpong, A.M.; Chetty, N. Mechanical properties of graphene and boronitrene. *Phys. Rev. B* **2012**, *85*, 125428.
43. Zhang, Z.; Yang, Y.; Penev, E.S.; Yakobson, B.I. Elasticity, Flexibility, and Ideal Strength of Borophenes. *Adv. Func. Mater.* **2017**, *27*, 1605059.
44. Zhong, H.; Huang, K.; Yu, G.; Yuan, S. Electronic and mechanical properties of few-layer borophene. *Phys. Rev. B* **2018**, *98*, 054104.
45. Mannix, A.J.; Zhou, X.F.; Kiraly, B.; Wood, J.D.; Alducin, D.; Myers, B.D.; Liu, X.; Fisher, B.L.; Santiago, U.; Guest, J.R.; et al. Synthesis of borophenes: Anisotropic, two-dimensional boron polymorphs. *Science* **2015**, *350*, 1513–1516.
46. Wang, H.; Li, Q.; Gao, Y.; Miao, F.; Zhou, X.-F.; Wan, X.G. Strain effects on borophene: ideal strength, negative Possion's ratio and phonon instability. *New J. Phys.***2016**, *18*, 073016.
47. De la Pena-Seaman, O.; de Cross, R.; Heid, R.; Bohnen, K.-P. Effects of Al and C doping on the electronic structure and phonon renormalization in MgB_2. *Phys. Rev. B* **2009**, *79*, 134523.
48. Ponce, S.; Margine E.R., Verdi, C.; Giustino, F. EPW: Electron-phonon coupling, transport and superconducting properties using maximally localized Wannier functions. *Comp. Phys. Commun.* **2016**, *209*, 116–133.
49. Margine, E.R.; Giustino, F. Anisotropic Migdal-Eliashberg theory using Wannier functions. *Phys. Rev. B* **2013**, *87*, 024505.
50. Damljanovic, V.; Gajic, R. Existence of Dirac cones in the Brillouin zone of diperiodic atomic crystals according to group theory. *J. Phys. Condens. Matter* **2016**, *28*, 085502.

51. Damljanovic, V.; Gajic, R. Addendum to 'Existence of Dirac cones in the Brillouin zone of diperiodic atomic crystals according to group theory'. *J. Phys. Condens. Matter* **2016**, *28*, 439401.
52. Poulet, H.; Mathieu, J.P. *Vibration Spectra and Symmetry of Crystals*; Gordon and Breach: New York, NY, USA, 1976.
53. Szalowski, K. Critical temperature of MgB_2 ultrathin superconducting films: BCS model calculations in the tight-binding approximation. *Phys. Rev. B* **2006**, *74*, 094501.
54. Zhang, C.; Wang, Y.; Wang, D.; Zhang, Y.; Liu, Z.-H.; Feng, Q.-R.; Gan, Z.-Z. Suppression of superconductivity in epitaxial MgB2 ultrathin films. *J. Appl. Phys.* **2013**, *114*, 023903.
55. Ao, B.; Zhang, Z.; Tang, T.; Zhao, Y. Potential enhancement of superconductivity in MgB_2 nanosheets: First-principles calculations. *Chem. Phys. Lett.* **2014**, *591*, 185–188.
56. Romero-Bermudez, A.; Garcıa-Garcıa, A.M. Shape resonances and shell effects in thin-film multiband superconductors. *Phys. Rev. B* **2014**, *89*, 024510.
57. Romero-Bermudez, A.; Garcıa-Garcıa, A.M. Size effects in superconducting thin films coupled to a substrate. *Phys. Rev. B* **2014**, *89*, 064508.
58. Acharya, N.; Wolak, M.A. ; Cunnane, D.P.; Karasik, B.S.; Xi, X.X. MgB2 ultrathin films fabricated by hybrid physical chemical vapor deposition and ion milling. *APL Mater.* **2016**, *4*, 086114.
59. Valentinis, D.; van der Marel, D.; Berthod, C. Rise and fall of shape resonances in thin films of BCS superconductors. *Phys. Rev. B* **2016**, *94*, 054516.
60. Narlikar, A.V. Small Superconductors: Introduction. In *The Oxford Handbook of Small Superconductors*, 1st ed., Narlikar, A.V., Ed.; Oxford University Press: Oxford, UK, 2017.
61. Gariglio, S.; Scheurer, M.; Schmalian, J.; Monteiro, A.M.R.V.L.; Goswami, S.; Caviglia, A. Surface and Interface Superconductivity. In *The Oxford Handbook of Small Superconductors*, 1st ed.; Narlikar, A.V., Ed.; Oxford University Press: Oxford, UK, 2017.

PROCEEDINGS OF SCIENCE

Linear dispersions in two-dimensional materials: a crystal with symmetry *pbma1'* as an example

Vladimir Damljanović[a,*] **and Nataša Lazić**[b]

[a] *Institute of Physics Belgrade, University of Belgrade, Pregrevica 118, Belgrade, Serbia*

[b] *NanoLab, Faculty of Physics, University of Belgrade, Studentski Trg 12, Belgrade, Serbia*

E-mail: damlja@ipb.ac.rs, natasal@ff.bg.ac.rs

Symmetry determines forms of band structures in the vicinity of special points in the reciprocal space of one-, two- and three-dimensional materials. Tight binding model on a crystal with four sites per primitive cell that belongs to gray layer single group *pbma* (45.2.315 or *pbma1'* in the magnetic layer groups notation) is calculated. Fortune teller states (FT) are obtained at the Brillouin zone (BZ) corners, as predicted by group theory for non-magnetic materials with negligible spin-orbit coupling. We show further that besides these FT states, another interesting band degeneracy arises as a consequence of symmetry.

11th International Conference of the Balkan Physical Union (BPU11),
28 August - 1 September 2022
Belgrade, Serbia

*Speaker

PoS(BPU11)107

1. Introduction

Symmetry is widely applied concept in solid-state physics. Predictions of crystal field splitting of electron energy levels in three-dimensional (3D) crystals [1], determination of phonon-displacement patterns in graphene [2, 3] and spin ordering in nano-tubes [4], are just a few among many examples. Group theoretical results are derived from irreducible (co)representations of little groups of the wave vector and the whole space groups. Those are tabulated and available for (3D) space groups [5, 6]. For layer groups, which are symmetries of two-dimensional (2D) materials, [7] tabulates little groups characters, while [8] gives characters of the (whole) graphene layer group. Recently, the representations of all layer groups, both single- and double-, with and without time-reversal symmetry (TRS), were also published [9].

Not only band degeneracies, but also dispersions near band contacts, are determined by symmetry. Ref. [10] gives analysis of band dispersions dictated by all symmorphic little groups in 3D. A few decades later, sufficient conditions for existence of Weyl fermions near high-symmetry points (HSPs) in Brillouin zone (BZ) of (3D) space groups were derived [11]. Recently, a full classification of linear dispersions near HSPs in layers has been reported [12]. Fully linear Hamiltonians are mutually distinguished not only by the dimensionality, but also by the functional dependence of energy on the wave vector near band contacts. Fortune teller dispersion (FT), theoretically predicted earlier [13], is seen in surface layers of silicone by angular resolved photo-emission spectroscopy (ARPES) [14].

While group theory gives band contacts and dispersions in their vicinity, it does not predict the position of the Fermi level. Also, symmetry alone does not guarantee that no other bands cross the Fermi level, once it is conveniently placed (*i.e.* it does not guarantee clean Fermi surface). Here we report the realization of FT states from a tight-binding model and show that it is impossible for FT states to be the only dispersions near given energy, at least when spin-orbit coupling (SOC) is neglected and for FT states arising from essential band contacts at HSP. Our proof relies on topologically protected accidental band contacts tabulated in the literature [15–20].

2. Results and discussion

When SOC is neglected and the material is non-magnetic, the combined crystal symmetry and TRS give FT states near BZ corners of layer groups 33, 43 and 45 [13]. From these layer groups, space groups 29, 54 and 57 are obtained by adding pure vertical translation (notation for layer and space groups is according to [21] and [22], respectively). We calculated the electronic band structure within tight-binding approximation on a structure that belongs to layer groups 45 (site $4c$ with $z = 0.6$Å, $x = 0.2$), which is shown in Figure 1.

Tight-binding Hamiltonian arising from s-orbitals is:

$$\hat{H}(\mathbf{k}) = [f_0 + f_1 cos(\mathbf{k}\cdot\mathbf{a}_1)]\hat{I}_4 + \begin{pmatrix} 0 & b_0\left(1+e^{i\mathbf{k}\cdot\mathbf{a}_1}\right) & c_0 e^{i\mathbf{k}\cdot\mathbf{a}_1}\left(1+e^{i\mathbf{k}\cdot\mathbf{a}_2}\right) & g_0\left(1+e^{i\mathbf{k}\cdot\mathbf{a}_2}\right) \\ b_0\left(1+e^{-i\mathbf{k}\cdot\mathbf{a}_1}\right) & 0 & g_0\left(1+e^{i\mathbf{k}\cdot\mathbf{a}_2}\right) & c_0\left(1+e^{i\mathbf{k}\cdot\mathbf{a}_2}\right) \\ c_0 e^{-i\mathbf{k}\cdot\mathbf{a}_1}\left(1+e^{-i\mathbf{k}\cdot\mathbf{a}_2}\right) & g_0\left(1+e^{-i\mathbf{k}\cdot\mathbf{a}_2}\right) & 0 & b_0\left(1+e^{-i\mathbf{k}\cdot\mathbf{a}_1}\right) \\ g_0\left(1+e^{-i\mathbf{k}\cdot\mathbf{a}_2}\right) & c_0\left(1+e^{-i\mathbf{k}\cdot\mathbf{a}_2}\right) & b_0\left(1+e^{i\mathbf{k}\cdot\mathbf{a}_1}\right) & 0 \end{pmatrix}, \quad (1)$$

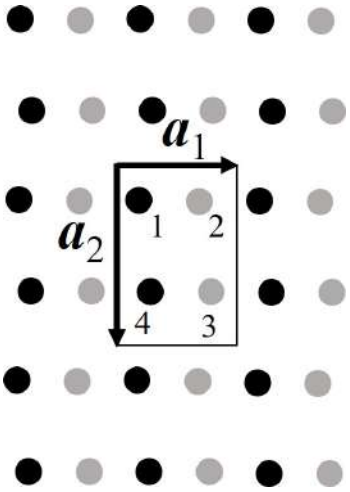

Figure 1: Crystal structure of the tight-binding model with $|\mathbf{a}_1|$ =2Å, $|\mathbf{a}_2|$ =3Å. All nuclei are of the same type. Black (gray) nuclei are located 0.6Å, above (below) the drawing plane. Fractional coordinates (in $\{\mathbf{a}_1, \mathbf{a}_2\}$-basis) for nucleus 1, 2, 3 and 4 are (0.2, 0.2), (0.7, 0.2), (0.8, 0.7) and (0.3, 0.7), respectively. We used program VESTA [23] for visualization.

where $\hat{I}_4$ is the four-dimensional unit matrix, $\mathbf{k}$ is a vector from the reciprocal space, while f_0, g_0, b_0, f_1 and c_0 (real numbers) are hopping parameters for the zeroth, first, second, third and fourth neighbor, respectively. The eigenvalues of $\hat{H}$ are bands denoted such that $E_1(\mathbf{k}) \leq E_2(\mathbf{k}) \leq E_3(\mathbf{k}) \leq E_4(\mathbf{k})$ for every wave vector $\mathbf{k}$. The full band structure for particular specified values of parameters is shown in Figure 2a) and near BZ corner in Figure 2b). Doubly degenerate lines are at BZ border as predicted by symmetry. The all four bands meet at the BZ corners. For closer look at dispersions near BZ corners, we expand the Hamiltonian in the vicinity of $(1/2, 1/2)$ in Taylor series up to linear (first) order:

$$\hat{H}(\mathbf{q}) \approx (f_0 - f_1)\hat{I}_4 + i \begin{pmatrix} 0 & -b_0\mathbf{q}\cdot\mathbf{a}_1 & c_0\mathbf{q}\cdot\mathbf{a}_2 & -g_0\mathbf{q}\cdot\mathbf{a}_2 \\ b_0\mathbf{q}\cdot\mathbf{a}_1 & 0 & -g_0\mathbf{q}\cdot\mathbf{a}_2 & -c_0\mathbf{q}\cdot\mathbf{a}_2 \\ -c_0\mathbf{q}\cdot\mathbf{a}_2 & g_0\mathbf{q}\cdot\mathbf{a}_2 & 0 & b_0\mathbf{q}\cdot\mathbf{a}_1 \\ g_0\mathbf{q}\cdot\mathbf{a}_2 & c_0\mathbf{q}\cdot\mathbf{a}_2 & -b_0\mathbf{q}\cdot\mathbf{a}_1 & 0 \end{pmatrix}. \tag{2}$$

The dispersion is:

$$E_{1,2,3,4} \approx f_0 - f_1 \pm \left| |b_0\mathbf{q}\cdot\mathbf{a}_1| \pm \sqrt{c_0^2 + g_0^2}\,|\mathbf{q}\cdot\mathbf{a}_2| \right|, \tag{3}$$

which is exactly FT type predicted in [13].

From (3) it follows that $E_1 = E_2$ and $E_3 = E_4$ if $\mathbf{q}\cdot\mathbf{a}_1 = 0$ or $\mathbf{q}\cdot\mathbf{a}_2 = 0$. These degeneracies are located at BZ borders and they are essential (caused by symmetry). However, there is another line of degeneracy $E_2 = E_3$, valid if $|b_0\mathbf{q}\cdot\mathbf{a}_1| = \sqrt{c_0^2 + g_0^2}\,|\mathbf{q}\cdot\mathbf{a}_2|$, which always has two solutions for sufficiently small $|\mathbf{q}|$. This degeneracy is accidental and it prevents the FT states to be the only states at the Fermi level, provided it continues across the whole BZ. Exact eigenvalues of full Hamiltonian (1) give lines of accidental degeneracies $E_2(\mathbf{k}) = E_3(\mathbf{k})$ for $|\mathbf{k}|$ not necessarily being small. These lines are indicated in red in Figure 2c). Such lines are not property of a model, but will always appear in group 45 as can be shown by the following argument. In the case with SOC included,

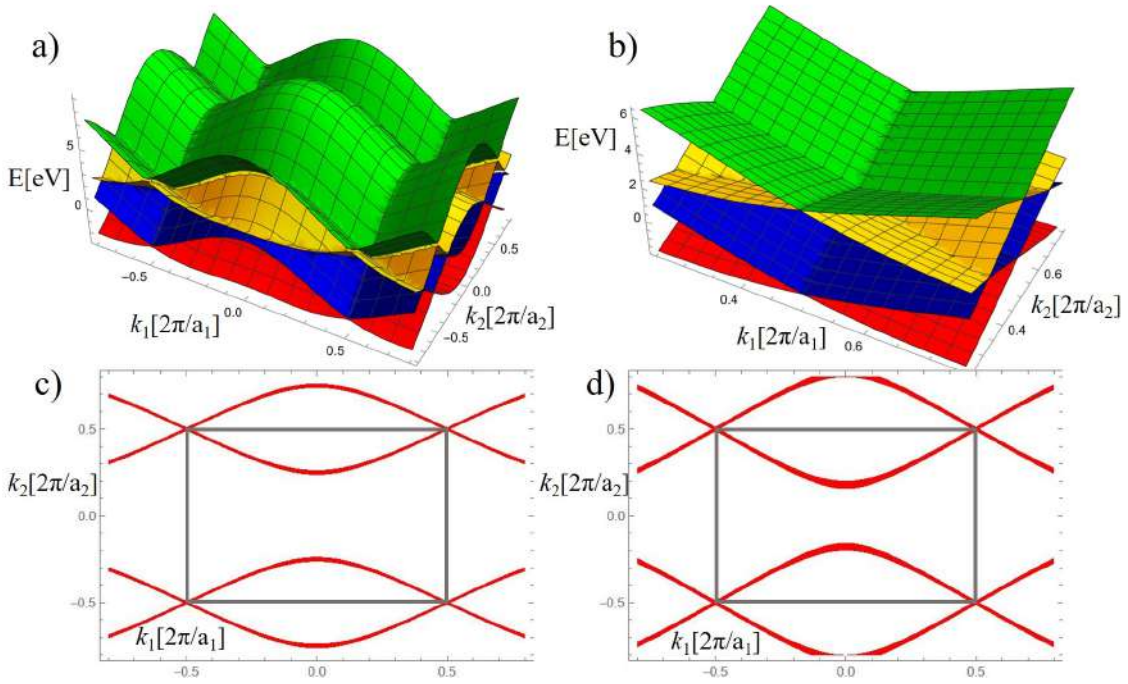

Figure 2: Band structure of the model: a) full band structure for f_0, g_0, b_0, f_1 and c_0 equal to $2eV$, $1.7eV$, $1.2eV$, $0.7eV$ and $0.3eV$, respectively, b) band structure near $(1/2, 1/2)$ showing FT dispersion, c) lines $E_2 = E_3$ (denoted in red) in **k**-space, d) lines $E_2 = E_3$ for f_0, g_0, b_0, f_1 and c_0 equal to $2.2eV$, $1.3eV$, $1.1eV$, $0.4eV$ and $0.1eV$, respectively. Grey rectangle in c) and d) denotes BZ border.

eight spinful non-degenerate bands are tangled together for groups 33, 43 and 45, giving electron filling of $8n$ as necessary condition for an insulator [17]. Since inclusion of SOC cannot close the gap, these eight bands (four if spin is not included) must be connected away from BZ corners, also in the absence of SOC. This means that the line $E_2 = E_3$ will always be present although its actual position depends on the parameters of the model. This is illustrated in Figure 2d) for slightly different values of parameters.

3. Conclusions

In summary we have confirmed that symmetry gives FT states unavoidably in the BZ corners of layer group 45, if the SOC is negligible and the magnetic order is absent. In addition, we showed that these FT states cannot be alone at the Fermi level and that there are always other bands that cross it. The same conclusion applies for remaining gray layer single groups with FT states (33 and 43). Our findings might help predicting new materials with anisotropic properties, or even suggest how to modify existing layered materials to obtain ones with these three symmetry groups.

Acknowledgments

Authors acknowledge funding by the Ministry of Science, Technological Development and Innovation of the Republic of Serbia provided by the Institute of Physics Belgrade (V.D.) and

Faculty of Physics (N.L.).

References

[1] H. Bethe, *Termaufspaltung in Kristallen*, *Annalen der Physik* **395**(2) (1929) 133–208.

[2] V Damljanović and R Gajić, *Phonon eigenvectors of graphene at high-symmetry points of the Brillouin zone*, *Physica Scripta* **T149** (2012) 014067.

[3] M. S. Dresselhaus, G. Dresselhaus, and A. Jorio, *Group Theory: Applications to the Physics of Condensed Matter*, Springer, 2008.

[4] Nataša Lazić and Milan Damnjanović, *Spin ordering in RKKY nanowires: Controllable phases in* ^{13}C *nanotubes*, *Phys. Rev. B* **90** (2014) 195447.

[5] Mois I. Aroyo, Asen Kirov, Cesar Capillas, J. M. Perez-Mato, and Hans Wondratschek, *Bilbao Crystallographic Server. II. Representations of crystallographic point groups and space groups*, *Acta Crystallographica Section A* **62** (2006) 115–128.

[6] Luis Elcoro, Barry Bradlyn, Zhijun Wang, Maia G. Vergniory, Jennifer Cano, Claudia Felser, B. Andrei Bernevig, Danel Orobengoa, Gemma de la Flor, and Mois I. Aroyo, *Double crystallographic groups and their representations on the Bilbao Crystallographic Server*, *Journal of Applied Crystallography* **50** (2017) 1457–1477.

[7] D. B. Litvin and T. R. Wike, *Character Tables and Compatibility Relations of the Eighty Layer Groups and Seventeen Plane Groups*, Plenum Press, 1991.

[8] V Damljanović, R Kostić, and R Gajić, *Characters of graphene's symmetry group Dg80*, *Physica Scripta* **T162** (2014) 014022.

[9] Božidar Nikolić, Ivanka Milošević, Tatjana Vuković, Nataša Lazić, Saša Dmitrović, Zoran Popović, and Milan Damnjanović, *Irreducible and site-symmetry-induced representations of single/double ordinary/grey layer groups*, *Acta Crystallographica Section A* **78** (2022) 107–114.

[10] A. A. Abrikosov and S. D. Beneslavskii, *Possible existence of substances intermediate between metals and dielectrics*, *Soviet Physics JETP* **32** (1971) 699–708.

[11] J. L. Mañes, *Existence of bulk chiral fermions and crystal symmetry*, *Phys. Rev. B* **85** (2012) 155118.

[12] N Lazić, V Damljanović, and M Damnjanović, *Fully linear band crossings at high symmetry points in layers: classification and role of spin–orbit coupling and time reversal*, *Journal of Physics A: Mathematical and Theoretical* **55** (2022) 325202.

[13] Vladimir Damljanović, Igor Popov, and Radoš Gajić, *Fortune teller fermions in two-dimensional materials*, *Nanoscale* **9** (2017) 19337–19345.

[14] Marek Kopciuszyński, Mariusz Krawiec, Lucyna Żurawek, and Ryszard Zdyb, *Experimental evidence of a new class of massless fermions*, *Nanoscale Horizons* **5** (2020) 679–682.

[15] Haruki Watanabe, Hoi Chun Po, Michael P. Zaletel, and Ashvin Vishwanath, *Filling-enforced gaplessness in band structures of the 230 space groups*, *Phys. Rev. Lett.* **117** (2016) 096404.

[16] Haruki Watanabe, Hoi Chun Po, Ashvin Vishwanath, and Michael Zaletel, *Filling constraints for spin-orbit coupled insulators in symmorphic and nonsymmorphic crystals*, *Proceedings of the National Academy of Sciences* **112** (2015) 14551–14556.

[17] Benjamin J. Wieder and C. L. Kane, *Spin-orbit semimetals in the layer groups*, *Phys. Rev. B* **94** (2016) 155108.

[18] J. Zhang, Y.-H. Chan, C.-K. Chiu, M. G. Vergniory, L. M. Schoop, and A. P. Schnyder, *Topological band crossings in hexagonal materials*, *Phys. Rev. Materials* **2** (2018) 074201.

[19] Moritz M. Hirschmann, Andreas Leonhardt, Berkay Kilic, Douglas H. Fabini, and Andreas P. Schnyder, *Symmetry-enforced band crossings in tetragonal materials: Dirac and Weyl degeneracies on points, lines, and planes*, *Phys. Rev. Materials* **5** (2021) 054202.

[20] Andreas Leonhardt, Moritz M. Hirschmann, Niclas Heinsdorf, Xianxin Wu, Douglas H. Fabini, and Andreas P. Schnyder, *Symmetry-enforced topological band crossings in orthorhombic crystals: Classification and materials discovery*, *Phys. Rev. Materials* **5** (2021) 124202.

[21] V Kopsky and D. B. Litvin, *International Tables of Crystallography Volume E: Subperiodic Groups*, Kluwer Academic Publishers, 2002.

[22] T Hahn, *International Tables of Crystallography Volume A: Space-Group Symmetry*, Springer, 2005.

[23] Koichi Momma and Fujio Izumi, *VESTA3 for three-dimensional visualization of crystal, volumetric and morphology data*, *Journal of Applied Crystallography* **44** (2011) 1272–1276.

BOOK OF ABSTRACTS

ADVANCES
IN SOLID STATE PHYSICS
AND NEW MATERIALS

ДОСТИГНУЋА У ФИЗИЦИ ЧВРСТОГ СТАЊА И НОВИХ МАТЕРИЈАЛА

30 година Центра за физику чврстог стања и нове материјале Института за физику у Београду

ADVANCES IN SOLID STATE PHYSICS AND NEW MATERIALS

30 years of the Center for Solid State Physics and New Materials at the Institute of Physics Belgrade

19 - 23 May 2025
Belgrade, Serbia

Group-Theoretical Study of Simple Bands in Two-Dimensional Materials

Vladimir Damljanović[a]

[a]*Institute of Physics Belgrade, University of Belgrade, Pregrevica 118, 11000 Belgrade, Serbia*

Abstract. In two-dimensional materials, simple bands are electronic or phononic bands that do not touch other bands near high-symmetry points of the Brillouin zone. In this contribution we found all possible simple bands in non-magnetic, two-dimensional materials using group theory. We found in total seven types of simple bands including bands of Mexican-hat shape. Our results are shown graphically for cases without and with spin-orbit coupling with the intention to made their usage easier [1].

REFERENCES

1. Damljanović, V., *Existence of Mexican-hat Dispersion and Symmetry Group of a Layer*, Physica E: Low-dimensional Systems and Nanostructures, Vol 170, 116224 (2025).

Advances in Solid State Physics and New Materials (5; 2025; Beograd)

Book of abstracts / Advances in Solid State Physics and New Materials - 30 years of the Center for Solid State Physics and New Materials at the Institute of Physics Belgrade, 19 – 23 May 2025, Belgrade, Serbia; editors Bojana Višić and Andrijana Šolajić. – Belgrade: Center for Solid State Physics and New Materials, Institute of Physics, 2025 (Belgrade: SASA).

ISBN 978-86-82441-65-6

1. Advances in Solid State Physics and New Materials

a) Физика чврстог стања - Апстракти

BOOK OF ABSTRACTS

ADVANCES
IN SOLID STATE PHYSICS
AND NEW MATERIALS

ДОСТИГНУЋА У ФИЗИЦИ ЧВРСТОГ СТАЊА И НОВИХ МАТЕРИЈАЛА

30 година Центра за физику чврстог стања и нове материјале Института за физику у Београду

ADVANCES IN SOLID STATE PHYSICS AND NEW MATERIALS

30 years of the Center for Solid State Physics and New Materials at the Institute of Physics Belgrade

19 - 23 May 2025
Belgrade, Serbia

Wettability of Covellite

Radoš Gajić[a], Marina Blagojev[b], Aleksandar Kremenović[b], Tijana Tomašević[a], Vladimir Damljanović[a], Marko Opačić[c], Borislav Vasić[a]

[a] *Laboratory for 2D materials, Center for Solid State Physics and New Materials, Institute of Physics Belgrade, University of Belgrade, Pregrevica 118, 11080 Belgrade, Serbia*
[b] *University of Belgrade - Faculty of Mining and Geology, Djušina 7, 11000 Belgrade, Serbia*
[c] *Center for Solid State Physics and New Materials, Institute of Physics Belgrade, University of Belgrade, Pregrevica 118, 11080 Belgrade, Serbia*

Abstract. Covellite (covelline) is a copper sulfide mineral (CuS). It has many interesting properties and applications including the first naturally occurring superconductivity or applications for lithium batteries cathodes, ammonium gas sensors or solar cells. In the mining engineering the froth flotation of covellite is an important issue. Therefore, the wettability of covellite (hydrophobicity) is a critical feature. In this this study we used ab-initio methods (density functional theory and molecular dynamics) to calculate the contact angle of covellite (the angle between a liquid and a solid surfaces). It turned out that the calculated value of the contact angle is in a good agreement with the experimental one we measured, proving that ab-initio methods are useful tools in the mining engineering.

Acknowledgement The authors would like to thank Professor Milena Kostovic from Faculty of Mining and Engineering in Belgrade for useful discussions.

REFERENCES

1. P. G. De Gennes, F. Brochard-Wayart, D. Quere, *Capillarity and Wetting Phenomena*, Springer (2004).
2. A. Gross, *Theoretical Surface Science*, Springer (2009).
3. S. R. Rao, J. Leja, *Surface Chemistry of Froth Flotation, 2nd, Vol. 1*, Springer (2004).
4. S. J. Clark, M. D. Segall, C. J. Pickard, P. Hasnip, M. J. Probert, K. Rafson, and M. C. Payne, *Z. Crystallogr*. **220**, 567-570 (2005).
5. A. M. Garcia, J. He, A. L. Soares Jr, and H. A. Duarte, *CrystEngComm*, **19**, 3078-3084 (2017)

Advances in Solid State Physics and New Materials (5; 2025; Beograd)

Book of abstracts / Advances in Solid State Physics and New Materials - 30 years of the Center for Solid State Physics and New Materials at the Institute of Physics Belgrade, 19 – 23 May 2025, Belgrade, Serbia; editors Bojana Višić and Andrijana Šolajić. – Belgrade: Center for Solid State Physics and New Materials, Institute of Physics, 2025 (Belgrade: SASA).

ISBN 978-86-82441-65-6

1. Advances in Solid State Physics and New Materials

a) Физика чврстог стања - Апстракти

BOOK OF ABSTRACTS

ADVANCES
IN SOLID STATE PHYSICS
AND NEW MATERIALS

ДОСТИГНУЋА У ФИЗИЦИ ЧВРСТОГ СТАЊА И НОВИХ МАТЕРИЈАЛА

30 година Центра за физику чврстог стања и нове материјале Института за физику у Београду

ADVANCES IN SOLID STATE PHYSICS AND NEW MATERIALS

30 years of the Center for Solid State Physics and New Materials at the Institute of Physics Belgrade

19 - 23 May 2025
Belgrade, Serbia

Raman Signatures Of Instabilities In $InSiTe_3$

T. Belojica[a], A. Milosavljević[a], S. Djurdjić Mijin[ba], J. Blagojević[a], A. Šolajić[a], J. Pešić[a], B. Višić[a], V. Damljanović[a], M. O. Ogunbunmi[c], S. Bobev[cd], Yu Liu[d], C. Petrovic[def], Z. Popović[g], R. Hackl[hi], and N. Lazarević[a]

[a]*Institute of Physics Belgrade, University of Belgrade, Pregrevica 118, 11080 Belgrade, Serbia*
[b]*Departamento de Fisica de Materiales, Facultad de Ciencias, Universidad Autónoma de Madrid, 28049 Madrid, Spain*
[c]*Departament of Chemistry and Biochemistry, University of Delaware, Newark, Delaware 19716, USA*
[d]*Condensed Matter Physics and Materials Science Departament, Brookhaven National Laboratory, Upton, NY 11973-5000, USA*
[e]*Department of Nuclear and Plasma Physics, Vinca Institute of Nuclear Sciences, University of Belgrade, Belgrade 11001, Serbia*
[f]*Shanghai Advanced Research in Physical Sciences (SHARPS), Shanghai 201203, China*
[g]*Serbian Academy of Sciences and Arts, Knez MIhailova35, 11000 Belgrade, Serbia*
[h]*School of Natural Sciences, Technische Universität München, Garching 85748, Germany*
[i]*IFW Dresden, Helmholtzstrasse 20, Dresden 01069, Germany*

Abstract. Layered van der Waals materials have gained considerable interest for their unique physical properties, yet $InSiTe_3$ remains largely unexplored due to uncertainties surrounding its crystal structure. In this work, we present a comprehensive experimental and theoretical investigation of $InSiTe_3$, confirming a rhombohedral structure with $P\bar{3}$ space group symmetry via single-crystal X-ray diffraction. Polarization-resolved Raman scattering reveals nine out of ten Raman-active modes expected for this symmetry, further validating the structural assignment. Beyond conventional phonon behavior, we identify strong anharmonicity and the emergence of a self-organized coherent phonon state associated with a high-energy A_g mode near 500 cm^{-1}. Analysis of phonon-phonon coupling parameters indicates that A_g modes exhibit coupling strengths up to eight times greater than E_g modes. Temperature-dependent Raman measurements from 80 to 300 K reveal notable changes in A_g mode intensities around 200 K and the appearance of broad spectral features in the phonon gap region, attributed to overtone excitations. Our findings point to an intrinsic lattice instability in $InSiTe_3$, driven by strong anharmonic interactions. However, further studies are required to fully uncover the microscopic origin of these instabilities and their implications for the material's physical properties.

*This research was supported by the Science Fund of the Republic of Serbia, 10925, Dynamics of CDW transition in strained quasi-1D systems – DYNAMIQS

Advances in Solid State Physics and New Materials (5; 2025; Beograd)

Book of abstracts / Advances in Solid State Physics and New Materials - 30 years of the Center for Solid State Physics and New Materials at the Institute of Physics Belgrade, 19 – 23 May 2025, Belgrade, Serbia; editors Bojana Višić and Andrijana Šolajić. – Belgrade: Center for Solid State Physics and New Materials, Institute of Physics, 2025 (Belgrade: SASA).

ISBN 978-86-82441-65-6

1. Advances in Solid State Physics and New Materials

a) Физика чврстог стања - Апстракти

IX International School and Conference on Photonics

PHOTONICA 2023

Book of abstracts

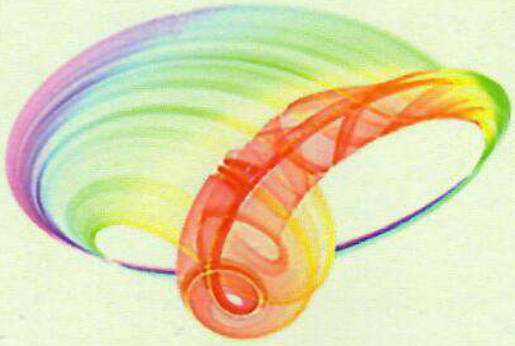

Editors

Jelena Potočnik, Maja Popović, Dušan Božanić

Belgrade, 2023.

Book of abstracts

IX International School and Conference on Photonics

PHOTONICA2023

with joint events:

Understanding interaction light - biological surfaces: possibility for new electronic materials and devices

&

Biological and bioinspired structures for multispectral surveillance

&

Quantum sensing integration within microfluidic Lab-on-a Chips for biomedical applications

August 28 - September 01, 2023, Belgrade, Serbia

Editors

Jelena Potočnik, Maja Popović, Dušan Božanić

Vinča Institute of Nuclear Sciences – National Institute of the Republic of Serbia, University of Belgrade

Belgrade, 2023

ABSTRACTS OF TUTORIAL, KEYNOTE, INVITED LECTURES, PROGRESS REPORTS AND CONTRIBUTED PAPERS

of

IX International School and Conference on Photonics

PHOTONICA2023

August 28 - September 01, 2023, Belgrade, Serbia

Editors
Jelena Potočnik, Maja Popović, Dušan Božanić

Publisher
Vinča Institute of Nuclear Sciences – National Institute of the Republic of Serbia, University of Belgrade
Mike Petrovića Alasa 12-14
11351 Vinča, Belgrade, Serbia

Printed by
Serbian Academy of Sciences and Arts

Number of copies
200

ISBN 978-86-7306-165-8

Centrosymmetric, non-symmorpic, non-magnetic, spin-orbit coupled layers without Dirac cones: a tight-binding example

V. Damljanović
Institute of Physics Belgrade, University of Belgrade, Pregrevica 118, Belgrade, Serbia
e-mail: damlja@ipb.ac.rs

It is believed that the existence of Dirac cones in the Brillouin zone (BZ) of time-reversal symmetric, two-dimensional (2D) materials with strong spin-orbit coupling (SOC) is closely connected with the presence of spatial inversion and non-symmorphic symmetry [1]. This belief is indeed confirmed in many cases published in the literature; however, a detailed group-theoretical analysis shows that this does not always hold [2]. Here we illustrate the mentioned fact by a tight-binding model from s-orbitals, on a structure that belongs to a non-symmorphic, gray, layer double group with spatial inversion. The band structure of the model consists of two double-degenerate bands touching only along a line at the BZ edge. Further, we show that neglecting SOC leads to unaltered Hamiltonian, up to numerical values of the parameters. Finally, we state some 2D materials described in the literature, with the symmetry of our model.

REFERENCES

[1] S.M. Young, C.L. Kane, Phys. Rev. Lett. 115, 126803 (2015).
[2] N. Lazić *et al.*, J. Phys. A: Math. Theo. 55, 325202 (2022).

CIP - Каталогизација у публикацији
Народна библиотека Србије, Београд

535(048)
621.37/.39:535(048)
621.37/.39:535]:61(048)
66.017/.018(048)

INTERNATIONAL School and Conference on Photonics (9 ; 2023 ; Beograd)
Book of abstracts / IX International School and Conference on Photonics PHOTONICA2023 with joint events: Understanding interaction light - biological surfaces possibility for new electronic materials and devices & Biological and bioinspired structures for multispectral surveillance & Quantum sensing integration within microfluidic Lab-on-a Chips for biomedical applications, August 28 - September 01, 2023, Belgrade, Serbia ; editors Jelena Potočnik, Maja Popović, Dušan Božanić ; [organizers] Vinča Institute of Nuclear Sciences-National Institute of the Republic of Serbia, University of Belgrade, Serbia ... [et al.]. - Belgrade : University, Vinča Institute of Nuclear Sciences, National Institute of the Republic of Serbia, 2023 (Belgrade : SASA). - XV, 148 str. : ilustr. ; 25 cm

Tiraž 200. - Bibliografija uz većinu apstrakata. - Registar.

ISBN 978-86-7306-165-8

а) Оптика -- Апстракти б) Оптички материјали -- Апстракти в) Оптоелектроника -- Апстракти г) Оптоелектроника -- Биомедицина -- Апстракти д) Телекомуникације -- Апстракти

COBISS.SR-ID 119913737

PHOTONICS CENTER

IPB

University of Belgrade
Institute of Physics Belgrade
Kopaonik, March 12-15, 2023

Book of Abstracts

16th Photonics Workshop

(Conference)

PHOTONICS
CENTER

16th Photonics Workshop (2023)

Book of abstracts

Kopaonik, Serbia, March 12-15, 2023

Publisher, 2023:

Institute of Physics Belgrade

Pregrevica 118

11080 Belgrade, Serbia

Editors:

Dragan Lukić, Marina Lekić, Zoran Grujić

ISBN 978-86-82441-59-5

Printed by:

NEW IMAGE d.o.o.

Tošin Bunar 185, Belgrade

Number of copies: 55

CIP - Каталогизација у публикацији - Народна библиотека Србије, Београд

535(048)
681.7(048)
66.017/.018(048)

PHOTONICS Workshop (16; 2023; Kopaonik)
Book of Abstracts / 16th Photonics Workshop, (Conference), Kopaonik, March 12-15, 2023; [organized by Institute of Physics Belgrade, Photonics center [and] Optical Society of Serbia]; [editors Dragan Lukić, Marina Lekić, Zoran Grujić]. - Belgrade: Institute of Physics, 2023 (Belgrade: New image). - 68 str.: ilustr; 25 cm

Тираж 55. - Registar.

ISBN 978-86-82441-59-5

а) Оптика -- Апстракти б) Оптоелектроника -- Апстракти в) Технички материјали -- Апстракти

COBISS.SR-ID 109912585

Atlas of electronic band structures in two-dimensional materials

V. Damljanović[1], N. Lazić[2]

(1) *Institute of Physics Belgrade, University of Belgrade, Pregrevica 118, 11080 Belgrade, Serbia*

(2) *NanoLab, Faculty of Physics, University of Belgrade, Studentski Trg 12, 11001 Belgrade, Serbia*

Contact: V. Damljanović (damlja@ipb.ac.rs)

Abstract. We have extended our previous work, devoted to full enumeration of layer groups and Brillouin zone high symmetry points hosting fully linear dispersions [1], to include dispersions beyond linear ones near all high symmetry points and lines for non-magnetic materials without and with spin-orbit coupling. Our results are presented graphically and fit into only two figures and a few pages of text/formulas [2]. Our graphical presentation enables easy access to information regarding which parts of Brillouin zone host particular quasiparticle in a certain layer (single- or double-) group.

REFERENCES

1. N. Lazić, V. Damljanović, M. Damnjanović, *J. Phys. A: Math. Theo.* **55** (2022), 325202.
2. V. Damljanović, N. Lazić, *arXiv*: 2212.09834 (2022).

BPU11 CONGRESS
The Book of Abstracts

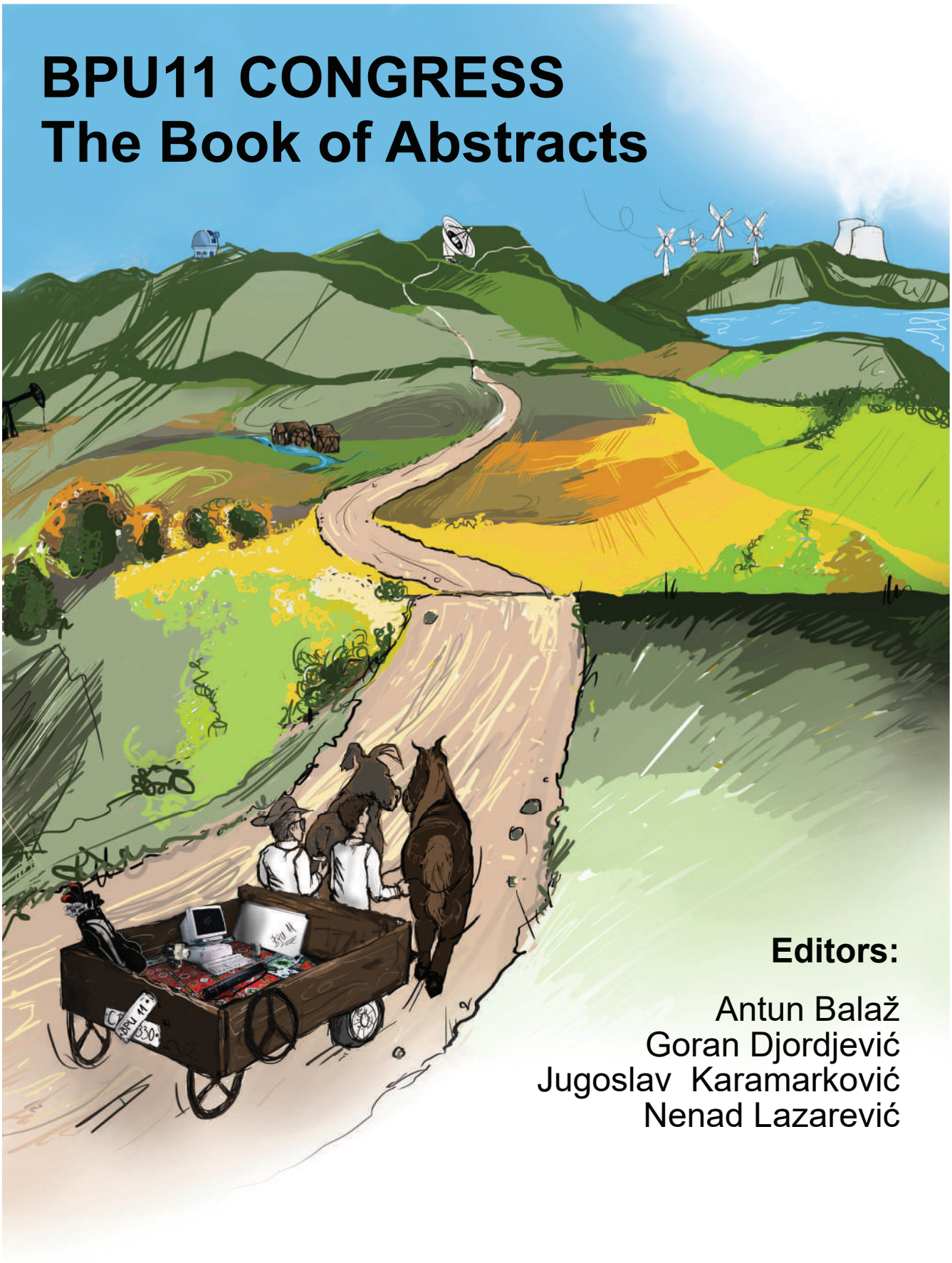

Editors:

Antun Balaž
Goran Djordjević
Jugoslav Karamarković
Nenad Lazarević

Belgrade, 2022

BPU11 CONGRESS

28 August 2022 - 1 September 2022

Book of Abstracts

Editors: Antun Balaž, Goran Djordjević,
Jugoslav Karamarković, Nenad Lazarević

Belgrade, 2022

BPU11 CONGRESS
The 11th International Conference of the Balkan Physical Union
The Book of Abstracts

Editors:
Antun Balaž, Goran Djordjević,
Jugoslav Karamarković, Nenad Lazarević

Technical Editor: Milan Milošević
Cover Design: Elena Denda

Printed by: Planeta Print, Belgrade
ISBN: 978-86-7025-950-8
Print run: 350

Co-organizers

- Serbian Academy of Sciences and Arts (SASA)
- Faculty of Sciences and Mathematics, University of Niš
- Faculty of Physics, University of Belgrade
- Vinča Institute of Nuclear Sciences, University of Belgrade, National Institute of the Republic of Serbia
- Faculty of Mathematics, University of Belgrade
- Mathematical Institute of Serbian Academy of Sciences and Arts, National Institute of the Republic of Serbia
- Faculty of Science, University of Kragujevac
- Faculty of Sciences, University of Novi Sad
- Faculty of Sciences and Mathematics, University of Pristina in Kosovska Mitrovica
- SEENET-MTP Centre
- European Physical Society (EPS)
- Institute of Physics Belgrade, National Institute of the Republic of Serbia

Partners and Sponsors

- International Centre for Theoretical Physics (ICTP), Trieste
- Central European Initiative (CEI), Trieste
- Ministry of Education, Science, and Technological Development, Republic of Serbia
- Conseil Européen pour la Recherche Nucléaire (CERN), Geneva
- Provincial Secretariat for Higher Education and Scientific Research, Autonomous Province of Vojvodina, Republic of Serbia
- The European Physical Journal (EPJ)

[1] *Ovidius University of Constanta: Academy of Romanian Scientists*

Presenter: V. Ciupina (vciupina@yahoo.com)

Using TVA technology, multilayer and composite C-Ti layers were deposited on silicon substrates. The C-Ti multilayers were constructed from the silicon substrate as follows: 100nm of carbon, followed by alternant 17nm Ti and 40 nm C three times, covered by one last 17 nm Ti layer, resulting a seven multilayer structure. For the composite layer, after the pre 100nm carbon one, we varied quasi continuously the Ti:C atomic ratio, from 1:9 and reaching 9:1 at the top of the 119 nm. For both composite and multilayer structures, several batches were obtained for comparison. We varied the substrate temperatures during the deposition (R. T.,100, 200, 300 and 400oC) and one deposition batch was obtained at 300oC with a -700V polarisation voltage on the substrates, in order to increase the ions energy reaching the layer, during the coating process.

Characterization of structural properties of films was achieved by Electron Microscopy technique (TEM) and GIXRD techniques. The measurements show that increase of the substrate temperature reveal changes in TixCy lattice parameters. Thus, according to GIXRD analysis it was found out that the Ti:C atomic ratio changes with increase of synthesis temperature. Also, in the case of composite films an increase of amount and sizes of TiC nanocrystals with the increase of energy of Ti ions determined by increase of polarisation voltage was observed. The tribological measurements were performed using a ball-on-disk system with normal forces of 0.5, 1, 2, 3N respectively. Was found that the coefficient of friction depends on the synthesis temperature and on the polarisation voltage. It is also noted that the friction coefficient depends on the pure C content, Ti content and amount of TiC nanocrystallites. These results are due to atomic diffusion at Ti/C interfaces and also are associated with amount of TiC nanocrystallites. Using Bruker Hysitron TI980 Triboindenter System, global hardness of the coating, in depth hardness and SPM imaging analysis were performed. By Nanoscratch Analysis, global and depth Young modulus was measured. To characterize the electrical conductive properties, the electrical surface resistance versus temperature have been measured, and then the electrical conductivity is calculated. Using the Wiedemann-Frantz law was obtained the thermal conductivity.

S06-CMPSP-101 / **Oral presentation**

Linear dispersions in two-dimensional materials: a crystal with symmetry pbma1' as an example

Authors: Nataša Lazić[1]; Vladimir Damljanović[2]

[1] *NanoLab, Faculty of Physics, University of Belgrade*

[2] *Institute of Physics Belgrade, University of Belgrade*

Presenter: V. Damljanović (damlja@ipb.ac.rs)

Symmetry determines forms of band structures in the vicinity of special points in the reciprocal space of one-, two- and three-dimensional materials. After short introduction to the complete classification of linear dispersions in 2D materials, [1] we will focus on a particular example. A tight binding model on a crystal with four sites per primitive cell that belongs to grey layer single group $pbma$ (45.2.315 or $pbma1'$ in the magnetic layer groups notation of Ref. [2]) is calculated. Fortune teller states are obtained in the Brillouin zone corners, as predicted [3,1] by group theory for non-magnetic materials with negligible spin-orbit coupling. We will discuss possible realizations of this model in realistic and hypothetical materials.

References
1. N. Lazić, V. Damljanović and M. Damnjanović, *arXiv*: 2108.11733 (2021).
2. D. B. Litvin, Acta Cryst. A **61**, 382 (2005).
3. V. Damljanović, I. Popov and R. Gajić, Nanoscale **9**, 19337 (2017).

S06-CMPSP-102 / **Oral presentation**

Influence of the Size of Cation on the Structure and Tribological Properties of Ionic Liquids Studied with Molecular Dynamics

Authors: Igor Stanković[1]; Miljan Dašić[1]

[1] *Scientific Computing Laboratory, Center for the Study of Complex Systems,Institute of Physics Belgrade, University of Belgrade, Pregrevica 118, Belgrade, 11080, Serbia*

Presenter: M. Dašić (mdasic@ipb.ac.rs)

Ionic liquids (ILs) are two-component systems composed of large asymmetric and irregularly shaped organic cations and anions. Physical properties of ILs like negligible vapour pressure, high-temperature stability, high ionic conductivity and also a great variety of ILs and their mixtures highlight them as potentially relevant to lubrication [1, 2]. A large number of variations in IL composition is possible, estimated at the order of magnitude of 10^{18} different ILs. From their variety stems the possibility of tuning their physicochemical properties which can affect lubrication, such as viscosity, polarity, surface reactivity. Hence, it would be advantageous to figure out general relations between the molecular structure and tribological properties of ILs.

In this study, we investigate a generic tailed-model (TM) of ILs which includes: an asymmetric cation consisting of a positively charged head ($\sigma_C = 5$Å) and a neutral tail of variable size ($\sigma_T = 3, 5, 9$Å) and a large spherical negatively charged anion ($\sigma_A = 10$Å). It represents a more realistic model compared to the simplest one, the so called Salt Model (SM) [3, 4]. We figured that, although simple, TM model results in striking differences in equilibrium bulk structure of IL governed by the tail size relative to cationic head: (i) simple cubic lattice for the small tail, (ii) liquid-like state for symmetric cation-tail dimer, and (iii) molecular layer structure for the

CIP - Каталогизација у публикацији
Народна библиотека Србије, Београд

53(048)

INTERNATIONAL Conference of the Balkan Physical Union (11 ; 2022 ; Belgrade)
Book of Abstracts / [The 11th International Conference of the Balkan Physical Union] [i. e] BPU 11 congress, 28 August 2022-1 September 2022 ; editors Antun Balaž ... [et al.]. - Belgrade : [САНУ] ; [Ниш] : [Природно-математички факултет Универзитета], 2022 (Belgrade : Planeta print). - 298 str. ; 25 cm

Tiraž 350. - Str. 1-2: Preface / Goran S. Djordjević. - Registar.

ISBN 978-86-7025-950-8 (SANU)

1. Balaž, Antun, 1973- [уредник]

a) Физика -- Апстракти

COBISS.SR-ID 72769545

Co-organizers

Partners and Sponsors

Hybrid 15th International Symposium on Flexible Organic Electronics

ISFOE22

BOOK OF ABSTRACTS

4-7 July 2022

Live in Thessaloniki, Greece

Virtual via Video Conferencing System

2022

ISFOE22 Committees

International Organizing Committee

S. Logothetidis, Department of Physics, Aristotle University of Thessaloniki, Greece (Chair)
Z. Cui, Printable Electronics Research Center, Suzhou Institute of Nanotech, Chinese Academy of Sciences, China (Co-chair)
G. Hadziioannou, LCPO, CNRS, University of Bordeaux, France (Co-chair)
J. Kallitsis, Department of Chemistry, University of Patras, FORTH-ICE-HT, Greece (Co-chair)
A. Laskarakis, Department of Physics, Aristotle University of Thessaloniki, Greece (Co-chair)
G. Malliaras, Department Of Engineering, University of Cambridge, UK (Co-chair)
R. P. Silva, Nano-Electronics Centre, Advanced Technology Institute, University of Surrey, UK (Co-chair)

Local Organizing Committee

S. Logothetidis, Department of Physics, Aristotle University of Thessaloniki, Greece
A. Laskarakis, Department of Physics, Aristotle University of Thessaloniki, Greece

International Scientific Committee

T. Anthopoulos, King Abdullah University of Science and Technology, Saudi Arabia
R. Baumann, Chemnitz University of Technology, Germany
F. Biscarini, University of Modena and Reggio Emilia, Italy
Y. Bonnassieux, LPICM, Ecole Polytechnique, CNRS, France
C. Brabec, Friedrich-Alexander-University of Erlangen-Nórnberg, Germany
D. Bradley, King Abdullah University of Science and Technology, Saudi Arabia
F. Castro, National Physical Laboratory (NPL), UK
A. Christou, Maryland NanoCenter, University of Maryland, USA
T. Claypole, Welsh Centre for Printing and Coating, Swansea University, UK
Z. Cui, Printable Electronics Research Center, Suzhou Institute of Nanotech, Chinese Academy of Sciences, China
M. Damnjanovic, Faculty of Physics, University of Belgrade, Serbia
G. Deligeorgis, FORTH IESL, Greece
B. Drevillon, CNRS, Ecole Polytechnique, France
V. Dyakonov, Julius-Maximilian University of Wuerzburg, Germany
D. Dykeman, ANSYS, Inc., UK
B. Fillon, CEA Liten, France
S. Forrest, University of Michigan, USA
M. Graetzel, LPI, ISIC, EPFL, Lausanne, Switzerland
G. Hadziioannou, LCPO, CNRS, University of Bordeaux, France
R. A. J. Janssen, Eindhoven University of Technology, The Netherlands
J. Kallitsis, Department of Chemistry, University of Patras, FORTH-ICE-HT, Greece
E. Kaxiras, Harvard University, Division of Engineering and applied Sciences, USA
J. Kido, Yamagata University, Japan
T. Kolbusch, COATEMA Coating Machinery GmbH, Germany
M. Krebs, Varta Microbattery GmbH, Germany
A. Laskarakis, Department of Physics, Aristotle University of Thessaloniki, Greece
K. Leo, Novaled & Dresden Technical University, Germany
N. Li Pira, Centro Ricerche Fiat, S.C.p.A, Italy
P. Lianos, General Department of Polytechnic School of Patras, Greece
L. Lidorikis, University of Ioannina, Greece
S. Logothetidis, Department of Physics, Aristotle University of Thessaloniki, Greece
G. Malliaras, Department Of Engineering, University of Cambridge, UK
M. McLachlan, Imperial College London, UK
N. Rikita, Mitsubishi Materials Corporation, Japan
M. Schrarber, Linz Institute for Organic Solar Cells, Austria
R. Silva, Nano-Electronics Centre, Advanced Technology Institute, University of Surrey, UK
F. Stelzer, Graz University of Technology, Graz, Austria
N. Stingelin, Georgia Institute of Technology, USA
D. Tsoukalas, National Technical University of Athens, Greece
J. Ulanski, Department of Molecular Physics, Technical University of Lodz, Poland
L. Van Langenhove, Department of Textiles, Ghent University, Belgium
A. Wedel, Fraunhofer Institute for Applied Polymer Research, Germany

Topological quantum chemistry for quasi-one-dimensional systems with either translational or helical periodicity

I. Milošević, S. Dmitrović, T. Vuković, M. Damnjanović

Faculty of Physics, University of Belgrade, Studentski trg 12, Belgrade, Serbia

Abstract:

By linking symmetry with combinatorial graph theory, topological quantum chemistry [1], in terms of elementary band representations (EBRs), gives universal description of electronic band structure topology of short-range entangled matter.

Here, derived are complete sets of nonequivalent (physical) EBRs, for symmetry groups of quasi-one-dimensional systems with either translational or helical periodicity. Apart from the system configuration symmetry described by line groups (LGs), considered also is the additional symmetry of time-reversal (grey-LGs) and the symmetry originating from spin degree of freedom (double-LGs and double-grey-LGs) [2,3]. The results obtained are complete and exhaustive, thus enabling thorough algorithmic search for topological compounds across the one-dimensional matter. As an illustration, a topological mirror chain model is considered.

[1] B. Bradlyn *et al.*, Nature 547 (2017) 298
[2] I. Milošević *et al.*, J. Phys. A 53 (2020) 455204
[3] S. Dmitrović *et al.*, J. Phys. A (2022)

Linear dispersions in low-dimensional structures: the role of crystalline symmetries, time reversal, and spin-orbit coupling

N. Lazić[1], V. Damljanović[2], M. Damnjanović[3], …

[1] NanoLab, Faculty of Physics, University of Belgrade, Studentski trg 12, 11001 Belgrade, Serbia
[2] Institute of Physics Belgrade, University of Belgrade, Pregrevica 118, 11080 Belgrade, Serbia
[3] Serbian Academy of Sciences and Arts, Kneza Mihaila St. 35, 11000 Belgrade, Serbia

Abstract: Crystalline symmetry imposes requirements on the band structure of material, which have consequences in the band topology. Besides gapped topological insulators, lattice symmetries are also important in describing gapless semi-metallic phases. They are characterized by band crossings on the Fermi level, and particularly interesting are those with linear energy-momentum dependence. Here, we study symmetry-enforced semi-metallic layered materials with dispersions linear in all directions around crossings hosted by high-symmetry Brillouin zone points. In particular, single and double, ordinary and grey layer groups are used to achieve the complete systematization of such fully linear band crossings and corresponding effective Hamiltonians. The resulting dispersion shapes are: single cone (with double degenerate crossing point and non-degenerate branches, or 4-fold degenerate crossing point with double degenerate conical branches), poppy-flower (4-fold degenerate crossing point with two pairs of non-degenerate mutually rotated conical branches), and a fortune teller (with nodal lines). Inclusion of spin-orbit interaction is analysed through the transition from single to double group; this results in interesting patterns at high symmetry points such as: gap closing, gap opening, cone preserving, cone splitting etc. Similarly, the role of time reversal symmetry is clarified through the ordinary to grey group transit

2022

ISFOE22

15th International Symposium on Flexible Organic Electronics

ISFOE22 is part of NANOTEXNOLOGY 2022

Organized by

Supported by

Under the Auspices of

www.nanotexnology.com

University of Belgrade
Institute of Physics Belgrade
Kopaonik, March 13-16, 2022

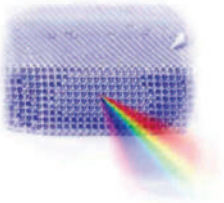

Book of Abstracts

15th Photonics Workshop

(Conference)

15th Photonics Workshop (2022)

Book of abstracts

Kopaonik, Serbia, March 13-16, 2022

Publisher, 2022:

Institute of Physics Belgrade

Pregrevica 118

11080 Belgrade, Serbia

Editors:

Dragan Lukić, Marina Lekić, Zoran Grujić

ISBN 978-86-82441-55-7

Printed by:

NEW IMAGE d.o.o.

Tošin Bunar 185, Belgrade

Number of copies: 55

CIP - Каталогизација у публикацији - Народна библиотека Србије, Београд
535(048)
681.7(048)
66.017/.018(048)
PHOTONICS Workshop (15; 2022; Kopaonik)
Book of Abstracts / 15th Photonics Workshop, (Conference), Kopaonik,
March 13-16, 2022; [editors Dragan Lukić, Marina Lekić, Zoran Grujić]. -
Belgrade: Institute of Physics, 2022 (Belgrade: New image). - 72 str.:
ilustr.; 25 cm
Tiraž 55. - Registar.
ISBN 978-86-82441-55-7
a) Оптика - Апстракти b) Оптоелектроника - Апстракти c) Технички
материјали - Апстракти

COBISS.SR-ID 60055049

Full classification of linear dispersions in two-dimensional materials

V. Damljanović[1], M. Damnjanović[2,3], N. Lazić[2]

(1) *Institute of Physics Belgrade, University of Belgrade, Pregrevica 118, 11080 Belgrade, Serbia*

(2) *NanoLab, Faculty of Physics, University of Belgrade, Studentski Trg12, 11001 Belgrade, Serbia*

(3) *Serbian Academy of Sciences and Arts, Kneza Mihaila St. 35, 11000 Belgrade, Serbia*

Contact: V. Damljanović (damlja@ipb.ac.rs)

Abstract. We present group-theoretical classification [1] of all possible dispersions, which are linear in all directions, in the vicinity of high-symmetry Brillouin zone points, in non-magnetic layered materials. Both spinless and spinfull cases in the presence and in the absence of time-reversal symmetry are covered. We found that only three types of such dispersions are possible: Dirac, fortune teller and poppy flower. Low energy effective Hamiltonians are also presented. Special attention will be given to some recently published results not supported by our theory [2-5].

REFERENCES

[1] N. Lazić, V. Damljanović, M. Damnjanović, *arXiv*: 2108.11733 (2021).
[2] B. J. Wieder. B. Bradlyn et al., *Science* **361** (2018), 246–251.
[3] S. M. Young and C. L. Kane, *Phys. Rev. Lett.* **115** (2015), 126803.
[4] P. J. Guo, Y. W. Wei et al., *Phys. Rev. Lett.* **127** (2021), 176401.
[5] W. Luo, J. Ji et al., *Phys. Rev. B.* **101** (2020), 195111.

6TH INTERNATIONAL CONFERENCE "NANOTECHNOLOGY"

4 – 7 October 2021
Tbilisi, Georgia

GTUnano2021

In memory of Prof. Alex Gerasimov

initiator of GTU's nanoconferences

BOOK OF ABSTRACTS

Publishing House
"Technical University"
Tbilisi
2021

Georgian Technical University

6th International Conference "Nanotechnology"

4 – 7 October 2021

Tbilisi, Georgia

G T U n a n o 2 0 2 1

In memory of Prof. Alex Gerasimov
initiator of GTU's nanoconferences

Book of Abstracts

Tbilisi
2021

Book of Abstracts contains more than 100 abstracts of papers submitted to the 6th International Conference “Nanotechnology”, 4 – 7 October 2021, Tbilisi, Georgia (GTUnano2021) organized by the Georgian Technical University (GTU). The GTUnano2021 is held in memory of Prof. Alex Gerasimov, the initiator of GTU’s regular series of nanoconferences in Georgia. The 6th conference participants represent universities, institutes, research centers, etc. leading in the field of nanotechnology and nanosciences from 20 countries (Armenia, Azerbaijan, Belarus, China, Czech Republic, Georgia, Germany, Hungary, India, Iraq, Japan, Kazakhstan, Mexico, Poland, Russia, Serbia, Spain, Turkey, Ukraine, and United States of America).

C o m p i l e r s :

Levan Chkhartishvili

Mikheil Chikhradze

© Publishing House “Technical University”, 2021
ISBN 978-9941-28-850-0
http://www.gtu.ge

PYRAMIDS AND COOTIE CATCHERS: NEW MASSLESS FERMIONS IN 2D MATERIALS

Igor Popov [1], Vladimir Damljanovic [2], Rados Gajic [2]

[1] Institute of Physics Belgrade
Institute for Multidisciplinary Research
University of Belgrade
Belgrade, Serbia
popov@ipb.ac.rs
[2] Institute of Physics Belgrade
University of Belgrade
Belgrade, Serbia

Dirac-like electronic states are the main engines powering the tremendous advances in research of graphene, topological insulators and other materials with these states. Zero effective mass, high carrier mobility and numerous applications are some consequences of linear dispersion that distinguishes Dirac states.

Here we report a new class of linear electronic bands in two-dimensional materials with zero effective mass and sharp band edges never seen in solid state matter before, and predict stable materials with such electronic structure utilizing symmetry group analysis and *ab initio* approach **[1]**. We make a full classification of completely linear bands in two-dimensional materials and find that only two classes exist: Dirac fermions on one hand and pyramidal-like and cootie catcher-like states on the other hand.

The new class supports zero effective mass and hence high carrier mobility similar to that of graphene, anisotropic electronic properties like that of phosphorene, and robustness of states with respect to electronic correlations.

Reference

[1] V. Damljanovic, I. Popov, R. Gajic. Fortune teller fermions in two-dimensional materials. Nanoscale, 2017, 9, 48, 19337-19345.

The collection of abstracts is provided by scientific committee.

Put into production 26.09.2021. Signed for printing 30.09.2021. Paper format 60X84 1/8. Cond. print. sheet. 7.

Publishing House – Technical University, Tbilisi, 77 M. Kostava Str.

WWW.GTU.GE

BOOK OF ABSTRACTS

NN20

17th International Conference on Nanosciences & Nanotechnologies

7-10 July 2020

2020

WS2-Computational	
16:30-16:45 16:45-17:00	**KEYNOTE (L)** **M. Damnjanovic, University of Belgrade, Serbia** Topological phases of layers: elementary band representations
17:00-17:15 17:15-17:30	**INVITED (L)** **V. Damljanović, University of Belgrade, Serbia** Electronic Dispersions in Two- and Three-Dimensional Single Crystals FromSymmetry Point of View
17:30-17:45 17:45-18:00	**INVITED (L)** **I. Miloević, University of Belgrade, Serbia** Electronic-band topology of group VI layered transition metal dichalcogenides
18:00-18:15 18:15-18:30	**INVITED (V)** **M. Zacharias, Cyprus University of Technology, Cyprus** Temperature dependence of the optical properties of silicon nanocrystals
18:30-18:45	**E. Antoniou Aristotle University of Thessaloniki, Greece (V)** Ab Initio Computational Investigation of Structure & Magnetic Properties of SmCo5-XNiX Intermetallic Compounds
18:45-19:00	**Ronald Columbié-Leyva, Instituto de Investigación en Materiales, UNAM, México. (V)** Theoretical studies of high-Tc Fe-superconductors based on BaFe2As2 in presence of dopants Rh and Pd.
19:00-19:15	**C. Simserides, National and Kapodistrian University of Athens, Greece (V)** Hole transfer in cumulenic and polyynic carbynes
19:15-19:30	**M. Witkowski , University of Warsaw, Poland (V)** DFT modeling of SERS spectra of dipeptides: A comprehensive study of vibrational structure for Cys-Trp and Trp-Cys adsorbed on Au and Ag

Topological phases of layers: elementary band representations

M. Damnjanovic[1]
NanoLab, Faculty of Physics, University of Belgrade Studentski trg 12, 11000 Belgrade, Serbia

Research of topological phases is probably the main stream of condensed matter physics. In brief, Bloch theory transforms band structure of the hamiltonian spectrum into the fibre bundle over Brillouin zone (BZ), in this way enabling topological characterization of such bundles. Extensive work is performed within differential-geometric framework: Berry phase and derived notions (connection, curvature and Wilson loop e.g.), are used to find topological invariants like winding and Chern numbers. However, 30 years ago Mischel and Zak, pathed the symmetry based combinatorial way to classify band structures. Reconsidered recently, these results are firmly related to topological phases of crystals. This purely algebraic method considers graphs graphs imposed by symmetry. The first one is graph of Brillouin zone: as a contractible manifold, each stratum of ***k***-vectors with equivalent (conjugated) stabilizers is a vertex of the graph, while (oriented) edges connect neighbouring strata. Bands are made of patches over strata, each corresponding to specific allowed irreducible representation (IR) associated to the stratum. Contraction of BZ to graph, causes simultaneous contraction of the band patches, and the whole band structure becomes IR-graph: vertices are IRs, while edges represent connected patches. These edges are subdued to compatibility relations, or better, they depict them. Therefore, having BZ-graph, and compatibility relations (the both are directly and fully symmetry-determined), all possible IR-graphs are found in a combinatorial manner. This procedure is implemented in POLSym code, and applied to all layer groups (single and double, with or without time reversal). The results are presented, together with various analyses. For example, the disconnected graphs are looked for, as pointing out topologically non-trivial phases. Also, selected are band structures with special subgraphs which indicate possible atomic limits.

Electronic Dispersions in Two- and Three-Dimensional Single Crystals From Symmetry Point of View

V. Damljanović[1]
Institute of Physics Belgrade, University of Belgrade, Pregrevica 118, Belgrade, Serbia

In spatially periodic atomic arrangements, the electronic energy depends on the wave vector and forms a band structure. The form of a band in the vicinity of some point in the Brillouin zone is called the electronic dispersion and determines many physical properties of a material. Examples of electronic dispersions are Dirac (e.g. in graphene), semi-Dirac (e.g. in black phosphorus) and quadratic (e.g. in MoS_2). On the other hand, every crystal periodic in two (three) directions belongs to one of 80 layer- (230 space-) groups. Here we present deep connection between the crystal symmetry and the types of electronic dispersions present in the crystal. Our contribution is based on works published for two- [1-3] and three-dimensional [4-7] single crystals. We show that new and unexpected types of dispersions often appear as a consequence of crystal symmetry. This may be the clue for discovery of new materials with interesting physical properties.

References:
[1] V. Damljanović, R. Gajić, Journal of Physics: Condensed Matter **28**, 085502 (2016).
[2] V. Damljanović, R. Gajić, Journal of Physics: Condensed Matter **28**, 439401 (2016).
[3] V. Damljanović, I. Popov, R. Gajić, Nanoscale **9**, 19337-19345 (2017).
[4] J. L. Mañes, Physical Review B **85**, 155118 (2012).
[5] B. J. Wieder, Y. Kim, A. M. Rappe, C. L. Kane, Physical Review Letters **116**, 186402 (2016).
[6] B. Bradlyn et al., Science **353**, 10.1126/science.aaf5037 (2016).
[7] B. J. Wieder et al., Science **361**, 246-251 (2018).

NN2020

NN20

17th International Conference on Nanosciences & Nanotechnologies

NN20 is part of NANOTEXNOLOGY 2020

Organized by

Supported by

Under the Auspices

www.nanotexnology.com

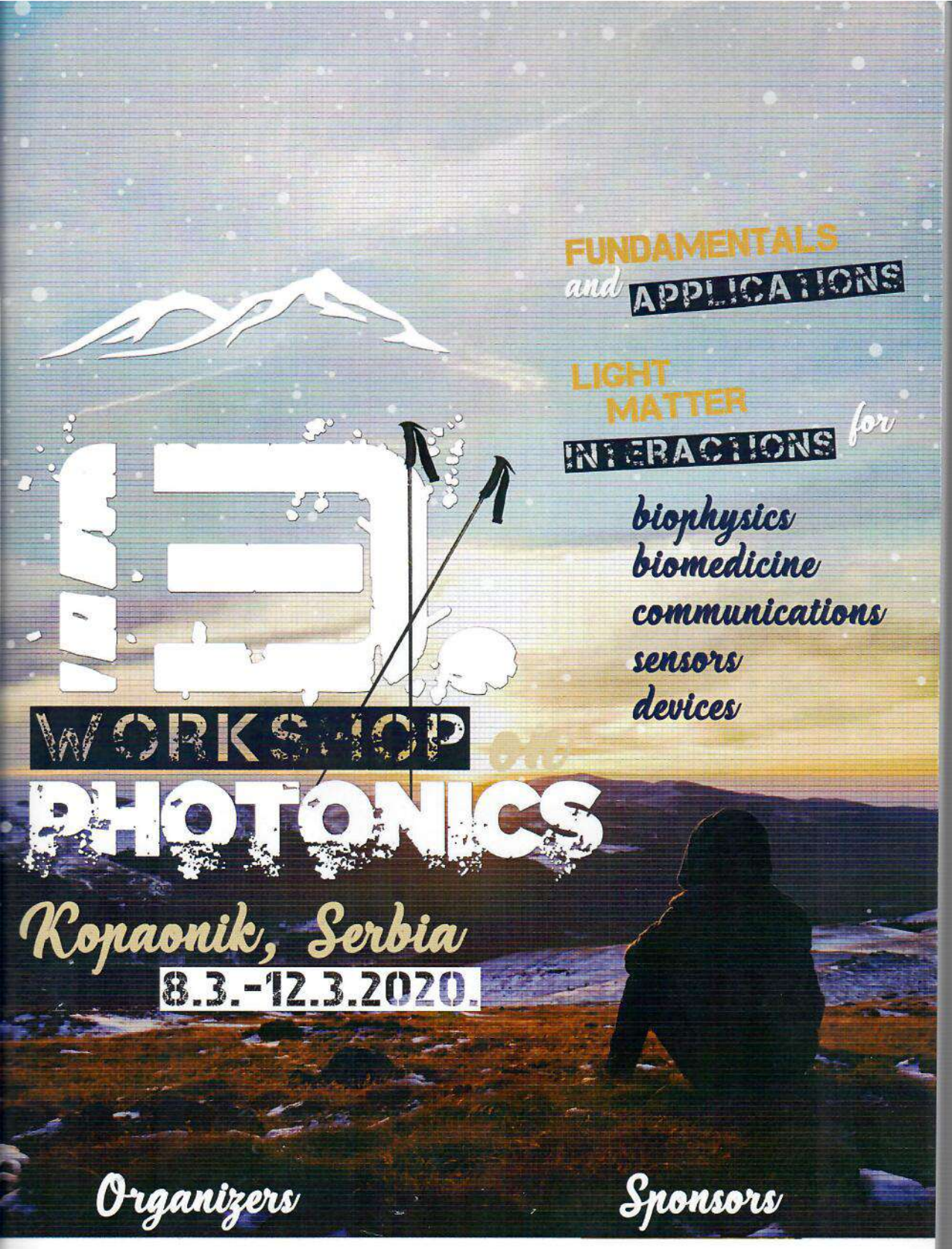

Organizers

PHOTONICS CENTER

IPB

Sponsors

Institute of Physics Belgrade
University of Belgrade
Kopaonik, March 08-12, 2020

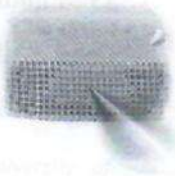

Book of Abstracts

13th Photonics Workshop

(Conference)

PHOTONICS
CENTER

13th Photonics Workshop (2020)

Book of abstracts

Kopaonik, Serbia, March 08-12, 2020

Publisher, 2020:

Institute of Physics Belgrade

Pregrevica 118

11080 Belgrade, Serbia

Editors:

Dragan Lukić, Marina Lekić, Zoran Grujić

ISBN 978-86-82441-50-2

Printed by:

NEW IMAGE d.o.o.

Cara Dušana 212, Zemun, Belgrade

Number of copies: 60

CIP - Каталогизација у публикацији Народна библиотека Србије, Београд

535(048)
681.7(048)
66.017/.018(048)

PHOTONICS Workshop (13 ; 2020 ; Kopaonik)
Book of Abstracts / 13th Photonics Workshop, (Conference), Kopaonik, March 08-12, 2020 ; [editors Dragan Lukić, Marina Lekić, Zoran Grujić]. - Belgrade : Institute of Physics, 2020 (Belgrade : New image). - 58 str. : ilustr. ; 25 cm

Tiraž 60. - Registar.

ISBN 978-86-82441-50-2

a) Оптика -- Апстракти b) Оптоелектроника -- Апстракти v) Технички материјали -- Апстракти

COBISS.SR-ID 283421708

Unusual electronic dispersions in non-magnetic, spin-orbit coupled, two-dimensional materials from double groups perspective

V. Damljanović[1]

(1) *Institute of Physics Belgrade, University of Belgrade, Pregrevica 118, 11000 Belgrade, Serbia*

Contact: V. Damljanović (damlja@ipb.ac.rs)

Abstract. When electron spin and orbital degrees of freedom are coupled, rotation in real space induces analogous transformation of two-component wave functions - Pauli spinors. Similarly, a symmetry group of an object in real space becomes a symmetry group in both real and spin space – so called double group [1]. In this contribution we used theory of layer double group representations to search for new electronic dispersions in non-magnetic, time-reversal symmetric two-dimensional materials with non negligible spin-orbit coupling [2]. Apart from known fortune-teller (FT) dispersion [3], we have found a new one: a generalization of both FT and Dirac dispersions. Our findings illustrate the fact that "to actually discover a feature in a band structure that provides the quasiparticle dispersion of a new and unexpected type is rare" [4] and that symmetry often provides such discovery.

REFERENCES

[1] H. Bethe, *Ann. Phys. (Leipzig)* **3** (1929), 133–208.
[2] V. Damljanović, N. Lazić, A. Šolajić, J. Pešić, B. Nikolić, M. Damnjanović, *submitted* (2020).
[3] V. Damljanović, I. Popov, R. Gajić, *Nanoscale* **9** (2017), 19337–19345.
[4] S. Banerjee, W. E. Pickett, *Phys. Rev. B* **86** (2012), 075124.

BOOK OF ABSTRACTS

16th International Conference on Nanosciences & Nanotechnologies

NN19

2-5 July 2019,
Porto Palace Conference Centre & Hotel
Thessaloniki, Greece

2019

Wednesday 3rd July 2019

09:00-09:30 Keynote Talk (Crystal Hall)

09:00-09:30 KEYNOTE	Linear dispersions in Q1D and Q2D crystalline structures M.Damnjanović University of Belgrade, Studentski trg 12, 11001 Belgrade, Serbia

Linear dispersions in Q1D and Q2D crystalline structures

M.Damnjanović[1], V. Damljanović[2]
[1]*NanoLab, Faculty of Physics, University of Belgrade, Studentski trg 12, 11001 Belgrade, Serbia*
[2]*Institute of Physics, University of Belgrade, Pregrevica 118,11000 Belgrade, Serbia*

Band structure with Dirac cone is origin of many amazing properties of graphene. Consequent Dirac equation of electron dynamics is one of the reasons for intensive research of this phenomenon during the past decade. In addition, topological band theory of insulators emphasized necessity of materials of this type as interphase for topologically different phases. In a search for other layers with similar band structure, several group theoretical conditions are singled out [1]. The conditions are applied to layer groups, and candidates for Dirac's points are singled out [2]. In fact, the band splitting occurs in a special point $\boldsymbol{P}$ in Brillouin zone; then an irreducible representation $D^{(P\alpha)}(\boldsymbol{G})$ of the layer symmetry group associated to this special point decomposes in several representations $D^{(P+k,\beta)}(\boldsymbol{G})$ associated to generic points $\boldsymbol{P+k}$ in the vicinity of $\boldsymbol{P}$. This gives compatibility relations which are strengthen by further restrictions providing linear dispersions of the split bands. Here, these group theoretical condition are revisited, and applied to line and layer ordinary and double groups, in order to find all Brillouin zone points with linear dispersions and the relevant irreducible representations (integer or half-integer). The results are discussed. For example, symmetries with linear crossing of bands only due to spin-orbit interaction are singled out.

[1] J. L. Manes, *Phys. Rev. B* **85**, 155118 (2012)
[2] V Damljanović and R Gajić, *J. Phys.: Condens. Matter* **28** (2016) 085502

LIGHT MATTER INTERACTIONS for

biophotonics
biosensing
biomedicine
optical materials
photonic structures
ultrafast phenomena
nonlinear and quantum optics

WORKSHOP on PHOTONICS

Kopaonik
10.3-14.3.2019.

Organizers

Sponsors

PHOTONICS

Копаоник, 10 – 14.03.2019.
УНИВЕРЗИТЕТ У БЕОГРАДУ
Институт за физику

Зборник апстраката

Дванаеста радионица фотонике (2019)

(Конференција)

Book of Abstracts

12th Photonics Workshop

(Conference)

PHOTONICS CENTER

Institute of Physics
University of Belgrade
Kopaonik, March 10-14, 2019

Дванаеста радионица фотонике (2019)

ЗБОРНИК АПСТРАКАТА

Копаоник 10-14.03.2019.

Издаје:

Институт за физику Београд

За издавача:

Др Александар Богојевић, директор

Уредници:

Др Драган Лукић, др Марина Лекић, др Зоран Грујић

Тираж: 70 primeraka

ISBN 978-86-82441-49-6

Штампа:

NEW IMAGE d.o.o.

Цара Душана 212, Земун, Београд

CIP - Каталогизација у публикацији - Народна библиотека Србије, Београд
535(048)
681.7(048)
66.017/.018(048)
PHOTONICS Workshop (12 ; 2019 ; Kopaonik)
Book of Abstracts / 12th Photonics Workshop, (Conference), Kopaonik, March 10-14, 2019. = Зборник апстраката / Дванаеста радионица фотонике (2019), (Конференција) ; [urednici Dragan Lukić, Marina Lekić, Zoran Grujić]. - Beograd : Institut za fiziku, 2019 (Beograd : New image). - 62
str. : ilustr. ; 25 cm
Tiraž 70. - Registar.
ISBN 978-86-82441-49-6
a) Оптика - Апстракти b) Оптоелектроника - Апстракти c) Технички материјали - Апстракти
COBISS.SR-ID 274585868

Effective masses, density of states and conductivities of various dispersions in 2D materials

Vladimir Damljanović[1]

(1) *Institute of Physics Belgrade, University of Belgrade, Pregrevica 118, 11000 Belgrade, Serbia*

Contact: V. Damljanović (damlja@ipb.ac.rs)

Abstract. Within the most simple, Drude model, the electrical conductivity of a crystal is inversely proportional to the electron effective mass and directly proportional to the concentration of free charge carriers [1]. At zero temperature, this concentration is determined by integration of density of states over partially filled energy bands. Situation becomes particularly interesting when the electron effective mass is zero. Dirac, semi-Dirac and Fortune-teller dispersions in 2D materials, support zero electron effective mass along at least one direction in the Brillouin zone. The conductivities of Dirac [2] and semi-Dirac [3] materials are well studied, both experimentally (graphene) and theoretically. On the other hand, the conductivity of recently discovered Fortune teller dispersion [4] remains an open question. In this talk we present conductivity analysis in [2, 3] and speculate that conductivity of the Fortune teller dispersion might be similar, with differences in detail left for future work.

REFERENCES

[1] N. W. Aschcroft and N. D. Mermin , *Solid State Physics*, Harcourt College, New York (1976).
[2] Y. V. Bludov, A. Ferreira et al., *Int. J. Mod. Phys. B* **27** (2013), 1341001.
[3] M. Sanderson, S. Huang et al., *J.Phys. D: Appl. Phys.* **51** (2018), 205302.
[4] V. Damljanović, I. Popov et al., *Nanoscale* **9** (2017), 19337-19345.

Book of abstracts

PHOTONICA2017

The Sixth International School and Conference on Photonics

& COST actions: MP1406 and MP1402

MultiscaleSolar

HERALD

&H2020-MSCA-RISE-2015 CARDIALLY workshop

CARDIALLY

28 August – 1 September 2017

Belgrade, Serbia

Editors

Marina Lekić and Aleksandar Krmpot

Institute of Physics Belgrade, Serbia

Belgrade, 2017

ABSTRACTS OF TUTORIAL, KEYNOTE, INVITED LECTURES, PROGRESS REPORTS AND CONTRIBUTED PAPERS

of

The Sixth International School and Conference on Photonics PHOTONICA2017

28 August – 1 September 2017
Belgrade Serbia

Editors
Marina Lekić and Aleksandar Krmpot

Technical assistance
Marko Nikolić and Danica Pavlović

Publisher
Institute of Physics Belgrade
Pregrevica 118
11080 Belgrade, Serbia

Printed by
Serbian Academy of Sciences and Arts

Number of copies
300

ISBN 978-86-82441-46-5

An example of two-dimensional crystal structure with semi-Dirac electronic dispersion

V. Damljanović[1] and R. Gajić[2]
[1]*Institute of Physics Belgrade, University of Belgrade, Pregrevica 118, 11080 Belgrade, Serbia*
[2]*Graphene Laboratory (GLAB) of Center for Solid State Physics and New Materials, Institute of Physics, University of Belgrade, Pregrevica 118, Belgrade, 11080, Serbia*
e-mail: damlja@ipb.ac.rs

In nanophysics, notion "semi-Dirac dispersion" denotes an electronic dispersion which is Dirac-like along certain direction in two-dimensional Brillouin zone (BZ) and quadratic along the orthogonal direction. Semi-Dirac materials are in the focus of research lately due to their intriguing physical properties. These include anisotropic Klein tunneling, characteristic response to magnetic field and peculiar photoresponse to circularly polarized light. To help search for new materials with the semi-Dirac cones, we have recently formulated a set of group-theoretical conditions that allow such dispersion and have provided the list of symmetry groups satisfying them [1]. In present contribution we have considered a tight-binding model on a structure that belongs to diperiodic (layer) group *p11b* (Dg5). This group belongs to our list [1] and should host the semi-Dirac cones in the vicinity of *A* and *B* points in the BZ. We have calculated electronic dispersion in the vicinity of these points. Obtained dispersion is of a semi-Dirac type thus confirming our theory. Here we also discuss other possible candidates for two-dimensional semi-Dirac materials by search Materials project database with particular attention to layered structures published in [2].

REFERENCES

[1] V. Damljanović, R. Gajić, J. Phys.: Condens. Matter 29, 185503 (2017).
[2] G. Cheon et al., Nano Letters 17, 1915 (2017).

Book of abstracts

PHOTONICA2017

The Sixth International School and Conference on Photonics

& COST actions: MP1406 and MP1402

MultiscaleSolar

HERALD

&H2020-MSCA-RISE-2015 CARDIALLY workshop

CARDIALLY

28 August – 1 September 2017

Belgrade, Serbia

Editors

Marina Lekić and Aleksandar Krmpot

Institute of Physics Belgrade, Serbia

Belgrade, 2017

ABSTRACTS OF TUTORIAL, KEYNOTE, INVITED LECTURES, PROGRESS REPORTS AND CONTRIBUTED PAPERS

of

The Sixth International School and Conference on Photonics PHOTONICA2017

28 August – 1 September 2017
Belgrade Serbia

Editors
Marina Lekić and Aleksandar Krmpot

Technical assistance
Marko Nikolić and Danica Pavlović

Publisher
Institute of Physics Belgrade
Pregrevica 118
11080 Belgrade, Serbia

Printed by
Serbian Academy of Sciences and Arts

Number of copies
300

ISBN 978-86-82441-46-5

Bifurcation in reflection spectra of holographic pullulan diffraction grating

S. Savić-Šević, D. Pantelić, V. Damljanović and B. Jelenković
Institute of Physics, University of Belgrade, Pregrevica 118, 11080 Zemun, Belgrade, Serbia
e-mail:savic@ipb.ac.rs

Reflection volume hologram gratings, fabricated using a single-beam method, usually have only one Bragg peak in the spectrum. Z. Wang et al. [1]noted the appearance of multiple peaks in the spectrum of volume diffraction grating recorded in dichromated gelatin, phenomenon that looks like bifurcation within the Bragg plateau. We also observed bifurcation phenomenain the spectrum of diffraction gratings recorded in dichromated pullulan (DCP), which is a polysaccharide doped with chromium. Compared to dichromated gelatin, the DCP material is simpler to prepare and process, it is insensitive to humidity, thusretaining high resolution and diffraction efficiency [2]. The typical number of appeared peaks in the spectrum is two, three, or four. It was found that a multi-peak phenomenon isaccompanied by wider band gap.

In order to understand multi-peak structure of band gaps, experimental results were compared with theoretically predicted results. The theoretical model investigates effects of several important parameters: absorption of radiation within the photosensitive layer, non-uniform thickness of the layer, refractive index modulation and non-uniform spatial period of the grating. Numerical reflection spectra of volume Bragg gratings have been calculated by the method of characteristic matrix [3]. Our model suggests that multi peak structures are produced by uneven modulation of Bragg layersinside the volume hologram. The results of calculation are in agreement with experimental results.

REFERENCES

[1] Z. Wang, D. Liu, J. Zhou, Opt. Lett.31, 3270 (2006).
[2] S. Savić-Šević, D. Pantelić, Applied optics 46, 287 (2007).
[3] M. Born, E. Wolf, *Priciples of Optics*, Pergamon (1980).

TWENTY-SECOND YOUNG RESEARCHERS' CONFERENCE

MATERIALS SCIENCE AND ENGINEERING

December 4 – 6, 2024, Belgrade, Serbia

Program and the Book of Abstracts

Materials Research Society of Serbia
&
Institute of Technical Sciences of SASA

2024

Book title:
Twenty-Second Young Researchers' Conference - Materials Science and Engineering: Program and the Book of Abstracts

Publisher:
Institute of Technical Sciences of SASA
Kneza Mihaila 35/IV, 11000 Belgrade, Serbia
Tel: +381-11-2636994, 2185263, http://www.itn.sanu.ac.rs

Conference organizers:
Materials Research Society of Serbia, Belgrade, Serbia
Institute of Technical Sciences of SASA, Belgrade, Serbia

Editor:
Dr. Smilja Marković

Technical Editor:
Aleksandra Stojičić and Dr. Ivana Dinić

Cover page: Dr. Smilja Marković
Cover photo: Dr. Nebojša Labus

Printing:
Gama digital centar
Otona Župančića No. 19, 11070 Belgrade, Serbia
Tel: +381-63 8616734
http://www.gdc.rs

Publication year: 2024

Print-run:
120 copies

CIP - Каталогизација у публикацији

Народна библиотека Србије, Београд

66.017/.018(048)

YOUNG Researchers Conference Materials Sciences and Engineering (22 ; 2024 ; Beograd)
Program ; and the Book of abstracts / Twenty-Second Young Researchers' Conference Materials Science and Engineering, December 4 – 6, 2024, Belgrade, Serbia ; [organizers] Materials Research Society of Serbia & Institute of Technical Sciences of SASA ; [editor Smilja Marković]. - Belgrade : Institute of Technical Sciences of SASA, 2024 (Belgrade : Gama digital centar). - XXII, 89 str. ; 23 cm
Tiraž 120. - Registar.

ISBN 978-86-80321-39-4

a) Наука о материјалима -- Апстракти b) Технички материјали -- Апстракти
COBISS.SR-ID 157262345

6-2

Study of crystal phases and temperature dependence of $InSiTe_3$

T. Belojica[1], J. Blagojević[1], S. Djurđić Mijin[1,2], A. Šolajić[1], J. Pešić[1], B. Višić[1], V. Damljanović[1], M. O. Ogunbunmi[3], S. Bobev[3,4], Yu Liu[4], C. Petrovic[4,5,6], Z.V. Popović[7], A. Milosavljević[1], N. Lazarević[1]

[1]Center for Solid State Physics and New Materials, Institute of Physics Belgrade, University of Belgrade, Pregrevica 118, 11080 Belgrade, Serbia, [2]Departamento de Fisica de Materiales, Facultad de Ciencias,Universidad Autonoma de Madrid, 28049 Madrid, Spain, [3]Department of Chemistry and Biochemistry, University of Delaware, Newark, Delaware 19716, U.S.A., [4]Condensed Matter Physics and Materials Science Department, Brookhaven National Laboratory, Upton, NY 11973-5000, USA, [5]Shanghai Advanced Research in Physical Sciences (SHARPS), Shanghai 201203, China, [6]Department of Nuclear and Plasma Physics, Vinca Institute of Nuclear Sciences, University of Belgrade, Belgrade 11001, Serbia, [7]Serbian Academy of Sciences and Arts, Knez Mihailova 35, 11000 Belgrade, Serbia

In recent years, quasi-low-dimensional materials have attracted significant attention due to their distinctive properties and possible applications in nanoeletronics and spintronics. The material of a specific interest within this group is $InSiTe_3$. Unlike related compounds, such as $CrSiTe_3$ and $CrGeTe_3$, research results $InSiTe_3$ are limited, most likely due to the unclear nature of its crystal structure. Detailed experimental and theoretical investigation was conducted to determine the crystal structure of $InSiTe_3$. Inelastic light scattering experiment performed on the $InSiTe_3$ reveals presence of six ($3A_{1g} + 3E_g$) out of eight and seven ($5A_g + 2E_g$) out of ten Raman active modes for proposed $P\bar{3}1m$ and $P\bar{3}$ space groups, respectively. These findings suggest a coexistence of two trigonal crystal phases: a high symmetry one corresponding to $P\bar{3}1m$ and athe lower symmetry one that corresponds to $P\bar{3}$ space group. Additional exitations were detected in parallel scattering configuration; two broad features in the gap of PDOS that can be a consequence of to two-phonon processes and a third one, at about 500 cm^{-1} that might indicate local symmetry breaking at nano scale. Temperature dependent measurements from 80 K to 300 K show monotonous decrease in energy and increase in linewidth up to 200 K at which point discontinuities appear across all analyzed modes. However, this anomaly overcomes the scope of this research and remains an open question.

26 - 30 June 2023
Belgrade, Serbia

21. СИМПОЗИЈУМ ФИЗИКЕ КОНДЕНЗОВАНЕ МАТЕРИЈЕ

THE 21st SYMPOSIUM ON CONDENSED MATTER PHYSICS

BOOK OF ABSTRACTS

Institute of Physics Belgrade

Vinca Institute of Nuclear Sciences

University of Belgrade, Faculty of Physics

Serbian Academy of Sciences and Arts

Ministry of Science, Technological Development and Innovation

Unmovable Nodal Points and Lines in Two-Dimensional Materials: Dispersions and Positions in the Reciprocal Space

V. Damljanović[a] and N. Lazić[b]

[a]*Institute of Physics Belgrade, University of Belgrade, Pregrevica 118, 11000 Belgrade, Serbia*
[b]*NanoLab, Faculty of Physics, University of Belgrade, Studentski Trg 12, 11001, Belgrade, Serbia*

Abstract. We have found all quasiparticles in non-magnetic, two-dimensional materials in the presence of time-reversal symmetry [1]. Analysis of all eighty layer groups, both single- and double-, indicates that nineteen sorts exist, which are located near high-symmetry points and lines in the Brillouin zone. Our results are presented graphically in analogy with space groups elements in International Tables for Crystallography. Our findings can pave the way towards realization of new 2D materials with unprecedent physical properties.

REFERENCES

1. Damljanović, V., and Lazić, N., *J. Phys. A: Math. Theor.* **56**, 215201 (2023).

7-11th October 2019
Belgrade, Serbia

http://www.sfkm.ac.rs/

The 20th Symposium on Condensed Matter Physics

BOOK OF ABSTRACTS

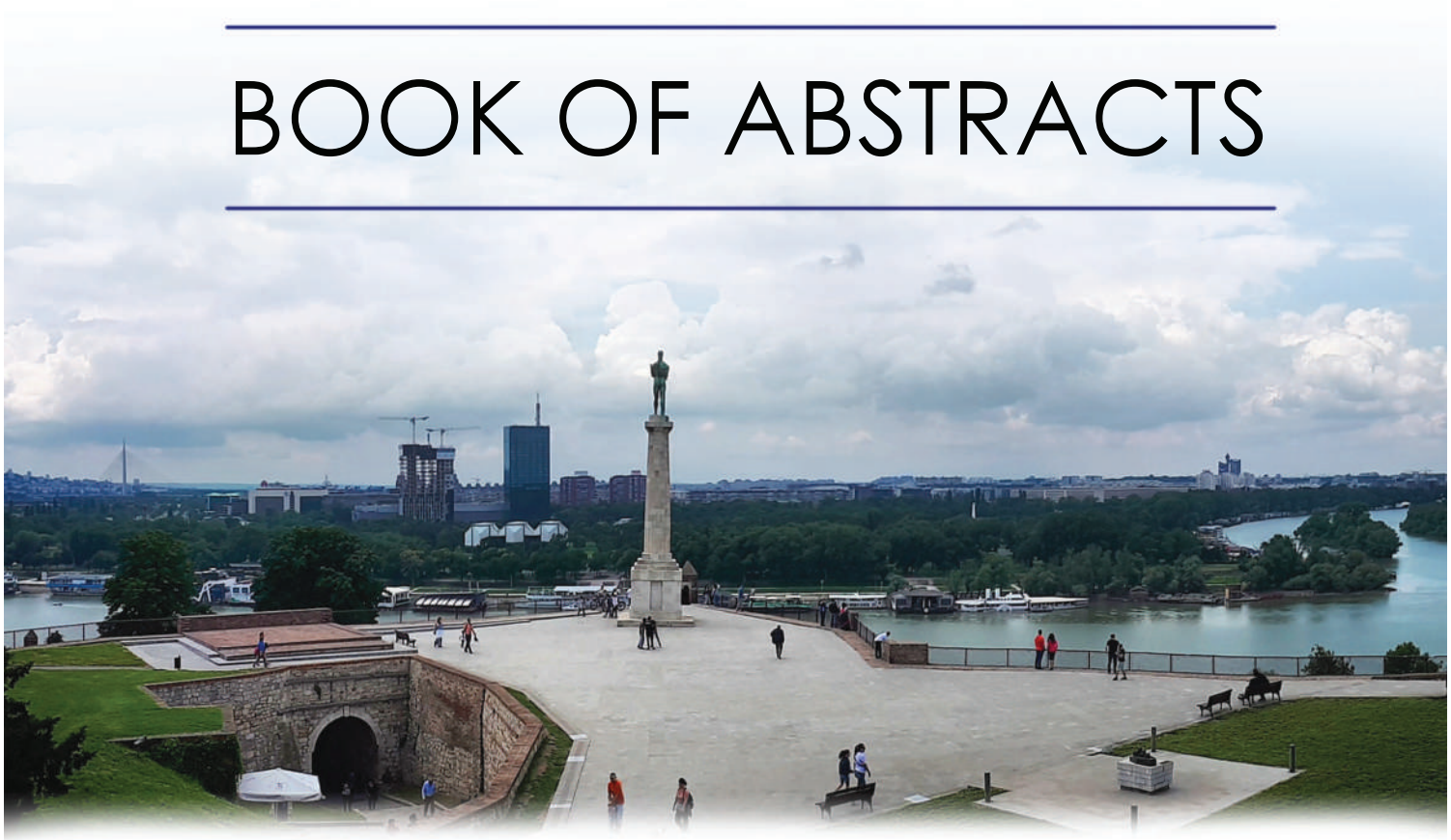

University of Belgrade, Faculty of Physics

Institute of Physics Belgrade

Vinca Institute of Nuclear Sciences

Serbian Academy of Sciences and Arts

Ministry of Education, Science and Technological Development, Republic of Serbia

Peculiar Electronic Dispersions in Two-Dimensional Materials Caused by Symmetry

Vladimir Damljanović[a]

[a]*Institute of Physics Belgrade, University of Belgrade, Pregrevica 118, 11080 Belgrade, Serbia*

Abstract. Two-dimensional materials are spatial atomic arrangements that are periodic in two directions, but are finite in the third, orthogonal direction. Most of their physical properties are determined by the functional dependence of the electronic energy near the Fermi level on the electron wave vector i.e. by the electronic dispersion. Until recently only three types of electronic dispersions were known in two-dimensional materials: Dirac (as in graphene), semi-Dirac (as in black Phosphorus) and quadratic (as in MoS_2). In this talk we show that certain symmetries of non magnetic, time-reversal symmetric, two-dimensional materials with no spin-orbit coupling (SOC) leads unavoidably to new, forth type of electronic dispersion we called the Fortune teller (FT) dispersion [1]. Even more, inclusion of SOC leads to another type of peculiar electronic dispersion, which is generalization of both Dirac and FT dispersions. The physical properties of materials which these new dispersions induce are still to be investigated theoretically.

REFERENCES

1. Damljanović, V., Popov, I., and Gajić, R., *Nanoscale.* **9**, 19337-19345 (2017).

PHOTONICS CENTER

UNIVERZITET U BEOGRADU
Institut za fiziku

Konferencija

Jedanaesta radionica fotonike (2018)

Zbornik apstrakata

Kopaonik, 11–14.3.2018.

Konferencija **Jedanaesta radionica fotonike (2018)**

ZBORNIK APSTRAKATA

Kopaonik 11-14.03.2018.

Izdaje

Institut za fiziku Beograd

Za izdavača

Dr Aleksandar Bogojević, direktor

Urednik

Dr Dragan Lukić

Tiraž

50 primeraka

ISBN 978-86-82441-47-2

Štampa

NEW IMAGE preduzeće d.o.o.

Cara Dušana 212, Zemun, Beograd

Symmetry induced electronic dispersions in two-dimensional materials

Vladimir Damljanović[1]

(1) *Institute of Physics Belgrade, University of Belgrade, Pregrevica 118, 11080 Belgrade, Serbia*

Contact: V. Damljanović (damlja@ipb.ac.rs)

Abstract. Two-dimensional (2D) materials are arrangements of atomic ions which are periodic in two spatial directions but finite in the third, orthogonal direction. Recent examples of such materials include graphene, silicene, transition metal dichalcogenide monolayers etc. Any 2D material belongs to one of eighty, so-called layer (or diperiodic) symmetry groups. In this talk, a deep connection between various types of famous electronic dispersions (Dirac, semi-Dirac, quadratic etc.) in a certain 2D material and a layer group to which the material belongs, is presented. In addition, previously unknown type of electronic dispersion obtained by applying symmetry arguments is also presented. Our talk is based on recently published results [1-4] refering to non-magnetic 2D materials with negligible spin-orbit coupling.

REFERENCES

[1]V. Damljanović, R. Gajić, *J. Phys.: Cond. Matt.* **28** (2016), 085502.
[2]V. Damljanović, R. Gajić, *J. Phys.: Cond. Matt.* **28** (2016), 439401.
[3] V. Damljanović, R. Gajić, *J. Phys.: Cond. Matt.* **29** (2017), 185503.
[4]V. Damljanović, I. Popov, R. Gajić, *Nanoscale* **9** (2017), 19337-19345